An investigation into the effects of inorganic element status on the accumulation and deposition of amyloid in various diseases.

Thesis submitted for the degree of

Doctor of Philosophy

UNIVERSITY
OF CENTRAL
LANCASHIRE

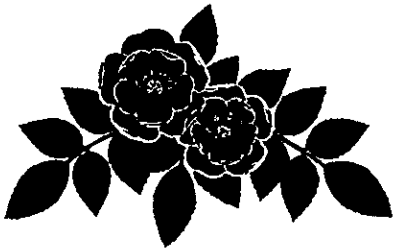

Edmund Lane

Department of Environmental Management

University of Central Lancashire

October 2000

An investigation into the effects of inorganic elements on the accumulation and deposition of amyloid in various diseases.

Abstract

Several human diseases are reported to be associated with amyloidogenic peptides and proteins, for example, β amyloid (Aβ) in senile plaques of Alzheimer's disease and β_2 microglobulin (β_2M) deposition in dialysis related amyloidosis. The major factor for amyloidosis appears to be an increase in the production of amyloidogenic proteins, resulting in the amyloid β sheet deposits. It is clear that conformational changes in amyloidogenic proteins lead to fibril formation and aggregation. Several trigger factors may be involved in the initiation and propagation of these amyloid deposits. Common components such as serum amyloid P component (SAP), glycosaminoglycans (GAGs) may be involved, and metals such as aluminium, copper, zinc and calcium have also been implicated. Metals have been shown to induce aggregations of amyloid and accelerate amyloid deposition. The present study involved the investigation of the effects of inorganic elements on the secondary structural integrity of amyloid proteins leading to aggregation and deposition.

The addition of Cu^{2+}, Zn^{2+}, Ca^{2+} and Al^{3+} (>50 μM) to the amyloids, particularly Aβ(1–40) and β_2M, showed some changes with a general decrease in α helix secondary structure and an increase in β sheets. Both the Aβ(1-40) and β_2M peptides treated with physiological concentration of either Al^{3+}, Ca^{2+}, Cu^{2+} or Zn^{2+} combined with the physiological concentrations of various GAGs showed that they had a synergistic effect, indicating that GAGs could play a role in conjunction with metals. This has not been previously reported in the literature. The binding of GAGs to the amyloids could provide further binding sites for metal ions, leading to an alteration in the protein conformation. There is evidence in the literature for metals as trigger factors in the deposition of the Alzheimer's disease Aβ peptides, but not for the dialysis related β_2M peptide. Similar changes occurred for the interaction of both Aβ(1-40) and β_2M with metals and also with metals in the presence of GAGs. This suggests that similar mechanisms may be involved and that metals may have an underlying role in the general process of amyloidosis independent of the type of amyloid protein involved.

Acknowledgements

I would like to thank Dr Alexis Holden for all her help and encouragement with this work. I would also like to thank Professor Ian Shaw and Dr Robert Coward, (Royal Preston Hospital, Preston, UK) for their valued discussion and advice. I am grateful to Dave Clarke, (Daresbury Laboratory, Warrington, UK) for his assistance with the circular dichroism station at Daresbury and for his help with the data analysis. Sincere gratitude is also extended to Dr Chris Morris (MRC, Neurochemicalpathology Unit, Newcastle, UK) for supplying the Alzheimer's disease brain tissue and the gift of Aβ(1-43) peptide.

I thank the many people in the Centre for Toxicology and the Chemistry department for their help and I also thank my family and friends for their support throughout the course of my PhD.

The PhD was jointly funded by the University of Central Lancashire and the Lancashire Centre for Medical Studies (LCMS).

Abbreviations

Aβ	beta amyloid from Alzheimer's disease
Aβ(1-40)	1-40 fragment of beta amyloid
Aβ(1-42)	1-42 fragment of beta amyloid
Aβ(1-43)	1-43 fragment of beta amyloid
Aβ(xx - xx)	other fragments of beta amyloid
AA	AA amyloid
Ads-ATR	adsorption attenuated total reflectance
AEF	amyloid enhancing factor
AIAPP	islet amyloid polypeptide
AL	AL amyloid
Al/Al^{3+}	aluminium / aluminium cation
$AlCl_3$	aluminium chloride
Apo	apoprotein
APP	amyloid precursor protein of Alzheimer's disease
Arg	arginine
Asn	asparagine
Asp	aspartic acid
ATR	attenuated total reflectance
β_2M	beta 2 microglobulin
BBB	blood brain barrier
BSA	bovine serum albumin
BSE	bovine spongiform encephalopathy
Ca/Ca^{2+}	calcium / calcium ion
$CaCl_2$	calcium chloride
CAPD	continuous ambulatory peritoneal dialysis
Cd	cadmium
CD	circular dichroism
CJD	Creutzfeldt-Jakob disease
CNS	central nervous system
Co/Co^{2+}	cobalt / cobalt cation
Cr	chromium
CS	chondroitin sulphate
CSA	camphor sulphonic acid
CSF	cerebral spinal fluid
CSPG	chondroitin sulphate proteoglycan
Cu/Cu^{2+}	copper / copper cation
$CuCl_2$	copper chloride
DNA	deoxyribonucleic acid

DRA	dialysis related amyloidosis
DS	dermatan sulphate
EAA	excitatory amino acids
ESRD	end stage renal failure
Fe/Fe^{3+}	iron / iron cation
FTIR/IR	Fourier transform infrared spectroscopy
GAG	glycosaminoglycan
Ge	germanium
Gly	glycine
H_2SO_4	sulphuric acid
HCl	hydrochloric acid
HD	haemodialysis
HDL	high density lipoprotein
HEP	heparin
HFIP	1,1,1,3,3,3 hexafluoroisopropanol
HIV	human immunodeficiency virus
HLA	human leukocyte antigen
hr	hour
HRP	horse radish peroxidase
HS	heparan sulphate
HSPG	heparan sulphate proteoglycan
IEF	isoelectric focusing
IRE	internal reflectance element
kDa	kilo Daltans
KS	keratan sulphate
Mg^{2+}	magnesium cation
$MgCl_2$	magnesium chloride
Mn/Mn^{2+}	manganese / manganese cation
Mo	molybdenum
MT	metallothionein
MW	molecular weight
Na_2SiO_3	sodium silicate
NaCl	sodium chloride
NaOH	sodium hydroxide
$(NH_4)_2\ SO_4$	ammonium sulphate
Ni/Ni^{2+}	nickel / nickel cation
NMR	nuclear magnetic resonance
NOE/NOESY	nuclear Overhauser effect / nuclear Overhauser enhancement spectroscopy
NP-40	nonylphenoxy polyethoxy ethanol (Tergitol)
NT	neurofibrillary tangles

PAGE	polyacrylamide gel electrophoresis
PAR	4-(2-pyridylazo) resorcinol
Pb	lead
PG	proteoglycan
Phe	phenylalanine
PHF	paired helical filament
pI	isoelectric point
PMSF	phenyl methly sulphonyl fluoride
Pro	proline
PrP*	prion protein intermediate
PrP^c	prion protein
PrP^{sc}	conformationally changed prion protein
r[hu]PrP^c	human recombinant prion protein
RNA	ribonucleic acid
rpm	revolutions per minute
SAA	serum AA amyloid
SAP	serum amyloid P component
Sb	antimony
SDS	sodium dodecyl sulphate (lauryl sulphate)
Ser	serine
SHaPrP(29-231)	Syrian hamster prion protein
SIMS	secondary ion mass spectrometry
SOD	superoxide dismutase
SP	senile plaque
TCBS	tween citrate buffered saline
TEMED	N,N,N',N'-tetramethylethylene diamine
TF-ATR	thin film attenuated total reflectance
TFE	2,2,2 - trifluoroethanol
Tris	tris[hydroxymethyl]aminomethane
Trp	tryptophan
TTBS	tween tris buffered saline
TTR	transthyretin amyloid
Tyr	tyrosine
UV	ultra violet (electromagnetic radiation)
Val	valine
VIS	visible (electromagnetic radiation)
Zn/Zn^{2+}	zinc / zinc cation
$ZnCl_2$	zinc chloride

Contents

Chapter 1. Introduction.

1.1 Proteins.

1.1.1 Protein introduction.

Proteins are abundant in all organisms and are indeed fundamental to life. Proteins are involved in virtually every biological process in a living system. The precise orchestration of cellular activity requires that various proteins are present in appropriate quantities at the correct times. The shear diversity of the protein structure underlies their large range of function. The information required to synthesise proteins is stored in DNA. Proteins are synthesised on ribosomes as linear chains of typically hundreds of amino acids.

Most of the chemical reactions that occur in biological systems are catalysed by enzymes, which are proteins. The rate of the reactions they catalyse are often increased by the order of at least a million-fold. Proteins are involved in the transmission of nerve impulses by acting as receptors of transmitter molecules that cross the junctions separating nerve cells. Proteins also act as hormone receptors and can themselves be hormones. The immune system depends on the production of antibodies: proteins, which bind to specific foreign particles such as bacteria and viruses.

Various ions, small molecules and other metabolites are stored in an organism as complexes with proteins; for example iron is stored bound to ferritin in the liver. Proteins are involved in the transportation of particles ranging from electrons to macromolecules. Haemoglobin in red blood cells is important for the transfer of oxygen and removal of carbon dioxide from the lungs to other tissues. The formation of pores in cellular membranes through which ions pass and the transport of molecules across membranes is also dependent on proteins. Some proteins have a structural role, providing mechanical support. The "skeleton" of a cell consists of a complex network of protein filaments. Muscle contraction depends on the action of large protein assemblies. Other organic materials are also based on protein, for instance hair. Collagen is found in all multi-cellular animals, occurring in almost every tissue; approximately a quarter of mammalian protein is collagen.

1.1.2 The importance of protein structure.

In order to function, protein chains must fold into the unique native three-dimensional structures that are characteristic of the individual proteins. The protein shape and function are inextricably linked. The importance of protein folding has been recognised for many years. In the 1950's, Linus Pauling [1] discovered that proteins consist of primarily two regular secondary structures - the α helix and the β sheet. And in the early 1960's, Christian Anfinsen [2] showed that proteins could adopt their native conformation spontaneously. What Anfinsen's experiments didn't show, however, was why a particular chain of amino acids folds into one and only one shape, i.e. the protein sequence determines its structure.

The formations of α helix and β sheet secondary structures are directly influenced by the presence of primary sequence of a protein. In proteins and nucleic acids the predominant regular structures are characterised by intra-chain hydrogen bonding within the backbone chain. The α helix is a right-hand spiral stabilised by hydrogen bonds between each amino acid's nitrogen atom and the oxygen atom of the fourth residue along the chain. This means that there are 3.6 amino acids for each turn of the helix (**Figure 1.1a**) [3].

The β sheet structure is essentially flat, with the side chains sticking out on alternate sides. The β sheet is also stabilised by hydrogen bonds between nitrogen and oxygen atoms. In this case, however, the hydrogen-bonded atoms belong to different amino acid chains running alongside each other. The sheets are `parallel' if all the chains run in the same direction and are `antiparallel' if alternate chains run in opposite directions (**Figure 1.1b**).

Antiparallel sheets are often, but not always, formed by a single chain looping back upon itself [3]. When a single chain loops back on itself to form an antiparallel β sheet, the one to three amino acids linking the two strands are known as a β-turn (**Figure 1.1c**). All other local arrangements of amino acids are described as `random coil,' although they are random only in the sense of not being periodic.

Figure 1.1

Typical secondary structure: (**a**) α helix, (**b**) anti-parallel β sheet, (**c**) β turn or hairpin. The dashed lines show hydrogen bonding between residues; arrows denote direction of β strand [3].

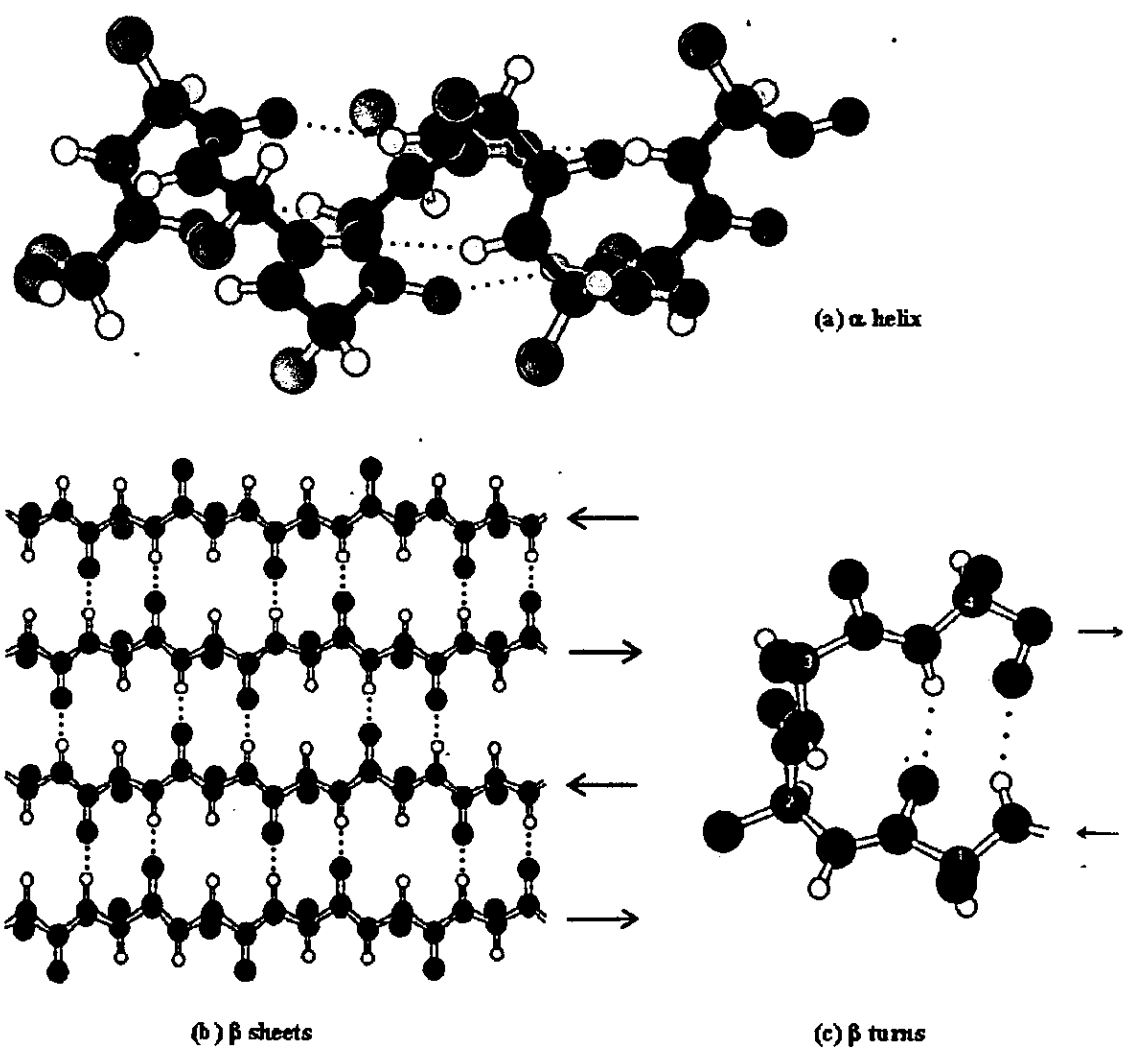

Tertiary folding is largely determined by the packing of the α helices and/or β sheets. For many proteins the tertiary structure can adequately be described by one of three motifs: an assembly of α helices with a predominantly β sheet (α/β), β sheets stacked together (β/β), or structures involving α helices (α/α). These arrangements satisfy the hydrogen bonding requirements of buried main-chain nitrogen and oxygen atoms while shielding a substantial fraction of the non-polar atoms from the solvent. Quaternary structure is formed by the combination of two or more chains. The interactions between the chains are not different from those in tertiary structure, but are distinguished only by being inter-chain rather than intra-chain [3].

1.1.3 Protein folding.

There are nearly 100,000 proteins encoded in the human genome, and there are thought to be more than a thousand fundamentally distinct structural architectures into which folded proteins can be classified. The number of possible conformations of a polypeptide chain is huge, yet the folding of a protein is fast with a typical folding time of 1 s. Protein folding occurs in multiple steps commonly referred to as *"The folding pathway"*.

The distribution of polar (hydrophilic) and non-polar (hydrophobic) residues along the polypeptide chain is now known to be a crucial factor in determining the overall fold and are important in both intra and inter-binding sites and ultimately their stabilisation. Protein folding involves complex mechanisms that depend on the co-operative action of a vast number of relatively weak non-covalent interactions involving thousands of atoms.

There are several families of cellular proteins whose job is to assist in the folding process of the other proteins, for example, molecular chaperones. The efficiency of protein folding can be compromised by aggregation of folding intermediates that have exposed hydrophobic surfaces. In a cellular environment, molecular chaperone proteins bind reversibly to folding intermediates, protecting the incompletely folded polypeptide chains from aggregating and promoting correct folding [4].

The formation of the protein structure that yields the lowest energy state, i.e. the "native conformation", is the process that drives the folding pathway. Protein folding is thought to start with the formation of elements of secondary structure independently of tertiary structure, or at least before tertiary structure is locked in place. First a very rapid formation of secondary structure such as α-helices and β–sheets. The folding of these compact shapes are presumed to be driven by hydrophobic collapse, so that most of the interior of the protein is occupied by hydrophobic amino acids, which have a low affinity for water. The second phase is slower; the secondary structure elements interact with each other to form the native tertiary structure.

The nucleus primarily consists of a few adjacent residues, which have some correct secondary structure interactions, but is stable only in the presence of further approximately correct tertiary structure interactions. These elements then assemble into the tightly packed native tertiary structure either by diffusion and collision or by propagation of structure in a stepwise manner. The protein subunits then assemble to the quaternary structure to form the final native conformation of the protein [4].

1.1.4 Protein misfolding and disease.

Even after the folding process is complete, however, a protein can subsequently experience conditions under which it unfolds, at least partially, and then it is again prone to aggregation. When we boil an egg, the albumin protein in the egg white unfolds. Upon cooling, the proteins don't return to their original shapes, instead, they form an insoluble solid, but tasty nonetheless.

It is becoming clear that the failure of proteins to fold correctly or to remain folded under all appropriate physiological conditions can give rise to a wide range of pathological conditions. Defective and misfolded proteins are normally rapidly degraded by proteolysis. It may therefore not always be obvious that a protein is misfolding, but rather, there seems to be a decrease in that protein.

The misfolding of a protein can be caused by:

- Mutations in the DNA so that the amino acid sequence differs from normal. Many single amino acid mutations have little affect on the folding, but in a number of cases results in a less efficient, or unstable protein.
- Lack of enzymes or molecular chaperone needed to fold a protein.
- Interaction with other misfolded proteins.
- Correctly folded protein becoming misfolded by accumulated damage due to oxidation, radicals or other chemical reactions.

Misfolding proteins can cause diseases in several ways:

- A protein becomes non-functional or ineffective.
- A protein is in short supply caused by a decrease in production or increased uptake/removal.
- A protein is unable to get to the right place, due to inability to fold correctly.
- The presence of protein aggregates, that have a damaging effect on the cell. The abnormal protein can, in some cases, propagate further misfolding of normal protein as in the prion diseases.

A number of diseases are caused by amyloid fibrils, in which a normally soluble protein deposits as insoluble fibrils. In most cases the exact cause is as yet unknown, but the protein involved is certainly misfolded. Examples are: Alzheimer's disease (β-amyloid protein), Primary systemic amyloidosis (immunoglobulin light chains), Senile systemic amyloidosis (transthyretin, TTR), Diabetes Type 2 (Amylin, IAPP), The prion diseases such as Bovine spongiform encephalopathy and Creutzfeldt-Jakob disease (prion, PrP). The resulting deposition of aggregated amyloid protein disrupts the normal function of tissue in which it is deposited [5].

Inherited diseases have examples of all types of consequences of misfolded protein: Emphysema is due to a lack of α-anti-proteinase. Osteogenesis imperfecta is due to an unstable fold. Cystic fibrosis, and familial hypercholesteremia may be due to a misfolded protein that cannot take up its proper position. Familial amyloidosis, Creutzfeldt-Jakob disease, and Alzheimer's disease involve aggregation of misfolded

proteins [5]. In Huntington's disease, the mutated gene codes for a protein that produces an increasing number of consecutive residues of the amino acid glutamine. When the number of residues expands past 40, the protein becomes insoluble, causing the protein to misfold.

1.1.5 Protein misassembly.

Various terms encompass protein misassembly [4]:

- ***Precipitation*** arises as a consequence of solvent changes, decreasing the solubility of the protein in a reversible manner.
- ***Denaturation*** refers to reversible, as well as irreversible structural changes in native proteins leading to altered solubility that does not change the primary structure.
- ***Coagulation*** occurs as a result of an increase in particle size caused by denaturation of a protein with subsequent gelation.
- ***Aggregation*** is used to describe the association or assembly of proteins that may involve quaternary structural changes or involve sidechain interaction [4].

Proteins may undergo a wide range of specific structural changes during their normal function. The biological activity of proteins is closely linked to its native structure, which is retained only if critical factors such as temperature, pH, solvent and concentration are kept within narrow limits. The relative reactivity of a protein often depends upon the nature of the solvent-protein interaction. Solvents such as di-chloroacetic acid, trifluoroethanol and formic acid can influence the secondary structure of the protein [4].

Protein folding can be studied in the test tube by dissolving a purified protein in aqueous solution and denature it using chaotropic agents which are polar and/or charged molecules (e.g. urea and guanidine-HCl), detergents (e.g. sodium dodecyl sulphate), heat, metals, reagents which cleave disulphide bridges (e.g. dithiothreitol, mercaptoethanol) and acids or bases which cleave salt bridges. Removing the denaturant by dialysis induces a *spontaneous refolding* of the polypeptide into its original, native fold.

Different denaturants can lead to different denatured states but common to all states is a reduction in solubility. Denaturants cause alterations in the conformation of the polypeptide chain, which can be reversed on their removal. Essentially the 'denaturation – renaturation' step is a two-state process involving a native protein state and an unfolded state. There are other intermediates but these are generally thermodynamically unstable. The increase in nucleus radius with increasing protein concentration leads to a gain in conformational entropy that drives the aggregation. As the concentration of denatured protein increases then the pool of component molecules that favour aggregation increases [4].

1.1.6 The binding of metals to proteins.

The solubility of proteins may be pictured as a balance between attractive and repulsive forces involving on the one hand the interaction of protein molecules with the solvent, and the interaction between the protein molecules. The balance of these forces determines the degree to which the protein molecules tend to disperse and surround themselves with other protein molecules. Some of the factors affecting this solubility include coulombic forces, hydrogen bonding between protein-protein and protein-solvent and the presence of hydrophobic groups in the protein.

The binding of ions depends on the intrinsic affinity of the ligand groups available for interaction that allows binding of ions non-specifically. The folding of a peptide chain means that side groups such as carboxyl, imidazole, or sulphydryl are usually more important than terminal amino or carboxyl groups. In general ion binding sites are composed of protein moieties, such as the carboxyl group, that interact simultaneously with the ion producing a co-operative affect that may afford some specificity. The amino acid groups in a polypeptide chain are restricted by intra- or inter-hydrogen bonding and steric hindrance and are not free to move and cluster around a metal ion in the way free amino acids and small peptides can. Proteins bind to particular ions due to the specific arrangement of residues.

The protein molecule normally bears a considerable number of positive and negative charges whose net potential field favours or hinders the approach of the metal ion. The effect of the counter ion depends on its size and ionic strength. At low ionic

strength, weak interaction of soluble organic molecules with proteins may lead to increased protein solubility (salting in). At high ionic strength, e.g. high salt concentration, the opposite holds and the solubility decreases (salting out).

Most of the groups available to bind to metal ions also bind to hydrogen ions and in general there will be competition for sites in the protein. Competition for hydrogen can be readily detected by a shift in pH following the addition of metal salts. The binding of metal ion may be mediated by the unfolding or denaturing of the protein, exposing ligands and chelatable sites. There is a linear relationship between the logarithm of solubility and ionic strength, i.e. the Hoffmeister effect. Decreased solubility favours aggregation and coagulation. These effects may be explained by competition for water of hydration between protein and excess electrolyte [4].

There are three separate ways in which metals could interact with proteins that may alter the solubility. It must also be highlighted that full saturation of metal ions may not be possible due to steric and electrostatic effects. The binding of metal to a protein could occur as in **Figure 1.2a** and may also form a chelate complex (**Figures 1.2b - 1.2c**).

The first form is probably encountered frequently in metal protein precipitates and may affect solubility in two ways: the charge effects are similar to that of H^+ (i.e. changing the net charge of the protein) and effects between protein-metal complex and the solvent. In the second mechanism, the aggregation occurs by cross linkages across metal ions. The cross-linking can occur when several ligands are exposed and the metal cation is able to chelate across either inter or intra protein molecule. Even if intermolecular cross-linking is the main mechanism which renders the protein insoluble, relatively few cross linkages may be necessary [4].

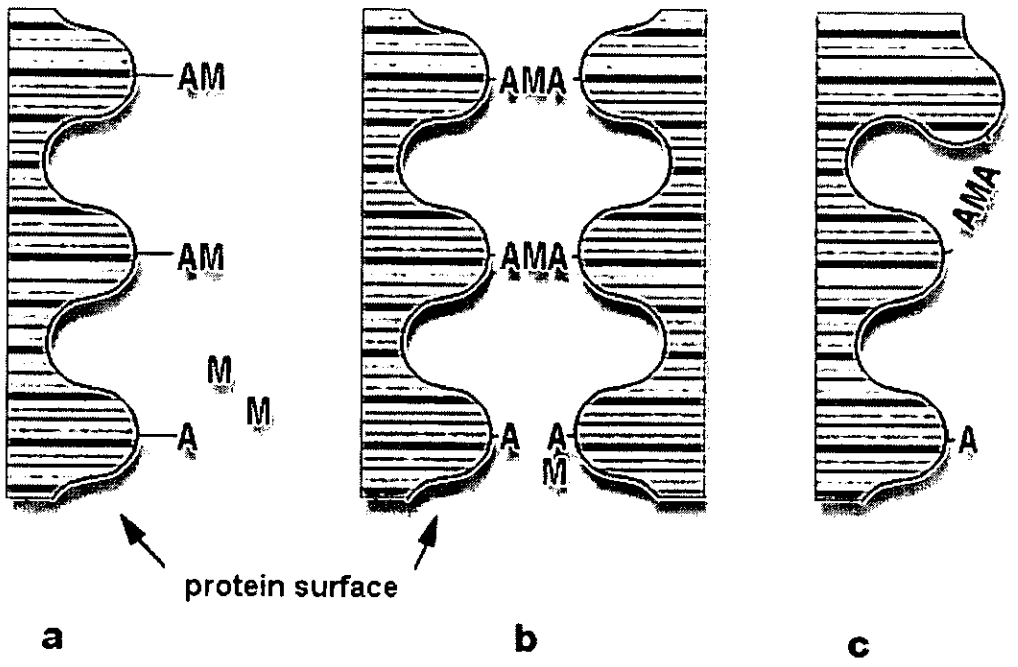

Figure 1.2 - Diagrams showing the possible interactions between protein ligand (A) and metal (M): (**a**) simple binding (**b**) inter and (**c**) intra chelate complex formation.

The two amino acids, which combine most strongly with metal ions, are the histidine and cysteine residues. Histidine may combine with a metal ion through all of its exposed donor groups, imidazole as well as the α amino group and carboxyl groups. Cysteine combines with metals strongly via the sulphur group. Ions tend to bind to groups for which they have some intrinsic affinity. Ca^{2+} ions bind to oxygen atoms, Zn^{2+} ions bind to imidazole rings of histidine residues. Fe^{2+}/Fe^{3+} ions bind to sulphur atoms on cysteine residues, and Cu^{2+} ions bind to thiol or imidazole groups.

1.2 Methods for the determination of secondary structure of proteins.

Techniques for protein structural elucidation include X-ray crystallography, NMR and fluorescence labelling and other spectroscopic methods. The complete three-dimensional structure of a protein at high resolution can be determined by X-ray crystallography. This technique requires the molecule to form well-ordered crystals, which may not be possible for all proteins. Nuclear magnetic resonance (NMR) spectroscopy has the advantage over crystallographic techniques in that experiments are performed in aqueous solution as opposed to a crystal lattice. However, the physical principles that make NMR possible limits the application of this technique to macromolecules of less than 30 kDa [6]. The interpretation of the NMR spectrum of large proteins is very complex and NMR peaks of larger proteins can be difficult to resolve and assign. In NMR, the secondary structures are localised to specific segments of the polypeptide chain and can thus provide a wealth of information about dynamics. However, obtaining secondary structural information from NMR data requires considerably concentrated solutions (15 mg ml^{-1} for a 15 kDa protein) [7 & 8]. These limitations have led to the development of alternative methods that are not able to generate structures at atomic resolution but provide structural information on proteins (especially secondary structure). Therefore, the use of circular dichroism and vibrational spectroscopy to determine the structure of biological macromolecules has been increasingly used.

Circular dichroism (CD) spectroscopy can be used to gain information about the secondary structure of proteins in solution. The advantages are that it is a non-destructive technique using small sample sizes of relatively low protein concentration (200 µl of a 0.5 mg ml^{-1} solution in standard cells). Relative changes due to the influence of the environment on the sample (pH, denaturants, temperature etc.) can be monitored very accurately. The major disadvantage is that a CD spectro-polarimeter is relatively expensive, and also some interferences occur with solvent absorption in the UV region which means that buffers used should be dilute and non-absorbing below 200nm [9]. Fourier transform infrared (FTIR) spectroscopy can be applied to the study of the secondary structure of proteins in aqueous solution [10-12]. The technique of FTIR spectroscopy requires only small amounts of proteins in a variety of

environments. The main strength of FTIR spectroscopy is the ability to investigate biological systems under non-invasive conditions. Therefore, high quality spectra can be obtained relatively easily without problems of background fluorescence, light scattering and those related with the size of the proteins. The ever-present water absorptions can be mathematically subtracted. Methods are now available that can separate sub-components that overlap in the spectrum of proteins. Since the potential sources of error in CD and FTIR analyses of secondary structure content are largely independent, the two methods are highly complementary and could be used in conjunction to increase accuracy. Despite limitations in the quantitative assessment of protein secondary structure content, FTIR and CD spectroscopy provide good tools to monitor conformational changes in polypeptides and proteins. The various techniques are described below. The spectroscopic methods of CD and FTIR, which were used in the actual studies, are discussed in more detail below.

1.2.1 X-ray crystallography.

The understanding of protein structure and function has been greatly enriched by X-ray crystallography, a technique that can reveal the precise three-dimensional positions of most of the atoms in a protein molecule. Crystals of the protein of interest are needed because the technique requires that all molecules be precisely orientated. Crystals can often be obtained by slow drying, or by adding ammonium sulphate or another salt to a concentrated solution of protein to reduce its solubility. A narrow beam of X- rays strikes the protein crystal, part of it penetrates through the crystal; the rest is scattered in various directions. Current detection methods include solid-state electronic detectors such as CCD instruments that can collect larger areas than single point scintillation counters. The molecular image obtained from x-ray crystallography is called an electron density map, because it is an image of the electron clouds of the molecule under study. Hence, the electron density map can give three-dimensional information about the structure of the protein [8]. If the sequence of amino acids in the protein is known, an accurate model can be obtained by fitting the atoms of the known sequence into the electron density map, calculations are carried out on sophisticated graphics computers.

1.2.2 Nuclear magnetic resonance (NMR) spectroscopy.

1.2.2.1 Physical principles of NMR.

Nuclear magnetic resonance is a spectroscopic method that is used to observe nuclear spin reorientation in an applied magnetic field. Sub-atomic particles possess a characteristic *spin angular momentum.* Many important nuclei (^{1}H, ^{31}P, ^{13}C) have a spin equal to a ½ giving rise to two energy states in the presence of a magnetic field. A transition from the lower (α) to the upper (β) state occurs when a nucleus absorbs electromagnetic radiation of appropriate frequency. NMR spectroscopy is a very informative technique because the local magnetic field around all the nuclei in the sample is not identical within the applied field B_0, because of shielding from the electron density around each molecule. Consequently, nuclei in different environments absorb energy at slightly different resonance frequencies, an effect termed the chemical shift. Thus each proton should, in principle, be characterised by a unique chemical shift. In practice, this is never observed as some protons, such as the three protons of each side chain, methyl group of Thr, Val, Leu, Ile, and Met and most pairs of equivalent (2,6 and 3,5) aromatic ring protons are found to have degenerate chemical shifts. Other protons (OH, SH, and NH_3) are in rapid chemical exchange with the solvent and thus have chemical shifts indistinguishable from the solvent resonance [6 & 7]. Near complete amino acid chemical shifts assignments are often possible [13].

1.2.2.2 Nuclear Overhauser effect.

The structural information of a protein can come from through space dipole-dipole coupling between two protons, called the nuclear Overhauser effect (NOE). The intensity of a NOE is proportional to the distance separating the two protons. Thus the NOE is a sensitive probe of short intramolecular distances. A two dimensional nuclear Overhauser enhancement spectroscopy (NOESY) spectrum graphically displays pairs of protons that are in close proximity [7]. The three-dimensional structure of a protein can be reconstructed from a large number of such proximity relations. This raises the problems complexity when analysing proteins and other biological macromolecules [6- 8].

1.2.2.3 Secondary structure in NMR.

Secondary structure determination by NMR techniques does not require a full three-dimensional structural analyses as X-ray crystallography does. Comparison of X-ray structures and amide proton chemical shifts for well characterised proteins reveals a simple correlation between chemical shift and secondary structure [7]. The α proton of all 20 naturally occurring amino acids has been shown to have a strong correlation with secondary structure [14]. Conformationally dependent chemical shifts of $^{13}C^{\alpha}$ and $^{13}C^{\beta}$ nuclei can also be used to identify regular α helix or β sheet regions in proteins. While obtaining the sequential resonance assignments is a time consuming task, the NMR method is perhaps the most powerful and certainly the most accurate method of secondary structure determination [6].

1.2.3 Circular dichroism (CD) spectroscopy.

Circular dichroism spectroscopy is a form of light absorption spectroscopy that measures the difference in absorption of right and left circularly polarised light by a substance. CD is a useful technique to determine the conformation of proteins and other biological macromolecules that exhibit chirality. Proteins are optically active because they are asymmetric. Amino acid residues other than glycine are intrinsically optically active because of the configuration about their α carbon atom. Threonine and isoleucine possess an additional chiral centre. Circular dichroism is very sensitive to the secondary structure of a polypeptides due to the dis-symmetric environment, which affects the electronic transitions to the excited state [15]. The electronic interaction between residues also contributes to the optical activity e.g. an α helical conformation results in a large contribution [8]. CD spectra rather than optical rotatory spectra are measured because CD spectra are more sensitive and simpler to interpret. The magnitude of $\Delta\varepsilon$ is $x10^3$ less than the ordinary molar absorption coefficient ε, corresponding to an ellipticity of a few 1/100th of a degree, hence sensitive instrumentation is required to measure CD [8].

1.2.3.1 Physical principles of CD.

Electromagnetic radiation is a complex waveform that can be considered as two components, a **magnetic** (B) and an **electric** (E) wave at right angles to each other

(**Figure 1.3a**). The differential absorption of radiation polarised in two directions as function of frequency is called dichroism. When applied to plane polarised light, it is called linear dichroism, and for circularly polarised light, it is called circular dichroism. After passing through an optically active sample, circularly polarised light will be changed in two aspects. The two components are still circularly-polarised, but the molar absorption coefficients for right- and left-polarised light now differ causing the E-vector to trace an ellipse (actually an elliptical screw) instead of a circle. There will also be a rotation of the major axis of the ellipse due to differences in refractive indices [16]. The synchrotronic light is circularly polarised in a photo elastic modulator (PEM) before passing through the sample chamber and detected using a photomultiplier tube (PMT) (**Figure 1.3b**).

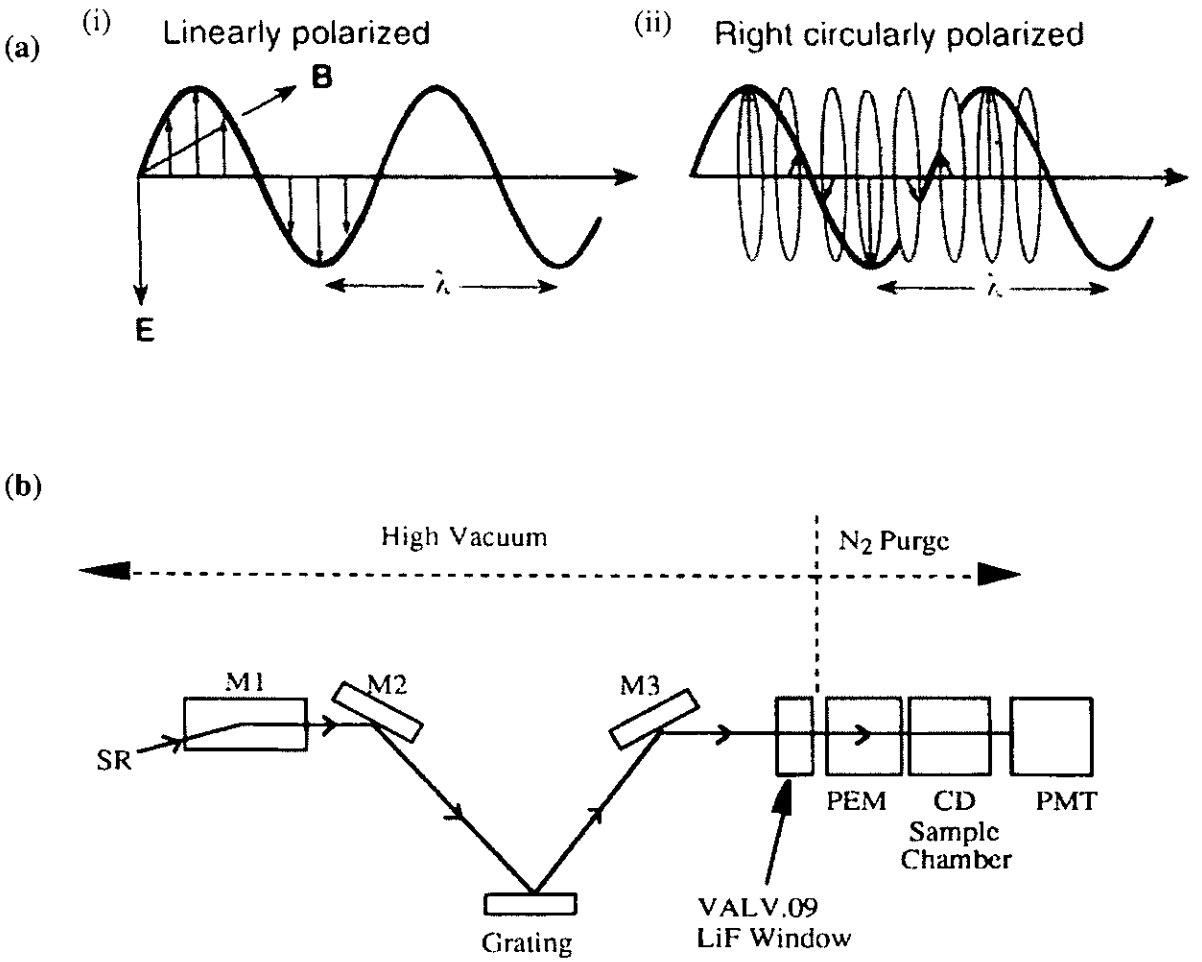

Figure 1.3 - Schematic diagrams of (**ai**) of linearly polarised light (λ - wavelength, B - magnetic and E - electric components), (**aii**) of right-handed circularly polarised light [16] and (**b**) the layout for CD **Station 3.1** at Daresbury Laboratories.

1.2.3.2 Secondary structure in CD.

Circular dichroism is particularly powerful in monitoring conformational changes. The far-ultraviolet CD spectrum of a protein is sensitive to its main-chain conformation. For proteins, the absorption in the ultraviolet region of the spectrum arises from the peptide bonds (symmetric chromophores) and amino acid side chains in proteins. Protein chromophores can be divided into three classes: the peptide bond; the amino acid side chains, and any prosthetic groups. The region of 178 - 260 nm can be monitored to observe effects of backbone conformational changes (**Figure 1.4**).

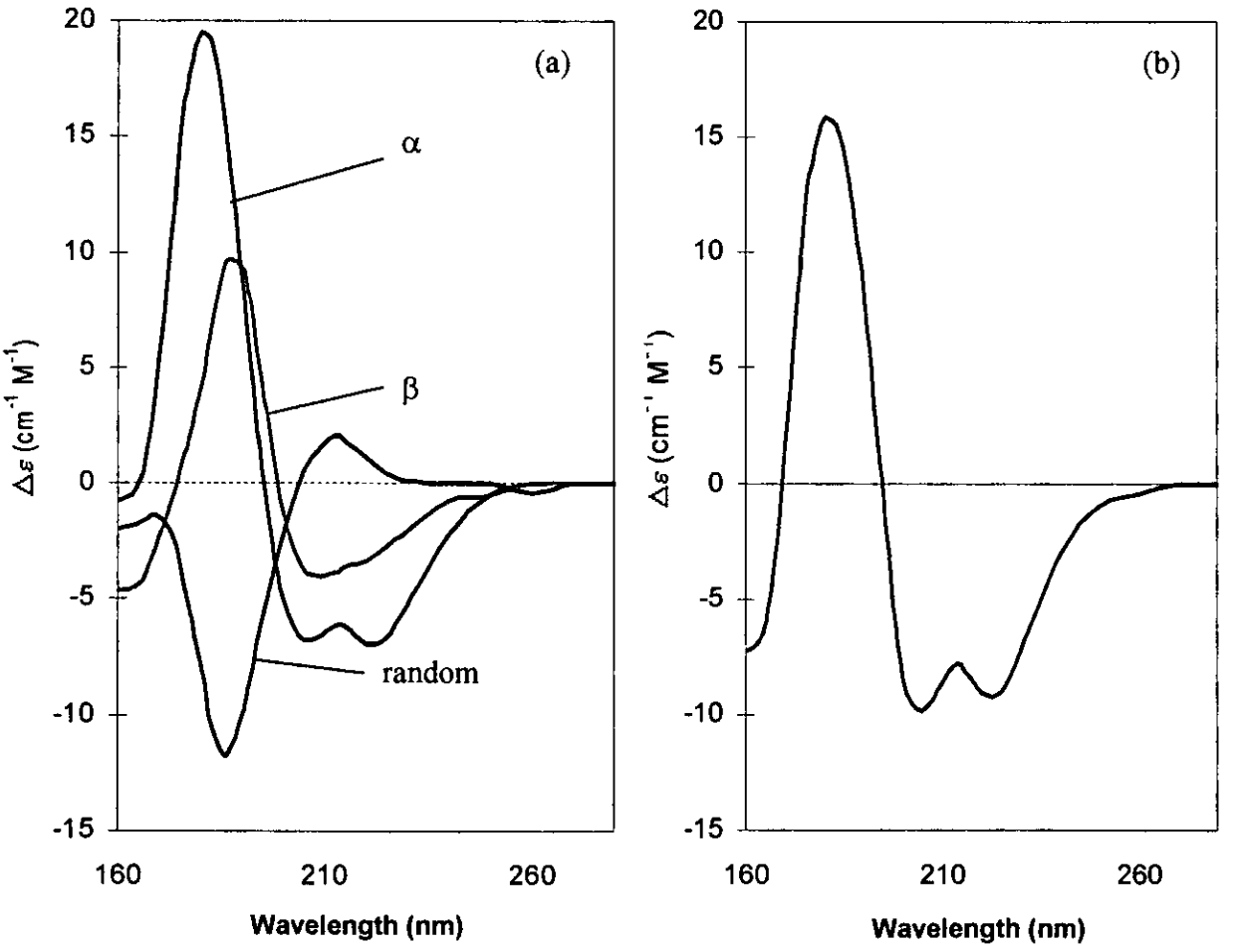

Figure 1.4 - The circular dichroism spectra of (**a**) secondary structural components; α helix (green), β pleated sheet (magenta) and a random coil (blue) of a model polypeptide and (**b**) the CD spectrum of combined secondary structure [8].

The protein microenvironment in solution, including solvent effects, influences secondary structural determination of peptides and proteins. The change in solvent environment can cause a change in the transition energy that leads to blue or red shifts of the CD maxima. These shifts contribute to a discrepancy in the determined

secondary structure [16]. The analysis of CD spectra can therefore yield valuable information of the secondary structure of biological macromolecules. Measurements of synthetic polypeptides and proteins of known structure define the α helices, β sheet structure and random coils motifs. The α helices have a dominant contribution with a negative band between 208 and 222 nm and a positive band at 192 nm. β sheets give a minimum around 218 nm and a maximum around 196 nm. A randomly arranged polypeptide chain has a negative CD band centred at 200 nm [8 & 16].

1.2.3.3 Secondary structural interpretation.

The secondary structural computer programs used to analyse the spectra may give differing values due to the program used for secondary structural calculations. Various methods including linear combination (LINCOMB), multi-linear regression (MLR), convex constraint analysis (CCA), neural network program single-value decomposition (SVD), CONTIN program for rigid regression analysis, and the self-consistent method (SELCON) to obtain secondary structural information from CD data [16-20]. Secondary structural analysis using the primary sequence has been improved by incorporating CD using a least-squares fit or best fit. Unfortunately, extraction of a secondary structure using the best fit does not necessarily give appropriate secondary structural elements of β sheet or β turn structures. It is generally accepted that the α helical secondary structural values are reliable.

1.2.3.4 Synchrotronic radiation.

The use of synchrotronic light allows CD measurements below 200 nm in far UV region, within the peptide backbone region of 178 – 260 nm. Conventional light sources diminish below this range, whereas the flux obtained from a synchrotronic light remains high. The synchrotronic light is produced as a result of loss of energy from electrons as they decelerate in a magnetic field. The electrons are held in an orbit in storage dipole magnets and accelerated to a velocity approaching that of the speed of light. Polarised synchrotronic radiation is emitted at a tangent and consists of a continuous spectrum of radiation ranging from the X-rays to the microwave region. The synchrotron radiation source (SRS) was housed at CLRC Daresbury Laboratory, Daresbury, UK.

1.2.4 Fourier transform infrared (FTIR) spectroscopy.

Fourier transform infrared (FTIR) spectroscopy has been used to evaluate structural characteristics of proteins, including secondary structure, hydrogen-deuterium exchange, thermal denaturation, and other properties. The hydrogen-deuterium exchange method can also be used to probe protein conformation, hydrogen bonding, exposed exchangeable hydrogens, and membrane-bound conformations. FTIR spectra of biological samples are usually complicated with numerous vibrational bands; therefore, a difference spectrum would be useful to observe changes purely due to the sample.

The O-H bending peak at 1644 cm^{-1} overlaps with the conformational sensitive amide I band. The high molar absorptivity of the O-H bending vibrations of water (~1640 cm^{-1}) and problems associated with non-linearity. This limits the path length used in studies of proteins dissolved in water to 10 μm or less. Longer path lengths result in significant distortions of water absoprtions, making background subtraction impossible. Therefore, digital subtraction of buffer and water spectra can generate the spectrum due to the protein. Adequate subtraction will only be obtained if the spectrum of the protein solution and water (or buffer) are recorded at the same temperature, due to the strong dependency of water absorptions on temperature. An alternative approach is to use ^2H_2O as a solvent. The water bend is shifted some 400 cm^{-1} to a lower frequency thus leaving a useful window free of absorptions in the amide I region of the spectrum. Much longer path lengths may then be used (50 μm is standard, although path lengths of 100 μm or more may be used), which allow a significant reduction in the concentration of samples (0.1 to 1 mg ml^{-1}).

1.2.4.1 Secondary structure in FTIR.

The infrared spectra of polypeptides exhibit a number of 'amide bands' that represent different vibrational modes of the peptide bond. There are up to 9 characteristic bands named amide A, B and I through to VII. Amide I and amide II bands are two major bands of the protein infrared spectrum. The amide I band (between 1600 and 1700 cm^{-1}) is mainly associated with the C=O stretching vibration (70-85%) and is directly related to the backbone conformation. Amide II (1510 and 1580 cm^{-1}) results from the N-H

bending vibration (40-60%) and from the C-N stretching vibration (18-40%). This band is conformationally sensitive. Amide III and IV (1350 – 1450 cm^{-1}) are very complex bands resulting from a mixture of several co-ordinate displacements. The out-of-plane motions are found in amide V, VI and VII bands (200- 800 cm^{-1}). Overall, the amide I bands are most useful primarily, because they arise predominantly from one type of vibration [21].

A critical step in the interpretation of IR spectra of proteins is the assignment of the amide I component bands of different types of secondary structure. Amide I bands centred around 1650-1658 cm^{-1} are generally considered to be characteristic of α helices. Unordered structure and turns also give rise to amide I bands in this region which complicates analysis. The β sheets give rise to highly diagnostic bands in the region of 1620-1640 cm^{-1}. There is a weaker band associated with antiparallel β sheets around 1680 cm^{-1} [22-24] (**Table 1.1**).

Secondary structure	Amide I frequency (cm^{-1})
Antiparallel β sheets/ aggregated strands	1675 - 1695
α helix	1648 - 1660
unordered	1640 - 1648
β sheet	1625 - 1640
Aggregated strands	1610 - 1628

Table 1.1 - shows the typical amide I frequencies corresponding to the secondary structural features [23 & 24].

1.2.4.2 Band assignment.

Band assignment depends on the nature and environment of the protein. For real proteins, the situation is much more complex than that discussed above, which assumes the presence of only one major structural motif. All proteins contain more than one secondary structural motif, and, consequently, give rise to more that one amide absorption. Unfortunately, the width and separation of these absorptions is such that they overlap and produce a composite, often featureless absorption profile as in **Figure 1.5**. It is also assumed that the absorptions arise from amide C=O groups involved in secondary structures.

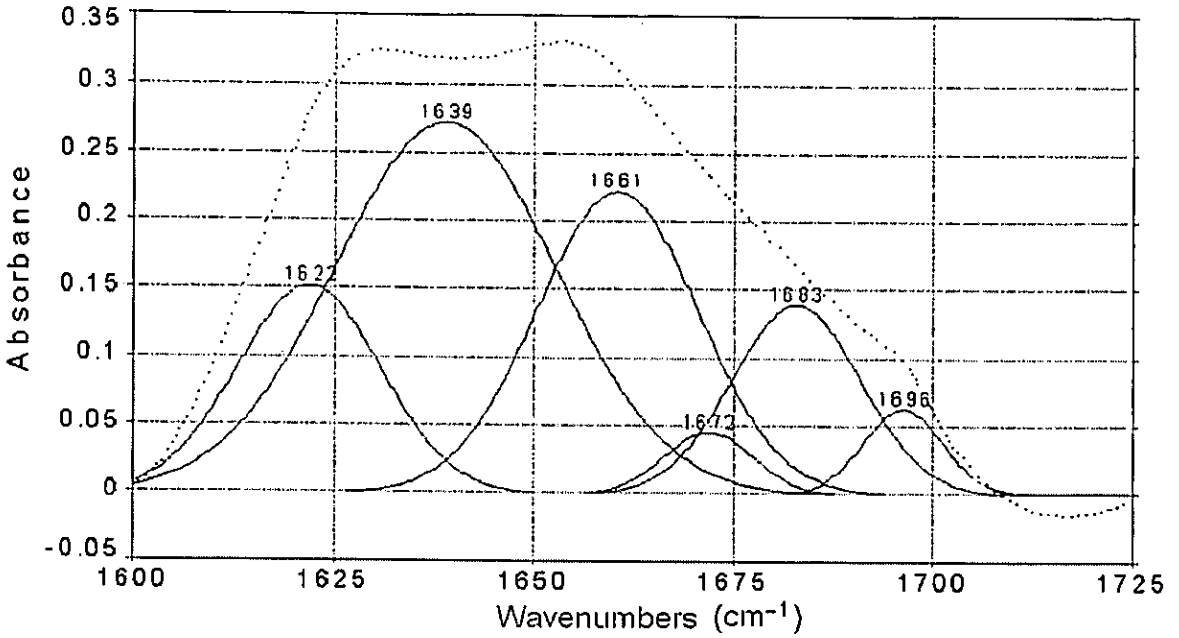

Figure 1.5 - A typical spectral profile for a protein containing a degree of secondary structure. The individual bands due to the secondary structure contribute to the overall featureless spectral envelope shown as the dotted black line.

In fact significant absorptions in this region of the spectrum may arise from amino acid side chains, including tyrosine, phenylalanine, glutamine, arginine and lysine [25]. In proteins containing significant amounts of these amino acids a nontrivial contribution from the side chains may in fact make up 10 - 15% of the total intensity of the amide I. Another source of error lies in the assignment of particular amide I absorptions to specific secondary structures, e.g. myoglobin is predominantly α helical in structure, with little or no β sheet structure present. However, the IR spectra exhibits a maximum at 1653 cm^{-1}, characteristic of an α helix and also a strong shoulder at 1632 cm^{-1} which may be mistaken for β sheet secondary structures. In fact, this most likely arises from turns within the protein. Although different types of secondary structures produce distinct band frequencies in the amide I region, it is difficult to distinguish between different parts of the protein that have the same secondary structure.

Information may be obtained by analysis of the frequency of the composite amide I spectral envelope along with any visible shoulders. However, changes in the positions of these maxima could make interpretation difficult. For example, a shift to a lower

wavenumber of a peak may mean that one or more of the underlying absorptions has shifted to a lower frequency. Alternatively, such a shift may be produced by an increase in intensity of a component band, resulting in a redistribution of intensities without any actual change in the frequency of the peak [23]. Analysis of the spectral envelope alone cannot be used to identify secondary structure and could lead to misinterpretation.

1.2.4.3 Second derivative and deconvolution spectra.

Methods such as deconvolution and derivation coupled with curve fitting can be used to assign specific bands. Deconvolution or derivation is performed on the original data to obtain an estimate of the number of discrete absorptions that make up the complex amide I band profile. Deconvolution or derivation are techniques used to obtain an estimate of the number of discrete absorptions that make up a complex spectral profile. Most of the band positions that are in the amide I band are easily found in second derivative spectra. Some difficulties arise in absorption bands showing as shoulder peaks in the derivative spectra. Deconvolution is an estimate of the number of components in the envelope, their width, height and shape. Therefore the bands overlap and can not be distinguished in the amide envelope. These parameters are then used as input parameters in an iterative least squares routine that attempts to reproduce the experimentally obtained amide I band profile by varying these parameters.

The most common method of quantitation of protein secondary structure involves curve fitting of the amide I region [26] of proteins in a variety of matrices and environments [27]. Curve fitting methods based on techniques such as singular value decomposition [28], factor analysis [29] and partial least squares analysis [30] of IR spectra are analogous to methods used for quantitation of CD spectral, i.e. comparison of spectra with spectra of known peptide structures. Although quantitative estimates of protein secondary structure are sought by many investigators, each of the techniques currently used suffers from significant shortcomings. Despite limitations in the quantitative assessment of protein secondary structure content, FT-IR provides a good tool to monitor conformational changes in polypeptides and proteins [31].

1.2.4.4 Attenuated total reflectance (ATR).

Attenuated total reflectance FTIR is a versatile and powerful technique for infrared sampling and is a method widely used in the study of proteins. Attenuated total reflectance spectroscopy can be used to analyse protein structures in different forms, including surface adsorbed proteins, membrane bound proteins, turbid solutions and proteins in biological samples [32]. The technique is ideal for rapid quantitative and qualitative analyses, as no sample preparation is required for most samples. The major advantage of ATR-FTIR over conventional FTIR is that proteins can be in aqueous solutions that can also be non transparent.

The ATR attachment comprises of a crystal of a material that is transparent to mid infrared. The internal reflectance element (IRE) has a refractive index such that incident radiation is internally reflected inside the crystal. Types of material used as the IRE include ZnSe and Ge. The refractive index of ZnSe is 2.4 whereas for Ge it is 4. The most common IRE is ZnSe and can be used at pH 5-9 whereas, Ge is recommended for use with acids; either can be used with bases.

Factors which affect the results obtained in an ATR experiment are: the wavelength of infrared radiation; refractive index of the IRE and sample; depth of penetration; effective path length; angle of incidence and sample contact with the ATR crystal material [33]. An evanescent wave is set up which actually penetrates the crystal surface by up to 5 μm dependent on the type of crystal and angle of incident of the infrared radiation. The attenuation of the internally reflected radiation results from the penetration of the electromagnetic radiation field into the matter in contact with the reflection surface. The consequence of this is that a sample in contact with the crystal can interact with the evanescent wave, which is then attenuated by absorption by the sample, hence the name attenuated total reflectance. The penetration depth is related to the effective path length. The effective path length can be used to approximate comparisons between transmission and ATR spectra [33].

1.3 Amyloidosis.

Amyloidosis is the generic term for the classification of diverse but specific conditions in which insoluble amyloid fibrils deposit. Amyloid deposits are observed in many different diseases including chronic renal dialysis, rheumatoid arthritis, B-cell malignancies, diabetes and Alzheimer's disease [34]. The term amyloid means "cellulose or starch like" derived from the first diagnostic tests and was first developed by Virchow [35]. The term has remained in use despite the fact that cellulose is not a constituent of amyloid.

At least 15 apparently unrelated types of proteins have been described as being responsible for amyloid deposition. These deposited proteins are diverse in nature but are, nevertheless, grouped together under the term amyloid. These include primary amyloid (AL), amyloid A (AA), transthyretin (TTR), Islet amyloid polypeptide (AIAPP), β_2 microglobulin (β_2M) and Alzheimer's amyloid β protein (Aβ) [36].

Although the protein deposits are chemically heterogeneous, they share common morphology, being fibrillar in nature with a β pleated sheet conformation. They stain with specific dyes such as Congo Red, and have a characteristic red-green birefringence appearance in polarised light. Amyloid fibrils are small (<30 kDa) and are about 7-10 nm in diameter. They are insoluble under physiological conditions and resistant to normal degradative processes *in vivo* [37]. In tissues, they are always associated with plasma extracellular matrix constituents such as glycosaminoglycans and proteoglycans.

The accepted overall mechanism in amyloidogenesis is thought to involve specific protein precursors that are produced in excess quantity. The processor proteins are subjected to genetic mutations or specific amino acid substitutions or are altered by proteolytic cleavage resulting in the generation of proteins or peptide fragments [38]. These amyloidogenic proteins self aggregate into fibrils with or without trigger factors.

1.3.1 Classification of amyloid.

The various amyloids can be classified according to their clinical setting or by the type of amyloid protein present. The most common forms of amyloid are shown in **Table 1.2.**

Type	Clinical disease	Type of amyloid protein
Primary amyloidosis	Primary amyloidosis appears *de novo* and is not associated with any underlying disease [39].	Consist of variable region of light chains deposited as the primary amyloid (AL).
Secondary amyloidosis	Amyloids that appear secondary to a disorder e.g. chronic inflammatory disorders, renal cell carcinomas and Hodgkin's disease [40].	The AA amyloid protein, derived from a naturally occurring serum protein (apo SAA).
Hereditary amyloidosis	Present in dominant autosomal disease such as Familial Amyloidotic Polyneuropathy (FAP) and Familial Mediterranean Fever (FMF) [41].	Most result from a variant of transthyretin (TTR).
Isolated amyloidosis	Localised deposits of amyloid in endocrine, lung, heart and cerebral in the case of Alzheimer's disease.	e.g. Dialysis related amyloid β_2 microglobulin (β_2M) and Alzheimer β amyloid (Aβ)

Table 1.2. - Classification of amyloid according to clinical setting.

AL amyloid protein is common to most primary amyloids such as systemic amyloidosis associated with myeloma, monoclonal gammopathy, and occult dyscrasia. AL amyloidosis is a disease of ageing that is influenced by gender, two thirds of patients are male with a median age of 62 [42]. Generally, AL fragments are deposited systemically, although deposits have been found in the heart, kidney, liver, spleen and in other organs. AL amyloid fibrils are derived from monoclonal immunoglobulin light chains, usually of λ type, which are produced by an abnormal clone of plasma B cells. AL deposits can consist of light chains of either κ or λ region of the light chain or the entire light chain [40]. The presence of light chain fragments

in amyloid deposits represents clear evidence that *in situ* proteolysis is a major mechanism predisposing to fibril formation.

The AA amyloid protein is a reactive systemic amyloid associated with acquired or hereditary chronic inflammatory disease. SAA consists of 76 amino acid residues with a molecular weight of 8500 Da, which corresponds to the terminal two thirds of a naturally occurring serum protein, apo SAA [43]. The apo SAA is an acute phase protein carried by plasma high density lipoproteins (HDL) in concentrations of 1 μg ml^{-1} but which increases by 1000 fold during an inflammatory process [44 & 45]. Multiple isoforms of AA are deposited but it is SAA production and its structure that are critical factors in AA amyloidogenesis [36].

The transthyretin (TTR) was also termed pre-albumin, as it migrates ahead of albumin in electrophoresis. Transthyretin consists of a 55 kDa non-glycoslyated plasma protein consisting of four 125 amino acid subunits. TTR serves as a transporter of retinol (Vitamin A alcohol). TTR amyloidosis may involve a variety of other proteins, for example apolipoprotein, gelsolin, cystatin C, fibrinogen Aα, and lysozyme. Mutant forms of this protein cause it to deposit with a predilection for peripheral and autonomic nerves [46].

Other forms of amyloid include localised deposits of amyloid that tend to involve a single organ including the lung, heart and various joints [40]. Islet amyloid polypeptide (AIAPP) is involved in endocrine amyloid deposits in the Islet of Langerhans in type II diabetes mellitus and insulinoma [47]. β_2 microglobulin is present in patients on chronic renal dialysis as dialysis-associated amyloidosis and is seen to precipitate into amyloid fibrils in various joints and other organs [48]. In Alzheimer's disease (AD), a 4 kDa amyloid β protein (Aβ) is deposited in cerebrovascular and intra-cerebral plaques. This form of amyloidosis can be sporadic or occur in a familial form and is also seen in Down's syndrome patients [49]. The prion protein (PrP^{sc}) found in Creutzfeldt-Jakob disease and Gertsmann-Staussler-Scheinker disease deposit as amyloid plaques and the brain pathology in these diseases resembles that of AD [50].

1.3.2 Common components of amyloid deposits.

Chemical analysis of solubilised amyloid fibrils obtained from different types of amyloid deposits has shown that amyloid fibrils are formed from two main components [51]. The first has a very high molecular weight consisting of a variety of macromolecules, including extracellular matrix proteins, fibronectin and proteoglycans [52]. The second protein constituent is a distinct fibril subunit with a low molecular weight ranging from 3 to 30 kDa, and is specific to each variety of amyloidosis. Amyloid fibrils may consist of two or more filamentous subunits of 3 nm diameter, which are polymerised with each other in an anti-parallel fashion giving a β sheet conformation [36]. This conformation is common to all amyloid proteins such as immunoglobulins, TTR, β_2M and Aβ.

1.3.2.1 Amyloid P component.

Regardless of the nature of the fibril protein, the majority of the amyloids are associated with glycosaminoglycans (GAG) and a specific protein known as the serum amyloid P component (SAP) [47]. The SAP is a normal serum plasma glycoprotein synthesised by the liver and formed as 25 kDa subunits [53]. The SAP has the ability to bind to different ligands and proteoglycan (HSPG) and to the GAGs such as heparan sulphate. Although fibrils can be formed *in vitro* without SAP, it seems that SAP and heparan sulphate proteoglycans are universal constituents of amyloid deposits formed *in vivo*. Their constant association with amyloid may be essential to establish or maintain appropriate conditions for amyloid fibril formation and deposit accumulation i.e. prevent resorption of fibrils [54]. Much more has to be learned about the significance of this association in the amyloidogenic process.

1.3.2.2 Glycosaminoglycans.

The presence of sulphated glycosaminoglycans has been reported in a range of amyloidogenic diseases including systemic amyloidosis and the cerebral amyloid plaques of AD, Down's syndrome [55], and transmissible spongiform encephalopathy (TSE) [56], Creutzfeldt-Jakob disease (CJD), Gerstmann–Straussler syndrome, Kuru, and experimental hamster scrapie [57]. GAGs have now been demonstrated in at least five distinct forms of amyloid and heparan sulphate appears to be one of the most

common glycosaminoglycans present [58]. Heparan sulphate as opposed to the other GAGs, increases β sheet structure in serum amyloid. In murine SAA the HSPG gene is over expressed in early amyloidosis and GAGs are reported *in situ* before the start of amyloidosis of AA fibrils [59]. There is high binding affinity of the SAP to heparan sulphate and dermatan sulphate. This indicates that the association of SAP and amyloid may be mediated by GAGs.

Glycosaminoglycans are linear polysaccharides composed of a repeating disaccharide unit of a N acetylated galactosamine or glucosamine and a uronic acid. They are negatively charged species with at least one sugar in the repeating unit having a negatively charged carboxylate or sulphate group. Proteoglycans (PG) are proteins containing one or more covalently linked glycosaminoglycans chains. They are present on cell surfaces and in the extracellular matrix of animals. Their main function is in the formation of basement membranes [40]. Proteoglycans are extracellular matrix components and also serve as ligands or receptors for mediators of cell adhesion, migration, and proliferation [60]. These highly negatively charged molecules can directly influence either the processing of the precursor, or the protein folding. GAGs and PGs may form templates to which the fibril protein precursors attach and multiply.

1.3.2.3 Amyloid enhancing factor.

Another factor that may influence amyloid deposition is the so called amyloid enhancing factor (AEF). AEF is a non inflammatory, non amyloidogenic substance that dramatically shortens the time necessary for the experimental induction of AA amyloid deposition in mice to within 24 - 36 hrs [61]. Amyloid enhancing factor was originally described in the context of AA amyloidosis. The activity has now been isolated from at least four forms of amyloid: AA, AL, transthyretin, and Alzheimer's amyloid, all of which vary considerably in terms of the protein subunit that is responsible for each amyloid [62]. Preliminary observations indicate that AEF is a protein-carbohydrate complex containing large quantities of GAGs or PGs, primarily heparan sulphate; the concentrations of AEF increases markedly during inflammation [63]. AEF activity cannot be destroyed by either nucleases or lipases, but can be destroyed by denaturing techniques and proteolytic enzymes [63].

1.3.3 Mechanisms of amyloidosis.

The pathogenesis of amyloidosis is thought to involve two key steps: (i) the over synthesis of specific amyloid protein as a result of point mutations in the genes coding of the amyloid precursor proteins [38] and (ii) the abnormal proteolysis of the precursor proteins to form amyloidogenic peptides. The general scheme in **Figure 1.6** shows the possible events that can lead to fibril formation, various components of amyloid deposits are common to all amyloidosis. The formation of amyloidogenic peptides can self aggregate to form fibrils which then aggregate to form amyloid deposits. The aggregation can occur with or without the participation of GAGs, SAP, other co-factors or trigger factors. The characteristic feature of the deposits is a large quantity of intra- or inter- crossed β pleated sheets.

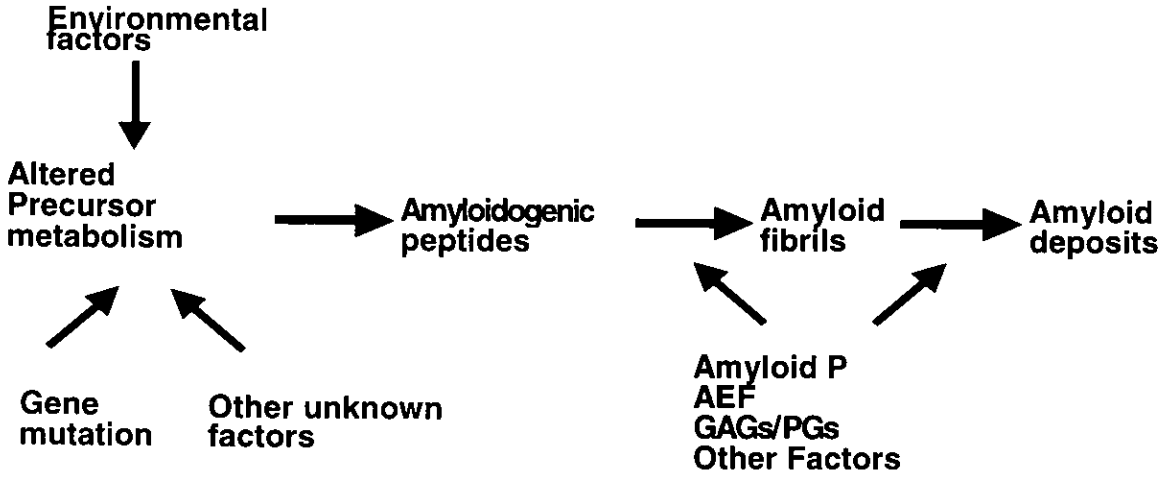

Figure 1.6 - The possible events leading to the deposition of amyloid adapted from Campistol et al. [64].

Amyloid deposition is a nucleation dependent process by which protein monomers add together to form the fibrils [65]. The fibril formation requires time because the nucleus forms via a series of association steps that are rate dependent. The lag phase is the period required for the formation of the nucleus, during which time, the protein appears to be soluble. The formation of the nucleus is thus the rate determining step. Once the nucleus has formed, further addition of monomers becomes thermodynamically favourable because monomers can add to the growing polymer at multiple sites, resulting in rapid polymerisation [66].

1.4. Alzheimer's disease.

Alzheimer's disease (AD) [67] is the fourth most common cause of death in the developed world. It accounts for over 60% of cases of dementia and its prevalence increases with age [68]. It is a degenerative condition caused by the progressive loss of brain neurones. AD is manifest with loss of memory, disorientation, impairment of intellect and changes in behaviour. Ultimately the sufferer becomes bedridden, doubly incontinent, and the deterioration leads to death [69].

1.4.1 Pathogenesis of Alzheimer's disease.

AD can be identified at post-mortem by two characteristic features; the neurofibrillary tangle (NT) and the senile plaque (SP), both of which are located in the brains of sufferers. The formation and contribution of these pathological structures in relation to the progression of the disease are largely unknown. Neurofibrillary tangles are found within affected neurones in the grey matter and surrounding the SP. They are composed of highly insoluble protein polymers, consisting of paired helical filaments (PHF). The PHF are seen to occupy most of the nerve cell cytoplasm, displacing cellular organelles [70]. The main component of the PHF is the microtubule associated protein tau, which is abnormally phosphorylated. Calcium regulated phosphorylation of tau may be involved in the formation of the PHF [71].

The senile plaques consist of roughly spherical deposits of extracellular amyloid fibrils and are 5-200 nm in diameter. They are surrounded by dystrophic neurites, microglia and astrocytes in the cerebral cortex, amygdala, hippocampus and in other brain regions [72]. The protein subunits are folded in a β pleated sheet conformation. Amino acid sequencing of the SP amyloid protein reveals a 39-42 amino acid peptide fragments, with a molecular mass of 4 kDa (Aβ), similar to cerebrovascular amyloid found in the brains of Down's syndrome sufferers [73]. The major component of the senile plaques is a 1-40 fragment, the Aβ(1-40) peptide [74]. Diffuse plaques are also seen deposited in AD. They seem to lack astrocytes and surrounding dystrophic neurites and are predominantly comprised of the Aβ(1-42) peptide [75].

1.4.1.1 Aβ protein formation.

Molecular cloning of Aβ fragment has shown it to be derived from a much larger amyloid precursor protein (APP) formed by proteolytic cleavage [76]. APP is a membrane glycoprotein that exists in various isoforms, APP-695, APP-751 and APP-770 (**Figure 1.7**). The APP-695, which lacks the Kunitz type serine protease inhibitor domain, is the most abundant in the CNS. APP has been shown to regulate cell growth and neurite length, participates in cell matrix adhesion, acts as a cell surface receptor, and is a protease inhibitor [77 & 78]. Normal proteolytic cleavage by the α secretase pathway at positions Lys16- Leu17 generates a soluble non-amyloidogenic APP ectodomain and a 10 kDa C-terminus domain that is further degraded to a 3 kDa and a 7 kDa peptide [79]. Abnormal processing by a γ secretase releases a 39-43 intact amyloidogenic Aβ fragment.

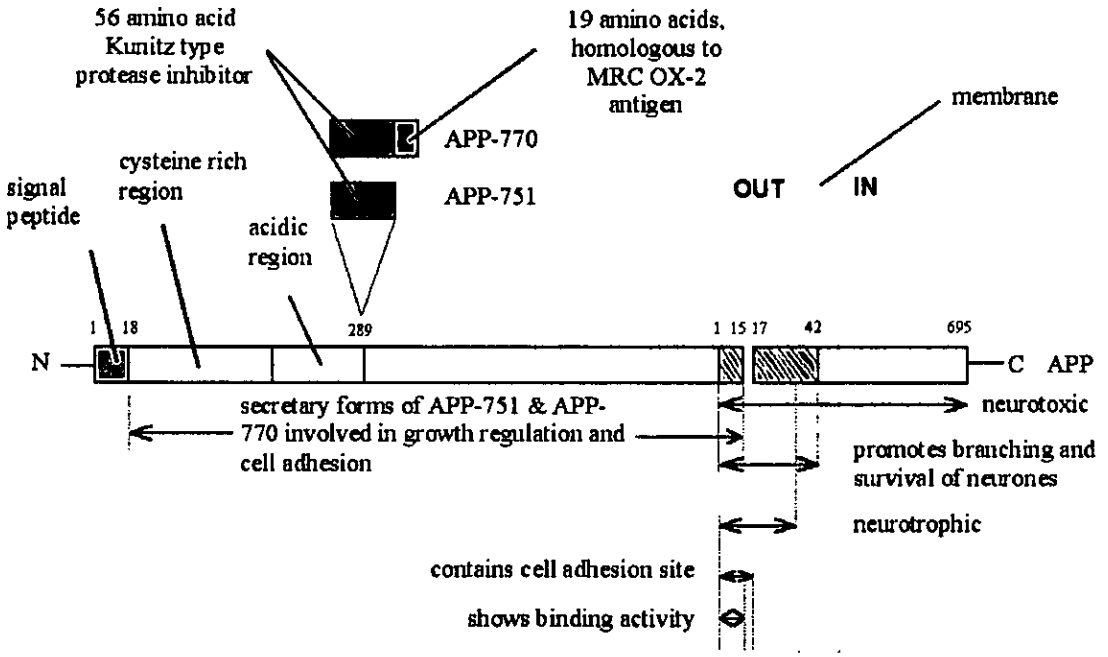

Figure 1.7 - Schematic diagram in shows the various pathways of metabolism of APP, the Aβ region is the hatched shaded area [72].

Aβ is released from many cells but its specific function has yet to be found and may be a metabolic by-product having no particular role [75]. Experiments with synthetic

fragments of Aβ indicate that the liberated peptide can spontaneously aggregate to form amyloid fibrils and this property may reside in the 25-35 region that also shows homology with tachykinin [80]. The hydrophobic C-terminus of the tachykinin neuropeptides is required for high-affinity receptor binding and biological activity; however the fragment Aβ(25-35) does not interact with tachykinin receptors. The precise mechanism of neurotoxicity is unknown, one hypothesis is that Aβ and interferon-γ (INF-γ) acts synergistically in triggering an increased release of tumour necrosis α-factor from microglia which mediates the release of reactive nitrogen species, both are involved in neuronal damage [81]. Among the possible metabolic consequences of Aβ accumulation and aggregation, altered ionic homeostasis, particularly excessive calcium entry into neurons could contribute to selective neuronal dysfunction and cell death [82 & 83].

1.4.1.2 Aβ deposition.

Aβ is found in the brains of individuals affected by AD and Down's syndrome as dense extracellular deposits of twisted β pleated sheet fibrils in the senile plaques and within cerebral blood vessels (amyloid congophilic angiopathy). The Aβ deposits are combined with other inflammatory proteins such as proteoglycans [84], amyloid P-component, and apolipoprotein E [85]. The deposition of Aβ, however, is not confined to the brain parenchyma, having been detected in amyloid deposits within the muscle, blood vessels, the kidneys, lungs, skin, subcutaneous tissue, and intestine of AD patients [86-89]. Aβ also aggregates to form diffuse amorphous deposits not only in AD but also following head injury [90] and in healthy aged individuals [91]. Cerebral Aβ deposition occurs in other aged mammals that have the human Aβ sequence [92] but is not a feature of aged rats [93].

Relatively large amounts of amorphous amyloid accumulate in healthy older brains and in Down's syndrome patients. This amyloid is presumably in a random coil form and is not associated with degeneration. Some additional event is required to transform this to the β sheet conformation [94]. The deposition of amyloid is thought to involve the seeding of a nucleus. The initial formation of a nucleus is slow and is the rate determining step and may result in a lag time in the disease [66]. Once the nucleus has been formed and the critical chain length has been reached addition of

further monomers is rapid as there are now several sites where the monomer can add to, resulting in aggregation [66 & 95]. As is the case with other amyloid proteins, Aβ originates as a normally soluble and constitutive protein found in biological fluids and tissue. According to recent *in vitro* studies the Aβ(1-40) is continuously produced and secreted as a soluble peptide during normal cellular metabolism but the peptide has not been detected intracellularly. These results suggest that Aβ is not simply an unwanted degradation product of a larger precursor molecule but may play a biological role by itself. The question then arises under which conditions an aggregation of this "normal" Aβ can be induced [96-99].

1.4.2 Aggregation is dependent on certain regions of Aβ.

Studies on Aβ peptides are diverse with respect to peptides size, region, and solvent conditions, but the initial formation of an intermediate with a high β sheet content appears to be the determining step in the Aβ self assembly. The β-amyloid protein (39- 43 amino acid residues) is the major constituent of the amyloid deposits found in the brain of patients with Alzheimer's disease (**Figure 1.8**). It has been shown that the first 28 residues constitute an extracellular domain whereas residues 29-40 anchor the peptide in the lipid membrane. The region Ile31 to met35 of the Aβ(1-40) peptide has been shown to be involved in formation of α helices in solution. The fibril formation could be accompanied by an α helix to β sheet transition in the region Ile31 to met35 [100]. Also Lys16 to Val24 and Lys28 to Val40 have been postulated on theoretical grounds [101].

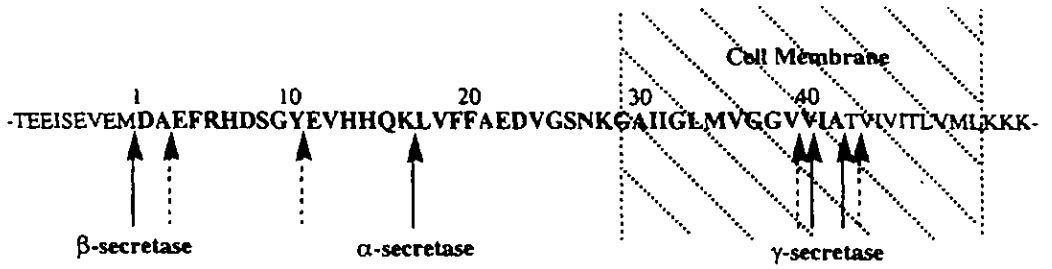

Figure 1.8 - The Aβ sequence, the shaded region is the cell membrane [102].

A number of endogenous Aβ peptides exist in AD brain tissue, the two most studied being Aβ(1-40) and Aβ(1-42), which differ by the position of their C-terminal cleavage from APP. More recently a number of Aβ variants have been identified in AD brain amyloid, including variants with modified aspartyl and glutamyl residues and shorter C-terminal forms such as the β peptide. The relationship of the relative abundance of these different peptides in brain, may be important in the development of AD neuropathology [102].

The solid state IR of the Aβ(1-28), Aβ(12-28), Aβ(14-28), Aβ(6-25), Aβ(1-38) and Aβ(1-40) peptides have all been shown to form amyloid-like fibrils *in vitro* [103-105]. Although the smaller synthetic peptide analogues of the Aβ peptide form amyloid-like fibrils *in vitro*, the solubility properties of these assemblies differ significantly from those reported from isolated brain senile plaques and cerebral vascular area [103, 104 & 106]. Based on X-ray diffraction and FTIR studies, Halverson et al. [107] proposed that the C-terminal residues of Aβ form a stable antiparallel β fibrillar core.

1.4.2.1 Main Aβ fragments: Aβ(1-40) and Aβ(1-42).

The relative formation of Aβ(1-40) and Aβ(l-42) appears to be critical to the pathology of AD. Both Aβ(1-40) and Aβ(l-42) have been widely studied to determine the influence of factors such as pH on their ability to form the β sheet structure of amyloid [108-110], the relative extent of deposition [66], and neurotoxicity [111]. Aβ(l-42) forms β sheet structure and amyloid fibrils much more readily than does Aβ(1-40) [112 - 115]. The increased polymerisation rate can be explained by increased hydrophobic interaction, first by the formation of a longer intra-molecular β sheet in the C terminus and second by the folding of this sheet over the core of the dimer [109]. The Aβ(l-42) peptide also deposits earlier than Aβ(1-40) in the disease process [116]. The aggregation behaviour of Aβ(1-40) bears a close resemblance to that observed for the fragment Aβ(25-35) [117].

1.4.2.2 Other Aβ fragments.

The synthetic Aβ peptide fragment having the same sequence as the N-terminal 28 residues, formed fibrils that share both antigenic and structural features with native Aβ amyloid filaments [103 & 104]. The β-amyloid peptide has been shown to fold into two antiparallel β-strands with a β-turn at residues 26-29 and with the nine N-terminal residues adopting a random coil configuration [118]. The Aβ(11-25) peptide is observed to possess the capability of α helix to β sheet transition [119].

It has previously been shown that amino acid residues 16-20, are essential for Aβ polymerisation. Peptides with substitutions of the 16-20 residues and peptides that bind to the Aβ(16-20) motif, prevent Aβ fibril formation [120]. Aβ(16-20) binds to the regions corresponding to 17-21 residues or/and 18-22 residues of adjacent Aβ forming antiparallel β sheet structure [120]. However, the 16-20 residues themselves are not sufficient for polymerisation, when Aβ(16-20) was incubated with full-length Aβ, only amorphous aggregates, not fibrils were formed [120]. Synthetic peptides consisting of residues 18-28 formed assemblies that showed extensive stacks of β pleated sheets. The Aβ(19-28) peptide also retains the ability to form amyloid-like fibrils with the characteristic cross-β conformation [103 & 104].

The most interesting property of Aβ(25-35) is its reversible β sheet - random coil transition at pH 4.0 and 5.5. Concentrated solutions of Aβ(25-35) contain microfibrils with β-structure which upon dilution disintegrate into random coil monomers [117]. The hydrophobic Aβ(29-42) peptide adopts exclusive intermolecular β sheet conformations in aqueous solution despite changes in temperature or pH. The Aβ(34-42) segment adopts anti-parallel β sheet structures forming filaments that are virtually insoluble in aqueous media [107]. This peptide is derived entirely from the hydrophobic transmembrane domain and the ability of this peptide to form stable β structure indicates that the C-terminal region could also be amyloidogenic [107].

1.4.4 The mechanism of Aβ amyloid deposition.

The polymerisation of the amyloid β peptide into protease resistant fibrillar deposits within the brain parenchyma and vasculature is a significant step in the pathogenesis of Alzheimer's disease [121]. The nucleation may occur, resulting from seeding of Aβ onto non amyloid peptide elements, such as GAGs and amyloid P component, present in the cellular milieu [122] or it may involve the self-assembly of Aβ(1–40) or Aβ fragments [113].

The Aβ(1-40) could be seeded by small amounts of the variants Aβ(1-42) or Aβ(1-43), which nucleate very rapidly and seed the aggregation of Aβ(1-40) (**Figure 1.9**). Aβ(1-42) and Aβ(1-43) could be produced in trace amounts by an abnormal C-terminal proteolysis [113]. This may occur in families with mutations in APP, that results in increased amounts of longer Aβ(1-42) or other stable aggregates [123 & 124]. Alternatively, the Aβ(1-40) can self aggregate with or without the presence of other components. In either case, once the slow lag phase of Aβ nucleation has occurred, a more rapid phase proceeds with the seeding of other Aβ peptides leading to fibril formation as shown in **Figure 1.9**.

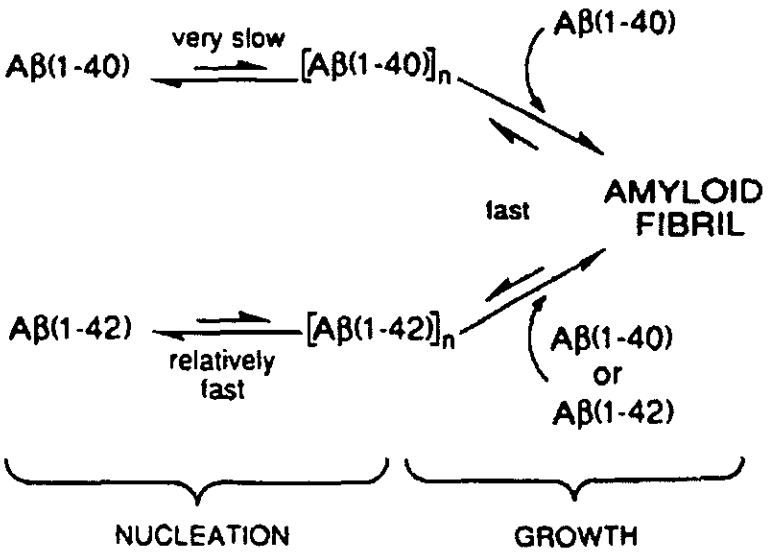

Figure 1.9 – The possible mechanism of Aβ deposition based on initial formation of nucleus and subsequent seeding [113].

The polymerisation starts with the formation of dimers, which in turn form tetramers and higher order oligomers. The existence of dimers and tetramers is supported by gel electrophoresis studies [125 - 127]. Since seeded polymerisation can be largely concentration dependent, a small increase in Aβ(1-40) could significantly increase the rate of amyloid formation it could support continued growth [128], which may explain some cases of early onset AD.

1.4.5 Risk factors for Alzheimer's disease.

Several neurobiological abnormalities have been associated with AD. These include abnormalities in cytoskeletal proteins of neurons and in the biology of the amyloid precursor protein and its proteolytic cleavage product, Aβ. The multifactorial puzzle of the disease includes a combination of age-related degenerative changes with additional genetic pre-dispositions and environmental factors, leading to increased vulnerability of the individual [68]. Genetic loci on chromosomes 14, 19, and 21 have been implicated. Mutations in the gene coding for the amyloid precursor protein on chromosome 21, may be the cause of a small number of familial cases of AD. The ε_4 allele of Apolipoprotein E (ApoE), on chromosome 19 is linked with an increased risk of both sporadic late onset and familial forms of AD [129]. A genetic determinant may increase susceptibility to amyloid deposition in late onset AD.

Recent interest in AD plaque development has focused on several proteins associated with amyloid accumulation: P component, sulphated glycosaminoglycans [55] and complement factors [130]; a-1 antichymotrypsin, apolipoprotein E. It is also suspected that there is an environmental component in the aetiology of Alzheimer's disease that could involve damage from chemical agents, which may accumulate over long periods of time [80]. Several studies have suggested a possible role of oxidative stress in the pathogenesis of AD [131].

1.4.5.1 Advanced Glycation End Products.

Advanced glycation end-products play a significant role in the evolution of vascular complications in normal ageing, especially in diabetes and renal failure [132]. Protein glycosylation first starts with the non-enzymatic spontaneous condensation of sugar aldehyde or ketone group with the free amino acid groups such as ε-NH_2 groups of lysine residues. The resulting adducts then undergo irreversible rearrangement to form cross-linked advanced glycation end products such as 3-deoxyglucosone [133 & 134]. Factors responsible for the increased cerebral AGE levels in Alzheimer's disease are not yet fully understood. An increased AGE level in plasma does not accompany the increased level of cerebral AGEs in AD patients, indicating accumulation in AD is probably a highly selective, brain specific event [135]. Increase in intracellular AGE could be due to increase of AGE reactive sugars as the consequence of a disturbed glucose metabolism, increase in unchelated copper and iron accelerating the oxidation of glycated proteins and depletion of the anti-glycation substances such as carnosine and anserine [136].

AGE related oxidative stress in AD is evidenced by chemical markers and also by the activation of the anti-oxidative defence system, and the up-regulation of heme oxygenase [137]. These AGE-mediated effects can be blocked by addition of antioxidants, such as probucol, or of antibodies to the AGE-receptor [138]. AGE modification and resulting crosslinking of protein deposits has been shown to occur in both plaques and tangles which is not unexpected since various long-lived and precipitated proteins become modified by AGEs. It has been shown that nucleation-dependent polymerisation of β amyloid is significantly accelerated by crosslinking through AGEs *in vitro* [134]. Susceptibility to AD is correlated with ε4 allele of apolipoprotein E (Apo E) and consequent substitution of cysteine by arginine creates more glycation sites and hence may facilitate the AGE-mediated crosslinking of Apo E to the insoluble deposits and hence accelerates plaque growth [139]. This suggests, that AGE represent a driving force in the acceleration of β amyloid deposition and plaque formation.

1.4.5.2 Cations as a trigger factor for the deposition of amyloid in AD.

Deficiency or excess of a number of trace elements has been reported in the tissues of patients with dementia. Some of these trace elements, both normal and abnormal levels, may be shown to have effects on cognition in experimental animals and possibly in man [140]. However, the relevance of the observed trace element imbalances, to the cognitive problems occurring in human neurodegenerative diseases, particularly Alzheimer's disease (AD), is uncertain. Aluminium has been consistently implicated as a risk factor for AD [94]. There is some evidence to show that the aluminium can be absorbed by normal individuals when present in excessive quantities. The high incidence of amytrophic lateral sclerosis in the Pacific island of Guam again shows a link between aluminium exposure and dementing disease [141]. Aluminium has been found associated with both SP and NFT in AD brains [142]. High levels of silicon have been reported to be associated with both isolated and *in situ* senile plaque rims using both chemical and X-ray microanalysis [143]. High-resolution solid-state nuclear magnetic resonance studies have detected the presence of aluminium and silicon co-localised as an aluminium silicate in the senile plaque cores [142].

Several metals Al, V, Cr, Mn, Fe, Co, Ni, Cu, Zn, Mo, Cd, Sb, and Pb have been detected in senile plaques using inductively coupled plasma mass spectrometry [144]. Zn^{2+}, Cu^{2+}, and Fe^{3+} are highly concentrated in the neocortex, regions most affected in AD. All three metal ions are significantly elevated in senile plaque deposits [145]. These metals could result from accumulation of physiological levels by AD patients over long periods of time. The presence of proteoglycans and glycosaminoglycans in the SP could also contribute to the accumulation of these metals. For instance heparan sulphate has an affinity for zinc [146-148]. Cations could act as a cofactor in several stages of SP formation. They could accelerate the proteolytic processing of APP and alter axonal transport and APP accumulation. APP contains multiple cysteine and carboxylic acid residues capable of binding metals ions in a non-specific manner. Zinc has been seen to have a binding site in the ecto domain (181-188) of APP (Kd = 764 nM) within exon 5 at the end of the cysteine rich region. [149]. APP has a high affinity copper binding site (10 nM at pH 7.5) located within residues 135-155 of the cysteine rich domain of APP 695 that is present in all APP splice isoforms [150]. It has been shown that APP can reduce copper Cu^{2+} to Cu^{+} [151].

1.5 Dialysis related amyloidosis.

Dialysis-related amyloidosis (DRA) is a serious complication of chronic dialysis therapy [152 & 153]. The protein deposited has been identified as a modified form of β2 microglobulin, levels of which are universally elevated in dialysis patients. β_2M amyloidosis is predominantly localised to osteoarticular tissues causing carpal tunnel syndrome, chronic synovitis, and progressive bone destruction [154 & 155]. Systemic deposition and visceral organ involvement have also been described. Older age at the onset of dialysis and the duration of dialysis are two important risk factors for development of this disease [156]. β_2M has clearly been identified as playing a central role as the amyloidogenic protein [157] but other factors must also be required, as the serum β_2M level is not predictive of the development of DRA.

1.5.1 Pathogenesis of β_2M amyloidosis.

The β_2M is a protein of low molecular mass, first isolated from the urine of patients with tubular proteinuria. It has about 30% homology to the immunoglobulin constant region domain [158] and is present on the surface of nucleated cells as a part of the HLA class I antigen complex and is also found in non HLA associated forms [158]. β_2M consists of 99 amino acid residues and has a molecular weight of 11.8 kDa. Its circulating pool in plasma and other body fluids is derived largely from the shedding of this protein from the surfaces of nucleated cells, where it is noncovalently associated will other molecules, notably class I histocompatibility antigens. The plasma concentration of β_2M is less than 2 mg l^{-1} and approximately 150-250 mg is cleared daily by glomerulofiltration [152]. Levels of β_2M are increased in diseases that impede glomerular filtration or re-absorption by the kidney and in chronic inflammatory diseases and malignancies, where synthesis is increased.

1.5.1.1 β_2M deposition.

In patients with chronic renal failure, β_2M is massively increased to more than 25-35 times the normal range because of the severe reduction in glomerulofiltration and levels of up to 60 times have been reported in anuric individuals due to the prolonged half life. Regardless of the serum β_2M concentration some subjects require very long periods of time to develop β_2M amyloidosis, while others do not [159]. It seems that

an increase in serum β_2M is not sufficient to induce amyloidosis but at least some degree of retention is required. It is likely that other factors could interact with the β_2M and accelerate the development of β_2M deposition [160]. The full amino acid sequence of monomeric β_2M has been identified in deposits of amyloid and has been shown to polymerise in tissue without apparent degradation. Aggregates of intact β_2M, consisting of dimers and tetramers have been isolated. The β_2M amyloid deposits are co-localised with SAP and are surrounded by macrophages. Electron microscopy shows the amyloid deposits consist of tightly packed bundles of parallel fibrils of 8–10 nm widths in a curvilinear configuration. The β_2M has a β sheet structure fibrillar configuration which may contribute to its deposition [161].

However, the genesis of DRA cannot be fully explained solely on the basis of simple precipitation of intact β_2M in body tissues. Other polypeptides, all of which originate from β_2M, have also been isolated from affected tissue samples. Two isoforms of β_2M the 5.7, 5.22 pI have been found with a single amino acid replacement Asn by Asp at the 17^{th} amino acid residue in the 5.22 pI isoform [161]. These more acidic isoforms of β_2M are modified with advanced glycation end products [162] and are suggested to be more amyloidogenic [163]. Proteolysed forms of β_2M have been found in the amyloid deposits, mainly associated with intact β_2M but complete sequence of the β_2M purified from the amyloid deposits and found to match with intact β_2M [157], indicating that proteolysis may not be necessary for amyloid formation. These results strengthen the view that DRA, although mainly consisting of β_2M, is not uniquely due to structural modifications of this protein. Rather, this condition probably has a multi-factorial pathogenesis, in which anti-proteases and other factors may play a role.

1.5.2 Aggregation is dependent on certain regions of β_2M.

β_2M has predominantly a β pleated sheet structure (>50 %) and has the basic fold of an immunoglobulin constant domain, where two antiparallel β sheets are closely packed face to face [164]. This β structure is most likely involved in the amyloidogenic properties of β_2M [165]. β_2M is a non glycosylated single chain polypeptide consisting of 99 amino acid residues with an inter-chain disulphide bridge between the half-cysteine residues in positions 25 and 80 [166]. Studies have shown

β_2M isolated from amyloid deposits to be composed of the monomer, dimer and higher polymers of intact β_2M. Two-dimensional gel electrophoresis studies have shown the presence of two or more isoforms of β_2M with pI co-ordinates (5.3-5.7) [157]. Acidic isoforms of β_2M have also been found with deaminated Asn at position 17. The presence and relevance of acidic β_2M isoforms in the pathogenesis of β_2M amyloidosis have been reported [167]. Tryptophan, tyrosine and methionine residues are also important in the protein folding of β_2M [163] and the 6 tyrosines of the β_2M are within the β sheet sandwich [168].

1.5.3 The mechanism of β_2M amyloid deposition.

Increased levels of β_2M most likely contribute to the formation of fibrils although β_2M alone is not the sole factor. It is likely that other factors could interact with the β_2M causing deposition [160 & 169]. Triggering of inflammatory processes due to stress could cause an increased production of β_2M [170]. It is also possible that the β_2M amyloid itself acts as a foreign material and thus initiate an inflammatory reaction. Deposits of β_2M are strongly associated with a heavy macrophage response [171]. A three-step molecular mechanism has been proposed by which these proteins form amyloid fibrils. The first step involves the association of two monomers to form a non-covalent dimer [172]. The second step leads to the formation of the pro-amyloid filament formed by head-to-tail interactions between dimers and polymerisation into tetramers or higher order complexes [172 & 173]. The final step results in the docking of two filaments creating a fibril assembly with enhanced stability through the multiple intra- and inter-filament interactions. As the nucleus size increases, the added monomers can interact at several interfaces on the fibril making it more thermodynamically stable. The formation of dimers, as well as aggregates, is a reversible process until the nucleation centre has formed [66].

1.5.4 Risk factors for the β_2M amyloidosis.

Several risk factors for β_2M deposition are already known, including that of age, duration of chronic renal failure, residual loss of renal function and the number of years on dialysis. Other factors such as water quality, purity of dialysate, and

membrane may have a contributory factor in β_2M clearance. Since β_2M does not seem to be the only factor influencing the occurrence of β_2M amyloidosis, a role for other proteins in amyloidogenesis has been hypothesised. In addition glycosaminoglycans, amyloid P component and apolipoprotein E have also been identified in β_2M amyloid deposits [161]. It is unknown whether these factors participate in amyloid deposit formation, its persistence, or are merely co-deposited.

1.5.4.1 Advanced Glycation End Products.

Advanced glycation end products have been demonstrated associated with the β_2M in amyloid fibrils [174]. The advanced products of the Maillard reaction, including N^{ε}-(carboxymethyl) lysine and pyrraline are present on surface of most AGE-modified proteins and may be involved in the β_2M dimer deposition [123]. β_2M amyloid fibrils are often surrounded by macrophages and it is known that AGE-modified proteins are chemotactic for monocytes, and that macrophages possess receptors for the endocytic uptake of these modified proteins [175 & 176]. Although this evidence strongly suggests that AGE modified β_2M is a major constituent of DRA [176], another possibility that needs to be ruled out is that the deposited β_2M undergoes secondary AGE modification. Circulating β_2M can also bind to AGE-modified collagen types I, II, and III present in osteoarticular tissue. The β_2M itself may be modified with AGE *in situ* to form crosslinks with the AGE-modified collagen. This complex could then trap other constituents of the β_2M amyloid deposits, such as amyloid P component, PGs and/or GAG - regulating the distribution and arrangement of these β_2M amyloid fibrils [158].

1.5.4.2 Cations as a trigger factor for β_2M deposition.

Some studies have suggested that kidney haemodialysis patients could be at risk from either moderate copper deficiency or copper toxicity [177 - 179]. There are many conflicting factors between these studies such as dietary copper intake, dialysis procedure, drug intake etc. [180]. Reduced zinc levels is common in patients with end-stage renal disease (ESRD) treated with continuous ambulatory peritoneal dialysis (CAPD). Other factors rather than zinc loss in dialysis effluents could result in redistribution of zinc from the extracellular to intracellular compartments. Decreased zinc nutritional intake, reduced absorption and hypoalbuminemia may be

factors affecting circulating levels of zinc [180]. In the past, patients with dialysis related amyloid deposition have been shown to have higher plasma and osseous levels of aluminium due to the transfer of aluminium in the dialysate during haemodialysis and through the use of oral aluminium preparations employed as phosphate binders [181]. Silicon levels were elevated in plasma and various tissues in chronic renal failure in man [182] and were found to be significantly higher both before and immediately after dialysis in the aluminium overload patients.

Calcium deposits have been found associated with β_2M in ectopic calcification of the heart [183] and in synovial amyloid deposits [184]. An association between β_2M amyloid deposition and aluminium, aluminosilicate and iron deposits has been reported in amyloid deposits in joints [185 - 187]. Recently, aluminosilicates have also been detected with secondary ion mass spectrometry [188]. These metals are thought to result in tissue damage mediated by the generation of oxygen free radicals. Another factor, which may favour β_2M amyloid deposition are the metallic particles derived from wear and tear of metal prosthesis. They may similarly act to produce tissue damage leading to leukocyte activation with associated β_2M amyloid formation and deposition. The relationship between the blood zinc, copper, and selenium concentrations and β_2M levels are widely considered as a marker of the disease progression such as with HIV [189 & 190]. Therefore changes in metal levels could be an indication of disease.

1.5.4.3 Aluminium and dialysis encephalopathy.

Dialysis patients under-going treatment for chronic renal failure were exposed to increased aluminium from dialysis fluids and from aluminium containing phosphate binders prescribed to prevent hyperphosphataemia [181]. They developed dialysis encephalopathy leading to mortality [191]. Strong positive correlations between the duration of the dialysis treatment and the index of the encephalopathy were apparent [192 & 193]. Patients with dialysis encephalopathy exhibited changes in proteins specifically characteristic of AD [194]. Thus there may be a link between aluminium and the expression or processing of the Aβ precursor protein in both dialysis encephalopathy and AD [195] in which eventually, in a complex cascade of events, leads to the extracellular deposition of the Aβ protein in senile plaques.

1.6 Other amyloids: The Prion protein and neurodegeneration.

The human prion diseases, Creutzfeldt-Jakob disease (CJD) and Gertsmann-Straussler-Scheinker disease are characterised by the slow onset of neurodegeneration [196]. Earlier terms used to describe the prion diseases include: transmissible encephalopathy and spongiform encephalopathy. Brain pathology in these diseases resembles that of AD [196] and is characterised by aggregation of a normal cellular prion protein (PrP^c) (rather than the β protein as in amyloid plaques) [50]. New variant CJD with a new specific neuropathological profile and with an early age of onset has been linked to exposure to bovine spongiform encephalopathy (BSE) infected food [197].

1.6.1 Pathogenesis of PrP amyloidosis.

Prions cause a group of human and animal neurodegenerative diseases, which are now classified together because their aetiology and pathogenesis involve modification of the prion protein. Prion diseases are manifest as infectious, genetic and sporadic disorders [196]. The diseases can be transmitted among mammals by the designated prion. Despite intensive searches over the pass three decades, no nucleic acid his been found within prions; yet, a modified isoform of the host-encoded PrP^c designated PrP^{sc} is essential for infectivity. In fact, considerable experimental data argue that prions are composed exclusively of PrP^{sc} protein [198].

While our understanding of the pathogenic role of PrP^{sc} has grown, the normal physiological function of PrP^c still remains unclear. The normal cellular PrP^c begins its metabolic cycle in the endoplasmic reticulum where the prion is anchored to the cell surface by the phospatidylinositol moiety. Possible roles of the PrP^c include a role in cell recognition, activation of lymphocytes and lymphoid cell and the control of the proliferation of astroglial cells.

1.6.1.1 Prion formation.

It has been shown that PrP^{sc} molecules do not differ from PrP^c at the level of an amino acid substitution or a post-translational chemical modification. It seems likely that it is in the secondary and tertiary structure in which the PrP^c and PrP^{sc} differ [199]. The

analysis shows that PrP^{sc} is predominantly composed of β-sheet, and β turns with a smaller amount of α-helix and minimal random-coil structure, which is consistent with its amyloid like properties [198 & 200]. Cleavage of the amino acid terminal region of PrP^{sc} also resulted in all β sheet PrP^{sc}. PrP^{c} contains ~45% α helix and little β sheets. Conversion to PrP^{sc} creates a protein, which contains 45% β sheet, little or no α helix, and 57% β turns and random coil [50, 196, 198 & 201]. However, nuclear magnetic resonance structure of the autonomously folding PrP^{c} domain comprising residues PrP^{c}(121-231) contains a two-stranded antiparallel β pleated sheet and three α helices. The presence of a β sheet in PrP^{c}(121-231) is in contrast to the model predictions of an all helical structure of PrP^{c}, which may have implications for the transition from PrP^{c} to PrP^{sc} protein [202].

1.6.1.2 Prion propagation.

Prions show virus like characteristics, with self replication and susceptibility to species barriers but is not an infectious pathogen for several reasons. Firstly, prions do not contain any nucleic acid, 'genetic coding' for the replication of the infectious PrP^{sc} agent. Secondly, the prion is a modified protein that is encoded by a cellular gene. Thirdly, the only, component of the prion is the infectious isoform of the prion protein PrP^{sc} which is pathogenically derived from cellular PrP^{c} [196]. The fundamental event in prion diseases seems to be a conversion reaction to the PrP^{sc} involving a dramatic reorganisation of secondary and tertiary structure of the PrP^{c}

The mechanism by which PrP^{c} is converted to PrP^{sc} remains unknown but PrP^{c} appears to combine with PrP^{sc} to form a PrP^{c}-PrP^{sc} complex with the former being transformed into another PrP^{sc} molecule. The two resulting molecules of PrP^{sc} combine with a further two molecules of PrP^{c} forming four molecules of PrP^{sc}. The process continues exponentially with the PrP^{sc} precipitating to form the amyloid plaques characteristic of transmissible spongiform encephalopathies (TSEs). The initial slow step is the conformational change from PrP^{c} to PrP^{sc}, which could be catalysed by the formation of a PrP^{sc}-PrP^{sc} heterodimer. Thus, the PrP^{sc} monomer would be the infectious species.

1.6.2 The mechanism of prion protein deposition.

A similar mechanism to that described in **Section 1.4.4** has been proposed for the prion diseases which involves a dramatic reorganisation of secondary and tertiary structure of the PrP^{c} to the PrP^{sc} (**Figure 1.10**) [50]. The PrP^{c} molecules appear to combine with PrP^{sc} to form a PrP^{c}-PrP^{sc} complex that initiates further transformation of PrP^{c} into another PrP^{sc} molecule. The slow step is the nucleus formation of the PrP^{sc} aggregate that then acts as a seed. Increases in cellular PrP^{c} levels could lead to sporadic prion disease. Similarly, PrP^{c} mutations that alter the PrP^{c} to PrP^{sc} equilibrium could have a major impact on the nucleation time [113].

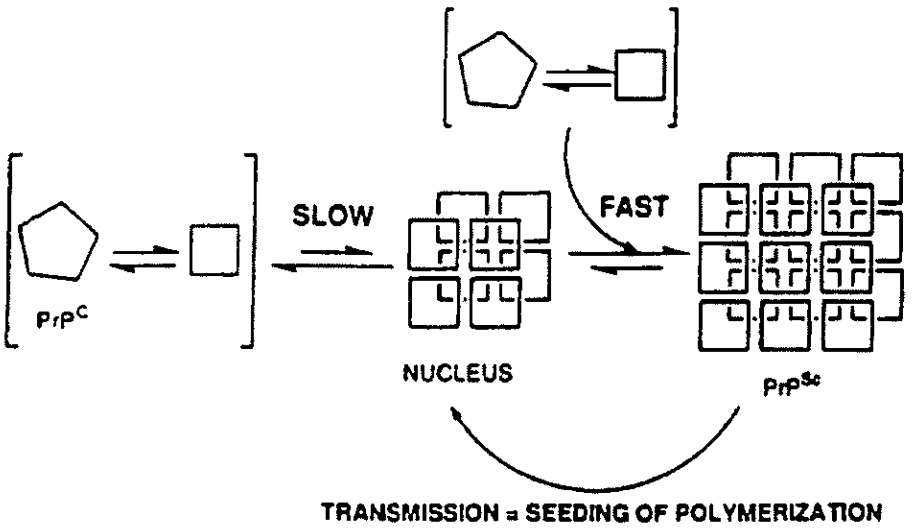

Figure 1.10 - The possible mechanism of prion propagation. The nucleus formation step is slow but subsequent seeding is fast [113].

1.6.2 Risk factors for PrP amyloidosis.

In familial CJD and Gertsmann-Straussler-Scheinker disease, it has been shown that there is a mutation in the gene coding PrP^c. The most common form of prion disease is the sporadic form of CJD and may result from spontaneous conversion of cellular PrP^c to PrP^{sc} but likely other factors are involved. Kuru is a prion disease spread amongst people in Papua New Guinea transmitted through cannibalism of human brains [203]. Thus the study of prions has shown it to be sporadic, genetic and transmissible.

In the 1980's, cattle were "exposed" to the ectoparasiticide, Phosmet, used to eradicate warble fly. The Phosmet was applied as a liquid preparation poured onto the back of the cattle. It was hypothesised that this method of application allowed the Phosmet to be absorbed into the spinal chord entering the brain after a delayed period. The Phosmet would then supposedly reach the brain causing a conformational change in cellular PrP^c to form the BSE prion PrP^{sc} that initiated the BSE epidemic [204]. However, the most likely cause was contaminated animal feed that originated from scrapie infected bone meal. Exposure to BSE infected meat as a foodstuff is considered to be the likely cause of the New variant CJD (nvCJD) [197].

1.6.2.1 Cations as a trigger factor for Prion deposition.

It has been shown using tryptophan fluorescence spectroscopy, that copper binds to recombinant Syrian hamster prion protein [SHaPrP(29-231)]. The binding sites are highly specific for Cu^{2+}, and binding of Cu^{2+} is preferable over other divalent cations; Ca^{2+}, Co^{2+}, Mg^{2+}, Mn^{2+}, Ni^{2+}, and Zn^{2+}. Copper may normally bind the PrP^c and may influence the formation of a conversion of PrP^c to PrP^{sc} or the formation of an intermediate PrP*. Binding of copper might also modify the second step of the conversion reaction where the activated PrP* is transformed into the PrP^{sc} molecule [205]. The binding of copper facilitates the thermodynamically formation of a β sheet aggregate [205]. A disturbance of copper binding in these PrP proteins might participate in the pathogenesis of prion amyloidosis.

1.7 Levels of trace elements in the human body.

The maintenance of normal health requires adequate protein, energy substrates, vitamins, and also trace elements. Trace elements in the human body are by definition present in tissues at concentrations of less than 0.01% dry mass. The essential trace elements are mostly transition elements and include Cr, Mn, Fe, Co, Cu, Zn and Mo (**Table 1.3**). In addition Se, I, and Sn are recognised as essential. Possible essential elements include Ni, F, Br, As, V, Ba, Si and Sr [206]. There are many 'non essential' elements, for which exclusively negative effects have been found so far. Potentially toxic elements include heavy metals such as Sb, Sn, Bi, Zr, and the lanthanides. The majority of the trace elements are key components of enzyme systems or proteins and are vital for their proper functions.

Element	Function	Total concentration ($mg\ kg^{-1}$)	Plasma concentration ($\mu g\ l^{-1}$)	Daily intake (mg)
Chromium	Deficiency causes glucose intolerance	<0.09	1.04	0.06
Cobalt	Component of vitamin B_{12}	0.014-0.029	0.59	0.006
Copper	Component of various enzymes	1.4	0.76-1.5 ($^{x}10^{3}$)	3.0
Fluorine	Present in bone and teeth	37-57	0.1-0.2	0.2-0.6
Iodine	Component of thyroid hormones	0.14-0.28	0.63	0.15
Iron	Component of haem pigments	57-70	0.56-1.1($^{x}10^{3}$)	10-14
Manganese	Cofactor for several enzymes	0.17-0.23	0.486	2.5-5.0
Molybdenum	Cofactor for xanthine oxidase	0.13-0.23	1.44	0.2
Nickel	Maintenance of membranes	<0.14	2.6	
Selenium	Glutathione peroxidase	0.3	100-300	0.05-0.2
Silicon	Possibly necessary in cartilage		0.39-1.09	
Zinc	Component of various enzymes	14-30	0.65-1.9($^{x}10^{3}$)	15

Table 1.3 - Trace elements and concentrations in the body [182, 207 - 213].

1.7.1 Essential trace elements.

1.7.1.1 Zinc as a trace element.

Zinc is crucial to the normal functioning of over two hundred proteins and enzymes [214 & 215] in their structural, catalytic, and regulatory roles [214]. It is essential for the activity of a number enzyme systems such as alkaline phosphatase, alcohol dehydrogenase, carbonic anhydrase, superoxide dismutase, collagenase, and leucine aminopeptidase. It is important in the binding of DNA and in enzymes involved in nucleic acid and protein synthesis. Zinc plays a role in maintaining immunological function in the zinc dependent interleukin-Iβ and tumour necrosing factor-α production in peripheral blood mononuclear cells [180].

Plasma zinc is mostly transported bound to albumin, α_2 macroglobulin and transferrin with a concentration in the blood of between 11-23 μM. Zinc is found throughout the mammalian brain, with the highest concentrations found in the neocortical and hippocampal areas of the brain [216 & 217]. Zinc concentrations are said to remain constant in the normal ageing brain [216 & 218]. The concentration of zinc in the neocortex is between 150 and 200 μM [217 & 219], three orders of magnitude greater than in the CSF (0.15 μM) [217]. The excitatory nerve terminals of the hippocampus and fascia dentata contain the highest concentrations of zinc 220-300 μM [217]. The body does not store zinc to any appreciable extent but non specific proteins such metallothionein (MT) can bind Zn^{2+} as well as Hg^{2+} and Cd^{2+}. Metallothionein is a major form of storage of zinc, and is important for cellular zinc metabolism [220]. Exogenous zinc has been shown to induce both necrotic and apoptotic death in neurons *in vivo* and *in vitro* [221 & 222].

1.7.1.2 Copper as a trace element.

Copper is essential for the activity of certain enzymes, notably cytochrome oxidase and superoxide dismutase (SOD). Copper is involved in the synthesis of several enzymes such as cytochrome oxidase, tyrosine monooxygenase, SOD and dopamine monooxygenase [223]. Copper also plays a critical role in the assimilation of iron into both microbial and mammalian cells [224]. Copper is primarily bound to ceruloplasmin (70%), albumin (18%) and transcuprein (12%) [180]. The

concentration of copper in blood is 11-24 μM. Low molecular weight amino acid complexes of copper [223] are the primary components of the exchangeable plasma copper pool responsible for the transmembrane transport of copper into the brain [225]. The brain contains the highest cellular concentrations of copper in the body besides the liver. Copper is most concentrated in the grey matter (60-110 μM) being consistently higher than in white matter (25-79 μM) [145 & 226]. These concentrations are about one order of magnitude greater than in CSF (1-8 μM).

1.7.1.3 Iron as a trace element.

Iron is important for oxygen transport and is found in haemoglobin, cytochromes, haemoproteins and catalases. Iron occurs in the blood as haemoglobin in erythrocytes and as transferrin in the plasma, in a ratio of nearly 1000 to 1. Average iron content of haemoglobin is 0.34% and functions as an oxygen carrier. Transferrin, a glycoprotein, acts as carrier for iron, where it is bound to the β_1 globulin group. Since even small quantities of free iron are toxic, the prevention of its occurrence in the plasma can be regarded as the function of transferrin. Iron deposits mostly occur in liver, spleen and bone marrow where dense hydrated ferric hydroxide form in core of ferritin [207]. Iron deficiency, particularly in pregnant women, can lead to anaemia. Iron overload, on the other hand, can cause siderosis. Copper deficiency can give rise to anaemia even if iron levels are normal as copper in ceruloplasmin is involved in the oxidation of $Fe^{2+}$to Fe^{3+} before it is taken up by transferrin.

1.7.2 Other trace elements.

1.7.2.1 Silicon as a trace element.

Silicon is generally agreed to be an essential trace element in humans. Nevertheless, its precise function is not known. It appears necessary for bone and collagen formation and growth in the chick and the rat. Silicon is also present in mitochondria in the rat liver [227]. Silicon is present in plasma mainly as silicic acid $Si(OH)_4$ and is also present as a complex anion or as a silicate polymer. The free form of silicic acid is able to penetrate biological membranes [182]. Silicon is handled via glomerular filtration during normal renal function and levels are elevated in plasma and various tissues in chronic renal dialysis. The chemistry of silicon shows it has a relatively

unique affinity for aluminium owing to the ionic size and charge and co-ordination geometry of the species involved. The two elements are accordingly commonly associated with each other in a range of minerals such as aluminosilicates [228]. This chemical inter-relationship of silicon and aluminium is of increasing interest in biology, particularly as a mechanism for the detoxification of aluminium. Research has in fact indicated that silicon may have no direct biological function other than to reduce the bioavailability of aluminium species by the formation of hydroxyaluminosilicates [211].

1.7.2.2 Aluminium as a trace element.

Aluminium, although ubiquitously distributed in the environment, has no known biological function. The reason for this may be the low solubility of Al^{3+} at around neutral pH when it is almost completely present as insoluble hydroxide, $Al(OH)_3$, or its condensation product Al_2O_3. The normal healthy individual is exposed to aluminium by inhalation of dust, skin contact and oral ingestion of foodstuffs, fluids and medicines. It is estimated that the average daily diet contains up to 5 mg of aluminium but less than 1% is absorbed [229]. Body uptake of environmental aluminium by gastro intestinal tract is complex and known to be influenced by numerous dietary factors. Dietary Zn^{2+} and Fe^{3+} intake and ligands such as citrate and maltol increases Al^{3+} uptake and accumulation in the brain [230].

Aluminium is present in blood plasma at a concentration of 10 $\mu g\ l^{-1}$ and present in all tissues at a concentration of about 2 mg kg^{-1} dry weight and appears to be cleared by the kidneys [229]. Aluminium in plasma is almost exclusively bound to transferrin (up to 95%) and the rest is bound to citrate [231]. Serum transferrin is only about 30% saturated with iron. Transferrin has a high affinity for aluminium and it is likely, Al^{3+} competes for Fe^{3+} for cellular transferrin, although $Al^{3+}$is not able to displace bound Fe^{3+} [232]. Aluminium can be taken up by various tissues including the liver, muscles, bone, brain and spleen [229].

1.7.3 Trace element levels and disease.

Distribution of trace elements in the body is tissue dependent and levels in blood are an important factor for determining disruption in trace element status. Deficiencies or excess of the trace element may have detrimental effect on the functions of enzymes [207]. Clinical and subclinical aluminium, lead and other heavy metal-induced toxic syndromes are known to occur in man [140]. Deficiency or excess of a number of trace elements has been reported in the tissues of patients with dementia. The anatomical functional integrity of the blood brain barrier is essential for heavy metal passage into brain tissue [233]. However, the relevance of the observed trace element imbalances to the cognitive problems occurring in neurodegenerative diseases, particularly Alzheimer's disease, is uncertain. The pathogenic impact of metals such as aluminium and lead might be to accelerate deposition of amyloids. The PrP^{sc}(27-30) polymeric aggregation and subsequent brain deposition [234] is similar to that reported with neurofibrillary tangles in AD patients [233 & 222].

1.7.3.1 Metal involvement and oxidative stress.

Redox-active metal ions are intimately involved in enhancing free radical generation via Haber-Weiss and Fenton reactions [235]. The Haber-Weiss reaction can form $OH^{\cdot}$ in a reaction catalysed by metal ions. The Fenton reaction, in which Fe^{2+}/Cu^{+} reacts with molecular oxygen, generates the superoxide anion ($O_2^{\cdot-}$) which undergoes dismutation either catalysed by SOD or spontaneously. The formation of H_2O_2 can generate the highly reactive hydroxyl radical ($OH^{\cdot}$). Cu^{+} catalyses this reaction at a rate constant magnitudes higher than that for Fe^{2+} [236]. The generation of free radicals and reactive oxygen species (ROS), if not scavenged, can result in lipid peroxidation, localised amino acid oxidation, and modifications to DNA [236]. Therefore metal disruption such as copper and zinc could lead to oxidative stress.

1.7.3.2 A disruption of metal levels.

Imbalances in metal status of an individual may be a contributory factor for metal toxicity. Inflammation generally induces local acidity and the mobilisation of both Zn^{2+} and Cu^{2+} [237 & 238], which are both found in high concentrations in the neocortex (~150, ~100 μM respectively) [239]. Systemic amyloidoses are often associated with chronic inflammation [240] e.g. the deposition of AA amyloid as a

consequence of inflammation [241]. Serum copper levels increase during inflammation, associated with an increase in ceruloplasmin. The release of reduced copper from ceruloplasmin is also greatly facilitated by acidic environments. Such an exchange of Cu^{2+} at low pH has been described as mediating the binding of serum amyloid P component to the cell wall polysaccharides. Brains from patients who die from AD are more acidic (pH 6.6) compared to brains from patients who die with no brain diseases (pH 7.1) [242]. Slight changes in the microenvironment of the brain may thus alter the solubility of Aβ [243]. Further disruption in elemental status occurs in conditions such as renal dialysis where clearance of metals is impaired.

Intracellular concentrations of Zn^{2+} and Cu^{2+} are approximately 1000- and 100- fold higher than extracellular concentrations, respectively [239]. This large gradient between intracellular and extracellular compartments is sustained by highly energy dependent mechanisms [244]. An energy dependent transport system has been described for the re-uptake of zinc into vesicles following synaptic transmission [219 & 217]. Therefore, alterations in energy metabolism, such as those seen in AD, trauma, or vascular compromise, may affect the compartmentalisation of these metal ions and possibly promote their pooling in the Aβ compartment.

1.7.4 Zinc in disease.

Zinc deficiency might render an individual more susceptible to oxidative injury through reduced Cu/Zn SOD function. Other zinc related disorders have been reported with subnormal plasma zinc levels in patients with arterio sclerocis, malignant tumours, chronic and acute infections and several liver diseases. The clinical manifestations include dermatitis and delayed wound healing.

1.7.4.1 Zinc levels and AD.

Studies of zinc in AD brain tissue have produced conflicting results. Studies have shown both normal serum zinc and copper levels [245 & 246], decreased serum zinc [247] and also decreased zinc concentrations in AD brain [248] particularly in the hippocampus [249] and the cortex [250]. Other groups have found no significant differences between AD patients and controls in cortical and hippocampal zinc level [216]. The highest brain zinc concentrations are found in the hippocampus, principally

in the axons of the dentate granule cells which normally synapse with the dendrites of the pyramidal cells in the hippocampus [217]. These areas are consistently affected by pathological Aβ deposition in AD [251].

Disruption in the blood brain barrier may result in an increased flow of zinc into the brain, as zinc levels in the brain are under homeostatic control. Zinc levels in the cerebral cortex, particularly hippocampus, increase from 0.15 to > 300 μM during glutamate synaptic transmission [251 & 252]. Glutamate is the major excitatory amino acid (EAA) neurotransmitter in the hippocampus and cortex. EAAs such as glutamate and aspartate have been reported to cause dissociation of zinc from metallothionein (MT) in the soluble fraction of rat hippocampus [253]. There must be some active removal mechanism as Zn^{2+} at 300 μM concentration is highly toxic [254]. Mechanisms of zinc-induced cell death have been observed in neuronal cells when exposed to concentrations of 7.5-200 μM [255] or 50-1000 μM [256]. It is likely that cellular homeostatic mechanisms that regulate zinc levels would be activated to eliminate the excess zinc. Synthesis of MTs to bind the excess ions is one such mechanism involved in stabilising levels of Zn^{2+}. During AD there is increased MT levels in the hippocampus [222]. High concentrations (0.15 to >300 μM) of zinc have been found in neurones in regions of the brain that are vulnerable in AD such as the cortex and the hippocampus during neurotransmission in the hippocampus up to 300 μM Zn^{2+} is released into the extracellular space [252 & 257]. This elevation in the concentration of zinc may be sufficient to induce aggregation of Aβ.

1.7.4.2 Zinc levels in renal dialysis.

Zinc levels have been found to be decreased in patients with end stage renal disease (ESRD) treated with continuous ambulatory peritoneal dialysis (CAPD) [177] and could result from loss of zinc in dialysis effluents. Factors other than the dialysis itself could account for the zinc disruption. The redistribution of zinc from the extracellular to intracellular fluid, decreased zinc nutritional intake, absorption, hypoalbuminemia and other factors may determine the circulating levels of zinc [180]. The normal ranges of serum zinc is 0.65–1.3 mg l^{-1} [178]. Particular attention has to be focused on other factors affecting dialysis such as variations in ambient pH, glucose concentrations, osmolality of dialysates and dwell times, and the effect of coexistent

conditions such as the uraemic milieu i.e. renal failure. Zinc depletion limits the ability of animals to achieve maximum circulating calcitriol hormone levels in response to the stress of calcium or phosphorus depletion [180]. Calcitriol levels are involved in maintaining calcium and phosphorous levels and may also modulate granulocyte and immune cell function of local tissue. Extracellular calcitriol levels are, at least in part zinc dependent, and could modulate intestinal zinc absorption, thereby perpetuating the cycle. Decreased zinc also causes an increase in interleukin-Iβ, tumour necrosing factor-α production. Zinc reduced serum levels in dialysis patients has been associated with disturbances in taste and sexual performance [179].

1.7.5 Copper in disease.

Disorders due to disruption in copper levels include acute leukaemia, Hodgkin's disease, leucopenia, haemochromatosis and myocardial infarction. Hereditary disorders such as Wilson's disease are characterised by excessive tissue deposition of copper, where as Menke's syndrome and fatal amytrophic lateral sclerosis are accompanied by changes in copper homeostasis and are characterised by severe neurodegeneration [182, 205, 207 - 213].

1.7.5.1 Copper levels and AD.

Compared to other tissues, the copper concentration in the brain has been reported to be relatively high [258 & 259]. During mild acidosis free copper is released and transferred to other proteins such exchange occurs with serum amyloid P component. Interestingly, the total copper content of different brain regions varies widely [133]. The highest values of copper are found in the locus ceruleus (1.3 mM) and in the substantia nigra (0.4 mM). More recently, it has been demonstrated that the normally high concentrations of copper in brain parenchyma (350 mM) are elevated in AD brain, reaching concentrations of 800 mM [145]. Copper is also further concentrated within the core and periphery of Aβ plaques. Copper and zinc are also significantly elevated in the serum of AD patients who carry an ε4 allele for apolipoprotein E (ApoE). Inheritance of the ε4 allele of ApoE is known to increase the risk of AD [129, 260 & 261].

1.7.5.2 Copper levels in renal dialysis.

Dialysis patients may be prone to a disruption in copper levels, although there may be many conflicting factors between these studies such as dietary copper intakes, dialysis procedures, drug intakes, and the prevalence of other health problems. One study showed that the mean serum concentration of copper in control patients and in those on dialysis are within the normal range of 0.7-1.41 mg l^{-1} [180]. Other studies have reported dialysis patients can have disrupted levels of copper and ceruloplasmin, ranging from low to high [178 & 262].

Serum ratios of copper to ceruloplasmin can be an indication of copper levels as ceruloplasmin contains nearly all of the serum copper. Using this indicator, copper levels have been shown to be moderately lower compared to the control groups [180]. Superoxide dismutase (SOD) levels as an alternative indicator can be misleading as moderate copper deficiency could result in above-normal SOD activities via a regulatory mechanism. Kidney dialysis patients on HD and CAPD, not dialysed with copper based membranes show decreased levels of copper ceruloplasmin [180]. This may indicate either increased excretion of copper in patients with renal failure or that the dialysis itself is removing copper.

1.7.6 Aluminium and silicon in disease.

Aluminium toxicity derives from its small crystal ionic radius of Al^{3+} (0.051 nm) and high positive charge, allowing it to displace magnesium in key metabolic reactions in brain cells and to interfere with their calcium utilisation [263]. The unique affinity of silicon for aluminium may play a role in biology as a mechanism for the detoxification of aluminium [211]. Aluminium is neurotoxic and has been associated with Alzheimer's disease and dialysis related encephalopathy. The neurotoxicity of aluminium is well established in experimental models [264] .

1.7.6.1 Aluminium and silicon levels in AD.

Aluminium was one of the first metal ions linked to AD. However, the influence of aluminium on the pathogenesis of AD remains controversial. Other researchers have been unable to find differences between control and AD brain [265]. Aluminium is the only metal which has been found in both plaques and neurofibrillary tangles in

brain from AD patients [266]. It has been proposed that the intracellular accumulation of Al^{3+} and also Ca^{2+} in tangle bearing neurones is secondary to a defect in brain mineral metabolism resulting from a chronic nutritional deficiency of calcium and absorption of toxic metals such as aluminium and manganese [267 & 268]. Aluminium is neurotoxic and has been associated with AD, induce neuronal cytoskeletal abnormalities *in vivo*, disordered whorls of neurofilaments, affect postsynthetis events, neurofilament subunit turnover, post-translational processing, axonal transport. Aluminium induces the accumulation of amyloid precursor protein, which gives rise to Aβ, the main substance of plaques. Aluminium induced build up of amyloid precursor protein within the axons and dendrites causes the threadlike extensions of nerve cells to thicken [269].

Aluminium loaded transferrin is able to pass through the blood brain barrier, into the cerebral cortex, hippocampus, septum and amygdala. These areas contain the highest level of transferrin receptors and are most prone to AD. The brain is calculated to take up 10 μg per annum of aluminium and is consistent with the levels found after 70 years [270-272]. Aluminium can directly bind to blood brain barrier endothelial cells and is capable of disrupting Fe^{3+} homeostasis. High level of aluminium have been found in ferritin isolated from AD brains. A feed back mechanism could stimulate over production of ferritin and lead to iron overload causing possible oxidative stress from release of Fe^{3+} [273]. The average AD brain aluminium concentrations are greater than 5.5 μg g^{-1} dry weight compared to control concentration of 4.7 μg g^{-1} [274 & 275]. Although, other studies have shown no elevations in brain aluminium concentration [276 & 277]. Amino acid-Al complexes such as D-Asp-Al and L-Glu-Al induce a larger random coil conformation in the Aβ peptide than the free Al^{3+} [278]. The acidic amino acids such as Asp and Glu are well studied excitatory neurotransmitters present in high concentrations in the central nervous system (CNS). It has been demonstrated that aluminium in the form of an L-glutamate complex was able to cross the blood-brain barrier and deposit in the brain [273].

Aluminosilicate, has been reported to be a specific feature of senile plaque core [279 & 280] and has been suggested that aluminium accumulation as aluminosilicate

complexes in SP. Using solid state NMR spectroscopy aluminium and silicon has been shown to be present in senile plaques. Selective increase by 2:3 fold of aluminium and silicon in cerebral cortex was detected by secondary ion mass spectrometry (SMS) and may be involved in an increased uptake in AD [281]. The initial event in the formation of the aluminosilicate deposits is likely to be the polymerisation of silicic acid either when its local concentration exceeds 100 μM or at much lower concentrations in the presence of aluminium [282]. If the total concentration of silicon during maturation of AD plaques (30 years) can exceed the critical polymerisation concentration >100 μM then it can precipitate with aluminium as aluminosilicates additionally it could react with numerous other protein ligands. Usually serum silicon levels are greater than aluminium levels. Levels of silicon have been found to be increased by 20 times in the CSF in AD patients, and age dependent silicon accumulation has been reported [283]. Elevated concentration of silicon could have a protective role in limiting aluminium bioavailability [279].

1.7.6.2 Aluminium and silicon levels in renal dialysis.

Both serum silicon and aluminium are elevated in renal dialysis patients compared with healthy controls [284]. In patients with chronic renal failure, aluminium accumulates through the use of oral aluminium preparations employed as phosphate binders [181] and from the transfer of aluminium in the dialysate during haemodialysis and adsorbed metals in the dialysis tubing could also be a possible source of metal contamination [285 & 94]. These patients have an increased body burden of aluminium due to impaired renal excretion and are at increased risk of accumulating the metal in their bodies. Deposition of aluminium, usually in the bone and brain, appears to be a major factor in the accumulation of aluminium in the brains of dialysis patients [229].

Al^{3+} levels in uraemic patients are greater than 100 μg l^{-1} and even up to 500 μg l^{-1} compared to the normal concentration of 47±8 μg l^{-1}. Serum Al^{3+} levels are increased in patients with bullous dermatosis recognised as a complication of chronic renal dialysis resulting in skin lesions and over photosensitivity [286]. Levels were also increased in patients treated with aluminium and calcium citrate phosphate binders, indicating an increased absorption with citrate [287]. Highest levels of aluminium are

found in those on haemodialysis with β_2M, 17.4±3.6 μg g^{-1} in synovial tissues and 20.2±6.6 μg g^{-1} in cartilage. Controls have 1.7±0.4 μg g^{-1} synovial tissue and 2.4±0.4 μg g^{-1} in cartilage [288]. The use of secondary ion mass spectrometry has shown Al^{3+} deposits in articular structures in renal dialysis. The ratio of Al:Si is 1 providing strong evidence that Al and Si are present as aluminosilicates [188].

Silicon levels are elevated in plasma and various tissues in chronic renal failure in man, and in patients on renal dialysis [284]. Serum silicon levels were found to be significantly higher both before and immediately after dialysis in the aluminium overload group. The observations indicate that silicon and aluminium show some evidence of association in serum [213]. Several studies show increased levels of serum silicon ranging from 0.52 to 2.8 mg l^{-1} [182, 213 & 279]. There is also evidence showing that an elevated concentration of silicon can limit aluminium bioavailability [289].

Dialysis patients under going treatment for chronic renal failure can develop dialysis encephalopathy leading to mortality [229]. These aluminium-induced dementias were associated with elevated aluminium in blood serum, of up to 200 μg l^{-1}, although it has been shown more recently that serum aluminium concentrations of 60 μg l^{-1} are associated with impaired cognitive function [193]. Concentration in CNS in particular the neocortex, are elevated and aluminium accumulates in lysosomes of dialysis patients. The mean aluminium concentration in the frontal cortex in the dialysis groups (6.3 μg g^{-1} dry weight) was significantly elevated compared with that in the control groups (2.5 μg g^{-1} dry weight) [194]. This encephalopathy was reversible if the aluminium burden was detected early enough, either by the dialysis regime or by the use of chelating agents such as desferrioxamine [290]. Alternative phosphate binders such as calcium compounds are now increasingly used [291]. There are profound differences in aluminium bioavailability between people with normal kidneys and people with kidney failure that display early AD like brain changes [292]. Also, the brains of about 30% of dialysis patients have plaques at ages when age matched controls do not [293]. Dynamic secondary ion mass spectrometry revealed focal accumulations of aluminium associated with cortical pyramidal neurones.

1.8 Summary.

Amyloid deposits have been associated with specific diseases such as chronic renal dialysis, prion disease and Alzheimer's disease. A change in the conformation of the amyloid proteins to a predominantly β sheet conformation results in the aggregation of amyloid proteins and their deposition. Trigger factors are required for this deposition of amyloid. A genetic determinant may increase susceptibility to the deposition of amyloid. Alternately an environmental factor may play a role and could involve damage from chemical agents, which may accumulate over long periods of time. For instance Phosmet and BSE. A disruption of the inorganic elemental status of an individual may be an important factor. Aluminium has been detected co-localised with silicon in the cores of senile plaques in Alzheimer's disease. Levels of silicon and aluminium in plasma are increased in patients on long term dialysis, who are prone to the deposition of amyloid. Glycosaminoglycans (GAGs) have been found universally in all amyloid deposits. The highly sulphated GAGs and proteoglycans (PG) may form templates to which the fibril protein precursors attach and multiply. Where these trigger factors interact in the amyloidosis pathway, and whether they act on their own or together is unknown.

1.9 Aims of study.

Aims of the present study were to:

Develop techniques to enable a trace element survey to be carried out in tissues obtained from various diseases in which amyloids are deposited and to determine if there are any imbalances in the levels of these trace elements.

Isolate and characterise amyloid materials and to determine the involvement of inorganic elements in the formation of these deposits.

Assess the manner of interaction of trace elements and amyloid materials using various methods to detect changes in secondary structure of the proteins.

Chapter 2. Materials and Methods.

2.1. Reagents.

All chemicals and reagents used were of analytical grade, unless otherwise stated. The reagents and their suppliers are listed in **Appendix A**.

2.1.1 Stock Solutions.

All solutions were prepared in distilled deionised water (17.6 MΩ cm^{-1}, Barnstead, UK) unless otherwise indicated. They were filtered through 0.45 μm Millipore filters and degassed. Those solutions asterisked (*) were not filtered or degassed.

17.5% w/v Acrylamide resolving gel: Acrylamide stock solution (17.5% w/v); Tris, (1.5 M, pH 8.8); SDS (0.1% w/v omitted for native); Ammonium persulfate (0.05% w/v); TEMED (0.25% v/v, added directly before use).

4% w/v Acrylamide stacking gel: Acrylamide stock solution (4% w/v); Tris, (1.0 M, pH 6.8); SDS (0.1% w/v)(omitted for native); Ammonium persulfate (0.05% w/v); TEMED (0.125% v/v, added directly before use).

Bradford reagent: Coomasie brilliant blue G (100 mg l^{-1}); Ethanol (0.05% w/v); Orthophosphoric acid (0.1% v/v).

Citrate buffered saline (10x): Citrate (200 mM); NaCl (5 M).

Coomasie stain: Coomasie Brilliant Blue R (0.025% w/v); Methanol (40% v/v); Acetic acid (7.0% v/v).

Destaining solution I*: Methanol (40% v/v); Acetic acid (7.0% v/v).

Destaining solution II*: Methanol (5.0% v/v); Acetic acid (7.0% v/v).

Equilibrium buffer (IEF)*: Tris (0.125 M,H 6.8); SDS (2.0% w/v); Dithiothreitol (4.9 mM); Bromophenol blue (0.02% w/v); Glycerol (10% v/v).

Electrophoresis buffer (PAGE)*: Tris (24.0 mM); SDS (0.1% w/v, omitted for native); Glycine (200 mM).

Homogenisation buffer*: SDS (1.0% w/v); PMSF (0.1 mM); tris (50 mM, pH 7.4); NaCl (150 mM).

IEF Anolyte solution*: Phosphoric acid (0.85% v/v).

IEF Catholyte solution: NaOH (20 mM).

IEF Denaturing tube gel: Acrylamide stock solution (3.3% w/v); Ampholytes (2.0% v/v); Urea (9.0 M); NP-40 (2.0% v/v); Ammonium persulfate (0.05% w/v); TEMED (0.125% v/v, added directly before use).

Kreb's Hensleit buffer: $NADP^+$ (0.4 µM); NADPH (0.4 µM); glucose-6-phosphate (8.0 µM); glucose-6-phosphate dehydrogenase (0.3 U ml^{-1}).

Lysis buffer (IEF)*: Ampholytes (2.0% v/v); Urea (9.5 M); NP-40 (2.0% v/v); Dithiothreitol (5.0% w/v).

Oxalate buffer*: Oxalic acid (50 mM); Lithium hydroxide (95 mM).

Post column reagent (transition metals)*: PAR (0.3 mM); Acetic acid (1 M); Ammonium hydroxide (3 M).

Post column reagent (aluminium)*: Tiron (30 mM), ammonium acetate (3 M made to pH 6.2 with NaOH 1 M).

Silver stain solutions*: i) Glutaraldehyde (10% v/v) ii) Dithiothreitol (5 µg l^{-1}); iii) silver nitrate (0.1% v/v), iv) Glutaraldehyde (0.0185% v/v), Sodium carbonate (3% w/v).

Sulphate buffer*: H_2SO_4 (0.01 M), $(NH_4)_2\ SO_4$ (0.2 M).

Treatment buffer (PAGE)*: Tris (0.125 M, pH 8.3); SDS (4.0% w/v, omit for native); Dithiothreitol (0.2 M); Bromophenol blue (0.02% w/v); Glycerol (20% v/v).

Tris buffered saline (10x): Tris (200 mM); NaCl (5 M).

Tris / TFE buffer*: 40% (v/v) Tris buffer (10 mM, pH 7.4), 60% (v/v) Trifluoroethanol (TFE)

2.2. Concentrations of trace metals in biological tissues.

2.2.1. Detection of trace metals in biological tissues and fluids.

All chemicals were of analytical grade and where possible all analyses were carried out in plastic-ware to reduce the risk of contamination during storage, transport and analysis. All containers and apparatus were acid washed by soaking in nitric acid (10% v/v) (BDH, UK) overnight, rinsed and then soaked in deionised water (Barnstead E-Pure, 17.6 $M\Omega\,cm^{-1}$) overnight. All calibration stock solutions were prepared daily from atomic absorption spectroscopy standards (Fisher, UK).

2.2.1.1. Sample preparation - Blood plasma.

Blood plasma samples (n=8) from renal dialysis patients were used. Samples were obtained from haemodialysis (HD) patients (n=4) and from patients on continuous ambulatory peritoneal dialysis (CAPD) (n=4). The age of the dialysis subjects ranged between 35-60 and the number of years that they had received dialysis treatment ranged between 2-25 years. These samples together with age matched control blood samples (n=4) were obtained from the Dialysis Unit, Royal Preston Hospital, Preston, UK.

The blood samples were centrifuged at 5,000 g for 10 minutes and the required plasma fractions were removed. The samples were stored in the refrigerator at 4 °C before use. The blood plasma (1 ml sample) was digested with 3 volumes of 70% v/v nitric acid (BDH, UK) in sealed pressurised 150 ml teflon bombs (CEM, UK). The samples were microwaved in an MDS 8D microwave (CEM, UK) at 70% power (Max temp 250 °C) for a total of 60 minutes in 3 x 20 minute periods. The bombs were allowed to cool for 10 minutes between each 20 minute period. After the final cooling, the digested material was diluted to a volume of 10 ml with deionised water.

2.2.1.2 Calibration of the internal standard method

The developed method used an internal standard to minimise errors due to sample loading, column variations etc. A cobalt internal standard was chosen and this was added to all of the samples. The standard addition samples were made as follows; four

1 ml aliquots of the plasma digest were spiked with copper (0, 0.2, 0.4 and 0.8 mg l^{-1}) and zinc (0, 0.2, 0.4 and 0.8 mg l^{-1}) made from atomic absorption spectroscopy standards (Fisher, UK). A 0.6 mg l^{-1} cobalt internal standard, made from an atomic absorption spectroscopy standard (Fisher, UK), was also added to each sample. The solutions were made up to 5 ml with deionised water. These samples were analysed immediately with the ion chromatography system.

2.2.1.3 Sample preparation - Human tissue.

Liver, kidney, heart and osseus joint (carpal tunnel) tissue samples were obtained at post mortem from a renal dialysis patient (n=1) diagnosed as having carpal tunnel syndrome from the Renal Unit, Royal Preston Hospital, Preston, UK. Control tissue samples of liver, kidney, heart and brain (cerebral cortex) were also obtained from the Royal Preston Hospital, Preston, UK. Alzheimer's disease brain tissue (n=4) (parieto-occipital cortex) was obtained from MRC Neurochemicalpathology Unit, Newcastle General Hospital, Newcastle, UK. All the samples were stored in sterile containers and were frozen until use.

A 5 g sample of tissue was digested in 10 ml of 70% v/v nitric acid (for the carpal tunnel tissue, 2.5 g was digested in 5 ml 70% v/v nitric acid) in 25 ml teflon beakers with loose fitting teflon lids. The samples were allowed to digest for 5 hours on a hotplate (250 °C). After complete dissolution of the tissue, the solution was evaporated for approximately 2 hours until only about 1 ml of sample was left. This was diluted to 20 ml with deionised water. Levels of copper, zinc, cobalt, and nickel and aluminium were directly measured using ion chromatography.

2.2.2 Measurement of metal levels by ion chromatography.

Ion chromatography was used to detect levels of transition metals in acid digested plasma and in acid digested tissue. Measurements were performed in triplicate on a Dionex DX500 ion chromatography system with a gradient pump connected to an Acer P100 personal computer running Hewlett Packard 'HP-ChemStation' chromatography software. The ion chromatography system also included a Dionex AS40 autosampler and postcolumn controller and reservoir (Dionex, UK). The

column used was a 25 cm HPIC-CS5 cation exchange column (Dionex, UK) with a 5 cm HPIC -CG5 guard column (Dionex, UK) with a 25 µl sample injection loop. The column packing consisted of a crosslinked styrene and vinylbenzene polymer with sulphonic functional groups. A Dionex A20 absorbance detector (Dionex, UK) in UV/VIS mode was used to detect the separated analytes. All eluents were degassed by passing helium gas through the solutions for 1 hour.

For the detection of transition metals, the eluent was 50 mM oxalic acid (BDH, UK) and 95 mM lithium hydroxide (BDH, UK) at pH 4.8 at a flow rate of 1 ml min^{-1}. The post column reagent used was 0.3 mM 4-(2-pyridylazo) resorcinol (PAR) (Dionex, UK) in 1 M acetic acid (Sigma, UK) and 3 M ammonium hydroxide (Sigma, UK) solution at a flow rate of 0.7 ml min^{-1}. The PAR metal complex was detected at 520 nm (VIS mode) using a Dionex A20 absorbance detector.

For the detection of aluminium, the eluent was 0.01 M H_2SO_4 and 0.2 M $(NH_4)_2$ SO_4 at a flow rate of 1 ml min^{-1}. The post column reagent was 3 x 10^{-4} M Tiron in 3M ammonium acetate (pH 6.2 with NaOH) solution at a flow rate of 0.7 ml min^{-1}. Detection of the tiron-aluminium complex was at 310 nm (UV mode) using a Dionex A20 absorbance detector .

2.2.2.1 Validation of the ion chromatographic technique.

The ion chromatography method for the detection of transition metals was compared to detection by inductively coupled plasma optical emission spectrometry (ICP-OES) (Analytical Model P, Spectro, UK) housed at the Sheffield Hallam University, Sheffield, UK. Copper was detected at 324.8 nm and zinc at 213.9 nm with a UV detector. The sample was introduced into the plasma at a flow rate of 1 ml min^{-1} through silicone tubing via a peristaltic pump. Five replicate measurements were made and approximately 0.5 ml of sample was required per sample. The system was flushed with deionised water between runs. The samples run on the ICP-OES contained the plasma digest spiked with copper (0, 0.2, 0.4 and 0.8 mg l^{-1}) and zinc (0, 0.2, 0.4 and 0.8 mg l^{-1}) and 0.6 mg l^{-1} cobalt internal standard.

2.3 Extraction of amyloid from Alzheimer's disease brain tissue.

A procedure of isolation based on the extreme insolubility of amyloid (Aβ) was used. The method employed was a slightly modified protocol as used by Naslund et al. [294]. Amyloid material was extracted from parieto cortex tissue from Alzheimer's disease sufferers from Norway. The brain tissue samples were obtained from the MRC Neurochemicalpathology Unit, Newcastle General Hospital, Newcastle, UK.

2.3.1 Homogenisation and centrifugation of the brain tissue.

Frozen sections of brain parieto cortex (30g of tissue) were thawed and homogenised in 5 volumes of homogenisation buffer (1% w/v SDS, 0.1 mM phenyl methyl sulphonyl fluoride, 150 mM NaCl and 50 mM tris pH 7.4). The SDS insoluble material was centrifuged for 60 minutes at 50,000 g (22 °C) in a Beckman L8 70M ultracentrifuge with a 70 Ti rotor (Beckman, UK). The pellet was re-homogenised in 5 volumes of homogenisation buffer and centrifuged as above. This step was repeated 5 times. The final pellet was washed with water and extracted with 5 volumes of 1,1,1,3,3,3 hexafluoroisopropanol (HFIP) (22 °C). The HFIP extract was filtered with glass wool to remove coarse material and dried using vacuum centrifugation in a Jouan RC10.22 Centrifugal vacuum evaporator, with an RDT 60 Vacuum unit (Jouan, UK) and Javac DD 150 high vacuum pump (Jouan, UK). The extracts were delipidated by adding 1 ml of a chloroform/methanol mixture (1:2) and centrifuged for 10 seconds at 20,000 g in a Jouan A10 centrifuge (Jouan, UK). Water (0.5 ml) was added to the supernatant and centrifuged at 20,000 g for 1 minute. Methanol (0.6 ml) was added to the aqueous upper phase and centrifuged at 20,000 g for 2 minutes. The pellet was dried under a stream of nitrogen and re-suspended in 70% v/v formic acid and centrifuged at 5,000 g for 3 minutes.

2.3.2 Size exclusion of protein extract and purification of the 4 kDa extract.

Amyloid proteins extracted from the brains of patients (n=4) with Alzheimer's disease were subjected to size exclusion chromatography to remove the 4 kDa amyloid β protein. Approximately 3-4 g of Sephadex (Sigma, UK) G75 was swelled in 40 ml of 70% v/v formic acid (Sigma, UK). The swelled Sephadex was degassed under

vacuum. Approximately 30 ml of the Sephadex was loaded onto a 1 x 50 cm glass chromatography column (Bio-Rad, UK) and allowed to settle for one hour. The column was equilibrated with 70% v/v formic acid for 3 hours. The flow rate was 100 ml min^{-1}. Collection volume of each fraction was 250 µl, equivalent to 20 drops. The total time for the running of the column was about 12 hours.

The column was calibrated with molecular weight markers (alcohol dehydrogenase, bovine serum albumin, carbonic anhydrase, cytochrome C and vitamin B_{12}, (Sigma,UK)) which have molecular weights of 150000, 66000, 29000, 12400, and 1335 Da respectively. Total protein was approximately 2 mg ml^{-1}. Dextran blue (MW 2,000,000) was also added to determine the 'dead volume'. The fractions were collected on a fraction collector. They were monitored by UV absorbance detection at 280 nm in a 1 mm quartz cuvette (sample volume 250 µl) in a Hewlett Packard (HP) diode array UV spectrometer (8452A). The system was connected to a HP Vectra QS/20 computer running the HP89531A UV/VIS operating software (Rev A.03.00, 1990). Collection was terminated when no more protein was detected.

The crude brain extract (390 mg) was subject to size exclusion using a 30 ml column of Sephadex G75 (Sigma, UK) in a 1 x 50 cm glass packing columns (Bio-Rad, UK) with a fraction collector (model 2110, Bio-Rad, UK). Alzheimer brain extract was re-suspended in 70% v/v formic acid and a small amount of dextran blue was added to determine the dead volume. The sample was applied to the column and the eluent was 70% v/v formic acid. The fractions corresponding to 4 kDa range of protein were pooled and vacuum centrifuged to dryness.

2.3.2.1 Protein quantification.

Extracted protein concentrations were quantified using the Bradford protein assay. The Bradford reagent was filtered in 0.45 µm filter (Millipore, UK) prior to use. The aliquot of the extracted protein (0.5 mg) was made up in 0.5 ml of deionised water. A range of standard proteins were prepared (1-100 µg ml^{-1}) using bovine serum albumin (BSA) (Sigma, UK). All tests were performed in duplicate. A 3 ml aliquot of the Bradford reagent was added to each solution in plastic cuvettes. After 5 minutes the absorbance of the solutions (Sarstedt, UK) was measured at 595 nm in a

spectrophotometer (Hewlett Packard, UK). A calibration curve was constructed from the BSA standards and the values of protein concentration of each extract were obtained by interpolation.

2.3.3 Immunblotting of β amyloid proteins.

The Immuno-Blot enzyme immunoassay kit (Bio-Rad, UK) was used in the detection of the amyloid Aβ (1-40) specific antigen and the procedure was followed as per kit instructions. The Immuno-Blot assay systems used a protein G - horseradish peroxidase complex that give sensitive detection of specific antigen - antibody complex. Protein can be transferred by dot-blotting, Western blotting, filter affinity transfers, and *in situ* colony or plaque lifts.

Approximately 10 μg of protein, synthetic Aβ(1-40), Aβ(1-42), Aβ(1-43), APP(125-135), the extracted amyloid and the pre-purified extracts were each solubilised in 100 μl of deionised water. The proteins were dot blotted onto a nitro-cellulose membrane. They were transferred drop wise and was allowed to dry before the next drop was added to ensure the radius of the drops were kept small. Following binding of each of the antigens, the remaining protein binding sites on the membrane surface were blocked with gelatin (3% w/v in tris buffered saline) with gentle shaking for 30 minutes. The gelatin will not react with the primary and secondary antibodies. The membrane was washed with tween tris buffered saline (TTBS) with gentle agitation for 10 minutes at room temperature. The membrane with bound antigens was then incubated overnight with the first antibody to Aβ(1-40) (Sigma, UK) at a concentration of 1:6000. The membrane was washed in tween citrate buffered saline (TCBS) to remove unbound antibody for 10 minutes. The solution was changed with fresh buffer after 5 minutes. The membrane was then incubated for 2 hours with gentle agitation with the conjugate. This was Protein G conjugated to horseradish peroxidase. The membrane was finally washed in TTBS for 5 minutes, at room temperature with agitation. This was repeated. The membrane was then exposed to the colour development reagent containing 4-chloro-l-naphtbol and hydrogen peroxidase, which yielded purple dots for the reacted antigen.

2.4 Circular dichroism spectroscopy studies of amyloid materials.

The circular dichroism spectroscopy (CD) was used to detect changes in secondary structure of proteins. The CD facility located on Station 3.1 was housed at CLRC Daresbury Laboratories, Daresbury, UK. This incorporated a 1 metre vacuum UV monochromator (Seya-Namioka) which was capable of operation between 30 and 500 nm wavelength range.

2.4.1 Calibration of the CD spectrometer.

The CD system was calibrated using (+)-10-camphorsulphonic acid (CSA) standard in water (1 mg ml^{-1} solution gave an absorbance of 0.149 in a 1 cm cell at 285 nm). The characteristic CD spectrum of camphorsulphonic acid has a positive band at 290 nm and a negative band at 192 nm. A 1 mg ml^{-1} solution in a 1 mm cell has a molecular ellipticity ($\Delta\varepsilon$) of -4.8 M^{-1} cm^{-1} at 192 nm. The value at the minimum divided by a constant gives a conversion factor for 1 mg ml^{-1} protein in a 0.1 mm cell.

2.4.2. Amyloid studies.

The buffer used in the CD studies contained 2,2,2-trifluoroethanol (TFE) and tris[hydroxymethyl]aminomethane (tris) (10 mM, pH 7.4) in a ratio of 3:2. The TFE acts as a 'secondary structure-inducing' agent. All metal stock solutions ($AlCl_3$, $CaCl_2$, $CuCl_2$, $ZnCl_2$ and $MgCl_2$) were prepared in tris/TFE buffer immediately prior to use. The silicon, as sodium metasilicate solution, was made in tris buffer and then diluted to the required concentration in tris/TFE (as the silicate precipitated in the tris/TFE at the stock concentration of 3 mM). The solutions were vortex mixed and allowed to stand at room temperature for 1 hour before analysis.

The synthetic amyloid proteins used were Aβ(1-40), Aβ(1-42) and Aβ(1-43). Other proteins used were; amyloid protein extracted from AD brains, β_2 Microglobulin and the recombinant mouse prion protein (r[mouse] PrP^c). The glycosaminoglycans used were sodium heparin, heparan sulphate (HS), dermatan sulphate (DS), chondroitin sulphate (CS), keratan sulphate (KS) and the proteoglycan used was heparan sulphate proteoglycan (HSPG) (Sigma, Poole, UK) and also sodium sulphate. The

concentrations of the various peptides, metals and glycosaminoglycans used are listed in **Tables 2.1, 2.2** and **2.3**.

Amyloid peptide	Stock solution (mg ml^{-1} (μM))	Final sample concentration (mg ml^{-1} (μM))
Aβ(1-40)	0.5 (115.5)	0.25 (57.7)
$β_2M$	0.5 (423)	0.25 (211.5)
Aβ(1-42)	0.3 (66.5)	0.15 (33.3)
Aβ(1-43)	2.0 (433.4)	1.0 (216.7)
Aβ(25-35)	0.25 (235)	0.125 (118)
Extract	1.0	0.5
PrP^c (90-231)	1.0	1.0

Table 2.1 – The concentrations of amyloid peptides used.

Sulphates and GAGs	Stock solution (mg ml^{-1} (mM))	Working solutions (μg ml^{-1})
Sodium sulphate (Na_2SO_4)	5.0 (35)	50, 500
Sodium heparin (HEP)	5.0 (0.83)	50, 500
Heparan sulphate (HS)	5.0 (0.67)	50, 500
Heparan sulphate proteoglycan (HSPG)	2.5	50, 500
Dermatan sulphate (DS)	5.0 (0.4)	50, 500
Chondroitin sulphate (CS)	5.0 (0.4)	50, 500
Keratan sulphate (KS)	5.0	50, 500

Table 2.2 – The concentrations of sulphates and glycosaminoglycans.

Inorganic element	Metal studies			GAG studies		
	Stock solution (mg l^{-1} (mM))		Working solution (μM)	Stock solution (mg l^{-1} (mM))		Working solution (μM)
Aluminium (as $AlCl_3$)	135	(5.0)	50, 150, 300, 400	4.3	(0.16)	1.6
Silicon (as Na_2SiO_3)	84.3	(3.0)	30, 300	39.3	(1.4)	14.0
Copper (as $CuCl_2$)	63.5	(1.0)	10, 50, 100	63.5	(1.0)	10.0
Zinc (as $ZnCl_2$)	65.4	(1.0)	10, 50, 100	0.65	(0.1)	10.0
Calcium (as $CaCl_2$)	40.1	(1.0)	100	0.65	(0.16)	16
Magnesium (as $MgCl_2$)	24.3	(1.0)	100	3.88	(0.16)	16

Table 2.3 – The concentrations of inorganic elements used in the metal studies.

Sample were analysed in 0.1 mm cells requiring approximately 80-100 µl of sample. Two scans were taken over 180 to 260 nm range at 0.25 nm increments with a dwell time of 3 seconds at each wavelength. The sample was kept at 37 °C using a circulating water jacketed 0.1 mm cell (Haake k20 water bath). Buffer scans were taken and the buffer spectrum was subtracted from the sample scan to give the final spectrum. The buffer scans were taken at regular intervals to correct for the changes in the synchrotronic light source output as this deteriorated with time.

2.4.2.1 Amyloid peptide treated with metals.

Aβ(1-40), Aβ(1-42), Aβ(1-43), the extracted amyloid and β_2M were treated with various metals: $CuCl_2$ (100 µM), $CaCl_2$ (100 µM), $ZnCl_2$ (100 µM). The Aβ(1-40) and β_2M were also treated with $MgCl_2$ (100 µM). The β(1-40) peptide was treated with $CuCl_2$ (10, 50 and 100 µM) and $ZnCl_2$ (10, 50 and 100 µM) and with combined $CuCl_2$ and $ZnCl_2$ (100 µM).

2.4.2.2 Amyloid peptide treated with aluminium and silicon.

Various amyloid proteins Aβ(1-40), Aβ(1-42), Aβ(1-43), Aβ(25-35), amyloid extract and β_2M in the tris/TFE buffer were treated with $AlCl_3$ (50, 150, 300 and 400 µM). The peptides Aβ(1-40) and β_2M were also treated with various combinations of $AlCl_3$ (50, 150, 300 and 400 µM) and Na_2SiO_3 (30 and 300 µM) as in shown below in **Table 2.4**.

Silicon (µM)	Aluminium (µM)				
	0	50	150	300	400
0	✓	✓	✓	✓	✓
30	✓	✓ + *	✓ + *	✓ + *	
300	✓	✓ + *	✓ + *	✓ + *	

Table 2.4 - The various combinations of aluminium and silicon. The + denotes silicon added before the aluminium, and * denotes the silicon added after the aluminium.

2.4.2.3 Amyloid peptide treated with glycosaminoglycans and metals

Synthetic amyloid peptides β_2M and Aβ(140) peptides were treated with various

sulphated glycosaminoglycans, heparan sulphate proteoglycan and sodium sulphate. Combinations of these GAGs and various metals were also investigated. Each peptide was treated with each of the glycosaminoglycans and also with sodium sulphate to investigate the sulphate group on its own. The GAGs were then added with various metals at concentrations found in serum: Al^{3+}, Ca^{2+}, SiO_4^{4-}, Cu^{2+} and Zn^{2+} (**Table 2.5**).

GAG	Al^{3+} (1.6 μM)	SiO_4^{4-} (14 μM)	Ca^{2+} (16 μM)	Cu^{2+} (10 μM)	Zn^{2+} (10 μM)
HEP			✓		
HS	✓	✓	✓	✓	✓
HSPG	✓	✓	✓	✓	✓
DS	✓	✓	✓	✓	✓
CS	✓	✓	✓		
KS	✓	✓	✓	✓	✓
Na_2SO_4			✓		

Table 2.5. - The peptides were treated with the various GAGs (500 μg ml^{-1}) combined with the metals.

2.4.3 The interaction of recombinant mouse PrP^c with the organophosphorous insecticide, Phosmet and its metabolites.

A specially designed rectangular cell was custom-made at Daresbury Laboratory. The cells consisted of a quartz cuvette (with outer dimensions of 2.5 x 4 x 2 cm) divided into two compartments separated by a semi permeable membrane (molecular weight exclusion >12 kDa) with a 0.1 mm path length. Due to the extreme toxicity of the prion protein these cells were manipulated in a Class III environment in a Class III hood (Royal Preston Hospital, Preston, UK) and were destroyed after use by incineration.

The effects of Phosmet and its metabolites on the secondary structure of recombinant mouse, r[mouse] PrP^c(90-231) was investigated by circular dichroism spectroscopy using synchrotron radiation at the CLRC facilities at Daresbury, UK. Spectra were recorded at 0.5 nm increments between 185 to 260 nm. The recombinant [mouse]PrP^c (1 mg ml^{-1}) in Kreb's Hensleit buffer and phosmet (25 mg l^{-1}) in Kreb's Hensleit

buffer were incubated in a cuvette for 2 hours before the spectrum were recorded. The spectrum was taken at 15 minute intervals for a total of 7 hours 15 minutes. The prion was treated with the metabolites of Phosmet. The metabolite generating system consisting of rat microsomes (2 mg ml^{-1}) was freshly prepared in Kreb's Hensleit buffer [295] and mixed with Phosmet (12.5 mg l^{-1}) in Kreb's Hensleit buffer. The r[mouse]PrP^c (1 mg ml^{-1}) in the Kreb's Hensleit buffer was injected into one side of the cell and the phosmet and rat microsomes in Kreb's Hensleit buffer (the metabolite generating system) was added to the reservoir.

The metabolite-generating system was studied by incubating microsomes (2 mg ml^{-1} of protein) with Phosmet (12.5 mg l^{-1}) in Kreb's-Hensleit buffer at 37°C for 30 minutes. Samples (100 µl) were taken at 15 minute intervals and extracted with hexane (500 µl). The hexane was evaporated and the residue dissolved in methanol (100 µl). Aliquots (20 µl) of the extract were analysed by high performance liquid chromatography (HPLC) with UV detection utilising a Sphereclone ODS 5 µm column (250 x. 4.6 mm; Phenomenex, Macclesfield, UK) eluted with methanol (1 ml min^{-1}) [296].

2.4.4 Manipulation of the CD data and determination of the amyloid secondary structure.

The data were analysed using 'Plotekx' (data analysis program on the Challenge L computers at CLRC, Daresbury) and Microsoft Excel (version 97). The buffer data were subtracted from the sample data and the resultant values corrected by a scaling factor obtained from calibrating the spectrometer with camphorsulphonic acid as described in **section 2.4.1**. The spectrum should tend towards zero after about 240 nm; this indicates correct buffer subtraction. The spectrum may need to be shifted by either a positive or negative constant. The SELCON program was used to determine empirically the secondary structures from the CD data by comparing with the peptide backbone (190 - 250 nm) for a set of model polypeptides [17-20].

2.5 Attenuated total reflectance Fourier transform infrared spectroscopy of amyloid materials.

Attenuated total reflectance Fourier transform infrared (ATR-FTIR) spectroscopy can be used to analyse protein structures in different forms, including surface adsorbed proteins, membrane bound proteins, turbid solutions and proteins in biological samples. Generally the α helical conformation of a protein is located around 1650 cm^{-1} and the β sheet band is around 1630 cm^{-1}. There is a weaker band associated with antiparallel β sheets around 1680 cm^{-1}. Monitoring of the changes in position and intensity of these amide I bands allows detection of conformational change within the protein.

Spectra were taken on a Mattson Galaxy series 3000, Fourier transform infrared spectrometer (Mattson, USA) connected to a Mitac PC computer running 'First' acquisition software. An attenuated total reflectance (ATR) element - model 0001-171/H133 (Spectratech, Nicolet, UK) was used with a germanium crystal in a horizontal mount for the two types of sampling (Spectratech, Nicolet, UK). This type of accessory comprises of a parallelogram prism of the internal reflectance crystal with mirrored ends. For a solid sampling attachment, the crystal is mounted flush with the top plate and the solid is clamped onto the surface by means of a fixing plate. The liquid sampling block has a well that holds the liquid sample, which was simply cleaned off when the acquisition was completed.

2.5.1 Modification of ATR attachment.

To minimise sample volume the solid sampling block was adapted for liquid sampling. An acetate cover (approximately 4 x 50 mm) was carefully placed over the pipetted sample on the germanium crystal. The liquid covered the crystal as with a cover-slip on a glass slide. This reduced the sample volume to 15 μl compared to 2 ml required in a typical liquid sampling block. (**Figure 2.1**). There was also less evaporation of the sample during measurement compared to open liquid sampling.

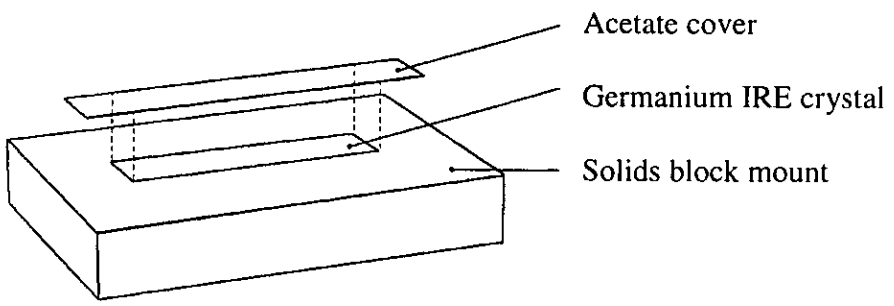

Figure 2.1 - A horizontal ATR attachment and solid sampling block with acetate cover slip (4 x 50 mm) to minimise sample volume (15 µl).

2.5.2 Measurement using ATR-FTIR.

Amyloid proteins Aβ(1-40) (57.7 µM), Aβ(1-42) (33.3 µM), Aβ(1-43) (216 µM), β amyloid extracted from human brain (0.5 mg ml^{-1}) and β_2M (211 µM) in tris buffer (10 mM, pH 7.4) were treated with $AlCl_3$ (50, 150, 300, and 400 µM), $CuCl_2$ (100 µM), $CaCl_2$ (100 µM), $ZnCl_2$ (100 µM) in tris buffer (10 mM, pH 7.4). The Aβ(1-40) and β_2M were treated with SiO_4^{4-} (300 µM), and Al^{3+} (300 µM). The Aβ(1-40) and β_2M were also treated with Ca^{2+} (100 µM) combined with heparan sulphate (500 µg ml^{-1}) or heparan sulphate proteoglycan (500 µg ml^{-1}). All the samples were left to incubate for 1 hour at room temperature before the ATR measurements.

Firstly, the crystal background was taken at 100 scans at 4 cm^{-1} resolution. Then three repeat scans of the tris buffer were taken. The crystal was wiped with tissue and three repeat scans of the sample were taken. The crystal was cleaned with detergent (10% w/v SDS), then wiped with ethanol and rinsed thoroughly with water and periodically checked for any adsorbed protein by running a blank spectrum which would show absorption bands between 1700-1600 cm^{-1} if protein was still present. The spectrum were converted to absorption spectrum and normalised using the 'First' spectral analysis program (V1.52, Mattson, USA). The tris buffer scans were subtracted from the sample spectrum.

2.6 Polyacrylamide gel electrophoresis of β_2M and Aβ(1-40).

Analysis of the amyloid proteins was carried out by polyacrylamide gel electrophoresis (PAGE) using a Hoefer SE600 water cooled dual unit gel electrophoresis kit (Hoefer, UK) with PS500XT power supply (Hoefer, UK). The gels were run either natively (which allows the separation by charge) and/or run as denatured proteins (which separates according to the size of the protein). The two dimensional analysis was carried out in a SE 6035, 1.5 mm tube gel adapter kit used with the above Hoefer SE600 gel electrophoresis equipment (Hoefer, UK).

Gels were cast according to the manufacturers instructions for the Hoefer SE 600 series gel electrophoresis unit. Solutions of 4% w/v and 17.5% w/v acrylamide, pH 6.8 and 8.8 respectively, were prepared from 30% w/v acrylamide, 0.8% w/v bisacrylamide stock solutions (Sigma, UK). Two clean glass plates of dimensions 16 x 18 x 0.03 cm (Hoefer, UK) were wiped with 70% v/v ethanol and allowed to dry. The plates were assembled with 1.0 mm spacers and clamped together and screwed onto the casting base to form a vertical slab gel unit. The 17.5% w/v acrylamide solution was syringed into the cavity up to 1 cm below the comb level (the acrylamide was initiated by adding TEMED immediately before filling). An overlay of water saturated iso-butanol was added and the gel allowed to set for 1 hour at room temperature. The overlay prevents the top edge of the resolving gel from polymerising so that the stacking gel can adhere to the main gel. Once the resolving gel had set the iso-butanol was thoroughly washed out with deionised water. A comb with 15 teeth (0.4 cm diameter) was inserted and the 4% w/v acrylamide solution was added making sure no air bubbles were trapped under the comb teeth. This was allowed to set at room temperature (about 30 minutes). The comb was then carefully removed and the wells washed with PAGE running buffer.

Synthetic amyloid proteins used were Aβ(1-43) (87 μM), Aβ(1-42) (44.4 μM), Aβ(1-40) (92 μM) and β_2M (170 μM) in tris buffer (10 mM, pH 7.4). All the metals and GAGs were made to twice the required concentration in tris buffer (10 mM, pH 7.4). The samples were then prepared by combining the solutions in equal amounts and were left to incubate at room temperature for 1 hour.

The amyloid peptides were treated with various metals; $AlCl_3$ (1 mM), $CuCl_2$ (1 mM), $ZnCl_2$ (1 mM), $CaCl_2$ (1 mM) and $MgCl_2$ (1 mM) and SDS PAGE gels run. The Aβ(1-40) and the β_2M peptides were also treated with increasing concentrations of aluminium (25, 50, 150, 300 and 400 μM). These samples were run both natively and under denaturing conditions. SDS PAGE gels were run of Aβ(1-40) and β_2M peptides treated with glycosaminoglycans (Heparan sulphate, heparan sulphate proteoglycan, dermatan sulphate and heparin Na_2SO_4 (all at a concentration of 500 μg ml^{-1})) and also with Na_2SO_4 (500 μg ml^{-1}). SDS PAGE of these GAGs also combined with various metals; Ca^{2+} (100 μM), Cu^{2+} (100 μM), Al^{3+} (300 μM), SiO_4^{4-} (300 μM) and Al^{3+} (300 μM) combined with SiO_4^{4-} (300 μM) were also run.

A mixture containing 10 μl of the protein sample and 10 μl of the treatment buffer were denatured by boiling the samples for 5 minutes at 95°C in a heat block. For SDS-PAGE the treatment buffer contained SDS and for native PAGE the SDS was omitted. The samples were loaded into the wells and 5 μl of low range molecular weight markers (1,060-26,600 kDa) (Sigma, UK) was also loaded. The gels were run in electrophoresis buffer (0.025 M tris, 0.192 M glycine) at 10 mA, 120 V for 1-2 hours (PS500XT, Hoefer, UK).

2.6.2 Isoelectric focusing of amyloid materials.

In two dimensional gel electrophoresis the first dimension gel is the isoelectric focused (IEF) gel. This first dimension separates the proteins according to their pI. The second dimension will separate the proteins according to their size as above. The 1.5 mm diameter glass tubes were cleaned and the ends capped by twisting Parafilm over the end three times. The tubes were assembled upright in the rack and held in a vertical position. The 3.3% w/v acrylamide solution containing ampholytes (3.5-10 pH) and urea was first degassed thoroughly and again initiated with ammonium persulfate and TEMED before casting. The solution was carefully syringed into the tubes, making sure no air bubbles were trapped in the gel and leaving about a 2 cm gap at the top. The ends were sealed with Parafilm and the gels were allowed to polymerise at room temperature for about 2 hours.

The β_2M peptide (85 μM) was treated with aluminium (300 μM) and allowed to incubate at room temperature for 1 hour. The sample was mixed with the IEF treatment buffer loaded on to the tubes and focused with the anolyte solution as a 10 mM phosphoric acid and the catholyte solution of 10 mM sodium hydroxide for up to 16 hours (PS500XT, Hoefer, UK). The tube gel was carefully removed from the glass tube by inserting a syringe over the end and expelling equilibration buffer until the gel slides out of the tube. The gel was equilibrated in a buffer containing dithiothreitol and SDS for 10 minutes. The tube gels were laid on top of the second dimension gel and sealed in place with a 1% w/v agarose melted in the electrophoresis buffer before being run as an SDS PAGE, as above.

2.6.3 Gel Staining.

Gels were stained with either coomasie blue or silver stain, following standard procedures. For coomasie blue stain, the gel was placed in a tray with coomasie blue and gently shaken for about 2 hours and preferably overnight. The gel was then destained in destain I solution overnight, then in destain II, again overnight. The silver stain method is highly sensitive but may also produce a higher background colour. Briefly, the gel was first stained with coomasie blue and destained as above. The gel was rinsed in destain II and then fixed in 10% v/v glutaraldehyde solution for 30 minutes. The gel was washed in deionised water for 2 hours with several changes or soaked overnight. Again it was rinsed in deionised water and placed in 200 ml of 5 μg ml^{-1} DTT in deionised water for 30 minutes. The solution was discarded and without rinsing, 100 ml of 0.1% w/v silver nitrate solution added and the gel shaken gently for 30 minutes. The silver nitrate was decanted and the gel washed twice with the developing solution and then left to develop in 100 ml of developer. Bands appear after about 30 minutes. The development was stopped by decanting the solution and addition of 100 ml of destain II.

Chapter 3. The determination of the levels of trace elements in biological fluids and tissues.

3.1 Introduction.

Levels of many trace elements are disturbed in various diseases for instance abnormal levels of copper and zinc have been found in patients on renal dialysis [284 & 288]. The disruption of trace element status, particularly the effects due to their accumulation, depletion or deficiency may have a detrimental effect on the functions of many enzymes [207]. Deficiency or excess of a number of trace elements has been reported in patients with dementias such as Alzheimer's disease [142] and clinical and subclinical aluminium, lead and other heavy metal induced toxic syndromes are known to occur in man [140].

Determination of a disruption in the levels of trace elements in an individual may indicate whether or not these elements play a role in the development of the disease. The detection of trace elements in blood is an important factor for determining any disruption in trace element status of the body. The method used to determine elemental levels needs to be sensitive enough to detect the concentration present in blood (< 1 mg l^{-1}) and in an all too often limited sample volume [262]. Analysis of trace elements in biological samples requires; precise and accurate separation of the analyte from the bulk matrix and a suitable means of detection, which is of the appropriate sensitivity. Careful consideration of factors such as diet and disease state are critical in the assessment of the results before any conclusions can be made about cause-effect relationships for the disruption of metal status [262].

Atomic absorption spectrometry (AAS) is widely used for the detection of many elements. Electrothermal atomic absorption spectrometry (ETAAS) is suitable for the detection of metals in biological tissues [297]. Detection limits for ETAAS are typically 0.3 μg l^{-1} and 0.1 μg l^{-1} for Cu and Zn respectively. However, for most of the AAS techniques, only one element can be determined at a time in many routine laboratories, although the relatively new Perkin Elmer method of simultaneous multi-element ETAAS (SIMAA) is able to detect up to 6 elements with the same detection limits as conventional ETAAS analysis due to the very low noise of the solid-state

detector [298]. Inductively coupled plasma optical emission spectrometry (ICP-OES) can be used in the direct analysis of biological fluids. The main advantage is the simultaneous detection of several elements in the one sample. The sample is efficiently desolvated, vaporised, excited and ionised in the plasma. Many chemical interferences are greatly reduced by the high temperature of 7000-8000 K. Typical levels of detection range from 0.5-100 mg l^{-1} for most metals [299].

Ion chromatography (IC) has gained wide acceptance over the last twenty years [178]. Advances in column technology and detection schemes have led to ion chromatography applications in a wide variety of matrices. One of the most important applications of IC in clinical chemistry is the analysis of physiological fluids and tissues both for inorganic and organic anions and cations. The analysis of physiological fluids requires a highly sensitive and selective analytical technique, since the matrix is complex and the concentrations of the ions of interest are often very low. While high-performance liquid chromatography has become an important technique for the determination of biological markers for the diagnosis of diseases, IC is being widely used for the analysis of ionic species.

3.1.1 The present study.

The current study involved the development of an IC method for the detection of the levels of trace metals from biological plasma and in various tissues in various disease states where amyloid is seen to deposit. A modified ion chromatographic method was used to detect levels of copper and zinc in blood plasma samples from patients on haemodialysis (HD) and continuous ambulatory peritoneal dialysis (CAPD). Standard methods were employed to detect copper, zinc, cobalt, nickel and aluminium in liver, heart, brain, kidney and carpal tunnel tissue [300].

3.1.2 Method.

Details of experimental method, instrumentation, and reagents are listed in **chapter 2 section 2.2.**

3.2 Results and discussion.

3.2.1 Determination of the levels copper and zinc in blood plasma.

The method of standard additions was used to detect copper and zinc. Copper, cobalt and zinc were easily resolved by ion chromatography with elution times of 2.9, 4.8 and 6.6 minutes respectively as shown in **Figure 3.1**. An unknown matrix component may account for the presence of the unidentified large peak. The reproducibility and the precision of the standard additions method was further improved by combining this with an internal standard. For this method to be reliable, the chosen internal standard must be well separated from the components but must appear close to the peaks of interest. The cobalt internal standard was subjected to the same conditions as the sample hence any fluctuations in the running conditions would be eliminated by plotting the absorbance ratio between copper and cobalt against the concentration of spiked copper. This was also applied to the analysis of zinc.

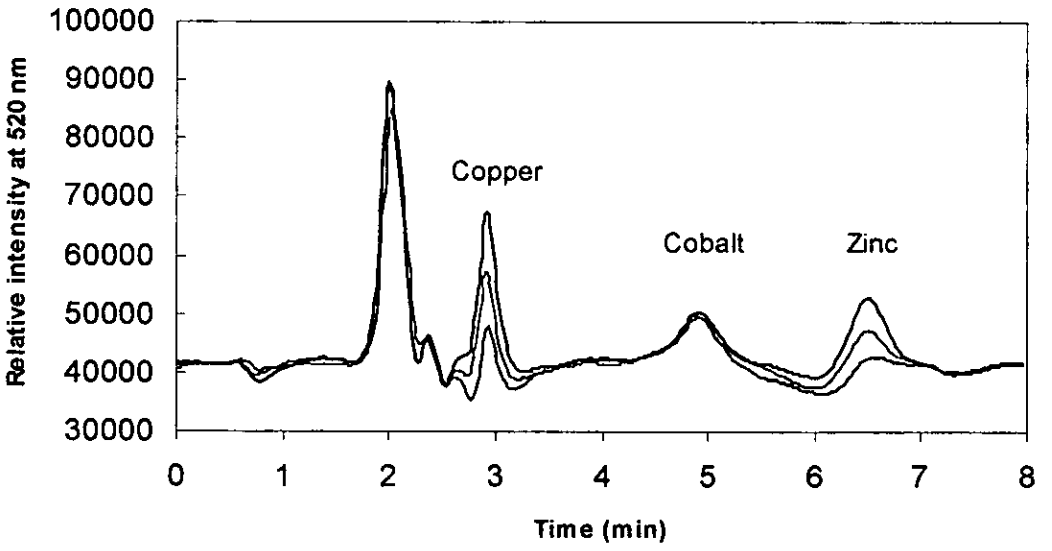

Figure 3.1 - Chromatograms of spiked blood plasma. Each of the samples was spiked with increasing concentrations of copper and zinc (0, 0.4, 0.8 mg l-1) and with cobalt (0.6 mg l-1). Copper, cobalt and zinc eluted at 2.9, 4.8 and 6.6 minutes respectively.

Cobalt can be used as an internal standard as it is found in serum at levels (< 0.05 $\mu g\ l^{-1}$) [207] well below the detection limit of IC with VIS. The detection limit for IC was calculated as 3 times the baseline signal to noise ratio. The signal to noise ratio was calculated as the standard deviation of a 0.05 mg l^{-1} sample of the analyte. The detection limits were calculated as 0.09 mg l^{-1} for copper and 0.03 mg l^{-1} for zinc.

Sample and Method		Copper (mg l^{-1})		Zinc (mg l^{-1})	
		Average	Range	Average	Range
IC-VIS	control (n=4)	0.501 ± 0.05	0.45 - 0.67	1.350 ± 0.05	0.73 - 1.83
	CAPD (n=4)	0.549 ± 0.05	0.33 - 0.68	1.576 ± 0.06	0.89 - 1.95
	HD (n=4)	0.594 ± 0.05	0.46 - 0.78	1.348 ± 0.06	0.98 - 1.79
ICP-OES	control (n=4)	0.534± 0.03	0.31 - 0.62	1.417 ± 0.02	0.79 - 1.95
	CAPD (n=4)	0.597 ± 0.02	0.51 - 0.70	1.789 ± 0.03	0.91 - 2.28
	HD (n=4)	0.575 ± 0.02	0.43 - 0.73	1.481 ± 0.02	0.93 - 2.02

Table 3.1 - Concentrations of copper and zinc in acid digested blood plasma as detected by IC with VIS detection using the standard additions method with a cobalt internal standard.

The levels of copper and zinc in CAPD patients, HD patients and controls are shown in **Tables 3.1** and **Table 3.2**. It must be stressed that these individual values represent the levels of copper and zinc in different patients and thus the concentrations of copper and zinc may vary from patient to patient due to factors such as sex, age, and time on dialysis. The normal range for copper in serum is 0.8 – 1.5 mg l^{-1} and for zinc it is 0.6 – 1.3 mg l^{-1} [178]. Overall, the average control copper levels were less than the normal levels expected in the blood. The measured copper concentration for this study was 0.501 ± 0.05 mg l^{-1} and was 1.350 ± 0.05 mg l^{-1} for zinc in the control samples.

The combination of the standard additions method and the use of an internal standard improved the precision of the measurements. This produced an overall improvement in the correlation coefficients of the standard addition plots for copper of 2.98 ± 1.89 % (in the range –0.3 % and 6 %) and zinc 2.92 ± 2.07 % (in the range –0.8 % and 5.7 %) as detailed in **Table 3.2**. The results obtained from the IC-VIS analysis were compared with the results with those obtained by inductively coupled plasma optical

emission spectrometry (ICP-OES). The copper and zinc levels in blood plasma in both dialysis groups were not significantly different to the copper and zinc levels in blood plasma of the control patients. A student t-test (at 95 % confidence limit) revealed no significant differences between the values obtained by the two methods (**Table 3.3**). There was reasonable agreement between both methods, although more samples would indicate if a better correlation were possible. The correlation coefficient for copper was 0.88 and the correlation coefficient for zinc was 0.89 for the two methods.

	Copper			Zinc		
	R^2 With IS	R^2 No IS	% Improvement	R^2 With IS	R^2 No IS	% Improvement
CAPD	0.97	0.92	6.05	0.94	0.95	-0.83
	0.95	0.92	3.35	0.95	0.91	4.64
	0.99	0.94	4.76	0.98	0.95	2.70
	0.99	0.95	3.75	0.98	0.92	5.64
HD	0.94	0.92	2.14	0.95	0.95	0.93
	0.95	0.94	0.82	0.93	0.93	0.43
	0.98	0.95	2.61	0.94	0.90	4.78
	0.98	0.93	5.23	0.95	0.92	3.05
Control	0.95	0.93	2.41	0.98	0.94	3.33
	0.93	0.92	1.18	0.98	0.95	2.25
	0.94	0.95	-0.33	0.95	0.93	2.31
	0.95	0.91	3.89	0.99	0.93	5.77
Average			2.98 ± 1.89			2.92 ± 2.07

Table 3.2 - The percentage improvement in the correlation (R^2) of standard additions of copper with and without an internal standard (IS) and zinc with and without an internal standard. (CAPD – continuous ambulatory peritoneal dialysis, HD – haemodialysis)

Methods and sample comparison	Copper (mg l^{-1})		Zinc (mg l^{-1})	
	t_{calc}	t_{crit}	t_{calc}	t_{crit}
IC-VIS / ICP-OES (n = 12)	0.189	1.717	0.265	1.717
IC- CAPD / control (n = 4)	0.448	1.938	0.747	1.943
IC- HD /control (n = 4)	0.938	1.938	0.007	1.943
IC- CAPD / HD (n = 4)	0.427	1.943	0.747	1.943

Table 3.3 - One tailed t-test for unequal variances was used to compare between the means of the dialysis group with the control groups and between the two methods ($p<0.05$). A total of 12 test samples were used in the comparison.

The Altmann-Bland plot, i.e. the plot of the differences between the two methods against the mean of the concentration, shows an overall positive bias for zinc of 0.128 mg l^{-1}. The positive bias for copper can be accounted for from experimental errors. This suggests that the results for zinc obtained from the ICP-OES method are higher than those obtained with IC-VIS analysis. This could result from interference from other elements within the plasma in the ICP-OES method.

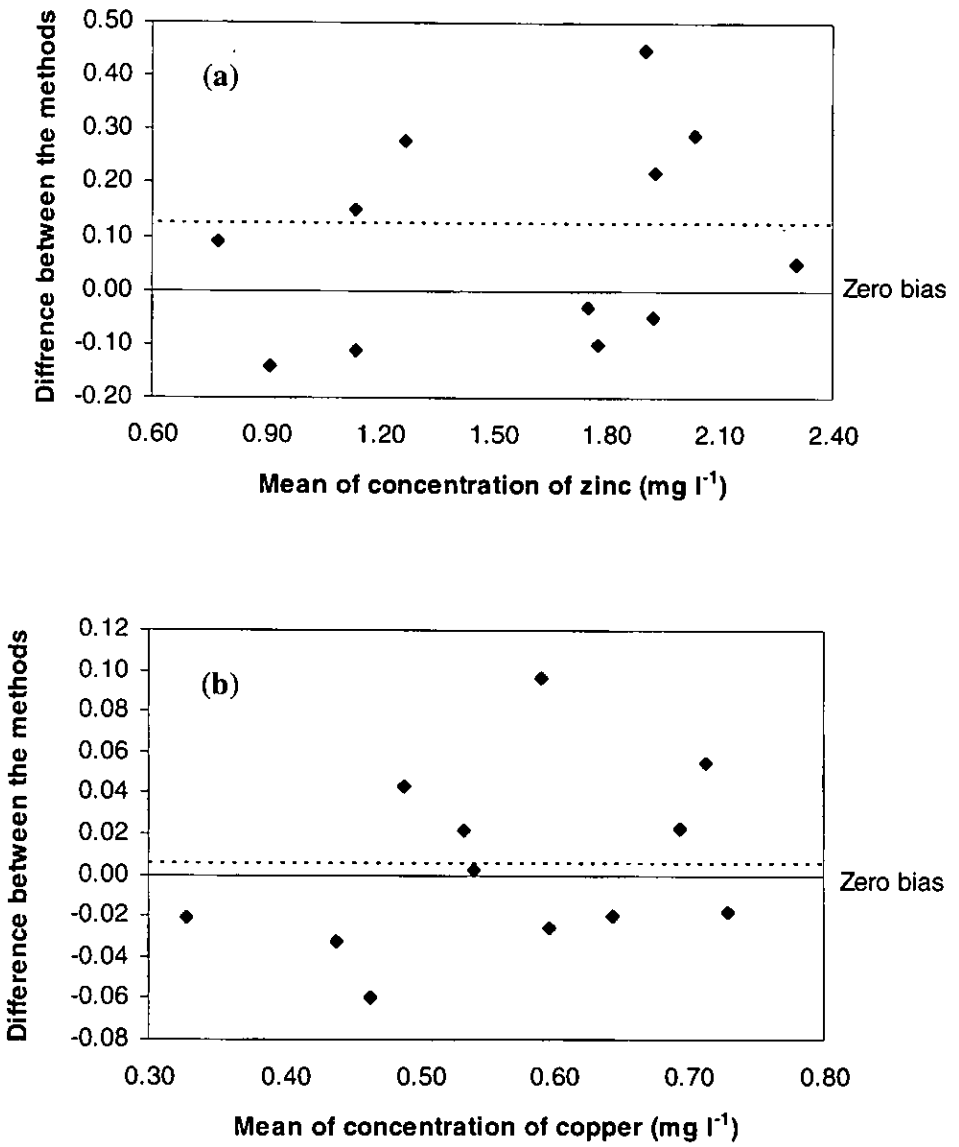

Figure 3.2 - The Altmann-Bland plots compare the two methods, IC-VIS and ICP-OES for copper (**a**) and zinc (**b**) The plots show a small positive bias for copper and larger bias for zinc indicating that the results obtained for zinc with ICP-OES are higher than those obtained using IC-VIS. The dotted lines show the mean difference between the two methods and the zero bias denotes no differences between the two methods.

3.2.2 Determination of the levels of copper, zinc, cobalt, nickel and aluminium in biological tissues.

The direct analysis of the acid digested tissues showed little matrix effect with the peaks being resolved easily. Copper, cobalt, zinc and nickel eluted at 2.9, 4.8, 6.6, 8.2 minutes respectively using an oxalate eluent and PAR post column reagent as shown in **Figure 3.3a**. The aluminium eluted at 6.1 minutes using an ammonium sulphate and tiron post column reagent as shown in **Figure 3.3b**. The concentrations of copper, zinc, nickel, cobalt and aluminium in acid digested tissues as detected by ion chromatography with UV/VIS detection are shown in **Table 3.4**.

Tissue sample	Concentration of analyte in the sample (mg l^{-1})				
	Al^{3+}	Cu^{2+}	Zn^{2+}	Co^{2+}	Ni^{2+}
Brain (n=4)	0.0294 ± 0.04	0.461 ± 0.04	0.392 ± 0.04	0.214 ± 0.05	0.062 ± 0.04
Heart (n=1)	0.0221 ± 0.04	0.107 ± 0.05	0.034 ± 0.03	0.615 ± 0.05	0.057 ± 0.04
Liver (n=1)	0.0120 ± 0.03	0.063 ± 0.04	0.095 ± 0.04	2.936 ± 0.06	0.040 ± 0.05
Kidney (n=1)	0.0179 ± 0.04	0.033 ± 0.03	0.027 ± 0.04	0.759 ± 0.04	0.029 ± 0.04
CT (n=1)	0.0155 ± 0.05	0.134 ± 0.04	0.037 ± 0.05	0.371 ± 0.06	0.021 ± 0.05
Brain (Control n=1)	0.0261 ± 0.04	0.642 ± 0.04	0.122 ± 0.04	0.930 ± 0.04	0.054 ± 0.04
Heart (Control n=1)	0.0124 ± 0.04	0.133 ± 0.04	0.055 ± 0.04	0.230 ± 0.03	0.033 ± 0.03
Liver (Control n=1)	0.0139 ± 0.03	0.051 ± 0.04	0.122 ± 0.03	1.041 ± 0.04	0.037 ± 0.04
Kidney (Control n=1)	0.0110 ± 0.04	0.055 ± 0.04	0.051 ± 0.04	0.625 ± 0.04	0.043 ± 0.04

Table 3.4 - Concentrations of copper, zinc, nickel, cobalt and aluminium in acid digested tissues as detected by ion chromatography with UV/VIS detection the standard deviations quoted relate to the replicate analysis.

Only one sample was measured for each tissue (except the AD brain) due to the small number of samples available. Inter-patient variations could account for the differences between the samples and controls. It should be noted that the high level of cobalt found in the tissue samples is most likely due to vitamin B_{12} (cobalamin). Vitamin B_{12}

is present in most organs and particularly high levels are found both in the liver and in the kidney. Therefore cobalt cannot be used as an internal standard for the detection of transition metals in tissues. A suitable internal standard should not be present in tissues and it should also be detectable by the current method.

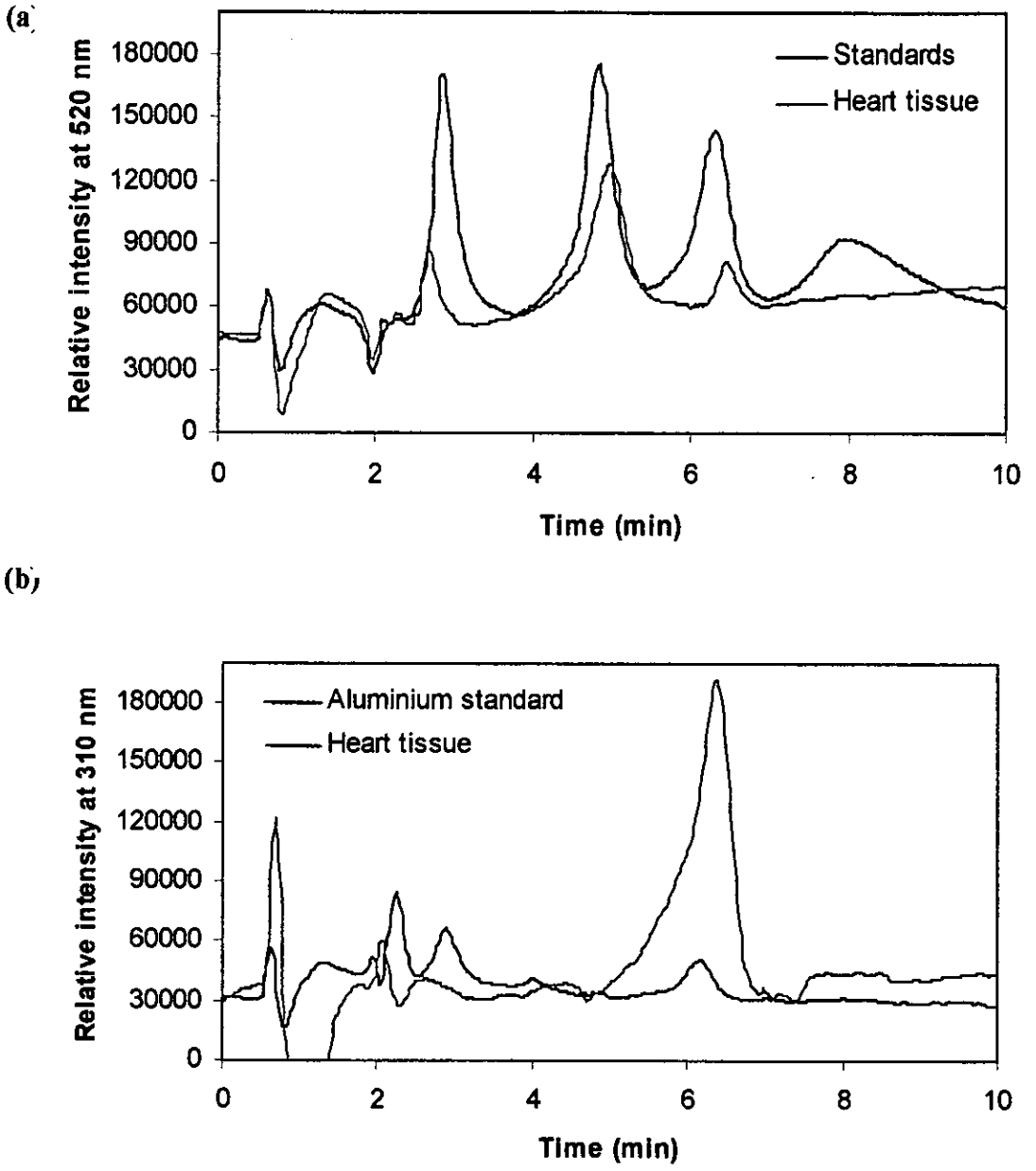

Figure 3.3 - **(a)** Detection of transition metals in heart tissue. Copper, cobalt, zinc and nickel eluted at 2.9, 4.8, 6.6, 8.2 minutes respectively using an oxalate eluent and PAR post column reagent (VIS mode). **(b)** Detection of aluminium in heart tissue. Aluminium elutes at 6.1 minutes using an ammonium sulphate and tiron post column reagent (UV mode).

3.3 Conclusions.

The above studies show that ion chromatography (UV/VIS detection) can be used to measure both transition metals and aluminium in a variety of acid digested tissues and transition metals in blood plasma. Although, no real conclusions can be made about the levels of these metals within each, due to the small number of samples analysed. A larger sample set is needed for a thorough investigation of the trace element levels. Even with an adequate number of samples, it is still difficult to determine if there are any overall disturbances in trace element levels in various disease states. Inter-patient variation and other factors such as age, sex, dietary condition, and disease state could affect the detected levels of trace elements.

The method developed method for the analysis of blood used cobalt as an internal standard to minimise errors due to sample loading and fluctuations that can occur during the running of the column. A suitable internal standard should not be present in tissues and it should also be detectable by the current method. Cobalt was successfully used as an internal standard for the analysis of blood plasma but high levels of cobalt were measured in the tissues samples. Therefore cobalt cannot be used as an internal standard for the detection of transition metals in tissues.

Ion chromatography has been increasingly used for the determination of metals and is becoming an alternative to conventional spectrometric methods [178].The most obvious advantages of this technique are that multiple elements can be determined in one sample of 25 μl volume and complete analysis can be performed when coupled with a suitable detection system or systems. Generally, the sample requires minimal sample pre-treatment [178]. The selectivity and peak sharpness in IC can be enhanced by the use of complexing agents such as PAR for the detection of cations followed by spectrophotometric detection giving a highly sensitive method. The use of the standard additions method and of an internal standard can improve the precision of the results.

Chapter 4. The extraction of amyloid from Alzheimer's disease brains.

4.1 Introduction.

Amyloid fibrils are known to be highly insoluble in neutral aqueous media of ionic strengths commonly used. At present, the examination of amyloid proteins from tissues of clinical significance is still based on the classical approach of water extraction, which is based on the insoluble nature of the amyloid deposits [301]. These techniques are still based on the initial method developed by Pras et al. [301]. The extracts were subjected to column gel chromatography, and the isolated proteins were analysed immunochemically and chemically.

Amyloid fibrils were originally isolated from amyloid rich tissue by alternate homogenisation in saline and water to obtain a top layer preparation. Further purification was achieved by centrifugation of the top layer amyloid material in a sucrose gradient. Solvents that the amyloid are soluble in are too harsh and may alter the structure of the amyloid material. In other procedures, the final top layer was homogenised in water in which some of the fibrils were suspended [76 & 112] Various methods of isolation and purification of amyloid from tissue deposits have at present been used [112, 302-303]. The majority of these methods are based on the insoluble nature of the amyloid protein [301] and have been used to obtain amyloid in a reasonably pure and stable state.

Analysis of the peptides suggests that Aβ(1-40) is the major variant in brain tissue and that cerebrovascular amyloid is composed primarily of Aβ(1-40), and Aβ(1-42) [304]. The Aβ(1-40) was predominant in sporadic AD, whereas Aβ(1-42) was predominant in elderly controls. The Aβ(1-40)/Aβ(1-42) ratio was seen to differ by 10 fold between non-demented controls and sporadic cases [301]. Therefore, a step that causes Aβ(1-42) to aggregate may seed further aggregation of either Aβ(1-40) or Aβ(1-42) [294]. Other variants or fragments of the β amyloid such as Aβ(11-42) have been isolated in amyloid deposits too.

Aβ fragments of differing lengths show characteristic differences for instance in solubility [305] and amyloid fibril formation, since slight differences in structure may affect amyloidogenesis. It is, therefore, important to have knowledge of the primary structure function and processing of the Aβ. This has major importance in the extraction and purification of amyloid from tissue. For instance, Aβ(1-40) is relatively soluble in aqueous media, whereas the C-terminally extended variant Aβ(1-42) rapidly forms fibril like, insoluble structures in aqueous solutions [113].

4.1.1 The present study.

A procedure of isolation based on the extreme insolubility of Aβ amyloid was used. Amyloid material was extracted from parieto cortex tissue from Alzheimer's disease sufferers (Obtained from MRC Neurochemicalpathology Unit, Newcastle General Hospital). The method employed was a slight modification to the protocol as used by Naslund et al. [294]. The ultra-centrifugation steps were carried out at 50,000 g for 1 hour compared to Naslund et al. [294] at 100,000 g for 20 minutes. Washings from subsequent re-homogenisations were run on a SDS polyacrylamide gel electrophoresis.

Amyloid was extracted by homogenisation with water after preliminary treatments, firstly to remove proteins soluble in saline and then to remove salts. The crude extract from brain tissue of patients with Alzheimer's disease containing insoluble amyloid protein was subjected to size exclusion to remove the 4 kDa amyloid protein. The immunoblot of this purified protein using antibody to the Aβ(1-40) was then performed.

4.1.2 Method.

Details of experimental method, instrumentation, and reagents are listed in **chapter 2 section 2.3.**

4.2 Results and discussion.

4.2.1 Extraction of Aβ peptide from Alzheimer's disease brain tissue.

The Aβ proteins are insoluble in the 1% w/v SDS lysis buffer, whereas other proteins and brain constituents are soluble and are able to be separated by subsequent centrifugations and rehomogenisation steps. After each centrifugation step, a sample of the supernatant was retained. These were run on SDS PAGE to determine if the sample contained Aβ peptides. The remaining pellet contains insoluble proteins and insoluble Aβ peptides. The Aβ were further purified by extraction with 1,1,1,3,3,3-hexafluoroisopropanol (HFIP). The Aβ amyloids are soluble in this solvent, which is a better solvent than trifluoroethanol for >40 residue Aβ amyloids [305]. The five supernatant fractions from the initial homogenisations contained progressively less protein as determined by UV spectroscopy at 280 nm. The final supernatant fraction recorded 0.01 absorbance units at 280 nm.

The supernatant from each of the centrifugation steps were run on a SDS PAGE together with the extracted peptide and synthetic Aβ(1-40) (**Figure 4.1**). The molecular weight markers are shown to the right of the lanes. There was no Aβ peptide in the supernatant fractions. The SDS PAGE also shows the progressive decrease in soluble brain proteins after each subsequent water homogenisation and centrifugation steps.

4.2.2 Purification of the β amyloid extract using size exclusion.

The column was calibrated with standard molecular weight markers: alcohol dehydrogenase, bovine serum albumin (BSA), carbonic anhydrase, cytochrome C and vitamin B_{12}. The dead time/dead volume was calculated to be the time from initial addition of the sample to the top of the size exclusion column, to the actual elution of the dextran blue, which is present as a blue coloured band. This was calculated to be about 1 hour for a 30 ml G75 column. The fractions were collected and monitored by UV absorbance detection at 280 nm in a 1 mm quartz cuvette (sample volume 200 µl) and collection was terminated when no more protein was detected.

Figure 4.1

Samples of the supernatant from each of the centrifugation steps were run on a SDS PAGE. The Molecular weight markers are shown to the right of the lanes. There was no Aβ peptide in the supernatant fractions.

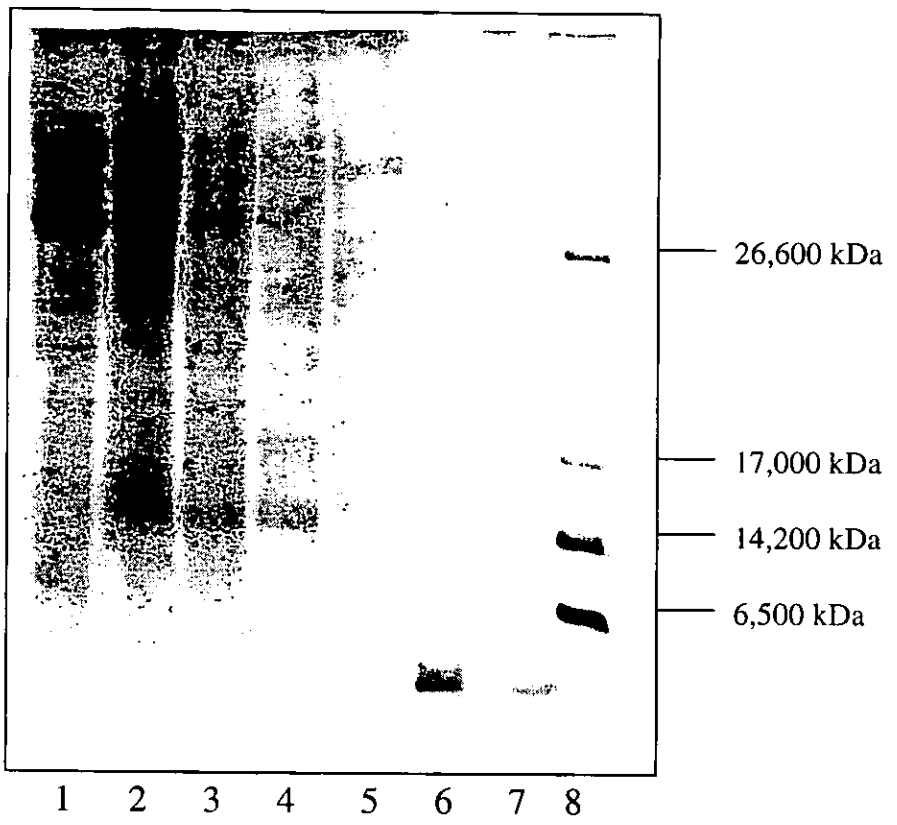

Lane	Sample
1	C1 – supernatant 1
2	C2 – supernatant 2
3	C3 – supernatant 3
4	C4 – supernatant 4
5	C5 – supernatant 5
6	Amyloid extract from AD brains
7	Aβ(1-40) standard
8	MW markers

The log of the molecular weight of the protein is proportional to mobility of the protein and hence the elution time, which is related to the length of the column or volume of packing. The smaller the protein the longer the retention time. Therefore, the column can be calibrated with markers of known molecular weight producing a linear plot for the log of the molecular weight against volume eluted as shown in **Figure 4.2.** The elution volumes are given in **Table 4.1**. The markers used were dextran blue, alcohol dehydrogenase, bovine serum albumin, carbonic anhydrase, cytochrome C and vitamin B_{12}.

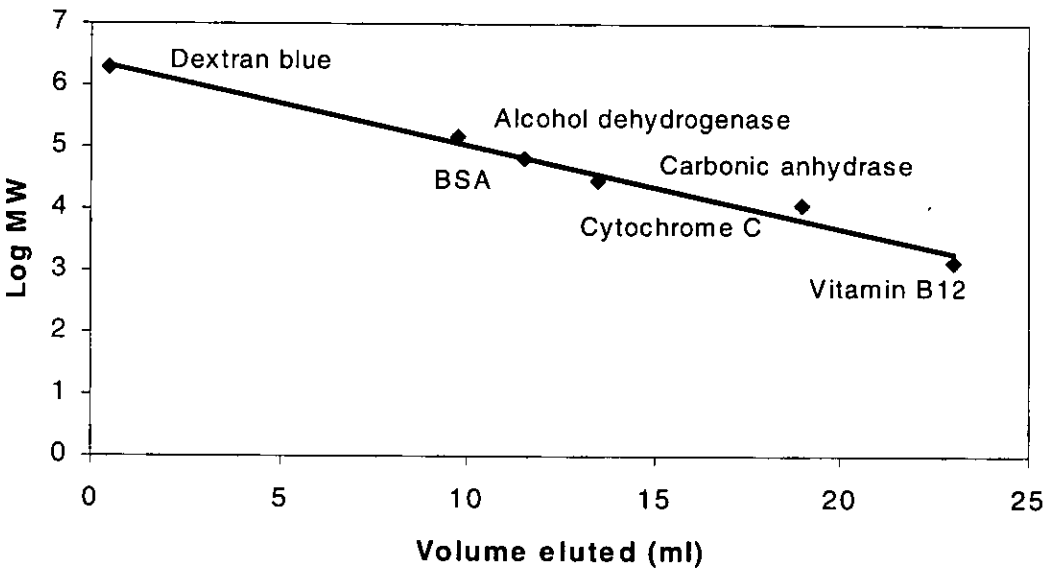

Figure 4.2 - The calibration plot for 30 ml column (Sephadex G75). The log molecular weight is directly proportional retention in the column i.e. the elution volume.

Molecular weight marker	Elution volume (ml)	log MW	MW
Dextran Blue	0.5	6.30	2000000
Alcohol dehydrogenase	9.75	5.17	150000
BSA	11.5	4.81	66000
Carbonic anhydrase	13.5	4.46	29000
Cytochrome C	19	4.09	12400
Vitamin B_{12}	23	3.12	1335
Extracted protein (4kDa) (calculated)	20.5	3.63	4330

Table 4.1 - The elution volumes of the standard molecular weight markers. The calculated elution volume for the 4 kDa peptide is also given.

There are several factors involved in the separation of proteins by size exclusion. The major factor in the resolution of size exclusion lies in the pore size of the packing. The stationary phase consists of a porous network of crosslinked polymers of carbohydrates and acrylamides that swell on absorption of water. The degree of crosslinking determines the size of the pores. Solvated molecules larger than the largest pores of the swollen gel cannot penetrate the pores of the gel particles and, therefore, will pass straight through the column through the spaces between the individual particles. Smaller molecules, however, will penetrate the open network in the particles to a varying degree, depending on their size and shape. They are therefore, retarded to varying degrees and will be eluted in order of decreasing molecular size. Dextran blue has a size of 2,000,000 MW and will therefore pass straight through the column and is consequently used to calculate the void volume. The two sizes of Sephadex (Sigma, UK) used were the G75 and G150 with fractionation ranges of 2,500-40,000 MW and 5,000–100,000 MW respectively.

Although separation of the proteins is reasonable for both the G75 and G150 the running time is almost doubled for the larger pore size Sephadex. **Figure 4.3** shows the comparison of two 30 ml size exclusion columns using G75 and G150 Sephadex sizes. This shows the effect of the choice of Sephadex on resolution of the peaks and the running time (or the volume of eluent required to remove all the components of the column). The larger pore size means that the proteins are retained for longer resulting in a better peak resolution but increasing the running time.

The length of column (or volume) also affects the degree of separation of proteins. The **Figure 4.4** shows the results from the three different column lengths of Sephadex G75. This illustrates that for a longer column there is better separation of proteins compared to the shorter column but the time taken to run the column is drastically increased. Therefore, the 30 ml column was chosen.

Figure 4.3

Comparison of two 30 ml size exclusion columns using **(a)** G75 and **(b)** G150 Sephadex sizes. The larger sized pores of the G150 retains the proteins longer resulting in a longer running time but better separation hence a sharper resolution. The peaks correspond to dextran blue (i), alcohol dehydrogenase (ii), bovine serum albumin (iii), carbonic anhydrase (iv), cytochrome C (v) and vitamin B_{12} (vi).

(a)

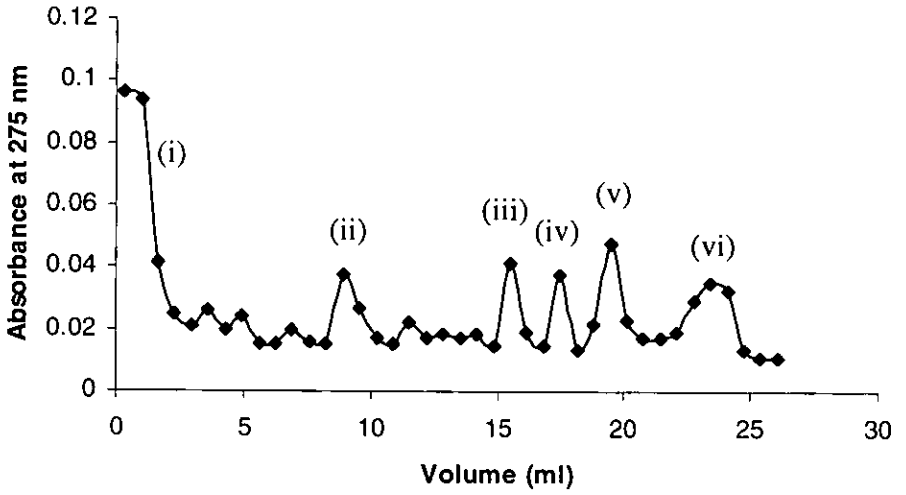

(b)

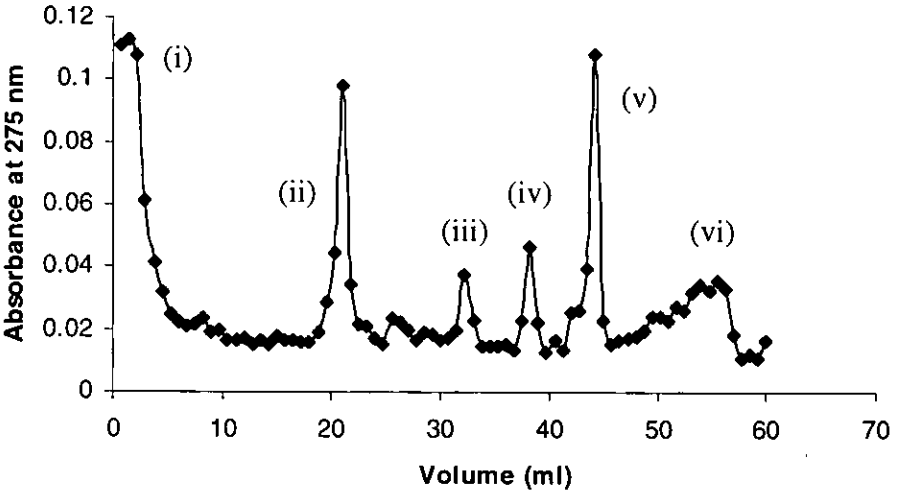

Figure 4.4

Comparison of different lengths of size exclusion column made with Sephadex G75 **(a)** 20 ml, **(b)** 30 ml, and **(c)** 50 ml columns. There is better separation of proteins in the longer column but the total time taken to run the column is drastically increased.

(a) 20 ml column

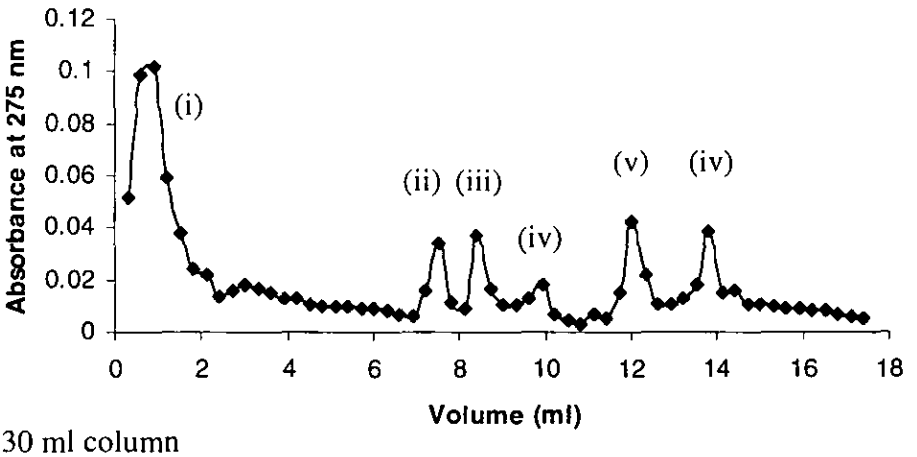

(b) 30 ml column

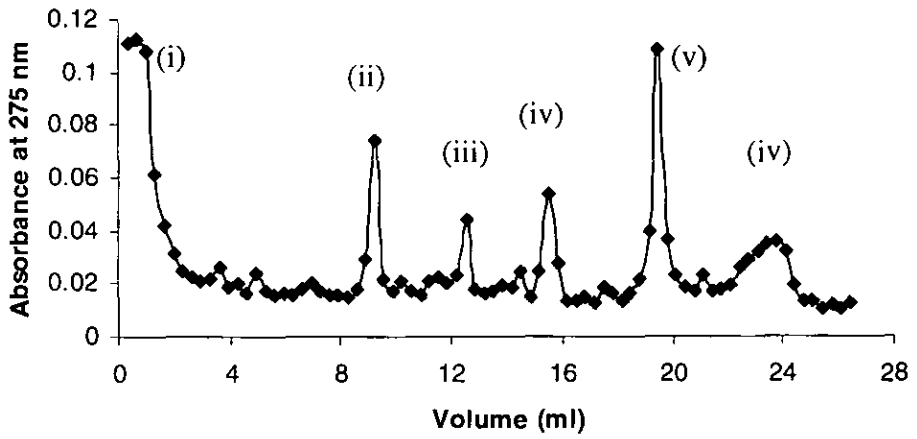

(c) 50 ml column

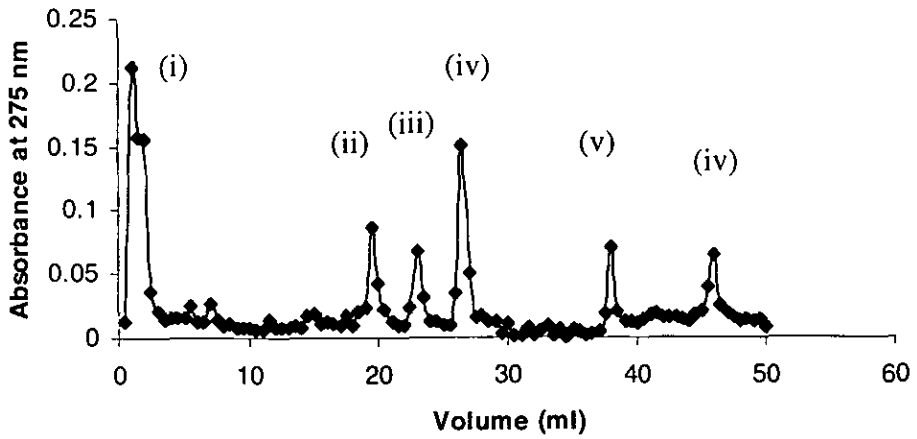

The crude Alzheimer brain extract (390 mg) was subject to size exclusion using 30 ml column of Sephadex G75 (Sigma). The final yield was 280 mg of extract protein, which approximated to about 1% weight of the original wet mass of brain tissue. Since the molecular weight is proportional to the degree of separation we can calculate the volume of elution of a 4 kDa fraction from the slope of the line.

The 4 kDa amyloid protein was calculated to be eluted in a volume of 20.5 ml. The actual volume in which our protein was eluted was about 21 ml (**Figure 4.5**). This is close to the calculated fraction number for a 4 kDa peptide (**Table 4.1**). The fractions corresponding to 4 kDa range of protein were pooled and vacuum centrifuged to dryness leaving a white powder.

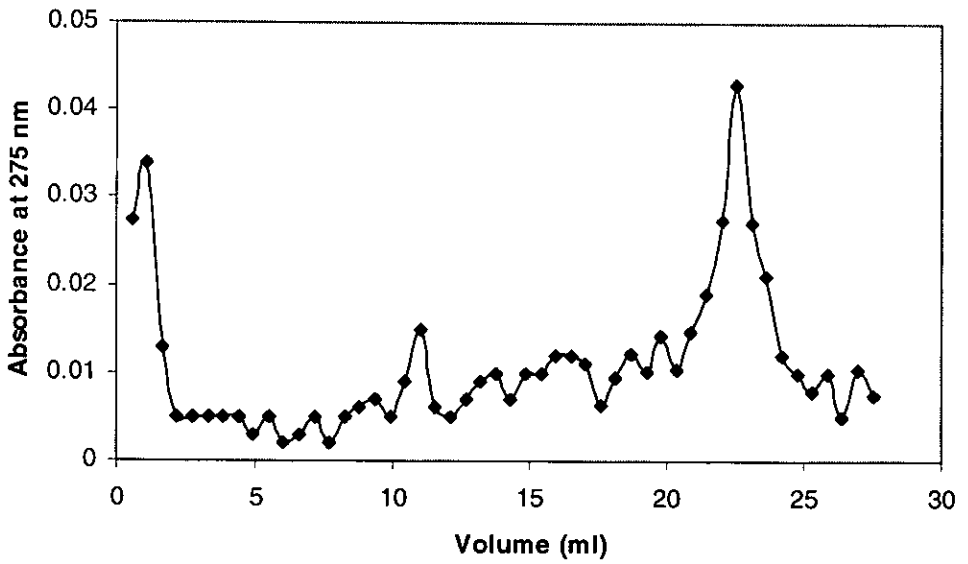

Figure 4.5 - The elution profile for the extracted protein shows a large absorption seen at around 21ml relating to the 4 kDa fraction

4.2.3 Immunoblot detection of the amyloid Aβ(1-40).

A dot blot of the extracted protein and the crude extract before size exclusion chromatography is shown in **Figure 4.6**. The synthetic Aβ(1-40), synthetic Aβ(1-42), synthetic Aβ(1-43) and synthetic APP(125-135) were also added for comparison. The primary antibody was an antibody to the Aβ(1-40) (Sigma, UK).

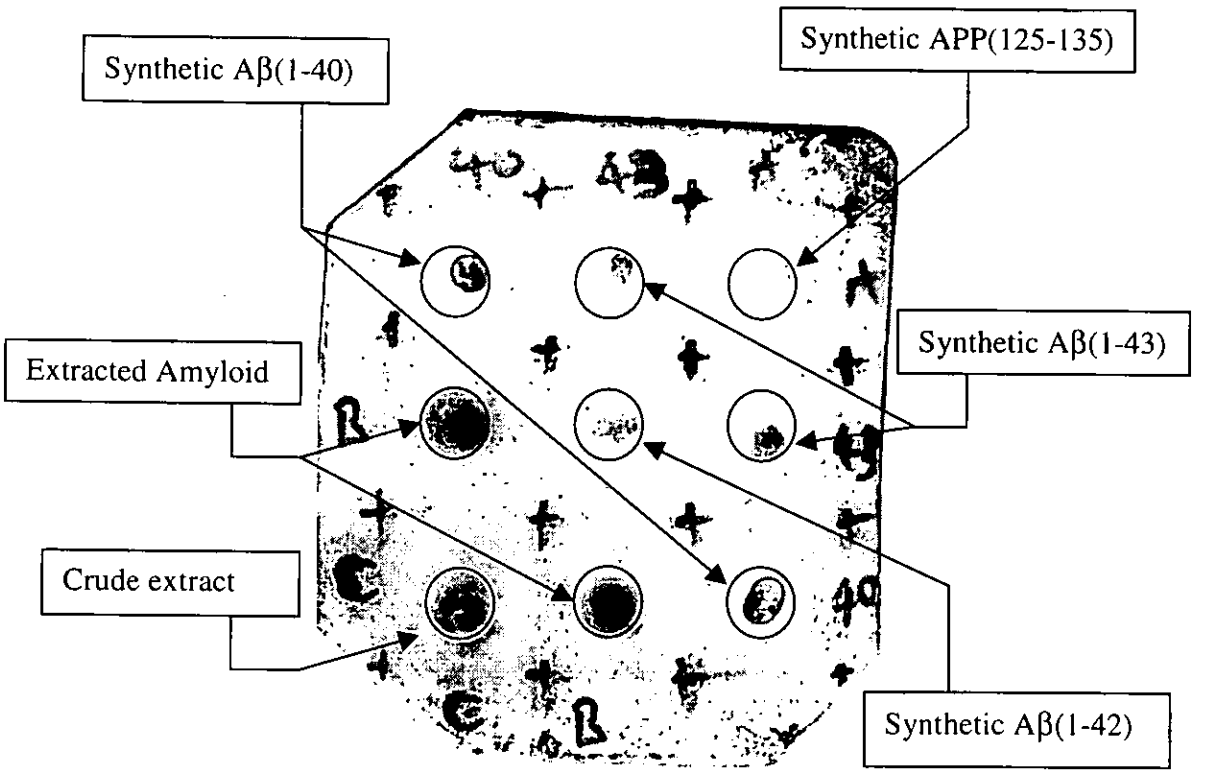

Figure 4.6 - A dot blot of the extracted protein and the crude extract before size exclusion chromatography. The synthetic Aβ(1-40), synthetic Aβ(1-42), synthetic Aβ(1-43) and synthetic APP(125-135) were also added for comparison. The primary antibody was an antibody to the Aβ(1-40).

Amyloid protein was extracted from Alzheimer's brain tissue using an extraction method that relied on the extreme insolubility of the amyloid. Several homogenisation/centrifugation steps are necessary to remove the majority of soluble proteins. It was then necessary to subject the crude extracted amyloid to size exclusion to yield the 4 kDa peptide. The purified 4 kDa extracted amyloid peptide reacted to the Aβ(1-40) antibody on the immunoblot.

It can be seen from **Figure 4.6** that there is strong reactivity between the Aβ(1-40) antibody and the synthetic Aβ(1-40). There was also strong reactivity with the extracted 4kDa peptide indicating that the extracted protein contains the Aβ(1-40). There is reactivity with the crude extract before purification by size exclusion. After purification the sample dot is more concentrated showing that the size exclusion step is needed to purify the amyloid extract. This indicates that the extracted protein most likely contains the Aβ(1-40).

There was no reactivity with the APP(125-135) fragment, which is a portion of the parent precursor molecule. There was some cross reactivity with Aβ(1-43) and Aβ(1-42) peptides. The anti-β amyloid Aβ(1-40) antibody is known to have weak cross reactivity with both Aβ(1-28) and Aβ(12-28) and may also have some reactivity with the above fragments. The modification of the Aβ lysine-16, either by derivatisation [306] or by the substitution of alanine reduces its ability to inhibit antibody binding to amyloid. Binding of amyloid antibody to Aβ(1-40) was found to be inhibited 80% by addition of Aβ(1-28) and 60% by [Ala^{16}]Aβ(1-28) but not all by Aβ(18-28). This suggests that the antigenic sites in AD amyloid are exposed in both Aβ(1-28) and the [Ala^{16}]Aβ(1-28) but is absent in Aβ(18-28) [104]. Fragments that contain an exposed Aβ(1-28) region will also react with this antibody. Therefore, although the extracted amyloid contains predominantly Aβ(1-40), it may also contain other Aβ fragments such as Aβ(1-43) and/or Aβ(1-42) as indicated by the immunoblot assay.

Aβ(1-40) is the predominant soluble species in biological fluids while Aβ(1-42) a minor species of Aβ that is more insoluble *in vitro* is the predominant species found in senile plaques and deposits associated with Alzheimer's disease and Down syndrome. Aβ(1-40) has been reported to be the predominant Aβ peptide in cerebral cortical extracts from AD brain [307] whereas diffuse SP have been reported as containing Aβ(1-42) [308].

Chapter 5. Circular dichroism spectroscopy studies of amyloid materials.

5.1 Introduction.

Circular dichroism spectroscopy (CD) is a useful technique for gaining information about the secondary structure of proteins and polypeptides in solution. The method requires only very small samples and it is non-destructive. Relative changes due to the influence of the environment on a sample can be monitored with CD. The technique of CD has been used increasingly to observe the conformational changes in the various amyloidogenic peptides.

5.1.1 The use of CD in the study of amyloid proteins.

A number of papers have used CD to observe conformational changes in the various amyloids [108, 117, 289, 309 & 310]. Murine serum amyloid A proteins have been shown to consist of a mixture of α helices and β sheets dependent on pH and solvent conditions [59]. The refolding of β_2M to its native state in vitro has been monitored using CD [311]. The interaction of amyloid Aβ peptides with neuronal membranes have been studied using CD to show that there was a specific binding of Aβ(1-40) to ganglioside containing membranes inducing a transition from unordered to β sheets. [312]. The amyloid peptides Aβ(1-28), Aβ(1-39), Aβ(1-40) and Aβ(1-42) incubated with rat neuronal cell lines showed a correlation between the toxicity and increasing β sheet secondary structure of the aged peptides [125].

CD has been used to study fragments of Aβ showing that the secondary structure is dependent not only on the specific fragment but also on experimental conditions. The Aβ(1-42) and Aβ(29–42), were seen to be predominantly β sheet at pH 7.3 in phosphate buffer, whereas the Aβ(1-28) was in random coil and Aβ(1-39) was a mixture of random coil and β sheets. In 50% TFE, the Aβ(29-42) remained in β sheet, but the other three formed α helices which is consistent with the stabilising effects of TFE [108]. Certain Aβ fragments undergo a reversible random coil to β sheet transition. The Aβ(12-28) will undergo such a transformation but this is temperature

dependent [313]. The Aβ(25-35) is also seen to undergo a reversible transition to β sheets at pH 4.0 and 5.5 [117].

The effects of aluminium with Aβ(1-40) and Aβ(25-35) have been monitored using CD. There was a loss of α helices with addition of increasing aluminium to the Aβ(1-40) with a shift to β sheets [289]. The effect of aluminium on the Aβ(1-42) has been shown to be reversed on addition of silicate in a 1:2 ratio. The addition of the silicate prevented the aluminium from interacting with the peptide [314]. Aβ(1-40) and Aβ(1-42) with glycosaminoglycans have also been studied using CD. The addition of various GAGs (heparan sulphate, keratan sulphate, chondroitin sulphate and heparin) to Aβ(1-42) caused an acceleration in the formation of β sheets but did not affect the less amyloidogenic Aβ(1-40) [315].

5.1.2 Factors affecting amyloid studies *in vitro*.

Synthetic amyloid proteins *in vitro* adopt a mixture of β sheet, α helix and random coil structures with relative proportions of each structure being dependent on conditions such as pH [305], length of time in solution [80 & 316], concentration and the solvent conditions [108]. Studies have shown that the conformational changes play an important role in β sheet aggregation and amyloid formation [317 & 318].

Different studies have also employed different amyloid proteins: Aβ(1-40) [125, 289 & 319]; Aβ(1-42) [109, 309 & 320]; Aβ(25-35) [117]; Aβ(1-39); Aβ(1-28) [108 & 109]; and from different origins such as synthetic [108, 117 & 134] and rat [125 & 314]. There are many different conditions under which amyloids have been analysed, e.g. buffers, temperature, and pH. Some studies have conducted analyses at room temperature [108, 124 & 319] whilst others have maintained the temperature at 37 °C [289 & 125]. At pH 1-4 and pH 7-10, α helix formation is favoured whereas β sheet formation is favoured at pH 4-7. Interestingly the maximum rate of aggregation is at pH 5.5, which is close to the isoelectric point of Aβ peptide is 6.1 [108 & 321]. The composition of buffers used in these studies also varied. In aqueous solution β sheet structure is favoured, whereas in aqueous solution containing trifluoroethanol (TFE) or hexafluoroisopropanol (HFIP) [322] the α helix is favoured [110]. Buffers, which

have been used, contain from between 50–100% TFE and have been combined with phosphate, tris, acetate or MES. The differing environments in these studies underscore the difficulties in assigning relevance to structural studies in peptides using CD spectroscopy.

5.1.2.1 Solvent effects.

The choice of solvent for the use in *in vitro* studies is important. The Aβ(1-40) peptide, has been shown to have a limited solubility in aqueous solutions. Organic solvents such as trifluoroethanol (TFE), hexafluoroisopropanol (HFIP) and chloroform may mimic membranes i.e. the lipid environment. These solvents acts as a 'secondary structure-inducing' agents as they weaken hydrophobic interactions in the tertiary structure. Fluorinated alcohols such as TFE and HFIP favour the production of α helices over the formation of β sheets and random coil structures. Less of the higher fluorinated HFIP is required to stabilise the α helical structure. However, the maximum α helical content in HFIP or TFE solvents are nearly the same, showing that HFIP does not cause additional α helix formation. This is consistent with the current understanding that these solvents do not induce α helix formation, but actually stabilise α helices in the protein regions that have an intrinsic tendency to form helical structure [323].

The dielectric constants of trifluoroethanol and the interior of biological membranes (26.6 and 1, respectively) are very different leading to a strengthening of charge interactions. TFE is a weaker proton donor than water and promotes structure formation by allowing intramolecular hydrogen bonding to occur, rather than intermolecular hydrogen bonding with the solvent i.e. stabilising of the α helix structure [108 & 324]. This indicates that hydrophobic interactions are probably important for stabilisation and formation of the β sheet conformation but are not important for the α helical conformation [108].

Trifluoroethanol may also induce β sheet structure. This has been demonstrated with CD spectroscopy for the related peptide Aβ(1-42), which is even less water soluble than Aβ(1-40) [108]. In the concentration range of 10 to 32% TFE, the Aβ(1-42) forms β pleated sheet structures, whereas the CD spectrum at 50 to 100% TFE reveals

α helices. Sha et al. [325] used CD to show that a 9 amino acid peptide (LLEELKEVL) in different solvents adopted different secondary structure. The peptide adopted a β sheet conformation in water, random coil in PBS buffer, α helical in SDS [323]. A β sheet conformation was also observed in TFE due to charge interactions of the peptide and hydrophobic clustering. Therefore, the use of TFE may alter the secondary structure, dependant on the ratio of TFE in the solvent. Nevertheless, TFE is widely used as a membrane mimetic solvent.

5.1.2.2 pH effects.

The pH has a significant effect on promoting the assembly of all amyloid peptides and influences the aggregation *in vitro*. The length of the hydrophobic carboxyl terminus of the Aβ peptide is important in determining the solubility and aggregation properties of the Aβ peptide and that acidic environments, high peptide concentration, and long incubation time would be predicted to be important factors in promoting amyloid deposition [305]. The Aβ(1-40) peptide exists in the α helical conformation and is stabilised in the pH ranges of pH 1-4 and pH 7-10. The 1-28 region is highly amphipathic, tending to stabilise the α helical conformation in the membrane-like environments. In the pH range 4-7, the peptide tends to be in β sheet-like conformation, e.g. Aβ(1-42) is insoluble in the pH range of 3.5-6.5 [108]. Only peptides of 42 residues or longer are showed to be significantly insoluble at pH 7.4. The solubility of Aβ analogues of the Aβ(2-43), Aβ(10-43), and Aβ(12-43) fragments are not dependent on pH in the range of pH 4.5-9.3 [118]. Both Aβ(1-47) and Aβ(1-52) are soluble in the α helix-promoting solvents such as HFIP [305] but have β sheet conformation in aqueous media.

The refolding conditions of β_2M are also dependent on pH. β_2M was seen to be stable at neutral pH where it displays a lower tendency to self-aggregate than in acidic conditions. It has been shown that low pH destabilises native β_2M. Aggregation studies with guanidine-HCl have shown that a reduction in the pH from 6 to 5 has the effect of reducing the stability of β_2M, increasing the aggregation [311]. The effect of temperature on the aggregation of β_2M is also pH mediated and no aggregation is

detected at pH 4. At this pH the β_2M is positively charged and the electrostatic repulsion can prevent protein aggregation [311].

5.1.3 The present study.

The present study extends the work of previous studies [289, 314 & 320], by using CD to study other amyloid peptides and with various inorganic anions and cations and GAGs. The first series of experiments used large concentrations of metals to elicit maximal effects. The later experiments used physiological concentrations for both the GAGs and metals. The amyloid materials used were the synthetic Alzheimer's disease proteins; Aβ(25-35), Aβ(1-40), Aβ(1-42), Aβ(1-43), and the extracted amyloid from Alzheimer's disease brains. The synthetic β_2M, as found in dialysis related amyloidosis was also used. In a separate experiment, the effect of the organophosphorous pesticide, Phosmet on the secondary structure of the recombinant mouse cellular prion protein (r[mouse] PrP^c) was investigated. Any changes in secondary structure were detected using CD spectroscopy.

The use of trifluoroethanol solvent to stabilise α helices was exploited in the current CD study. This work used TFE (60% v/v) the same as Exley et al. [289]. Barrow et al. [108] reported that the optimum concentration which induced an α helical conformation was TFE (60% v/v). In contrast the experiments of Fasman et al. [314 & 320], used a 100% TFE environment. Any change due to the interaction of metals can be detected from the initial conformation of the native peptides in the TFE/tris (3:2) buffer. In the present studies, the pH of the amyloid peptide solutions was maintained at physiological pH 7.4 with TFE/tris buffer. All other solutions, where possible, were also buffered with TFE/tris at pH 7.4.

5.1.4 Method.

Experimental methods, instrumentation and reagent details are given in **chapter 2, section 2.4**.

5.2 Results.

Relatively high protein concentration and lowest path length afforded the best results. Typically, for a 0.01 cm cell, 50-100 µl of a protein concentration of 0.2-0.5 mg ml^{-1} was needed to record a CD spectrum to 180 nm. Two scans were taken over 180 to 260 nm range at 0.25 nm increments with a dwell time of 3 seconds at each wavelength. To achieve adequate signal-to-noise ratio, a spectrum for secondary structure determination required 30-60 minutes to record and an equivalent amount of time for the recording of the background.

Buffer spectra need to be taken regularly because the synchrotronic light source diminishes exponentially with time (**Figure 5.1**). The buffer data were subtracted from the sample data to give the resultant spectrum due to the peptide itself. Problems may arise if the buffer and sample scans are taken too far apart, ripples may appear in the subtracted data.

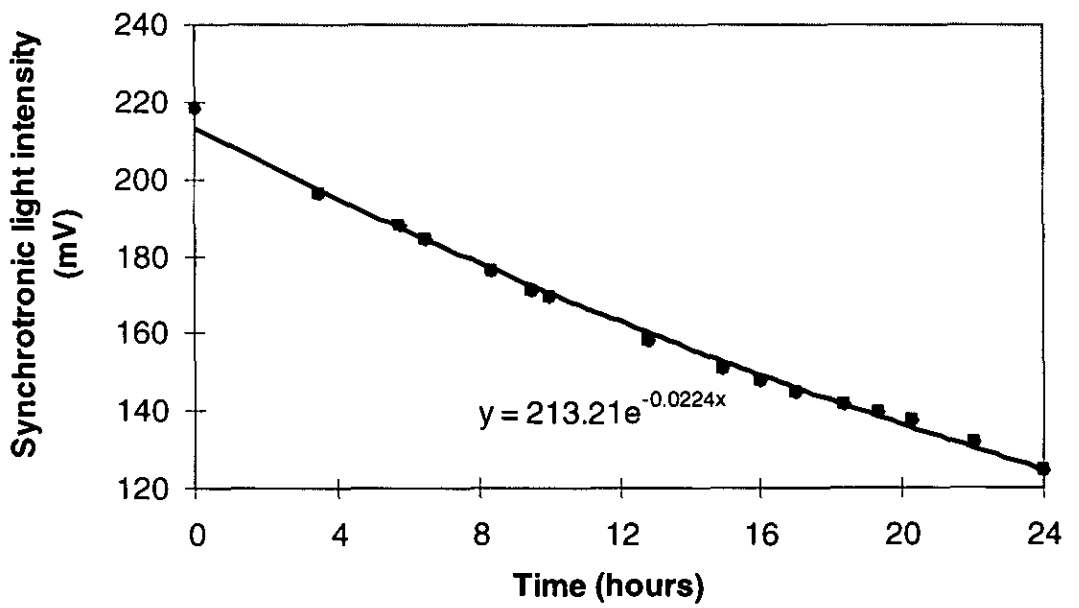

Figure 5.1 - The synchrotronic light output plotted against time. The light source diminishes exponentially with time over a 24 hour period.

The spectral data was analysed using the SELCON program [17]. This used a self consistent method to fit the CD data with a combination of spectral data from proteins with known structure. Secondary structural analysis using the primary sequence has been improved by incorporating CD data constraints. Several new methods have been developed to analyse the secondary structures of peptides and proteins from CD data, to obtain secondary structural information from CD data [17-21]. Most methods were developed by comparing the CD experimental curve with the reference protein using a least-squares fit or best fit.

Many interpretation difficulties arise from: ionisation of groups; binding ligands; temperature; pH; disulphide bridges; aromatic side rings and β turns etc. The contributions of the side chains can become significant below 200 nm. It is generally accepted that the α helical content, as calculated by data fitting programs, are accurate. The β sheet structural elements are predicted to give a negative minimum near 218 nm and positive maximum around (195-197 nm). A positive maximum at 192 nm and two negative minima at 207 and 222 nm are characteristic of α helices [325]. The SELCON program gives good correlation for the fitting of the secondary structures with coefficients of 0.95 for α helix and 0.84 for β sheet [326].

Interference can occur with solvents that absorb in the region of interest between 170 and 260 nm. A buffer or detergent or other chemical should not be used unless it can be shown that the compound in question will not mask the protein signal. For instance imidazole cannot be used below 220 nm because it overwhelms the spectrum from then on. Only very dilute, non-absorbing buffers that allow measurements below 200 nm, should be used. Unfolded protein, peptides, particulate matter (scattering particles), and anything that adds significant noise to the CD spectrum must be avoided. The protein itself should be as pure as possible, any additional protein or peptide will contribute to the CD signal.

The error in the CD spectra is shown in **Figure 5.2**, this was calculated for both repeat scans of the prion protein in Krebs Hensleit buffer (n = 20) and the Aβ(1-40) amyloid protein in TFE/tris buffer (n = 6) obtained on different days and different runs. The spectra clearly show that there is a large inherent error in the Δε values at lower

wavelengths below 190 nm. The error at low wavelength is greater for the Krebs Hensleit buffer than for the TFE/tris buffer and is most likely due to the fact that the Krebs Hensleit buffer absorbs more energy than the TFE/tris buffer in that region.

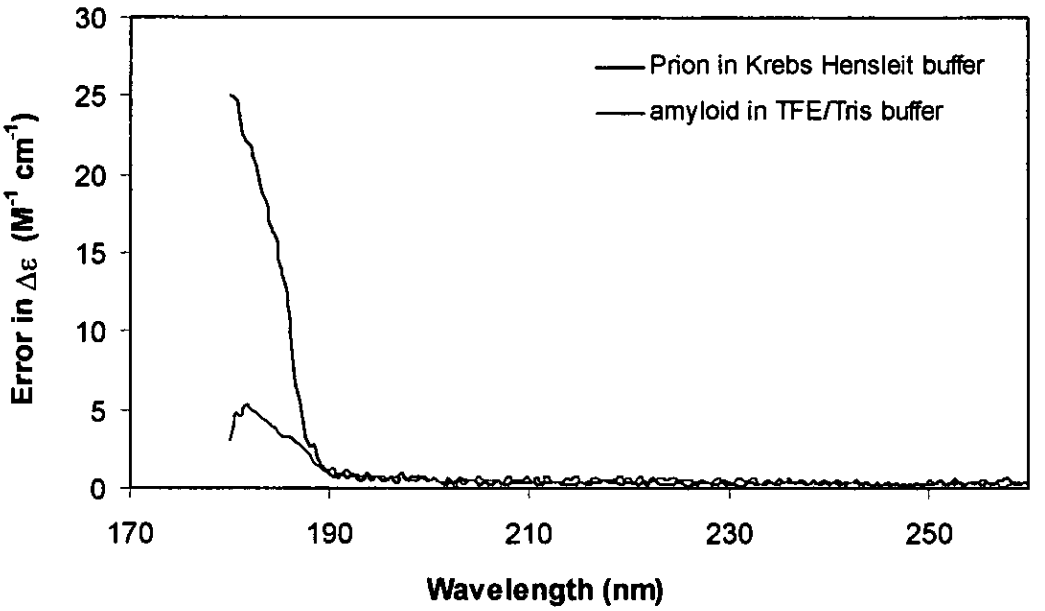

Figure 5.2 - A plot of the error against wavelength for the CD spectra for both the prion in Krebs Hensleit buffer (n = 20) and amyloid in TFE/tris buffer (n = 6).

The CD measurements are subject to a number of experimental errors and due to errors in the fitting process. The overall accuracy of the secondary structural values as calculated by SELCON was determined to have a 3% error for the spectral region between 190-260 nm. Experimental values quoted as significant if the changes in the secondary structure are greater than 3%. Errors within results obtained between different runs on different days and were within the error limits and so it was possible for comparison of the results intra- and inter- run. The quoted secondary structural values for the amyloid peptides are an overall average of the values over the different runs.

5.2.1 Amyloid peptides.

The CD spectra of several of the fragments of the Alzheimer's disease amyloid fragment are shown in **Figure 5.3a.** The spectra for the amyloid peptides clearly showed the diversity of secondary structure for the different fragments of the same protein. This demonstrates both the unique ways in which certain amino acid residues can contribute to the overall structure and the possibility that different parts of the molecule may be involved in the deposition of amyloid.

In the TFE/tris solvent, the longer Aβ(1-43) was predominantly α helical (40.3%) in nature, whereas the Aβ(25-35) fragment is predominantly β sheet (51.7%) in nature. The Aβ(25-35) is thought to be involved in the mediation of β sheet formation within the amyloid deposition [327]. The Aβ(1-40) (α - 36.9%, β - 17.6%) had a higher α helical and lower β sheet content than the Aβ(1-42) (α - 20.5%, β - 24.9%) (**Figure 5.3a**). Both are found in senile plaques within Alzheimer's disease brains [74 & 75].

The amyloid protein extracted from Alzheimer's disease brains (α - 11.3%, β - 35.5%) shows a larger percentage of β sheets than α helices. This indicates that the extracted protein had more β sheets than either Aβ(1-40) or the Aβ(1-42) but less than the Aβ(25-35). The extracted amyloid could also contain many β amyloid protein fragments such as the Aβ(1-42) or Aβ(25-35). The CD method is not able to distinguish between a mixture of proteins and the secondary structure from each protein within the mixture contributes to the overall spectrum.

Comparison of the Aβ(1-40), β_2M and the prion protein are shown in **Figure 5.3b**. The spectral profiles of the Aβ(1-40) and β_2M are very similar The Aβ(1-40), β_2M and r[mouse]PrP^c prion all have similar percentages of β sheet (17.6, 18.2 and 15.2% respectively). The CD spectrum (**Figure 5.3b**) shows that PrP^c is predominantly composed of α-helix (42.5%). Changes in the secondary structure of PrP^c to form PrP^{sc} lead to the deposition of β pleated sheets in a manner similar to amyloid deposition [200]. Conversion to PrP^{sc} creates a protein, which contains 45% β sheet, little or no α helix, and 57% β turns and random coil [50, 196, 198, 201 & 319] which is consistent with its amyloid like properties [198 & 318].

Figure 5.3a

The CD spectra of the Aβ(1-40) (57.7 μM), Aβ(1-42) (33.3 μM), Aβ(1-43) (216 μM), Aβ(25-35) (118 μM) and Aβ extract (0.5 mg ml^{-1}) in TFE/tris buffer. The percentage secondary structures of various amyloid materials are shown below.

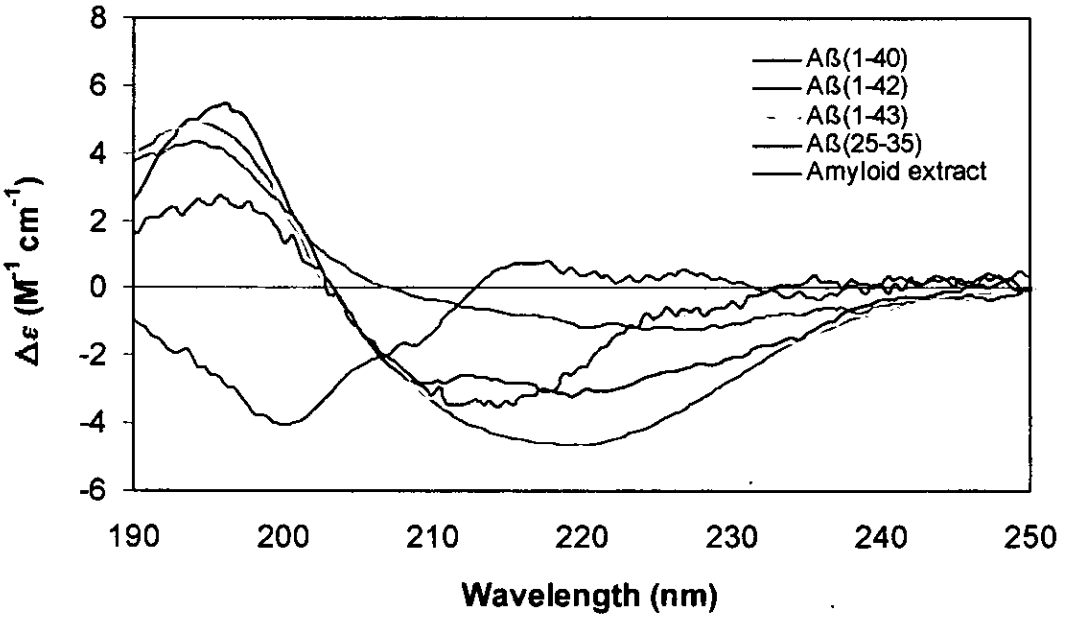

Secondary structure	Percentage secondary structural values (%)				
	Aß(1-40)	Aß(1-42)	Aß(1-43)	Aß(25-35)	Aβ Extract
Helix	36.9	20.5	40.3	9.9	11.3
Beta Sheets	17.6	24.9	15.3	51.7	35.5
Beta-Turn	16.8	15.8	17.7	15.4	17.6
Random Coil	33.8	38.8	26.7	23.9	37.1

Figure 5.3b

The CD spectra comparing Aβ(1-40) peptide (57.7 μM), β_2M (211.5 μM) and prion protein (r[mouse]PrP^c) (1.0 mg ml^{-1}) in TFE/tris buffer. The percentage secondary structures of various amyloid materials are shown below.

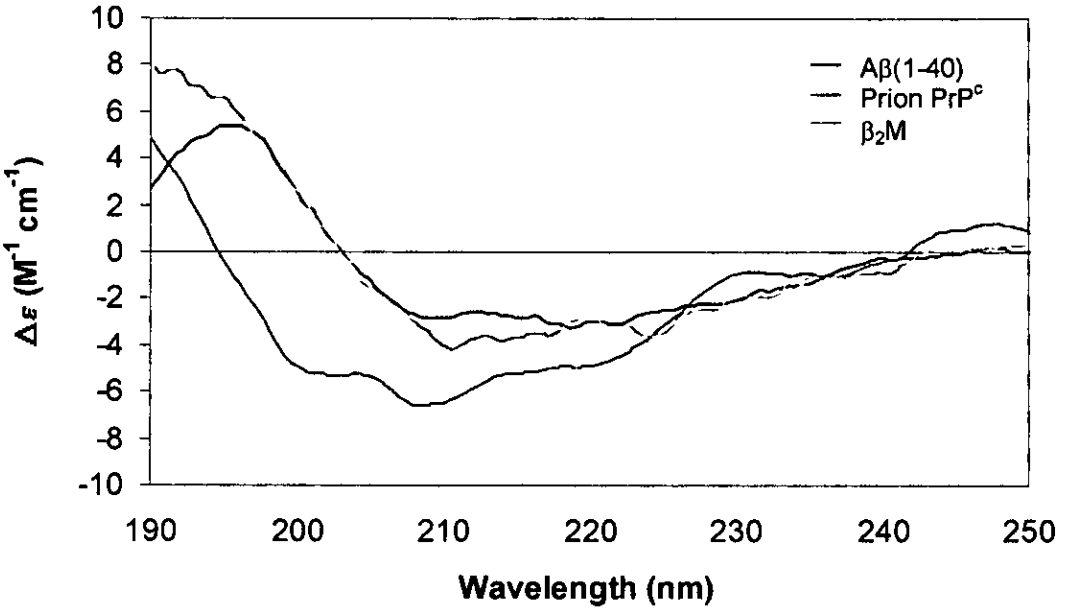

Secondary structure	Percentage secondary structural values (%)		
	Aß(1-40)	Prion PrP^c	$ß_2$M
Helix	36.9	42.5	37.3
Beta Sheets	17.6	18.2	15.2
Beta-Turn	16.8	13.0	15.8
Random Coil	33.8	28.2	31.4

5.2.2 The secondary structural changes of recombinant mouse PrPc treated with Phosmet and its metabolites.

The exposure of the r[mouse]PrP^c (90-231) to Phosmet is shown in **Figure 5.4.** There was no overall change in the CD spectrum over a 7 hour period. This indicates that the Phosmet does not change the secondary structure of the prion protein over the 7 hour incubation period.

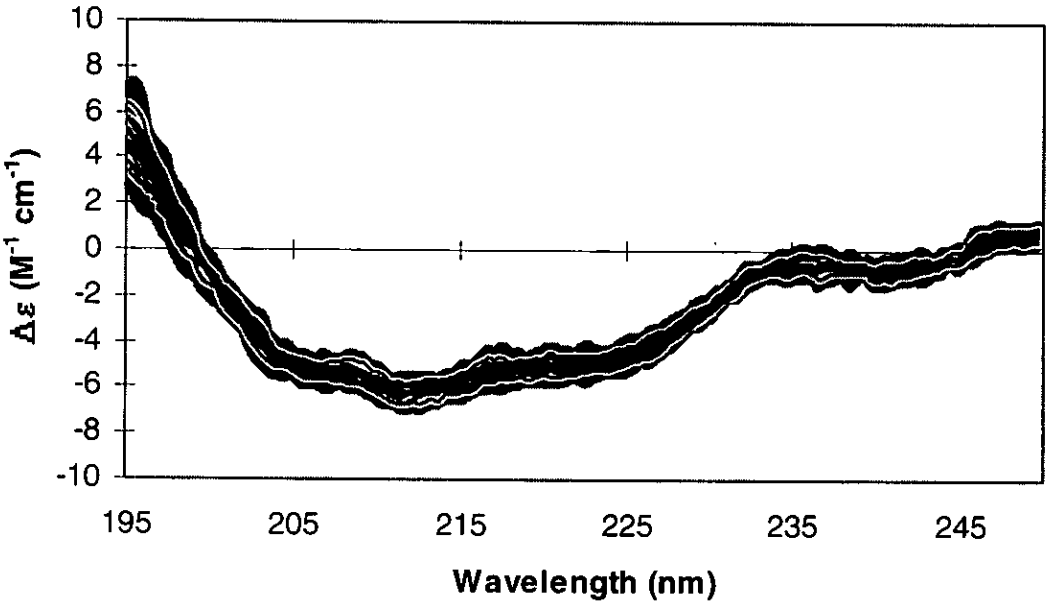

Figure 5.4- The CD spectra of r[mouse]PrP^c in Krebs Hensleit buffer following incubation with Phosmet. The shaded region is the error.

PrP^c exposed to the metabolites of Phosmet generated *in situ* in the CD cuvette, showed no change in the CD spectrum of the protein (**Figure 5.5**). The exposure of r[mouse]PrP^c to Phosmet or its metabolites did not result in any changes in the conformation of the prion. This indicates that Phosmet does not act as a trigger factor for the initiation of PrP^{sc}. This experiment was designed to ensure a short time period between generation of the active Phosmet metabolites and their potential contact with the PrP^c. This is important because it is likely that the metabolites, which might interact with PrP^c, are reactive oxidation products that have a short half-life in aqueous environments.

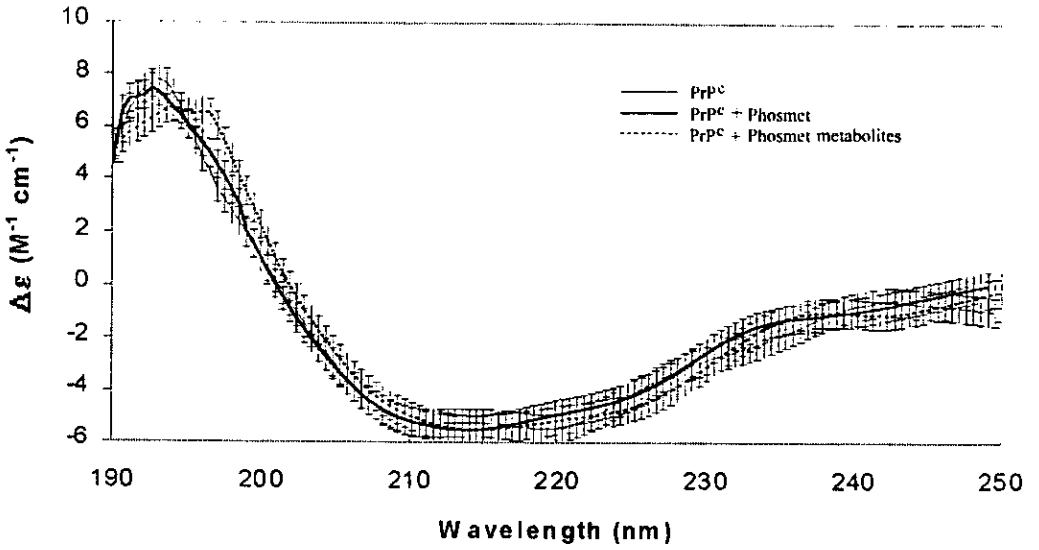

Figure 5.5 - The CD spectra of r[mouse]PrP^c with Phosmet and its metabolites.

In order to check the Phosmet metabolite-generating capacity of the rat microsomal preparation, rat microsomes were incubated with Phosmet and the incubation medium solvent extracted and subjected to HPLC analysis. The major metabolite (likely to be oxo-phosmet) was generated plus at least 2 minor metabolites. The overall metabolic conversion of Phosmet was 0.16 μM h^{-1} (this is equivalent to 50% Phosmet metabolism h^{-1} in our experiment). Generation of the oxo-metabolite is important because this is very reactive and is a likely candidate for interaction with proteins and these experiments show they were available for reaction with PrP^c.

Secondary structures	Percentage Secondary structures (%)		
	Control r[mouse]PrP^c	r[mouse]PrP^c + Phosmet	r[mouse]PrP^c+ Phosmet metabolites
Helix	38	42	42
Beta sheets	19	17	16
Turn and Others	42	41	42

Table 5.1 - The secondary structural values for the prion with Phosmet and its metabolites.

The proportions of the different conformational forms of the prion protein are shown in **Table 5.1**. The secondary structure values show no change in the conformation of the prion, irrespective of the treatment to which the PrP^c was subjected in our experiments.

5.2.3 Amyloid proteins treated with metals.

The various amyloid peptides Aβ(1-40), Aβ(1-42), Aβ(1-43), Aβ extract and β_2M were treated with the metals Ca^{2+} (100 μM), Cu^{2+} (100 μM), Zn^{2+} (100 μM) and Al^{3+} (150 μM). In addition, the Aβ(1-40) and β_2M were also treated with Mg^{2+} (100 μM). The CD spectrum for the Aβ(1-43) peptide showed little or no change on addition of the metals. The secondary structural values also indicated no change from the native peptide values (**Figure 5.6a**). The CD spectrum for the Aβ(1-42) peptide showed a general increase in random coil by more than 5% and a decrease in the α helix of about 3% for all of the metals. A decrease in the β sheets resulted from treatment with Ca (↓ 13%) (**Figure 5.6b**). The CD spectrum for the extracted amyloid protein again showed a general decrease in α helix of less than 4% for all the metals. There was also a decrease in the minimum around 220 nm for the Cu^{2+} treated peptide. This related to a large increase in β sheet with a corresponding decrease in both β turns and random coil secondary structural values (**Figure 5.6c**). The CD spectrum for the β_2M amyloid showed small changes in the metal treated protein spectrum. There was a small decrease in α helices and random coil together with a small increase in β sheets for all the metal treated peptides (**Figure 5.6e**).

The CD spectrum for Aβ(1-40) amyloid protein showed little change with Mg^{2+} but with Ca^{2+} and Al^{3+} there was a significant decrease in the maximum around 195 nm and a decrease in the minimum around 220 nm (**Figure 5.6d**). The secondary structural values for Cu^{2+}, Zn^{2+} and Al^{3+} treated peptides showed large decreases in α helix and random coil with large increases in β sheet secondary structures. The peptide treated with either Cu^{2+} (100 μM) or Zn^{2+} (100 μM) caused a complete inversion in the minimum and maximum. Ca^{2+} also showed similar effects but to a lesser extent. The Aβ(1-40) amyloid peptide was also treated with Cu^{2+} and Zn^{2+} (10, 50, 100 μM) and with Cu^{2+} and Zn^{2+} combined (100 μM). The results showed that the lower concentration of Cu^{2+} (> 10 μM) and Zn^{2+} (> 10 μM) also elicited large changes in the secondary structure of the Aβ(1-40) (**Figure 5.6f and 5.6g**). The combined effect of Cu^{2+} (100 μM) and Zn^{2+} (100 μM) was similar to either Cu^{2+} (100 μM) or Zn^{2+} (100 μM) alone, but interestingly to a lesser degree.

Figure 5.6a

CD spectra of the synthetic Aβ(1-43) treated with Ca^{2+}, Cu^{2+}, Zn^{2+} (100 μM) and Al^{3+} (150 μM) in TFE/tris buffer. The percentage secondary structures are shown below.

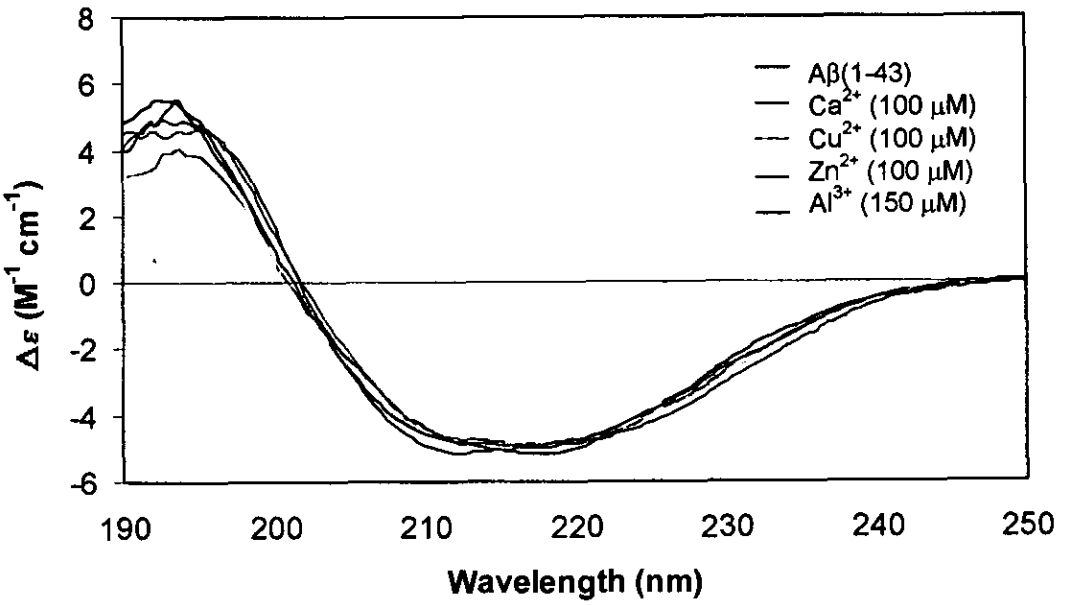

Secondary structure	Percentage secondary structural values (%)				
	Aß(1-43)	Ca^{2+}	Cu^{2+}	Zn^{2+}	Al^{3+}
Helix	40.7	40.3	38.0	42.7	40.3
Beta Sheets	15.0	15.0	14.3	13.8	14.7
Beta-Turn	17.5	17.3	20.5	19.4	18.4
Random Coil	26.8	27.0	28.2	26.1	26.4

Figure 5.6b

CD spectra of the synthetic Aβ(1-42) treated with Ca^{2+}, Cu^{2+}, Zn^{2+} (100 μM) and Al^{3+} (150 μM) in TFE/tris buffer. The percentage secondary structures are shown below. Shaded values are changes greater 3% from the native peptide.

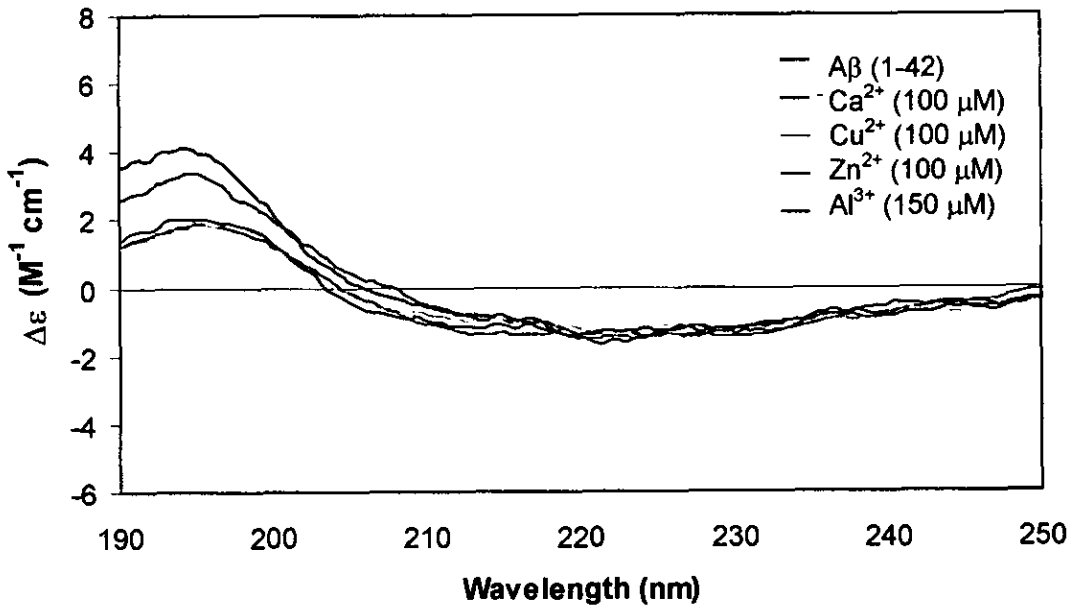

Secondary structure	Percentage secondary structural values (%)				
	Aβ(1-42)	Ca^{2+}	Cu^{2+}	Zn^{2+}	Al^{3+}
Helix	20.5	17.0	15.1	16.7	17.9
Beta Sheets	24.9	19.6	24.4	21.5	23.7
Beta-Turn	15.8	19.2	17.9	19.1	16.1
Random Coil	38.8	50.3	43.5	46.5	42.6

Figure 5.6c

CD spectra of the Aβ extract treated with Ca^{2+}, Cu^{2+}, Zn^{2+} (100 μM) and Al^{3+} (150 μM) in TFE/tris buffer. The percentage secondary structures are shown below. Shaded values are changes greater 3% from the native peptide.

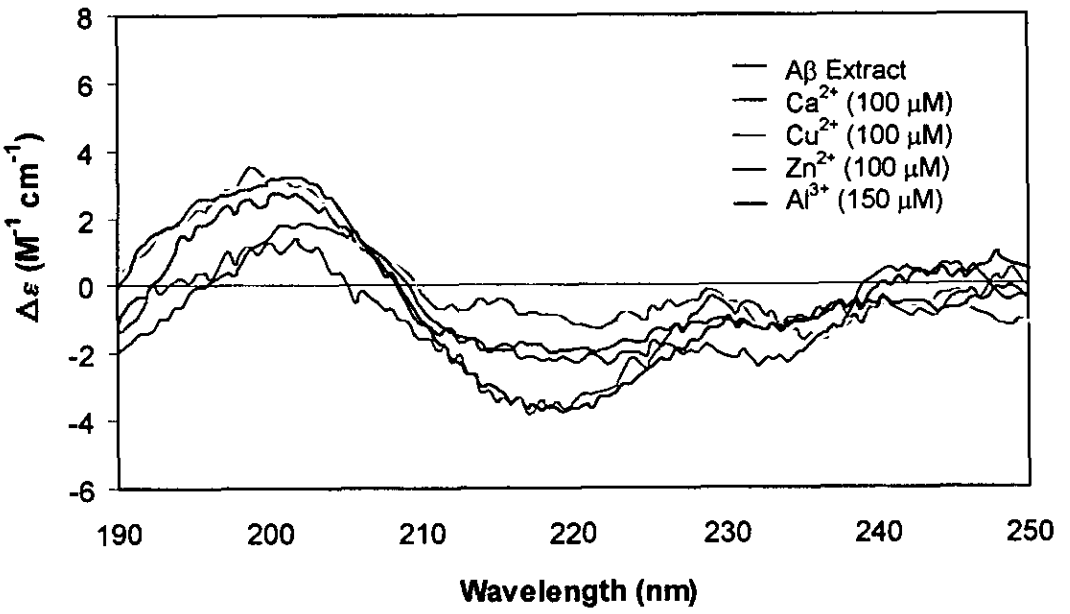

Secondary structure	Percentage secondary structural values (%)				
	Extract	Ca^{2+}	Cu^{2+}	Zn^{2+}	Al^{3+}
Helix	11.3	9.6	7.3	7.6	10.0
Beta Sheets	35.5	32.2	61.7	29.4	34.3
Beta-Turn	17.6	18.9	12.2	17.4	17.4
Random Coil	37.1	37.7	23.7	41.4	38.0

Figure 5.6d

The CD spectra of β_2M treated with Mg^{2+}, Ca^{2+}, Cu^{2+}, Zn^{2+} (100 μM) and Al^{3+} (150 μM) in TFE/tris buffer. The percentage secondary structures are shown below. Shaded values are changes greater 3% from the native peptide.

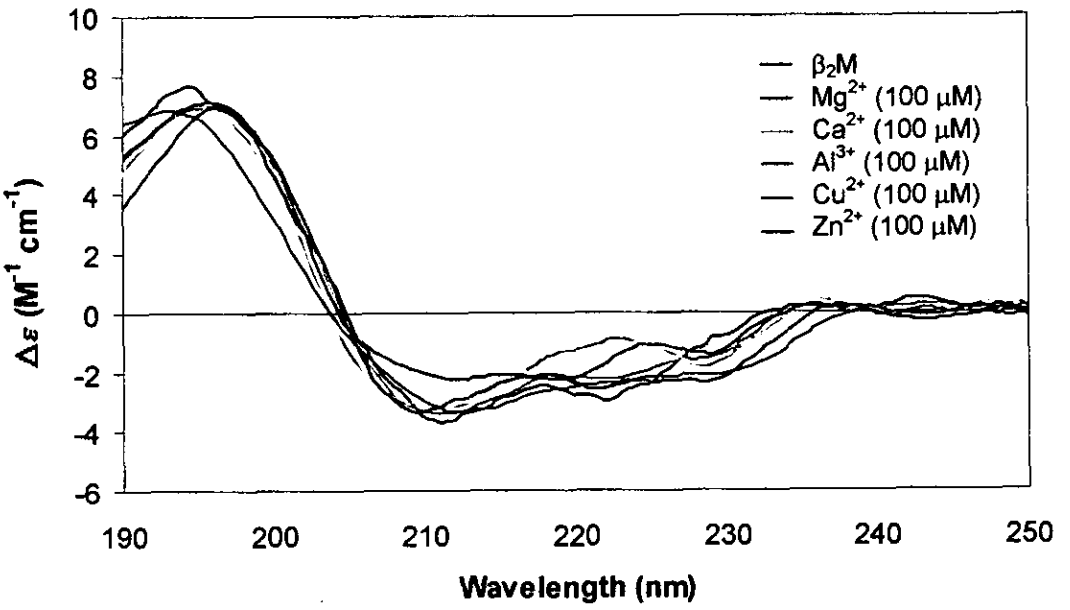

Secondary structure	Percentage secondary structural values (%)					
	β_2M	Mg^{2+}	Ca^{2+}	Cu^{2+}	Zn^{2+}	Al^{3+}
Helix	37.3	36.0	34.0	32.7	35.8	34.1
Beta Sheets	15.2	16.3	18.1	17.4	16.8	17.7
Beta-Turn	15.8	17.4	17.7	17.0	17.6	17.4
Random Coil	31.4	30.3	30.1	32.9	29.8	30.8

Figure 5.6e

The CD spectra of Aβ(1-40) amyloid peptide treated with Mg^{2+}, Ca^{2+}, Cu^{2+}, Zn^{2+} (100 μM) and Al^{3+} (150 μM) in TFE/tris buffer. The percentage secondary structures are shown below. Shaded values are changes greater 3% from the native peptide.

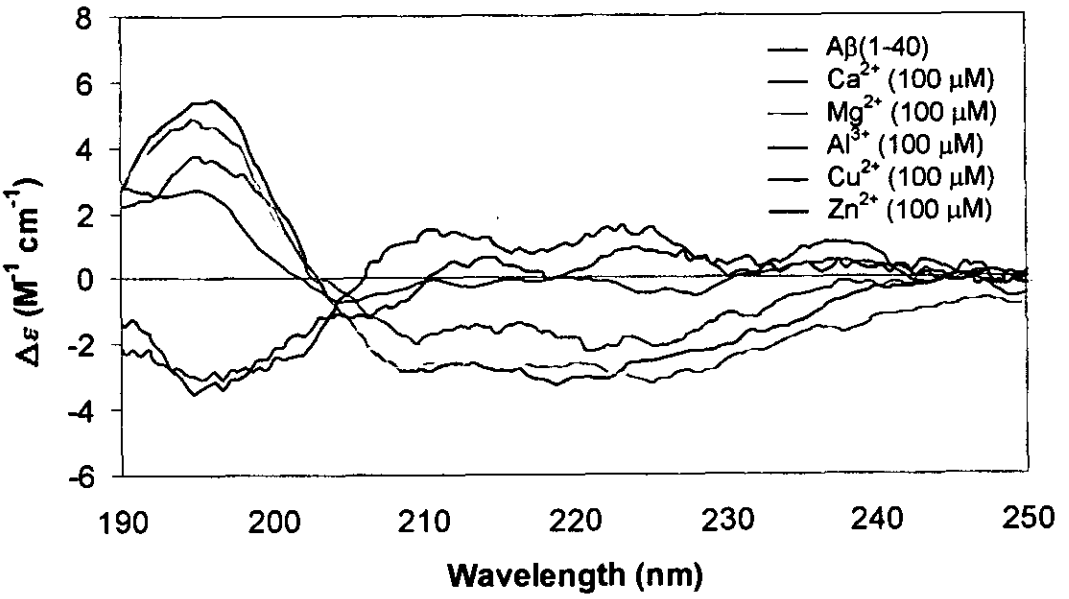

Secondary structure	Percentage secondary structural values (%)					
	Aβ(1-40)	Mg^{2+}	Ca^{2+}	Cu^{2+}	Zn^{2+}	Al^{3+}
Helix	36.9	31.2	21.4	7.9	9.4	16.3
Beta Sheets	17.6	16.6	28.6	50.1	49.5	34.1
Beta-Turn	16.8	16.7	16.7	14.2	14.9	16.0
Random Coil	33.8	34.4	34.4	27.8	26.2	33.6

Figure 5.6f

The CD spectra of Aβ(1-40) peptide with Cu^{2+} (10, 50, and 100 μM) in TFE/tris buffer. The percentage secondary structures are shown below. Shaded values are changes greater 3% from the native peptide.

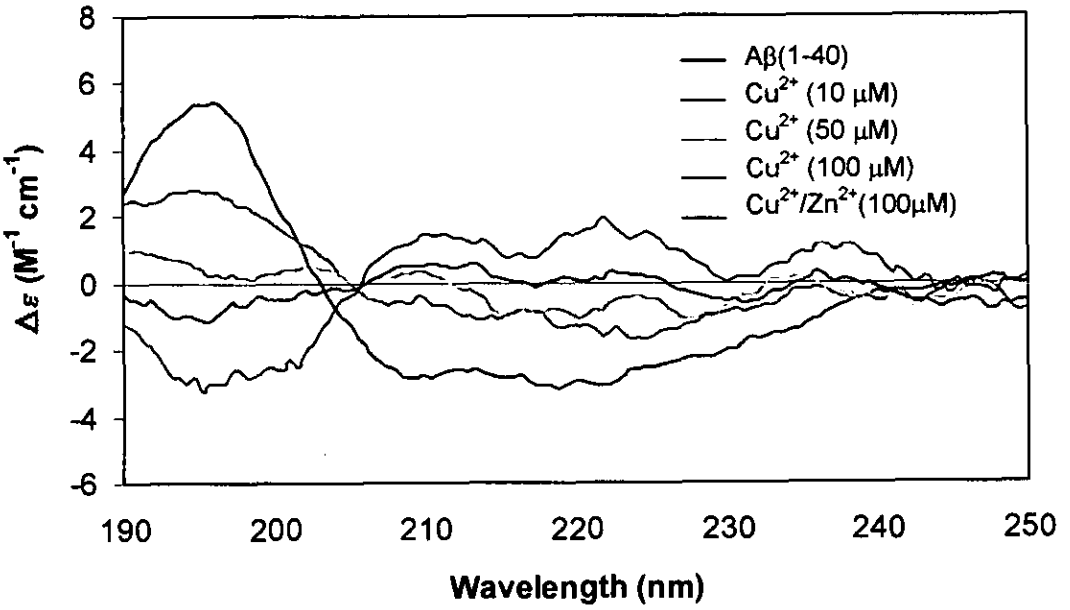

Secondary structure	Percentage secondary structural values (%)				
	Aβ(1-40)	Cu^{2+} (10 μM)	Cu^{2+} (50 μM)	Cu^{2+} (100 μM)	Zn^{2+}/Cu^{2+} (100 μM)
Helix	36.9	19.5	13.9	7.9	11.2
Beta Sheets	17.6	27.8	36.5	50.1	43.3
Beta-Turn	16.8	16.2	15.3	14.1	14.8
Random Coil	33.8	36.5	34.4	27.8	31.7

Figure 5.6g

The CD spectra of Aβ(1-40) peptide with Zn^{2+} (10, 50, and 100 μM) in TFE/tris buffer. The percentage secondary structures are shown below. Shaded values are changes greater 3% from the native peptide.

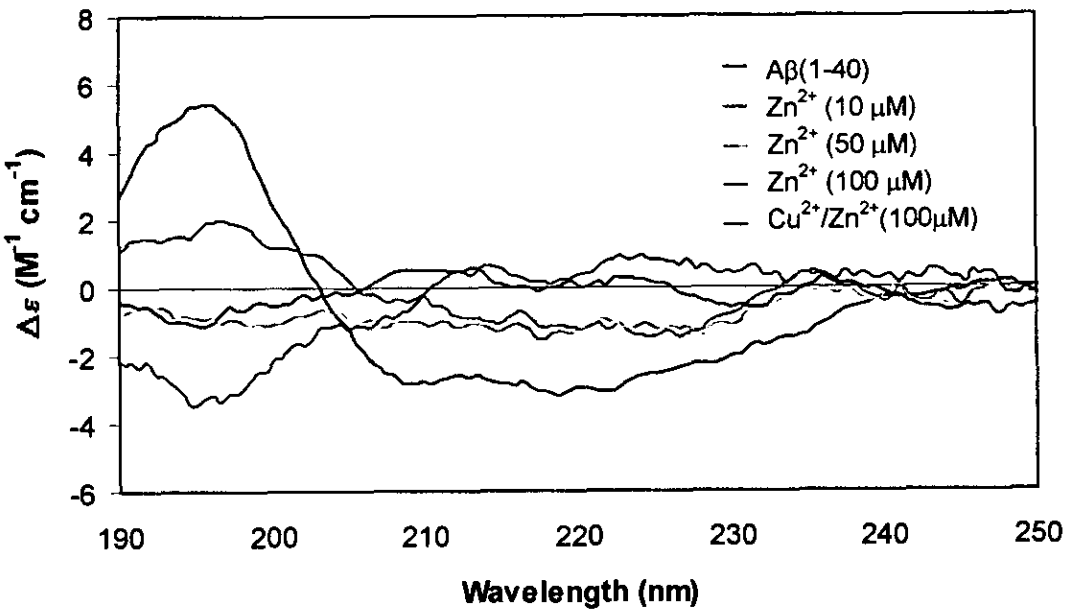

Secondary structure	Percentage secondary structural values (%)				
	Aβ(1-40)	Zn^{2+}(10μM)	Zn^{2+}(50μM)	Zn^{2+}(100μM)	Zn^{2+}/Cu^{2+}(10μM)
Helix	36.9	17.1	14.1	9.4	11.2
Beta Sheets	17.6	31.6	39.8	49.5	42.3
Beta-Turn	16.8	15.9	15.8	14.9	14.8
Random Coil	33.8	35.3	30.1	26.2	31.7

5.2.4 Amyloid proteins treated with aluminium.

The CD spectrum for the Aβ(1-43) peptide showed little change on addition of increasing concentration of Al^{3+}. The secondary structural values also showed no significant changes although there was a small decrease in α helices and slight increase in β sheets (**Figure 5.7a**). The CD spectrum for Aβ(1-42) with Al^{3+} showed a decrease in both α helices and random coil and a general increase in β sheets on addition of high concentrations of Al^{3+} (**Figure 5.7b**). The CD spectrum of the extract with Al^{3+} showed a small decrease in the minimum around 220 nm although the secondary structural values indicate no significant changes (**Figure 5.7c**).

The spectrum for the Aβ(1-40), on the other hand, showed more of a marked change on addition of increasing concentration of Al^{3+}. There was a gradual decrease in the maximum around 195 nm coupled with a gradual decrease in the minimum around 220 nm. There was a decrease in α content and small increases in β sheets and random coil with increasing concentration up to Al^{3+} (300 μM). With Al^{3+} (400 μM), there was a slight reversal in the above trend i.e. up to Al^{3+} (300 μM) the β sheets decreased from 36.9% in the native peptide to 15.5% but for the addition of Al^{3+} (400 μM) there was an increase back to 18.5% (**Figure 5.7d**). With the β_2M, there was a general decrease in α helices and an increase in β sheets with increasing Al^{3+} (**Figure 5.7e**). Al^{3+} may have a similar effect on β_2M as with Aβ(1-40) but to a lesser extent. On addition of increasing concentration of Al^{3+} (150, 300 and 400 μM), the α helix values decrease to 24.4% and the β sheet values increase to 31.2%.

The solution chemistry of aluminium is complex. A variety of aluminium species exist as a result of a series of hydrolytic equilibria as $Al(H_2O_6)^{3+}$, $Al(OH)^{2+}$, $Al(OH)_2^+$, $Al(OH)_3$, $Al(OH)_4^+$, and other polycationic species. The amount of each species present is dependent on pH, concentration and time [328, & 232]. At pH 7, Al^{3+} is almost completely present as insoluble hydroxide, $Al(OH)_3$ [232]. It is this insolubility that limits the concentration of aluminium in aqueous biological systems.

The 5 mM Al^{3+} stock solution in tris buffer was prepared immediately prior to use from $AlCl_3$ salts (pH 7.4). The required working solutions were then prepared and

added to the samples and allowed to incubate for 1 hour. Flame atomic absorption spectroscopy experiments indicated that the concentration of the 5 mM Al^{3+} in tris buffer (pH 4.8) was stable for up to 72 hours. Hence, the concentrations of the working solutions made immediately from this 5 mM stock solution were reliable. The equilibrium of Al^{3+} in solution is also time dependent and it may be the case that the 1 hour incubation period is sufficient to allow a certain degree of Al^{3+} to transform into insoluble species. At the 400 μM Al^{3+} concentration, less of the Al^{3+} had remained in the soluble monomeric state at pH 7.4 and at 20 °C over the incubation period. The availability of the aluminium in solution may thus account for a higher β sheet content of Aβ(1-40) of the 300 μM compared with the 400 μM concentrations.

5.2.5 Amyloid proteins treated with both aluminium and silicon.

Addition of Al^{3+} (150 and 300 μM) to the Aβ(1-40) peptide caused a decrease in α helices and an increase in β sheet as shown in **Section 5.2.4**. Addition of SiO_4^{4-} (30 μM) after the Al^{3+}, had little effect in reversing the changes in secondary structure caused by Al^{3+} (150 and 300 μM) as shown in **Figure 5.8a**. A higher concentration of SiO_4^{4-} (300 μM) caused a reversal in both the α helices by 5% back towards the native peptide for the Al^{3+} (150 μM) treated peptide.

Addition of SiO_4^{4-} (300 μM) after Al^{3+} (300 μM) caused similar effects but to a lesser extent with a further increase in α helices of 3% compared to Al^{3+} (300 μM) alone. **Figure 5.8b** showed that the addition of SiO_4^{4-} (300 μM) added before the Al^{3+} (300 μM) further reverses the structural changes with an increase in α helices of 5% and a decrease in β sheets of 4%, back towards the native peptide. The β_2M showed similar trends to Aβ(1-40) though to a lesser degree (**Figure 5.8c**). Addition of SiO_4^{4-} (100 μM) after the Al^{3+} (300 μM) seems to have little effect on reversing the changes due to the Al^{3+} and when added before the Al^{3+} increased the α helices by 4%, towards the native value. However, a higher concentration of SiO_4^{4-} (300 μM) added both before and after the Al^{3+} (300 μM) resulted in a slight reversal in the changes caused by the Al^{3+} with further increases in α helices (6% for SiO_4^{4-} added before) and decreases in β sheets of (4% for SiO_4^{4-} added before).

Figure 5.7a

CD spectra of the synthetic Aβ(1-43) treated with Al^{3+} (50, 150, and 300 μM) in TFE/tris buffer. The percentage secondary structures are shown below.

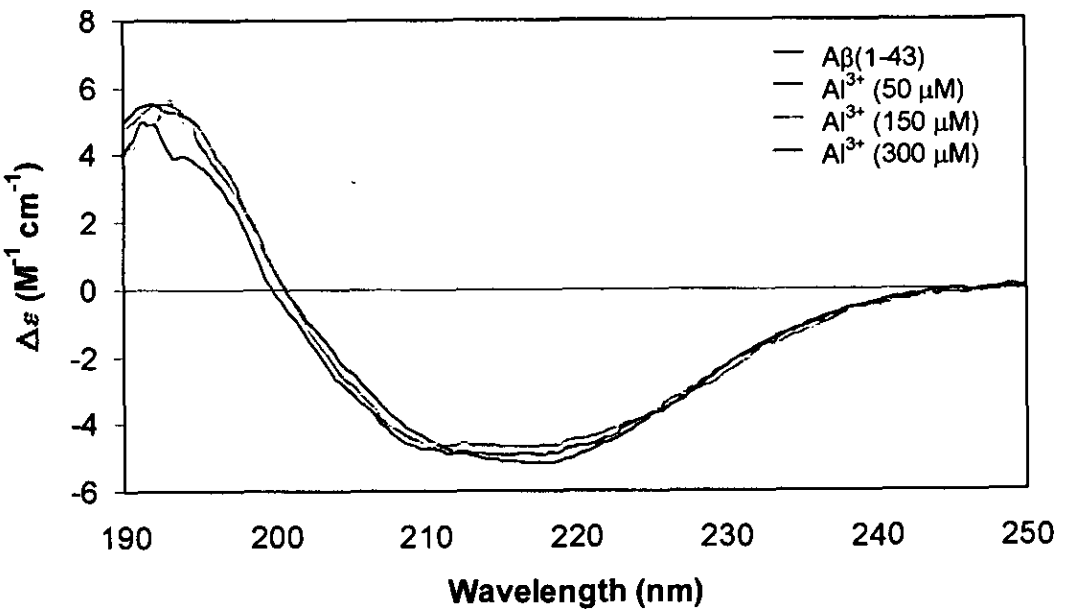

Secondary structure	Percentage secondary structural values (%)			
	Aβ(1-43)	Al^{3+} (50 μM)	Al^{3+} (150 μM)	Al^{3+} (300 μM)
Helix	40.7	40.3	40.3	38.9
Beta Sheets	15.0	15.3	15.6	17.2
Beta-Turn	17.5	17.7	17.9	18.1
Random Coil	26.8	26.7	26.3	25.8

Figure 5.7b

CD spectra of the synthetic Aβ(1-42) treated with Al^{3+} (50, 150, 300, and 400 μM) in TFE/tris buffer. The percentage secondary structures are shown below. Shaded values are changes greater 3% from the native peptide.

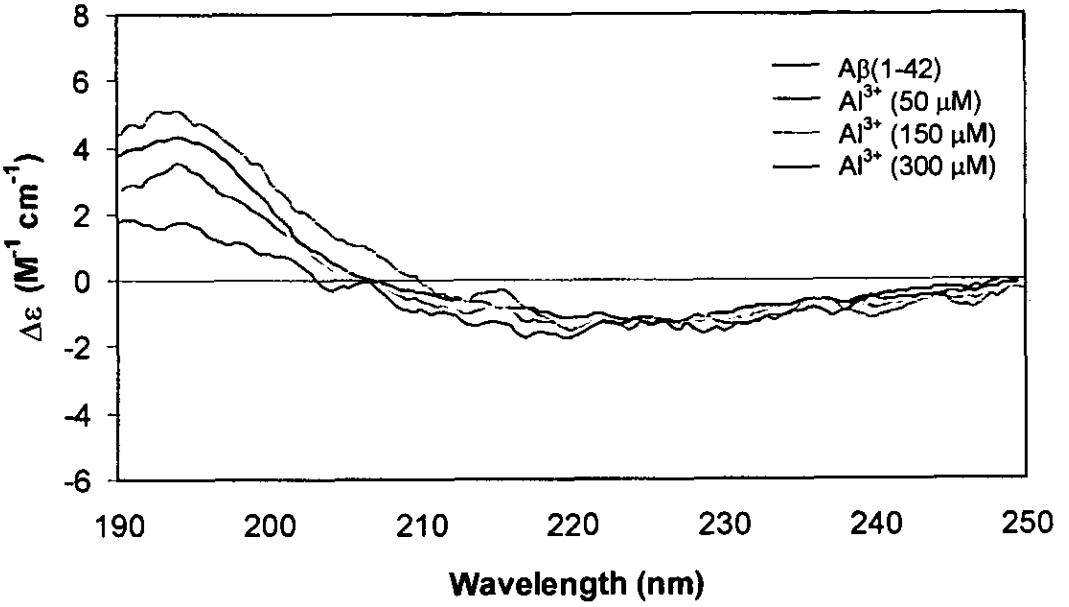

Secondary structure	Percentage secondary structural values (%)			
	Aβ(1-42)	Al^{3+} (50 μM)	Al^{3+} (150 μM)	Al^{3+} (300 μM)
Helix	20.5	20.8	19.6	18.5
Beta Sheets	24.9	22.5	27.3	31.7
Beta-Turn	15.8	15.3	16.1	16.6
Random Coil	38.8	42.1	38.7	37.3

Figure 5.7c

CD spectra of the Aβ extract treated with Al^{3+} (50, 150, 300 μM) in TFE/tris buffer.

The percentage secondary structures are shown below.

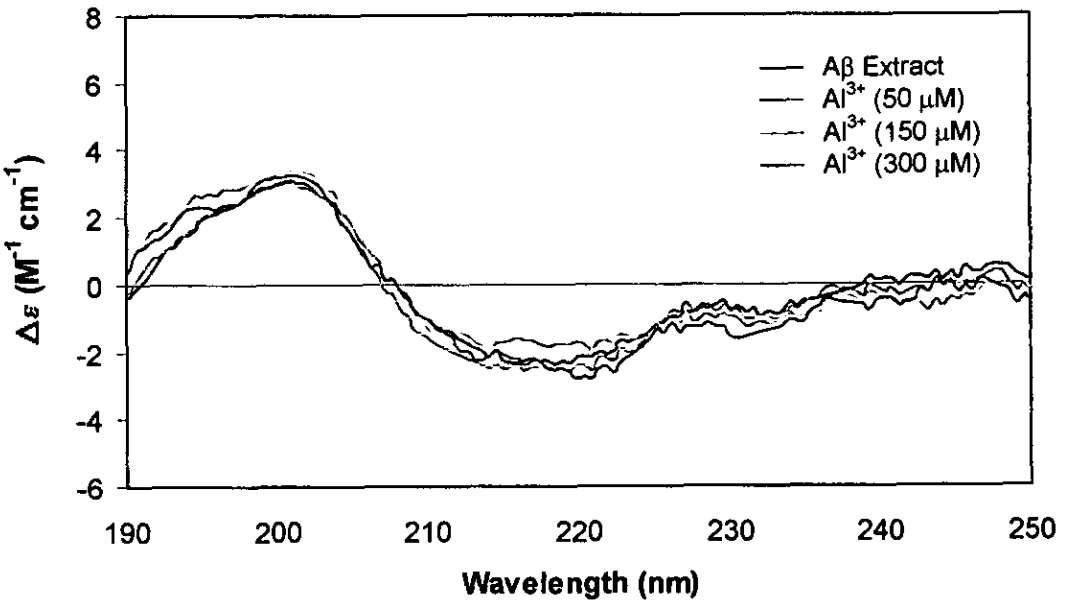

Secondary structure	Percentage secondary structural values (%)			
	Extract	Al^{3+} (50 μM)	Al^{3+} (150 μM)	Al^{3+} (300 μM)
Helix	11.3	11.1	11.0	10.9
Beta Sheets	35.5	36.0	35.3	35.0
Beta-Turn	17.6	17.5	17.4	17.3
Random Coil	37.1	37.3	38.0	38.6

Figure 5.7d

CD spectra of the synthetic Aβ(1-40) treated with Al^{3+} (50, 150, 300 and 400 μM) in TFE/tris buffer. The percentage secondary structures are shown below. Shaded values are changes greater 3% from the native peptide.

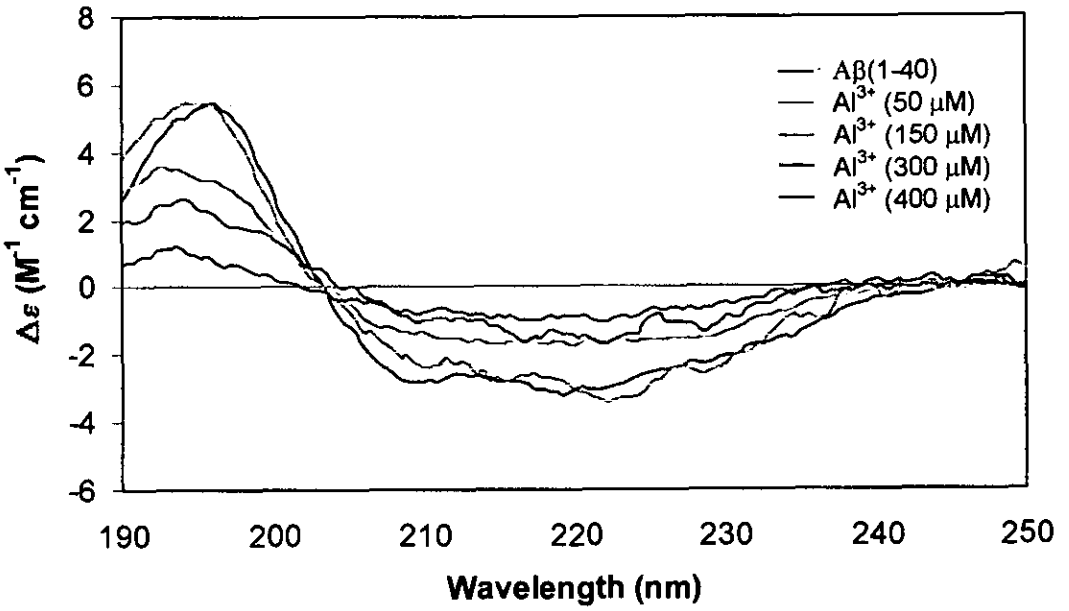

Secondary structure	Percentage secondary structural values (%)				
	Aβ(1-40)	Al^{3+} (50 μM)	Al^{3+} (150 μM)	Al^{3+} (300 μM)	Al^{3+} (400 μM)
Helix	36.9	30.8	21.9	15.5	18.5
Beta Sheets	17.6	18.1	22.8	26.3	25.1
Beta-Turn	16.8	16.8	16.7	16.9	16.3
Random Coil	33.8	34.3	37.2	40.3	38.1

Figure 5.7e

CD spectra of the synthetic β_2M treated with Al^{3+} (50, 150, 300 and 400 μM) in TFE/tris buffer. The percentage secondary structures are shown below. Shaded values are changes greater 3% from the native peptide.

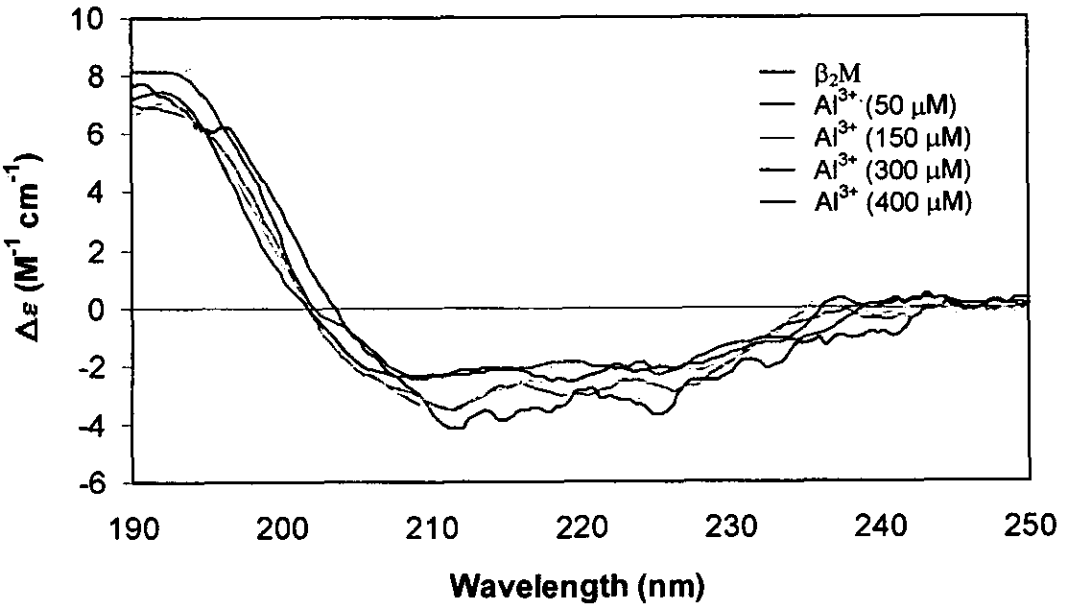

Secondary structure	Percentage secondary structural values (%)				
	β_2M	Al^{3+} (50 μM)	Al^{3+} (150 μM)	Al^{3+} (300 μM)	Al^{3+} (400 μM)
Helix	37.5	35.8	34.2	23.2	24.4
Beta Sheets	15.2	16.1	17.7	23.7	31.2
Beta-Turn	15.8	17.1	17.4	16.5	16.6
Random Coil	33.4	30.9	30.8	36.7	33.7

Figure 5.8a

The CD spectra of Aβ(1-40) peptide with Al^{3+} (150, 300 μM) and SiO_4^{4-} (300 μM) in TFE/tris buffer. The percentage secondary structural values are shown below. Shaded values are changes greater 3% from the native peptide.

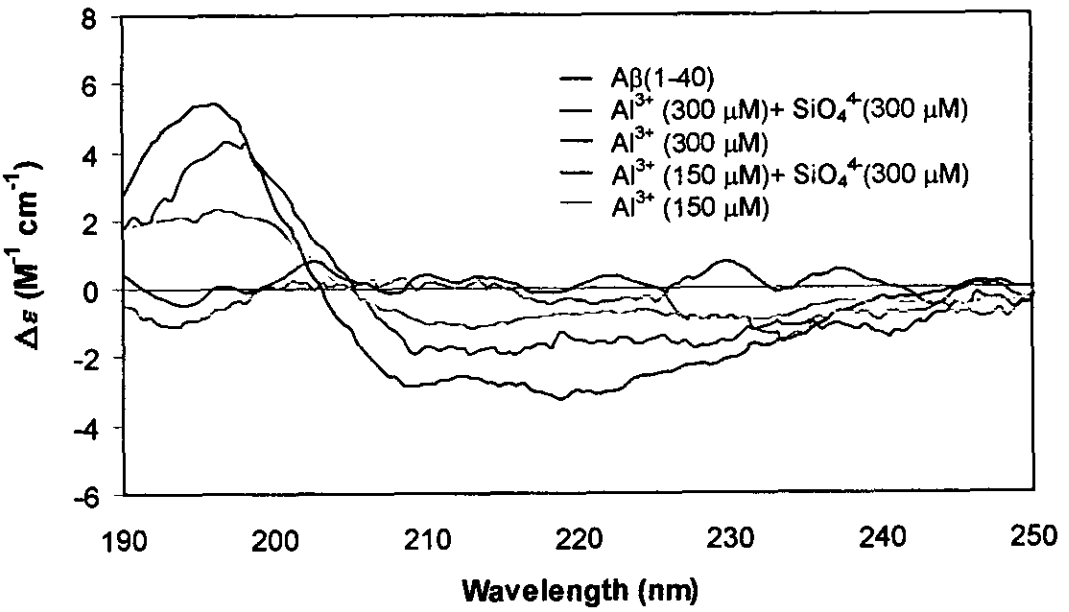

Secondary structure	Percentage secondary structural values (%)				
	Aβ(1-40)	Al^{3+} (150 μM)	Al^{3+} (300 μM)	Al^{3+} (150μM)/ SiO_4^{4-} (300μM)	Al^{3+} (300μM)/ SiO_4^{4-} (300μM)
Helix	36.9	21.9	15.5	26.2	18.4
Beta Sheets	16.6	22.8	26.3	20.8	28.3
Beta-Turn	16.8	16.7	16.9	16.5	15.9
Random Coil	33.8	37.2	40.3	36.5	38.4

Figure 5.8b

The CD spectra of Aβ(1-40) peptide with Al^{3+} (300 μM) and SiO_4^{4-} (300 μM) in TFE/tris buffer added before and after the Al^{3+}. The percentage secondary structural values are shown below. Shaded values are changes greater 3% from the native peptide.

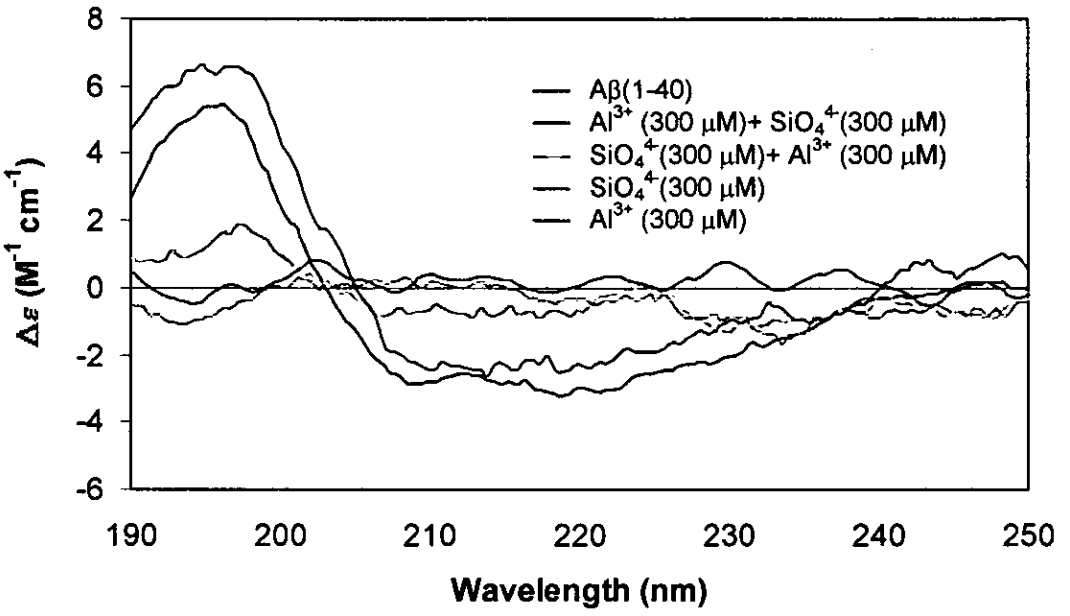

Secondary structure	Percentage secondary structural values (%)				
	Aβ(1-40)	SiO_4^{4-} (300 μM)	Al^{3+} (300 μM)	Al^{3+} (300μM)/ SiO_4^{4-} (300μM)	SiO_4^{4-} (300μM)/ Al^{3+} (300μM)
Helix	36.9	31.5	15.5	18.4	20.5
Beta Sheets	17.6	17.1	26.3	28.3	22.4
Beta-Turn	16.8	16.5	16.9	15.9	16.6
Random Coil	33.8	34.9	40.3	36.4	37.5

Figure 5.8c

The CD spectra of β_2M peptide with Al^{3+} (300 μM) and SiO_4^{4-} (300 μM) in TFE/tris buffer. The percentage secondary structures are shown below. Shaded values are changes greater 3% from the native peptide.

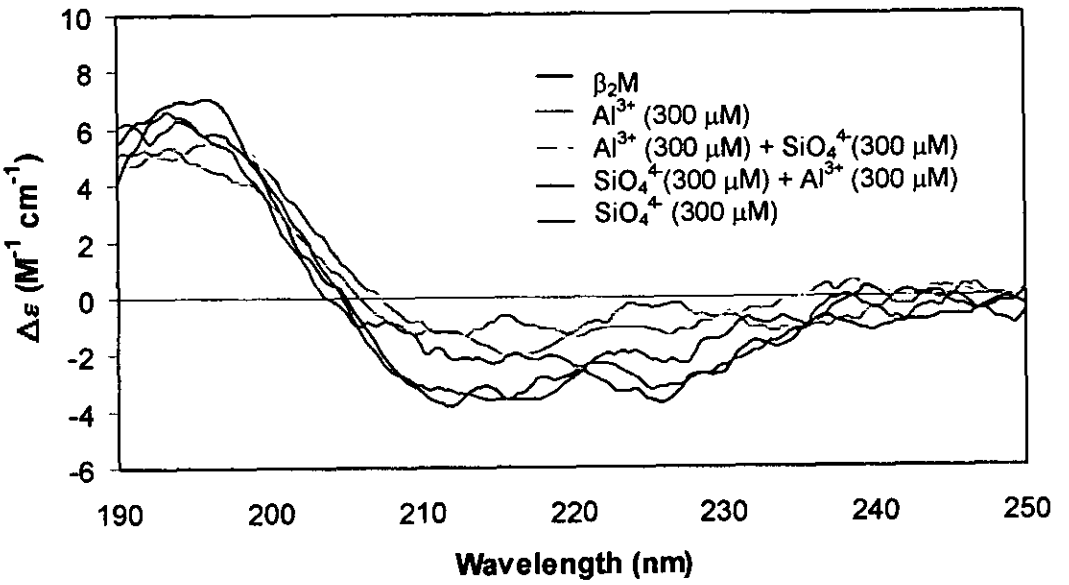

Secondary structure	Percentage secondary structural values (%)				
	β_2M	SiO_4^{4-} (300 μM)	Al^{3+} (300 μM)	Al^{3+} (300μM)/ SiO_4^{4-} (300μM)	SiO_4^{4-} (300μM)/ Al^{3+} (300μM)
Helix	37.5	32.5	23.2	24.0	29.3
Beta Sheets	15.2	16.1	23.7	21.3	18.8
Beta-Turn	15.8	16.3	16.5	16.0	16.6
Random Coil	31.4	35.2	36.7	38.7	35.3

5.2.6 Amyloid proteins treated with glycosaminoglycans.

The Aβ(1-40) amyloid peptide and β_2M peptide were both treated with various glycosaminoglycans; heparin (HEP) (50, 500 μg ml^{-1}), HS (50, 500 μg ml^{-1}), HSPG (50, 500 μg ml^{-1}), KS (50, 500 μg ml^{-1}), DS (50, 500 μg ml^{-1}), CS (50, 500 μg ml^{-1}) and sodium sulphate (50, 500 μg ml^{-1}). The β_2M and Aβ(1-40) peptides did not appear to undergo any significant change in the spectral profiles on binding sulphates and GAGs.

The addition of the lower concentration GAGs (50 μg ml^{-1}, data not shown) showed very similar spectrum to the spectrum of the higher concentration of GAG (500 μg ml^{-1}). The GAGs on their own seem to have little effect on the secondary structure of the Aβ(1-40) and β_2M with maximum change of about 5%. The most notable changes for Aβ(1-40) are with Na_2SO_4 (α ↓5% and β ↑3%) and DS (α ↓4.5%) (**Figure 5.9a**). The most notable changes for β_2M are with HS (α ↓4%) and KS (α ↓5%) (**Figure 5.9b**).

5.2.7 Amyloid proteins treated with glycosaminoglycans combined with aluminium.

The CD spectrum in **Figure 5.10a** showed that the Aβ(1-40) peptide treated with physiological concentrations of Al^{3+} (1.5 μM) and Aβ(1-40) with the GAGs alone, both showed little change in the secondary structures. There was a slight change of in both α helices (↓6%) and β sheets (↑8%) when the aluminium was combined with HS, HSPG or DS. Similar effects were seen with β_2M. β_2M treated with Al^{3+} (1.5 μM) or GAGs showed little change with slight changes of about 3% in both α helices and β sheets. There was a change of in both α helices (↓10%) and β sheets (↑9%) when the Al^{3+} was combined with HS, DS or CS (**Figure 5.10b**).

5.2.8 Amyloid proteins treated with glycosaminoglycans combined with copper or zinc.

Aβ(1-40) peptide with both DS/Cu^{2+} and HSPG/Cu^{2+} show little difference in the secondary structures compared to Cu^{2+} (10 μM) alone. With HS/Cu^{2+} there was a slight reversal in the changes of secondary structure caused by copper itself (**Figure 5.11a**). β_2M with both DS/Cu^{2+} and HSPG/Cu^{2+} seem to enhance the effects due to copper itself i.e. further decreases in α helices and increases in β sheets. Again, with HS/Cu^{2+} there was a slight reversal in the changes of secondary structure caused by copper itself (**Figure 5.11b**). Similar results are also seen with β_2M and zinc. β_2M with DS/Zn^{2+} and KS/Zn^{2+} seem to enhance the effects due to Zn^{2+} (10 μM) itself i.e. a further decrease in α helices and an increase in β sheets, where as HS appears to have no effect. (**Figure 5.11c**).

5.2.9 Amyloid proteins treated with glycosaminoglycans and calcium.

Aβ(1-40) peptide and β_2M were treated with combinations of Ca^{2+} (16 μM) and HEP, Na_2SO_4, HS, HSPG, KS, DS and CS. The CD spectra of Aβ(1-40) peptide treated with HSPG, CS, KS and DS with Ca^{2+} (16 μM) are shown in **Figure 5.12a.** The CD spectra show that combinations of KS or DS and calcium do not seem to alter the secondary structural changes with just the Ca^{2+} (16 μM) itself. Both HSPG and CS combined with calcium cause further decreases in α helices but only the CS/Ca^{2+} caused a further increase in β sheets. Where as HEP, HS, and Na_2SO_4 with Ca^{2+} show a further increase in α helix and a decrease in β sheet compared to Ca^{2+} itself, i.e. decreasing the effects of calcium, as shown in **Figure 5.12b**. β_2M with Na_2SO_4/Ca^{2+}, DS/Ca^{2+} and HEP/Ca^{2+} cause no further changes with respect to calcium (**Figure 5.12c**). With KS/Ca^{2+}, CS/Ca^{2+}, HS/Ca^{2+} and HSPG/Ca^{2+} there are further decreases in α helices and increases in β sheets indicating that these combinations enhance the effects of Ca^{2+} (**Figure 5.12d**).

Figure 5.9a

CD spectra of the Aβ(1-40) treated with sodium sulphate sodium heparin (HEP), heparan sulphate (HP), dermatan sulphate (DS), chondroitin sulphate (CS), keratan sulphate (KS) and heparan sulphate proteoglycan (HSPG) (all 500 μg ml^{-1}) in TFE/tris buffer. The percentage secondary structures are shown below. Shaded values are changes greater 3% from the native peptide.

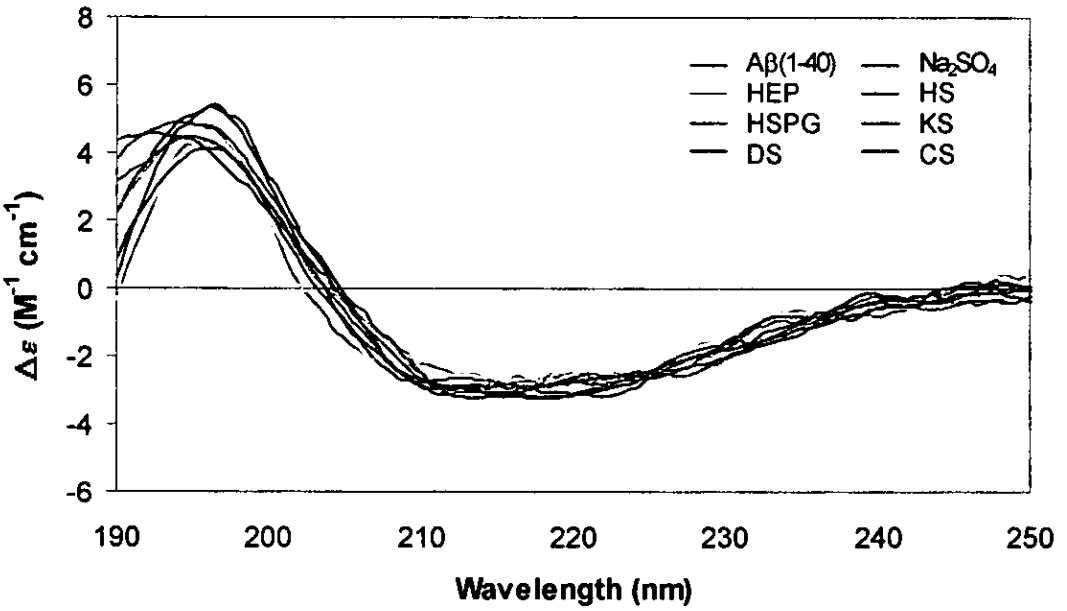

Secondary structure	Percentage secondary structural values (%)							
	Aβ(1-40)	Na_2SO_4	HEP	HS	HSPG	KS	DS	CS
Helix	36.9	32.4	31.2	30.4	31.4	29.5	32.4	30.9
Beta Sheets	17.6	19.1	19.0	18.9	17.1	18.1	17.2	19.1
Beta-Turn	16.8	16.5	17.7	17.1	16.4	16.8	16.7	16.5
Random Coil	33.7	35.0	31.0	33.5	35.0	34.4	33.6	35.5

Figure 5.9b

CD spectra of the β_2M treated with sodium sulphate sodium heparin (HEP), heparan sulphate (HP), dermatan sulphate (DS), chondroitin sulphate (CS), keratan sulphate (KS) and heparan sulphate proteoglycan (HSPG) (all 500 $\mu g\ ml^{-1}$) in TFE/tris buffer. The percentage secondary structures are shown below. Shaded values are changes greater 3% from the native peptide.

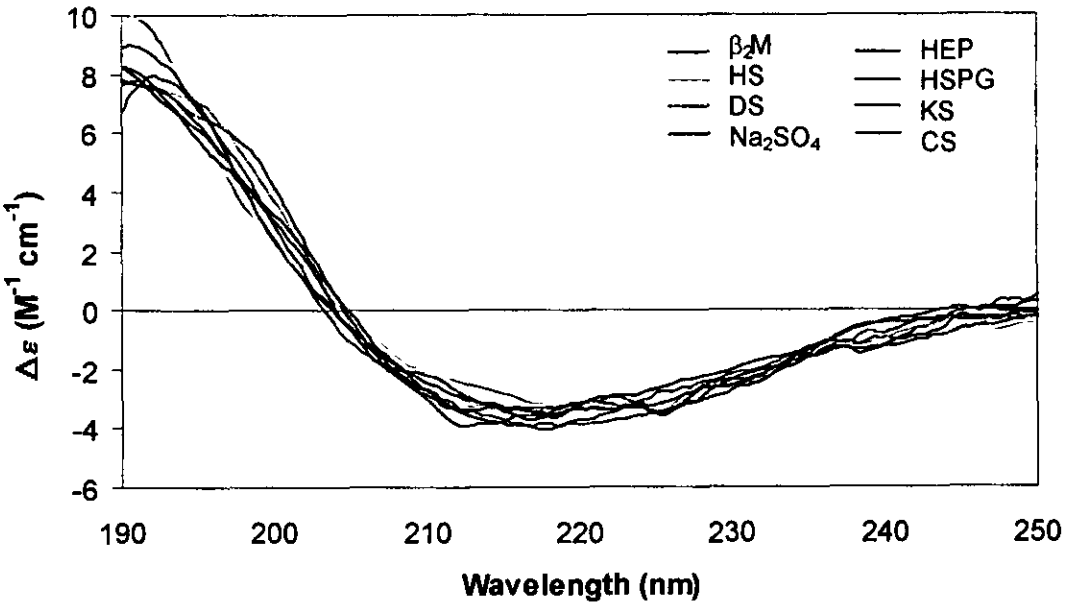

Secondary structure	Percentage secondary structural values (%)							
	β_2M	Na_2SO_4	HEP	HS	HSPG	KS	DS	CS
Helix	37.5	35.4	36.4	33.3	35.1	32.5	35.8	35.7
Beta Sheets	15.2	13.8	13.1	15.8	16.7	15.8	15.7	12.8
Beta-Turn	15.8	15.6	15.3	16.3	17.6	17.7	17.3	16.4
Random Coil	31.4	34.9	35.2	34.4	29.4	32.7	31.4	33.1

Figure 5.10a

The CD spectra of Aβ(1-40) peptide treated with HS, HSPG and DS with Al^{3+} (1.5 μM) in TFE/tris buffer. The percentage secondary structures are shown below. Shaded values are changes greater 3% from the native peptide.

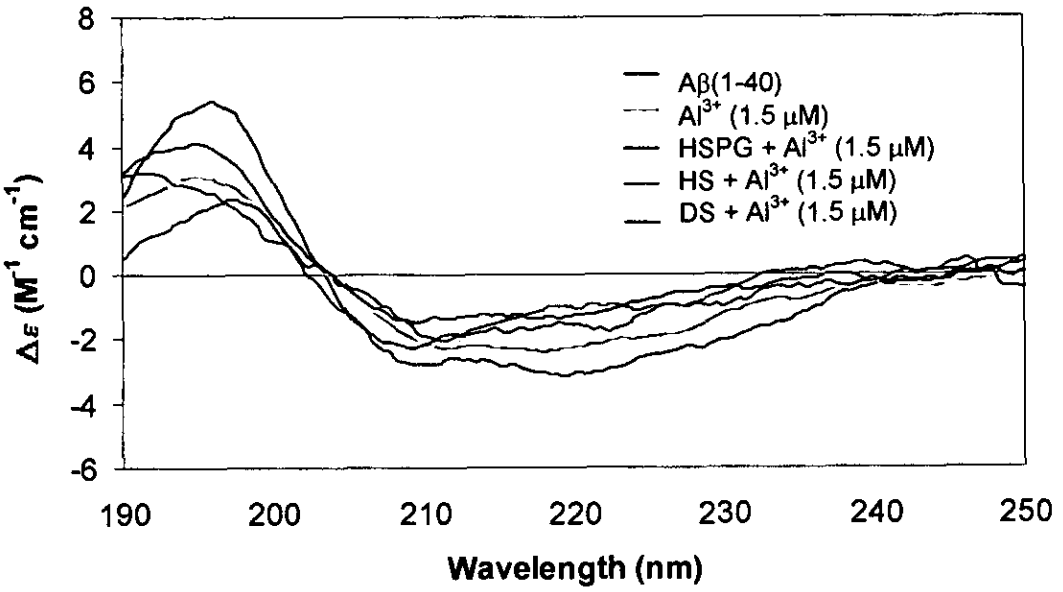

Secondary structure	Percentage secondary structural values (%)							
	Aβ(1-40)	HS	HSPG	DS	Al^{3+}	HS+Al^{3+}	HSPG+Al^{3+}	DS+Al^{3+}
Helix	36.9	30.4	31.5	32.4	29.8	25.2	25.1	26.8
Beta Sheets	17.6	18.9	17.0	17.2	18.5	23.3	23.5	25.2
Beta-Turn	16.8	17.1	16.5	16.7	16.7	16.8	17.2	16.9
Random Coil	33.8	33.5	35.0	33.6	34.3	35.1	33.4	34.3

Figure 5.10b

The CD spectra of β_2M peptide treated with HS, DS and CS with Al^{3+} (1.5 μM) in TFE/tris buffer. The percentage secondary structures are shown below. Shaded values are changes greater 3% from the native peptide.

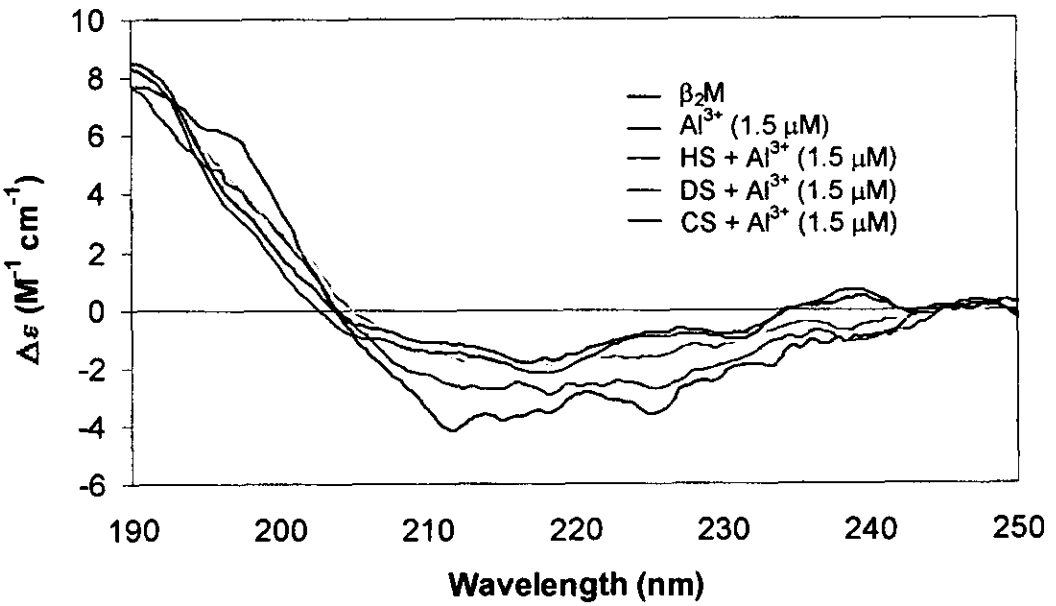

Secondary structure	Percentage secondary structural values (%)							
	β_2M	HS	DS	CS	Al^{3+}	HS+Al^{3+}	DS+Al^{3+}	CS+Al^{3+}
Helix	37.5	33.3	35.8	35.7	29.8	24.3	25.6	26.0
Beta Sheets	15.2	15.9	15.7	14.9	18.4	20.9	22.5	21.8
Beta-Turn	15.8	16.4	17.3	16.4	16.5	15.9	16.9	16.7
Random Coil	31.4	34.4	31.5	33.1	32.9	38.9	34.9	35.6

Figure 5.11a

The CD spectra of Aβ(1-40) peptide treated with HS, HSPG, KS and DS with Cu^{2+} (10 μM) in TFE/tris buffer. The percentage secondary structures are shown below. Shaded values are changes greater 3% from the native peptide.

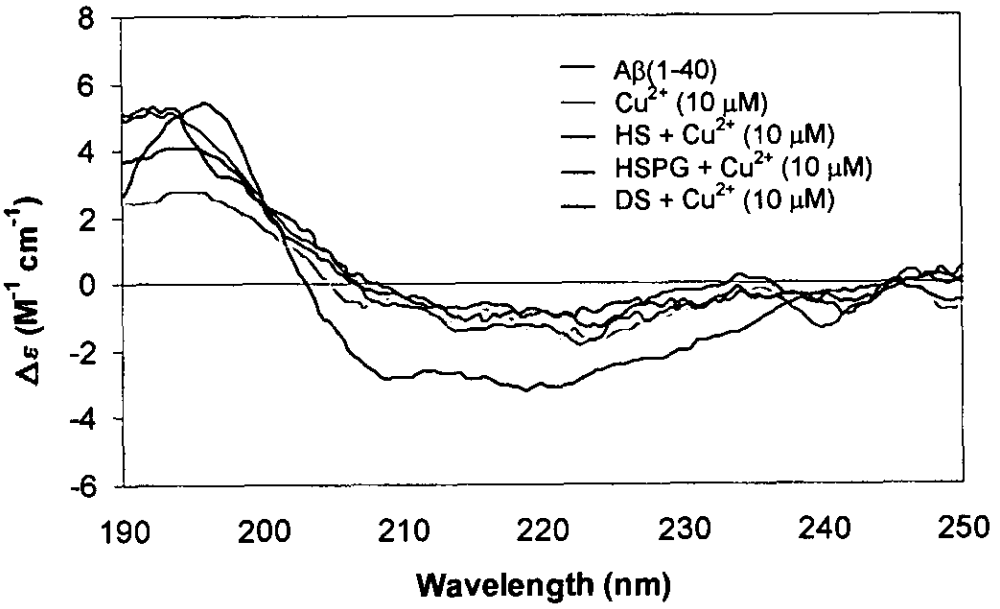

Secondary structure	Percentage secondary structural values (%)							
	Aβ(1-40)	HS	DS	HSPG	Cu^{2+}	HS+Cu^{2+}	DS+Cu^{2+}	HSPG+Cu^{2+}
Helix	36.9	30.4	32.4	31.5	19.5	27.1	21.8	20.7
Beta Sheets	17.6	18.9	17.2	17.0	27.8	19.3	25.3	24.6
Beta-Turn	16.8	17.1	16.7	16.5	16.2	16.1	16.3	15.9
Random Coil	33.8	33.5	33.6	35.0	36.5	37.5	36.5	38.9

Figure 5.11b

The CD spectra of β_2M peptide treated with HS, HSPG and DS with Cu^{2+} (10 μM). The percentage secondary structures are shown below. Shaded values are changes greater 3% from the native peptide.

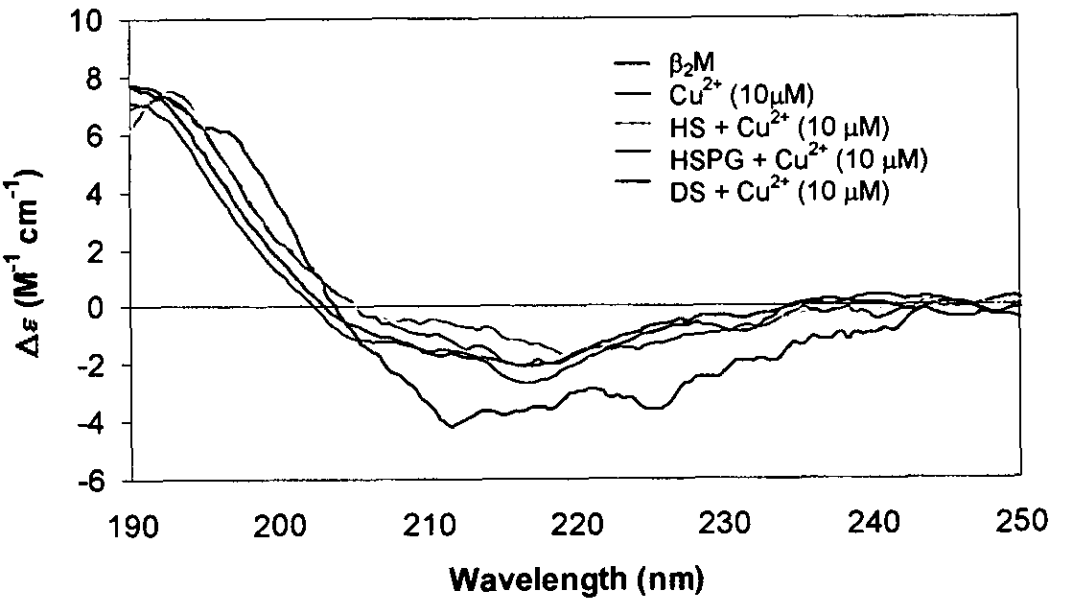

Secondary structure	Percentage secondary structural values (%)							
	β_2M	HS	DS	HSPG	Cu^{2+}	HS+Cu^{2+}	DS+Cu^{2+}	HSPG+Cu^{2+}
Helix	37.5	33.3	35.8	35.1	34.2	35.4	28.2	26.7
Beta Sheets	15.2	16.0	15.7	16.8	16.4	14.6	21.7	20.0
Beta-Turn	15.8	16.4	17.3	17.6	15.0	16.2	17.3	16.4
Random Coil	31.4	34.4	31.5	29.4	32.2	33.7	32.5	36.7

Figure 5.11c

The CD spectra of β_2M peptide treated with HS, DS and KS with Zn^{2+} (10 μM). The percentage secondary structures are shown below. Shaded values are changes greater 3% from the native peptide.

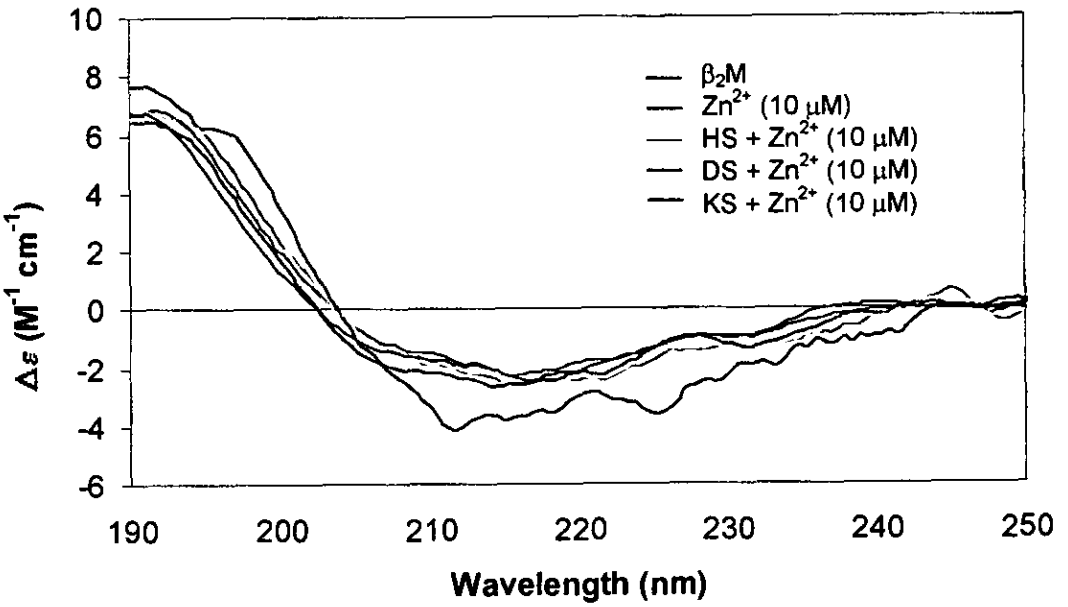

Secondary structure	Percentage secondary structural values (%)							
	β_2M	HS	DS	KS	Zn^{2+}	HS+Zn^{2+}	DS+Zn^{2+}	KS+Zn^{2+}
Helix	37.5	33.3	32.9	32.5	36.5	32.4	29.7	31.1
Beta Sheets	15.2	16.0	18.3	15.8	15.8	18.4	25.2	19.7
Beta-Turn	15.8	16.4	17.3	17.7	16.2	17.1	18.5	17.6
Random Coil	31.4	34.4	31.5	32.7	30.4	31.2	26.7	30.5

Figure 5.12a

The CD spectra of Aβ(1-40) peptide treated with HSPG, KS and DS with Ca^{2+} (16 μM) in TFE/tris buffer. The percentage secondary structures are shown below. Shaded values are changes greater 3% from the native peptide.

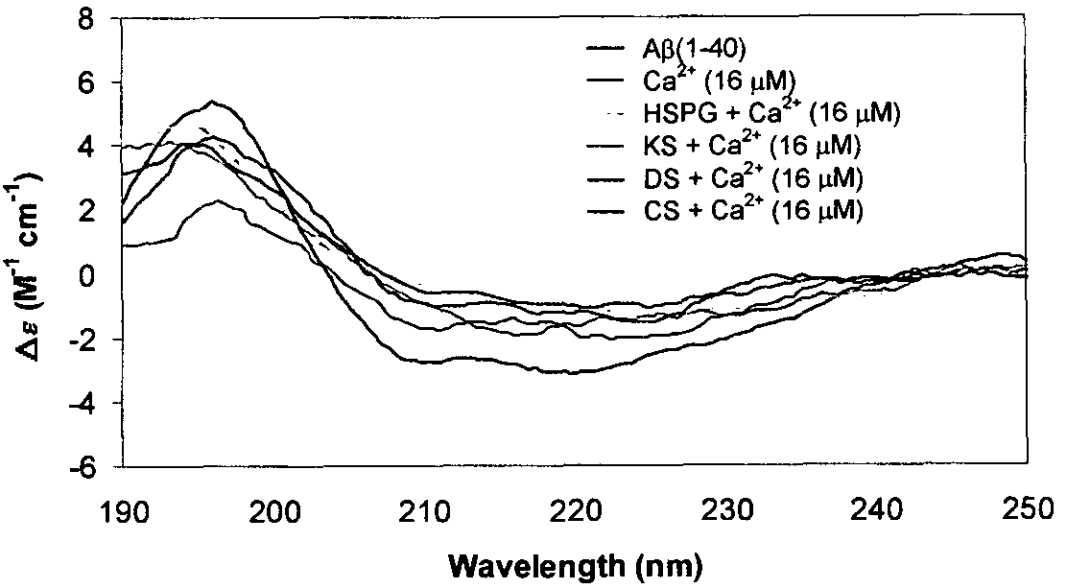

Secondary structure	Percentage secondary structural values (%)									
	Aβ(1-40)	KS	DS	HSPG	CS	Ca^{2+}	KS+Ca^{2+}	DS+Ca^{2+}	HSPG+Ca^{2+}	CS+Ca^{2+}
Helix	36.9	29.5	32.4	31.5	30.9	22.4	22.6	21.6	19.9	20.2
Beta Sheets	17.6	18.1	17.2	17.0	19.0	26.6	25.8	26.6	26.2	29.1
Beta-Turn	16.8	16.8	16.7	16.5	16.5	16.2	16.5	15.9	15.4	15.5
Random Coil	33.8	34.4	33.6	35.0	35.5	34.4	36.3	39.0	40.7	40.1

Figure 5.12b

The CD spectra of Aβ(1-40) peptide treated with heparin, HS, Na_2SO_4 and CS with Ca^{2+} (16 μM) in TFE/tris buffer. The percentage secondary structures are shown below. Shaded values are changes greater 3% from the native peptide.

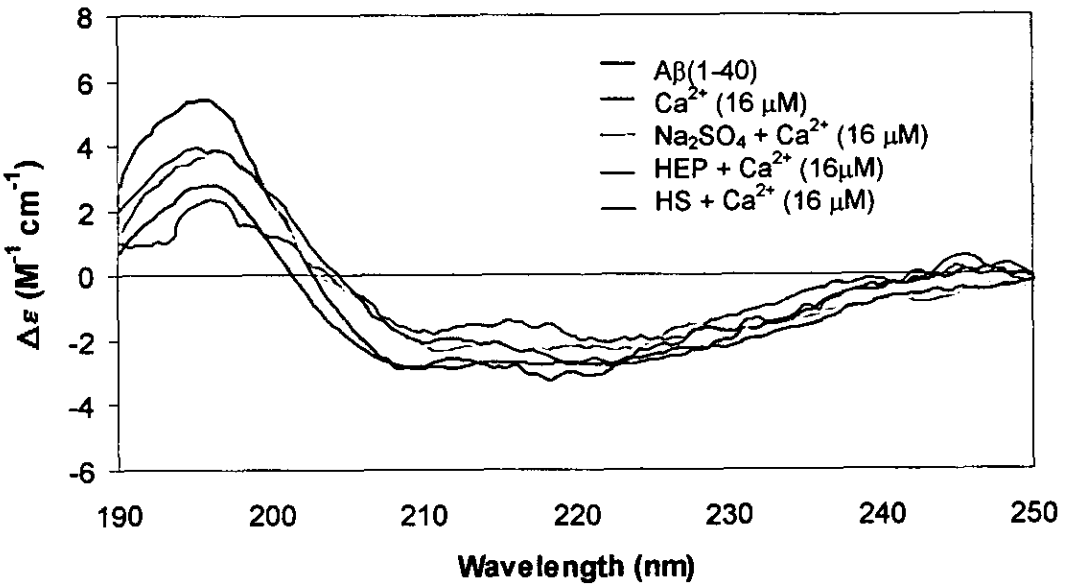

Secondary structure	Percentage secondary structural values (%)							
	Aβ(1-40)	HEP	HS	Na_2SO_4	Ca^{2+}	HEP+Ca^{2+}	HS+Ca^{2+}	Na_2SO_4+Ca^{2+}
Helix	36.9	31.3	30.4	32.4	22.4	26.3	26.6	25.4
Beta Sheets	17.6	19.1	18.9	19.1	26.6	20.9	19.3	22.6
Beta-Turn	16.8	17.7	17.1	16.5	16.2	16.8	17.0	16.7
Random Coil	33.8	31.0	33.5	35.0	34.4	34.8	31.6	35.4

Figure 5.12c

(c) The CD spectra of β_2M peptide treated with Heparin (HEP), HSPG and CS with Ca^{2+} (16 μM) in TFE/tris buffer. The percentage secondary structures are shown below. Shaded values are changes greater 3% from the native peptide.

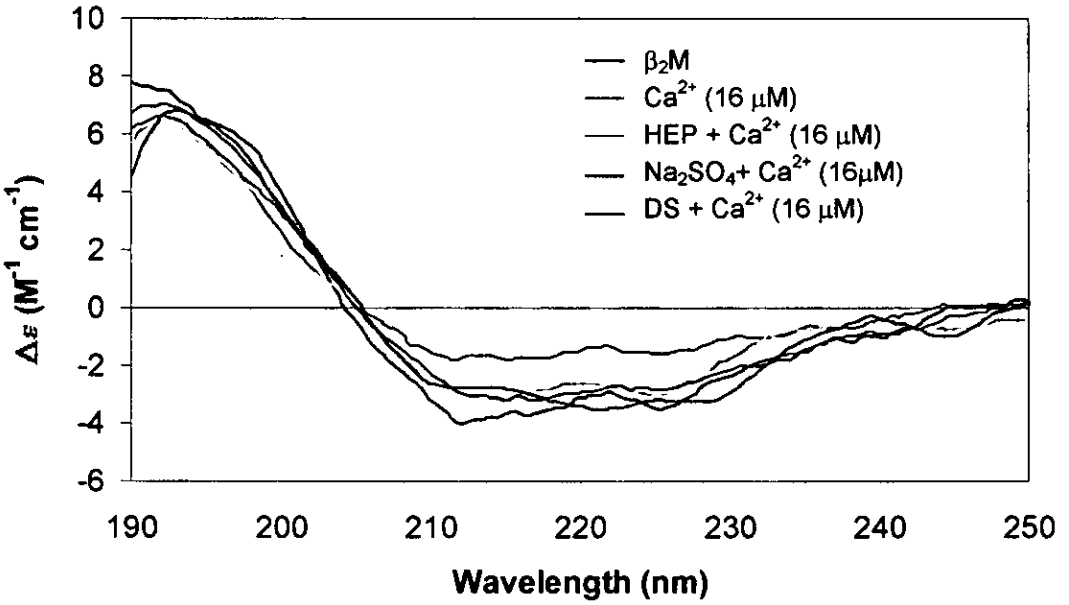

Secondary structure	Percentage secondary structural values (%)							
	β_2M	HEP	DS	Na_2SO_4	Ca^{2+}	HEP+Ca^{2+}	DS+Ca^{2+}	Na_2SO_4+Ca^{2+}
Helix	37.5	36.4	26.4	28.3	35.0	31.2	30.4	29.3
Beta Sheets	15.2	13.0	20.9	19.1	17.1	14.5	17.6	18.9
Beta-Turn	15.8	15.3	16.6	17.7	16.7	14.9	16.7	16.8
Random Coil	31.4	35.2	36.0	31.0	32.1	39.1	35.4	34.8

Figure 5.12d

The CD spectra of β_2M peptide treated with sodium HS, DS, KS and Na_2SO_4 with Ca^{2+} (16 μM) in TFE/tris buffer. The percentage secondary structures are shown below. Shaded values are changes greater 3% from the native peptide.

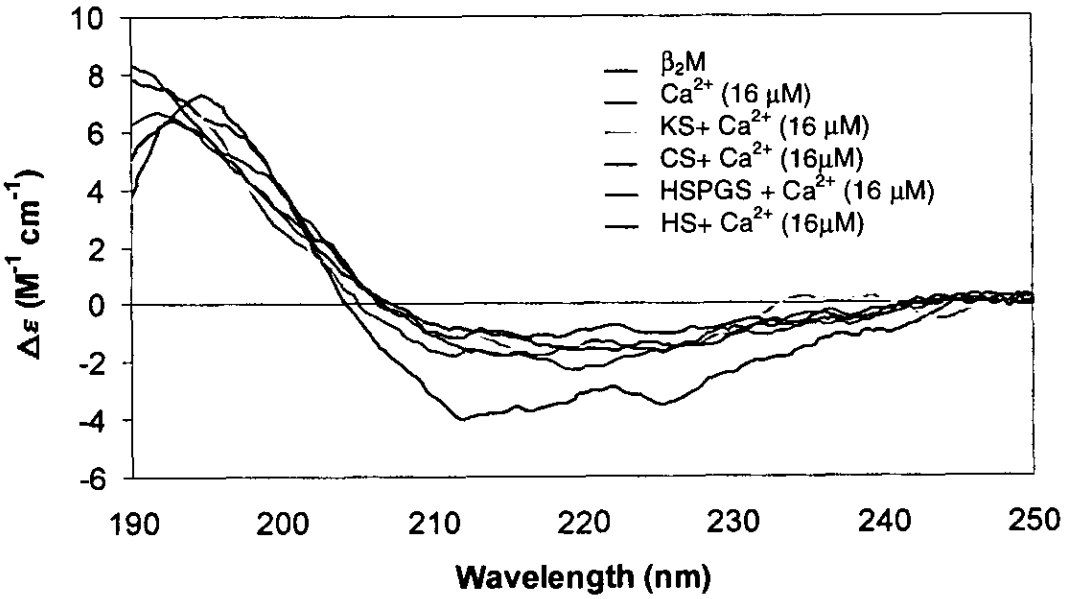

Secondary structure	Percentage secondary structural values (%)									
	β_2M	HSPG	HS	CS	KS	Ca^{2+}	HSPG+Ca^{2+}	HS+Ca^{2+}	CS+Ca^{2+}	KS+Ca^{2+}
Helix	37.5	35.1	29.4	35.7	28.9	35.0	28.9	26.6	26.8	20.2
Beta Sheets	15.2	16.7	19.0	14.8	19.0	17.1	19.2	20.3	19.3	20.1
Beta-Turn	15.8	17.6	17.1	16.4	16.5	16.7	16.3	17.0	15.7	15.5
Random Coil	31.4	29.4	33.5	33.1	35.5	32.1	36.2	31.6	38.9	40.1

5.3 Summary of results.

The following tables (**Table 5.3**) show a summary of all the results.

Aβ(1-40)	α helix	Random	β sheet
Ca (100 μM)	↓↓	–	↑↑
Mg (100 μM)	–	–	–
Cu^{2+} (10μM)	↓↓	–	↑↑
Cu^{2+} (50 μM)	↓↓	–	↑↑↑
Cu^{2+} (100 μM)	↓↓↓	↓	↑↑↑
Zn^{2+} (10 μM)	↓↓	–	↑↑
Zn^{2+} (50 μM)	↓↓	↓	↑↑↑
Zn^{2+} (100 μM)	↓↓↓	↓	↑↑↑
Cu^{2+} / Zn^{2+} (100 μM)	↓↓↓	–	↑↑↑
Al^{3+} (50 μM)	↓	–	–
Al^{3+} (150 μM)	↓↓	–	↑↑
Al^{3+} (300 μM)	↓↓↓	–	↑↑↑
Al^{3+} (400 μM)	↓↓↓	–	↑↑↑
SiO_4^{4-} (300 μM)	–	–	–
Al^{3+} (150 μM) / SiO_4^{4-} (300 μM)	↓↓	–	↑↑
Al^{3+} (300 μM) / SiO_4^{4-} (300 μM)	↓↓	–	↑↑
SiO_4^{4-} (300 μM) / Al^{3+} (300 μM)	↓↓	–	↑↑
Na_2SO_4 (500 μg ml^{-1})	↓	–	↑
HEP (500 μg ml^{-1})	↓	–	–
HS (500 μg ml^{-1})	↓	–	–
HSPG (500 μg ml^{-1})	–	–	–
KS (500 μg ml^{-1})	↓	–	↑
DS (500 μg ml^{-1})	–	–	–
CS (500 μg ml^{-1})	–	–	–
HS (500 μg ml^{-1}) / Al^{3+} (1.5 μM)	↓	–	↑
HSPG (500 μg ml^{-1}) / Al^{3+} (1.5 μM)	↓	–	↑
DS (500 μg ml^{-1}) / Al^{3+} (1.5 μM)	↓	–	↑
HS (500 μg ml^{-1}) / Cu^{2+} (10 μM)	↓	–	↑
HSPG (500 μg ml^{-1}) / Cu^{2+} (10 μM)	↓	–	↑
DS (500 μg ml^{-1}) / Cu^{2+} (10 μM)	↓	–	↑↑
HS (500 μg ml^{-1}) / Ca (16 μM)	↓↓	↑	↑↑
HSPG (500 μg ml^{-1}) / Ca (16 μM)	↓↓	–	↑↑
KS (500 μg ml^{-1}) / Ca (16 μM)	↓↓	↑	↑↑
DS (500 μg ml^{-1}) / Ca (16 μM)	↓	–	↑
CS (500 μg ml^{-1}) / Ca (16 μM)	↓	–	↑
HEP (500 μg ml^{-1}) / Ca (16 μM)	↓	–	↑
Na_2SO_4 (500 μg ml^{-1}) / Ca (16 μM)	↓↓	↓	↑↑

Table 5.2a - Experiments with Aβ(1-40) (↑ (>3%), ↑↑ (>6%), ↑↑↑ (>10%) difference from the native peptides).

β_2M	α helix	β sheet	Random
Cu^{2+} (100 μM)	↓	—	—
Zn^{2+} (100 μM)	—	—	—
Ca (100 μM)	↓	↑	—
Mg (100 μM)	—	—	—
Al^{3+} (50 μM)	—	↑	↓
Al^{3+} (150 μM)		↑	↓
Al^{3+} (300 μM)	↓↓	↑↑	↑
Al^{3+} (400 μM)	↓↓	↑↑	—
SiO_4^{4-} (300 μM)	—	—	—
Al^{3+} (300 μM)/SiO_4^{4-} (100 μM)		↑↑	↑
Al^{3+} (300 μM)/SiO_4^{4-} (300 μM)		↑↑	↑
SiO_4^{4-} (100 μM)/Al^{3+} (300 μM)		↑↑	—
SiO_4^{4-} (300 μM)/Al^{3+} (300 μM)		↑	—
Na_2SO_4 (500 μg ml^{-1})	—	—	—
HEP (500 μg ml^{-1})	—	—	—
HS (500 μg ml^{-1})		↑	—
HSPG (500 μg ml^{-1})	—	↑	—
KS (500 μg ml^{-1})	↓	↑	—
DS (500 μg ml^{-1})	↓	↑	—
CS (500 μg ml^{-1})	—	—	—
HS (500 μg ml^{-1})/ Al^{3+} (1.5 μM)	↓	↑	↑
HSPG (500 μg ml^{-1})/ Al^{3+} (1.5 μM)	↓	↑	—
KS (500 μg ml^{-1})/ Al^{3+} (1.5 μM)	↓	↑	—
HS (500 μg ml^{-1})/ Cu^{2+} (10 μM)	—	—	—
HSPG (500 μg ml^{-1})/ Cu^{2+} (10 μM)	↓	↑	↑
DS (500 μg ml^{-1})/ Cu^{2+} (10 μM)	↓	↑	—
HS (500 μg ml^{-1})/ Zn^{2+} (10 μM)		↑	—
DS (500 μg ml^{-1})/ Zn^{2+} (10 μM)		↑↑	↓
KS (500 μg ml^{-1})/ Zn^{2+} (10 μM)		↑↑	↓
HS (500 μg ml^{-1})/ Ca (16 μM)	↓↓	↑↑	—
HSPG (500 μg ml^{-1})/ Ca (16 μM)	↓	↑	↑
KS (500 μg ml^{-1})/ Ca (16 μM)	↓↓	↑↑	↓
DS (500 μg ml^{-1})/ Ca (16 μM)	↓	↑↑	↓↓
CS (500 μg ml^{-1})/ Ca (16 μM)	↓	↑	↑
HEP (500 μg ml^{-1})/ Ca (16 μM)	↓	—	↑
Na_2SO_4/ Ca (16 μM)	↓↓	↑↑	—

Table 5.2b - Experiments with β_2M (↑ (>3%), ↑↑ (>6%), ↑↑↑ (>10%) difference from the native peptides).

Aβ(1-43)	α helix	Random	β sheet
Cu^{2+} (100 μM)	—	—	—
Zn^{2+} (100 μM)	—	—	—
Ca (100 μM)	—	—	—
Al^{3+} (50 μM)	—	—	—
Al^{3+} (150 μM)	—	—	—
Al^{3+} (300 μM)	↓	—	↑

Table 5.2c - Experiments with Aβ(1-43) (↑ (>3%), ↑↑ (>6%), ↑↑↑ (>10%) difference from the native peptides).

Aβ(1-42)	α helix	Random	β sheet
Cu^{2+} (100 μM)	↓	↑	↓
Zn^{2+} (100 μM)	↓	↑	↓
Ca (100 μM)	↓	↑	↓
Al^{3+} (50 μM)	—	↑	—
Al^{3+} (150 μM)		—	—
Al^{3+} (300 μM)	↓	—	↑↑
Al^{3+} (400 μM)	↓	↓	↑↑

Table 5.2d - Experiments with Aβ(1-43) (↑ (>3%), ↑↑ (>6%), ↑↑↑ (>10%) difference from the native peptides).

Extract	α helix	Random	β sheet
Cu^{2+} (100 μM)	↓	↓	↑↑↑
Zn^{2+} (100 μM)	↓	↑	↓
Ca (100 μM)	↓	—	↓
Al^{3+} (50 μM)	—	—	—
Al^{3+} (150 μM)	—	—	—
Al^{3+} (300 μM)	—	—	—

Table 5.2e - Experiments with Aβ extract (↑ (>3%), ↑↑ (>6%), ↑↑↑ (>10%) difference from the native peptides).

Prion Protein	α helix	Random	β sheet
Control r[mouse]PrP^c	—	—	—
r[mouse]PrP^c + Phosmet	—	—	—
r[mouse]PrP^c + Phosmet	—	—	—

Table 5.2f - Experiments with prion protein (↑ (>3%), ↑↑ (>6%), ↑↑↑ (>10%) difference from the native peptides).

5.4 Discussion

CD spectroscopy has been used to study the secondary structures of various amyloid peptides Aβ(1-40), Aβ(1-42), Aβ(1-43), the Aβ extract from Alzheimer's disease brain and β_2M. CD spectroscopy has been previously used to study Aβ(1-40) and Aβ(25-35) treated with Al^{3+} [289] and Aβ(1-42) treated with Al^{3+} and SiO_4^{4-}, [289, 314 & 320]. The present experiments extend the work of these studies by the use of other amyloid peptides, with various inorganic elements and GAGs.

5.4.1 Comparison of secondary structural values in other CD studies.

The secondary structural values obtained in various studies are shown in **Table 5.3**:

Sample and conditions		Secondary structure (%)			
		α Helix	β sheet	β Turn	R Coil
Aβ(1-40) (57.7 μM in TFE 60%/tris 10 mM pH 7.4)	A	36.9	17.6	16.8	29.4
Aβ(1-40) (40 μM in TFE 60%/tris) [289]	A	21	58	21	
Aβ(1-40) (TFE 70%/HEPES pH 6.7) [278]	A	46	0	32	
Aβ(1-40)-Al(300 μM) (TFE 60%/tris 10 mM pH 7.4)	A	15.5	26.6	16.9	40.3
Aβ(1-40)-Al(350 μM) (TFE 70%/$H_2$0 pH 6.7) [278]	A	29	29		27
Aβ(1-40)-D-Asp-Al^{3+} (TFE 70%/$H_2$0 pH 6.7) [278]	A	13	27		47
Aβ(1-40)-L-Glu-Al^{3+} (TFE 70%/$H_2$0 pH 6.7) [278]	A	17	21		54
Aβ(1-42) (TFE 60%/tris 10 mM pH 7.4)	B	20.5	24.9	15.8	38.8
Aβ(1-42) (60% TFE ph7.4) [108]	B	38	3		35
Aβ(1-43) (TFE 60%/tris 10 mM pH 7.4)		40.3	15.2	17.7	26.7
Aβ(23-35) (TFE 60%/tris 10 mM pH 7.4)	C	10	50	15.3	23.9
Aβ(25-35) (0.23 mM, TFE 60%/tris) [289]	C	5	61	34	
Aβ(25-35) (250μM in 5mM AcONa pH4.0) [117]	C	20	60	3	22
Aβ(25-35) (60% TFE pH7.4) [108]	C	2.1	39	15.2	43.7
Aβ(1-28) (60% TFE pH7.4) [108]		42	5		39
Aβ(1-39) (60% TFE pH7.4) [108]		50	0		30
Aβ(29-42) (60% TFE pH7.4) [108]		15	61		28
Extract (TFE 60%/tris 10 mM pH 7.4)		11.3	35.9	17.6	37.9
β_2M (TFE 60%/tris 10 mM pH 7.4)		36.9	15.2	15.8	31.4
Control r[mouse]PrP^c	D	42.5	18.2	41.2	
r[mouse]PrP^c + Phosmet	D	42	17	41	
r[mouse]PrP^c + Phosmet metabolites	D	42	16	42	
Human PrP^{sc} [200]	D	0	45	57	
Hamster PrP^c [200]	D	42	3	55	
Hamster PrP^{sc} [200]	D	30	43	27	

Table 5.3 - The secondary structural values of the various amyloid peptides compared with other CD studies. The shaded values were obtained in the present studies.

The studies differed in terms of experimental conditions, the solvent environment, and the methods of data analysis. Several methods have been developed to analyse the secondary structures of peptides and proteins from CD data, to obtain secondary structural information from CD data [16-20]. Each method has been shown to have its own advantages and pitfalls; for example, the wavelength range of data acquisition and the precision of protein concentration determination have been shown to affect the reliability of each method. The differing conditions could account for the differences in the secondary structural values. Most alarming is a paper by Simmons et al. [125], which identified variation in results with amyloid materials from different suppliers as well as within the same batches from the same supplier. The method of analysis of the data could affect the way the results are interpreted.

The following conclusions were made for the differences in the values obtained and the values quoted in various studies:

A) Although, the native Aβ(1-40) peptide values differ from those in the literature, the values follow the general trends of decreasing α helix and increasing β sheet on addition of aluminium.
B) The effects of solvents could alter the overall secondary structure, as is the case for Aβ(1-42). The secondary structural values differ in TFE (60%)/ water (40%) showing more α helix and less β sheets.
C) All the values show increased β sheets for Aβ(25-35) indicating that this peptide or peptide region may be involved in Aβ aggregation.
D) The PrP^{c} prion protein is predominantly α helix in nature. Conversion to the PrP^{sc} results in an abolishment of the α helix with an increase in β sheets.

5.4.2 Extracted Aβ may contain different fragments of the Aβ protein.

In the present study, the CD spectrum for the various Aβ amyloid peptides clearly showed the diversity of secondary structures of the different fragments of the same protein. This suggests that certain fragments or residues within the Aβ contribute to the overall structure. The secondary structural values for the Aβ extract from brain

tissue were closest to that of Aβ(1-42) and Aβ(25-35) but not the Aβ(1-43). The α helical content for the Aβ extract was too low compared with the Aβ(1-43). Secondary structural values from the CD study are shown in **Table 5.4.**

Amyloid protein	Secondary structure (%)			
	α Helix	β sheet	β Turn	R Coil
Aβ(1-40)	36.9	17.6	16.8	29.4
Aβ(1-42)	20.5	24.9	15.8	38.8
Aβ(1-43)	40.3	15.2	17.7	26.7
Aβ(23-35)	10.0	50.0	15.3	23.9
Extract	11.3	35.9	17.6	37.9
β_2M	36.9	15.2	15.8	31.4
Control r[mouse]PrP^c	42.5	18.2	13.0	28.2

Table 5.4 – The secondary values of the amyloid proteins obtained from CD spectra.

The amyloid plaques are composed of β sheet aggregates and are formed as a result of a conversion from α helices to β sheets. Therefore, a large β sheet content was expected for the extracted protein. The extracted amyloid could also contain many β amyloid protein fragments such as the Aβ(1-42) or Aβ(25-35). The CD method is not able to distinguish between a mixture of proteins and the secondary structure from each protein within the mixture contributes to the overall spectrum. The secondary structural values for the extracted amyloid protein from Alzheimer's disease were between that of the Aβ(1-42) and the Aβ(25-35).

The secondary structural values for the Aβ extract from brain tissue were closest to that of Aβ(1-42) and Aβ(25-35) but not the Aβ(1-43). The α helical content for the Aβ extract was too low compared with the Aβ(1-43). The immunoblot detection with the antibody to Aβ(1-40) indicated that the extracted amyloid contains Aβ(1-40), but may also contain Aβ(1-42) and/or Aβ(1-43). It can be concluded that from both the immunoblot assay and the CD results that the Aβ extract contained a mixture of amyloids, predominantly Aβ(1-40) but possibly also Aβ(1-42) and Aβ(25-35).

The β-amyloid peptide has been shown to fold into two antiparallel β-strands with a β-turn at residues 26-29 and with the nine N-terminal residues adopting a random coil

configuration [118]. The synthetic Aβ peptide fragment having the same sequence as the N-terminal 28 residues, formed fibrils that share both antigenic and structural features with native Aβ amyloid filaments [103 & 104]. The hydrophobic Aβ(29-42) peptide adopts exclusive intermolecular β sheet conformations in aqueous solution despite changes in temperature or pH. This peptide is derived entirely from the hydrophobic transmembrane domain and the ability of this peptide to form stable β structure indicates that the C-terminal region could also be amyloidogenic [107]. Both Aβ(1-40) and Aβ(1-42) have been widely studied, the Aβ(1-42) forms β sheet structure and amyloid fibrils much more readily than does Aβ(1-40) [112 - 115 & 329]. The Aβ(1-43) formed stable α helices in solution indicating that the intact entire length peptide behaves differently to the other fragments. The Aβ(25-35) undergoes a reversible β sheet - random coil transition at pH 4.0 and 5.5 [117].

5.4.3 The prion protein interaction with Phosmet.

A truncated recombinant mouse, r[mouse]PrP^c (90-231) was used in these experiments. The primary sequence of PrP^c has been determined for a number of species [100]. The human PrP exhibits 87.3% homology with hamster PrP that has over 94% homology with mouse PrP. The PrP has several definable regions within the primary sequence. The N terminus (region 7-69) contains a series of octa repeats of amino acid rich in prolines and glycines, which are known to bind to Cu^{2+}. A hydrophobic cluster (residues 113-128) with a core domain (residues 125-228) consisting of three α helices and two short antiparallel β strands. The hydrophobic region (113-128) has been shown to be necessary for α to β conversion [152]. Studies with recombinant Syrian hamster PrP, r[SHa]PrP(29-231) compared to the r[SHa]PrP(90-231) show that they both exhibit identical core structures and similar backbone dynamics. The 29-124 residues of the r[SHa]PrP(29-231) displays a substantial amount of flexibility and little structure and indicates that the N terminus may be disordered in vivo [202]. Little information exists for the involvement of the N terminus region. It has been shown that the truncated PrP(121-231) without N terminal, caused cerebrallar disorders in transgenic mice.

The amino acids 1-22 of PrP^c comprise a single peptide that is removed during biosynthesis [330] and therefore not involved in the secondary structure of PrP^c. Spectral data is available from the suppliers of the r[mouse]PrP^c used in the experiments show the folding of the α helix from β pleated sheet form in reducing acid conditions. Therefore, the recombinant mouse PrP(90-231) is likely to refold in a similar manner to the intact mouse prion protein. It can also be used to detect changes in secondary structure on exposure to the Phosmet and its metabolites. The mouse prion protein has over 80% homology to the human prion and the region of interest which displays the ability to form β sheets lies within the hydrophobic cluster (residues 113-128). It was not possible to determine the conformational structure of isolated mouse PrP^{sc} in these experiments because of its extreme insolubility in the buffers used. It would also be of interest to perform these experiments with the human full-length prion protein.

In this experiment, the exposure of r[mouse]PrP^c to Phosmet or its metabolites did not result in any changes in the conformation of the prion. A change from predominantly α helix to β sheets would indicate that the PrP^c had been converted to PrP^{sc}. This indicates that Phosmet does not act as a trigger factor for the initiation of mouse PrP^{sc}. The ectoparasiticide, Phosmet, was used to eradicate BSE in cattle in the '80s. This external treatment was applied as a liquid preparation, poured onto the back of the cattle. It was hypothesised that this method of application allowed the Phosmet to be absorbed into the spinal chord, entering the brain after a delayed period. One possible mechanism is the interaction of Phosmet with cellular PrP^c transforming it into PrP^{sc} and this would initiate the BSE disease [204]. The mechanisms for this proposed transformation of PrP^{sc} can be divided into two distinct groups; those not involving a direct interaction with the Phosmet and those involving interaction between Phosmet and/or its metabolites with the prion protein. Indirect interaction is mechanistically diverse and could include esoteric cellular changes which result in altered cellular metabolism or altered immune responses or interactions between Phosmet and the cell membrane or prion anchor proteins, which might indirectly affect PrP^c. The direct interactions are perhaps the most likely mechanisms if Phosmet did play a role in the BSE epidemic.

However, the most likely cause was animal feed containing scrapie-infected bone meal [147]. Cattle that were fed on this infected bone meal then contracted BSE via cross species contamination. Exposure to BSE infected meat as a foodstuff is considered to be the likely cause of the new variant CJD (nvCJD) [197].

5.4.4 Amyloids treated with metals.

The addition of copper, zinc, calcium and aluminium to Aβ(1-40), Aβ(1-42), the Aβ extract and to β_2M show some change with the exception of Aβ(1-43). Addition of metals with the Aβ(1-42) and Aβ extract generally caused a decrease in the α helix. The effects of both copper and zinc were concentration dependent showing an almost complete abolition of α helices with a shift to β sheets with Aβ(1-40). Aluminium has a concentration dependent effect on the secondary structure as seen with a decrease in α helices and an increase in β sheet for both Aβ(1-40) and β_2M. Calcium also showed similar affects with the Aβ(1-40) but to a lesser extent.

Iron, nickel and aluminium all caused amyloid to deposit to a degree whereas barium, silver, lead, magnesium and calcium had the least effect on Aβ(1-40) deposition [331]. These metals may have similar effects on the other Aβ fragments and indeed other amyloids such as β_2M and the prion protein. Studies have reported metal-induced aggregations of amyloid if the metals are present in a high enough concentration [331 - 333]. Bush et al. [331] found that at a concentrations of 25 μM or less of zinc, less than 20% of amyloid β protein remained in solution. There is evidence that prolonged exposure to fragments of Aβ can have toxic effects on neurons *in vitro* either directly or by calcium dependent mechanisms [254]. Calcium has been reported to cause the same effects on the structure of the Aβ peptide as with aluminium [320].

5.4.5 Amyloids treated with copper and zinc.

Addition of a mixture of copper and zinc to the Aβ(1-40) did not show a combined effect. In fact, the resultant changes were less than that of the metals on their own. Copper is able to displace of ^{65}Zn from Aβ when co-incubated with excess Cu^{2+}

[319]. The Cu^{2+}-induced Aβ aggregation at pH 7.4 is considerably less than that induced by Zn^{2+} [331, 332 & 335]. Aβ has binding sites for both copper and zinc, but copper ions can displace zinc ions, hence a co-operative effect is not seen with the addition of both copper and zinc [331 & 336]. Aβ(1-40) may be capable of binding Cu^{2+} and Zn^{2+} simultaneously [331 & 335] and like the prion protein, Aβ is able to bind multiple copper ions [319]. Clements et al. [319], reported that the binding of zinc to the peptide was dependent upon the amount of free zinc and the relative affinities of any competing proteins. Therefore, the overall binding and hence interaction of both the Zn^{2+} and Cu^{2+} is actually decreased because of competition for the same binding sites.

5.4.6 Amyloids treated with aluminium.

The Aβ(1-40) and the β_2M both showed similar results with the treatment of increasing concentration of Al^{3+}. There was a general decrease in α helix with an increase in β sheets. The results obtained for Aβ(1-40) are similar to, and a progression of, those previously reported by other workers. The peptide and aluminium results mirrored trends reported by Exley et al. [289] except for the addition of 400 μM Al^{3+}, which they did not report. They also found that the addition of an increasing concentration of aluminium up to 300 μM caused a general decrease in α helices although there was also a decrease in the β sheets with an increase in random coil. In contrast there was a decrease in α helices and increases in both β sheets and random coil, in this study. Experiments by Fasman et al. [314] also showed that on addition of upto 4 molar equivalents of Al^{3+} to rat Aβ(1-42) caused a decrease in the α helix and an increase in β sheets. Thus, an increase in the β sheet content of the amyloid peptide Aβ(1-40) treated with Al^{3+} may indicate a possible mechanism for its aggregation.

Exley et al. also reported that aluminium (50 μM) had a small effect on the Aβ(25-35) [289]. In the present study, the initial CD spectrum of the Aβ(25-35) showed that there was a significant amount of β sheet (>50%) and treatment of aluminium would not have any effect on the secondary structure. Although the solvent conditions were similar, the suppliers of the peptides differed. This may account for the differences in

the results as amyloid materials have been shown to vary from different suppliers [125].

5.4.7 Amyloids treated with aluminium and silicon.

Addition of SiO_4^{4-} after the aluminium had the effect of reversing the changes in secondary structure caused by Al^{3+} for both the Aβ(1-40) and β_2M. This reversal was enhanced by the addition of the silicate before the aluminium. The effect of silicate on Aβ(1-42) has previously been reported [314 & 320] but not for Aβ(1-40) or β_2M. The results presented here differ from those of Fasman et al. [314 & 320] with respect to (i) the amyloid peptide (ii) the matrix environment within which the peptide was analysed and (iii) the peptide concentration. The amyloid used by Fasman et al. was rat amyloid Aβ(1-42) whereas the amyloids used in the present study were all synthetic human amyloid peptides. The experiments by Fasman et al. were conducted in a 100% TFE environment. The solvent used in the current study consisted of 60% TFE/ 40% tris (pH 7.4, 10 mM) environment. This environment more closely resembles *in vitro* conditions than that of Fasman et al [314].

The effect of aluminium on the Aβ(1-42) has been shown to be reversed on addition of silicate in a 1:2 ratio [314 & 320], where as the above experiments show that there is a reversing effect with a 1:1 ration of Al^{3+} and SiO_4^{4-}. There was a greater reversal in the secondary structure with SiO_4^{4-} (300 mM) and with a lower concentration of Al^{3+} (50 and 150 μM). The chemistry of aluminium also shows that it has a unique affinity for silicon forming insoluble aluminosilicates. Therefore, addition of SiO_4^{4-} before the Al^{3+}, as above, could allow the formation of aluminosilicates thereby reducing the amount of soluble aluminium available to interact with the peptide [314].

5.4.8 Amyloids treated with GAGs.

The β_2M and Aβ(1-40) peptides did not appear to undergo any significant conformational change on binding sulphates and GAGs. Even if sulphate did not influence fibrillogenesis via conformation changes, binding of the GAG could provide a high-affinity binding ligand that could then bind other factors such as metal ions.

Similar experiments by McLaurin et al. [315] show comparable results for the Aβ(1-40) treated with various GAGs using CD. In their experiments, the Aβ(1-40) showed little change on addition of the GAGs (heparin, heparan sulphate, keratan sulphate or chondroitin-4-sulphate and chondroitin-6-sulphate) at high concentration and at different pH (7.0 and 6.0). The concentrations of the GAGs they used ranged from 0.5–5 mg ml^{-1}, the lowest was 10 times the concentration used in our experiments.

They also looked at Aβ(1-42), which is far more amyloidogenic than Aβ(1-40). They showed it formed β sheets with the GAGs [315]. They used a phosphate buffer, and in the presence of phosphate (50 mM at pH 7.0 and pH 6.0), the chondroitin-4-sulphate was seen to induce a β sheet structural change in Aβ(1-40) only after 4 hrs. They also showed that after 48 hrs at pH 7.0, the Aβ(1-40) aggregated formed with or without either chondroitin 4 sulphate or heparin [315]. The interaction of the GAGs showed no time or pH dependence or effect from other molecules such as phosphate. Therefore the choice of buffer may influence the outcome of the GAG induced change in Aβ. Thus, the inability of GAGs to induce a β conformational switch in Aβ(1-40) may be as a result of specific shielding of charges by counter ions present in the buffer [315].

5.4.9 Amyloids treated with GAGs and metals.

Aβ(1-40) and β_2M peptide treated with physiological concentrations of Al^{3+} combined with the GAGs showed a synergistic effect. In the above experiments, it was observed that Al^{3+} had an effect on the secondary structure of both Aβ(1-40) and β_2M but only at the higher concentrations. The levels of aluminium were lower (1.5 μM) compared to previous experiments (50 μM upwards). Neither the GAGs nor the aluminium on their own caused an appreciable change in the secondary structure. These results indicate that the highly sulphated GAGs were somehow enhancing the effects of the Al^{3+}. These changes seemed to occur with several types of GAG, which suggests that the highly negatively charged sulphate groups may be involved.

Similar effects were also seen with copper and zinc, although the Cu^{2+} and Zn^{2+} initially alter the peptides at the concentrations used. The Aβ(1-40) peptide treated with combinations of Ca^{2+} and various GAGs showed different effects depending on the GAG. Most notably, the combinations of heparin, HS, and Na_2SO_4 with calcium, appears to increase the α helices and decrease the β sheets. For β_2M, the combined calcium and GAGs generally decreased the α helices and increased the β sheets, with the exception of HSPG, HS, KS, and CS causing further decreases in α helices and β sheets with increases in random coil.

Highly sulphated glycosaminoglycans and proteoglycans are common constituents of amyloid deposits. The sulphate may represent an ideal distribution of sulphate groups for amyloid interactions. GAGs could affect the nucleation and propagation of these fibres by serving as an anchor for amyloid fibril organisation [315]. GAGs also possess substituent groups, which permits complex co-ordination with metal cations. These complexes could further interact with the amyloid fibrils.

5.5 Conclusion.

The present results show that metals with both Aβ(1-40) or β_2M caused an increase in the peptide β sheets secondary structure and thus may accelerate amyloid deposition. It was seen that the effects on the amyloids of metals such as copper, zinc, aluminium and calcium are enhanced when combined with GAGs. The results for β_2M are interesting because there is little work on β_2M with metals in the literature. The work with the GAGs and Metals has not been previously reported. The similarity in the results for both the above amyloids indicates that common mechanisms are involved.

Calcium under certain conditions with certain GAGs is seen to have increased or decreased effects on the amyloids. Abnormal metabolism of PGs including specific GAGs is closely involved in the production of amyloids. Though it is not known if elevated levels of PGs has any influence on amyloidosis. Given that in all amyloids highly sulphated GAGs are present, one can postulate that these highly negatively charged molecules may play a role in the presence of other factors, such as metals.

Chapter 6. Detection of secondary structural changes in amyloid proteins using attenuated total reflectance (ATR-FTIR).

6.1 Introduction.

The technique of attenuated total reflectance Fourier transform infrared spectroscopy is a method widely used in the study of proteins. ATR-FTIR is more versatile than conventional transmission FTIR spectroscopy because the spectra of peptides can be obtained in such a wide range of matrices. ATR spectra can be collected of non-transparent samples, and proteins can be detected in aqueous solutions. It is also possible to study proteins in the presence of strongly absorbing solutes (such as denaturants). A broad range of ATR-FTIR accessories is becoming available to overcome the problems of studying biological samples [337 - 342]. Small amounts of sample are required and only very low protein concentrations (< 0.3 mg ml^{-1}) are necessary.

Traditionally ATR has been used for the analysis proteins as films and can be extended to study the orientation of molecules in thin films, such as lipids and peptides in bio-membranes. Such studies involve drying the protein as a hydrated thin film on the surface of an internal reflectance element (IRE) as in thin film ATR (TF-ATR). The other strategy for collecting ATR spectra is to allow proteins or peptides to adsorb to the surface of the IRE from solution as in adsorption ATR (Ads-ATR). Significant structural disturbances may occur with drying of proteins onto the IRE. Proteins adsorb onto the surface will also interact with the IRE material. The structural distortion caused by protein-IRE interactions can be substantial; hence the secondary structure will be disrupted [23]. There are several factors that can affect the ATR spectra. A number of these parameters are fixed such as the angle of incidence of the infrared radiation and the length of the crystal. Other factors include the need for regular background spectrum and good contact between sample and the surface of the IRE, but this is not a problem with liquid samples, where the liquid is in direct contact with the surface of the IRE.

Water-soluble protein samples are best analysed in adequately buffered aqueous solutions (in ^2H_2O, H_2O or preferably both) rather than as solids or as hydrated films.

Unfortunately, problems still remain when studying proteins dissolved in water or aqueous buffers due the high molar absorptivity of the O-H bending vibrations of water (~1640 cm^{-1}) and problems associated with non linearity. This limits the path length used in studies of proteins dissolved in water to 10 μm or less. Longer path lengths result in significant distortions of water absoprtions, making background subtraction impossible. This can be overcome in ATR-FTIR as the germanium crystal used has an effective path length of 2.59 μm (the internal critical angle is 22.02° with the external angle of 45° giving the number of internal reflections as 12 and the depth of penetration as 0.664 μm).

6.1.1 The use of FTIR in the study of amyloids

FTIR has previously been used in the analysis of Alzheimer's disease amyloid proteins; changes in the SO_3^- spectral region have been used to determine the binding of the congo red dye-protein complexes [343]. Other studies have used FTIR to detect changes in AD amyloid fragments in deuterated solvents and at various pHs [344]. In another study FTIR was used in the correlation of the solubility and the β sheet structure formation of the amyloid proteins Aβ(26-33) and Aβ(34-42) [107]. The solubility of the above fragments in various solvents such as 1,1,1,3,3,3 hexafluoroisopropanol (HFIP), 2,2,2, trifluoroethanol (TFE) and deuterated water has been determined by FTIR. The Aβ(26-33) in deuterated water and HFIP and Aβ(34-42) in HFIP reveals a broader amide I band centred around 1650 cm^{-1} indicative of a random coil or alpha helix formation.

The formation of amyloid gel aggregates leads to a band at 1625 cm^{-1}, which is indicative of β sheets, demonstrating that precipitation is linked to the formation of β sheets. Fragments Aβ(34-42) in deuterated water also show positions of the amide I band at 1625 cm^{-1} and the weak absorption band at around 1700 cm^{-1} are characteristic of antiparallel β sheet structures, indicating that the amyloid fragments are predominantly β sheet. Solid state FTIR also reveals the Aβ(34-42) to be a β sheet structure [107]. The FTIR of Aβ(11-25) shows that it exists as predominantly β sheet at pH 3 to 8 similar to the Aβ(1-40). A substitution of the histidines at position 13 and 14 of the Aβ(1-28) fragment showed less β sheets at all pHs indicating that histidines are involved in the β sheet formation or stabilisation [344]. Again, the different

peptide environments illustrate the difficulty in comparing the results between the various studies. A detailed discussion of the effects solvent and pH conditions on *in vitro* studies can be found in **Chapter 5, section 5.1.2.1**.

6.1.2 The present study.

The present study investigated amyloid proteins treated with metals and glycosaminoglycans using a novel ATR-FTIR method. The synthetic amyloid peptides used were synthetic Aβ(1-40), Aβ(1-42) and Aβ(1-43) peptides, as found in senile plaques in the brains of Alzheimer's disease sufferers. The extracted amyloid protein from Alzheimer's disease brains and the synthetic β_2 microglobulin, as found in dialysis related amyloidosis, were also investigated. The changes in the protein secondary structure were detected using ATR-FTIR spectroscopy.

The system developed here used an acetate 'cover-slip' to minimise the sample volume needed to cover the germanium crystal surface. The system is 'open' and the sample may be prone to evaporation. The total time for each analysis was approximately 10 minutes, which was short enough so as to prevent evaporation of the sample in the tris buffer. The solvent used in the ATR study contained only tris buffer (10 mM, pH 7.4), where as, trifluoroethanol would evaporate during the short sample analysis time. Again, we are measuring the changes in the secondary structure from the initial conformation in the tris buffer. Further spectral deconvolution was necessary for the determination of the percentages of secondary structures, but this was not possible with the current system. However, much information can be obtained by monitoring changes within the spectra for individual peptides. The tris buffer itself would have a different effect on the overall ratios of α helix and β sheet secondary structures of the proteins compared to the tris/TFE buffer used in the CD experiments. Therefore, the overall changes in the amyloid secondary structure, rather than absolute values were compared between the results of the CD studies and ATR studies.

6.1.3 Method.

Experimental methods, instrumentation and reagent details are given in **Chapter 2, section 2.5.**

6.2 Results.

The developed ATR method used a strip of acetate that covered the sample on the germanium crystal. The sample was sandwiched between the acetate and the IRE surface much like a cover slip on a glass slide, thus reducing the sample volume to 15 µl. It is necessary to obtain regular buffer spectra as the subtraction of the sample spectra from the buffer spectra is prone to discrepancies due to the presence of air and water vapour as the system is 'open'. The tris buffer (10 mM, pH 7.4) used was not a deuterated buffer as the small path lengths of the ATR system meant that water was not totally absorbing.

6.2.1 Validation of the ATR system.

Cleaning of the ATR element is also important as protein may adsorb onto the surface of the crystal and add to successive spectra. **Figure 6.1** shows that cleaning with 10% SDS was necessary to remove all the adsorbed protein. The protein may adsorb onto the crystal surface and this would contribute to the next spectrum. After several sample runs the protein may not be removed by cleaning with ethanol and rinsing with water, but is completely removed with a detergent. The total time for each analysis was approximately 10 minutes and the protein concentration (1 mg ml^{-1}) was low enough so as to prevent adsorption onto the crystal surface within this time.

The validation of any technique is important for quantitative work. **Figure 6.2** shows the reproducibility of the method. Running four replicate samples of bovine serum albumin (BSA, 1 mg ml^{-1}) in tris buffer (10 mM, pH 7.4) to test the reproducibility. The spectra were obtained independently and on different days. The buffer spectrum were subtracted and the spectrum were normalised to the maximum peak intensity of amide I (1600 – 1700 cm^{-1}). The overall standard deviation was calculated to be 0.0035 absorbance units. It is necessary to take into account the overall error; therefore, any changes must be greater than 0.003 absorbance units.

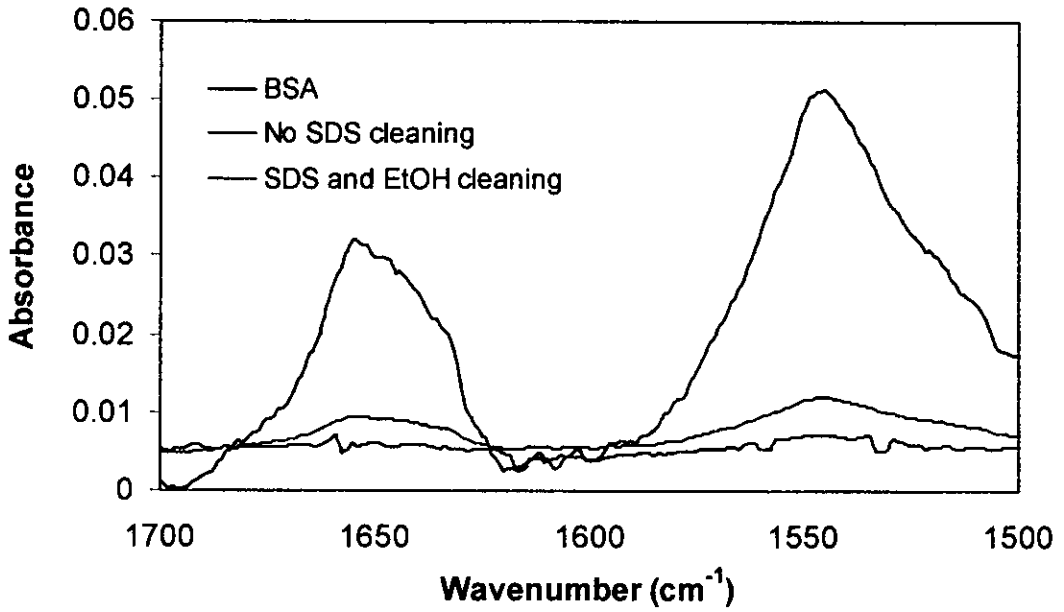

Figure 6.1. – Spectra of BSA (1 mg ml^{-1}), after cleaning with ethanol and after cleaning with SDS (10% w/v) and ethanol. Cleaning the ATR crystal with 10% SDS and with ethanol is necessary is to remove all traces of protein adsorbed onto the IRE.

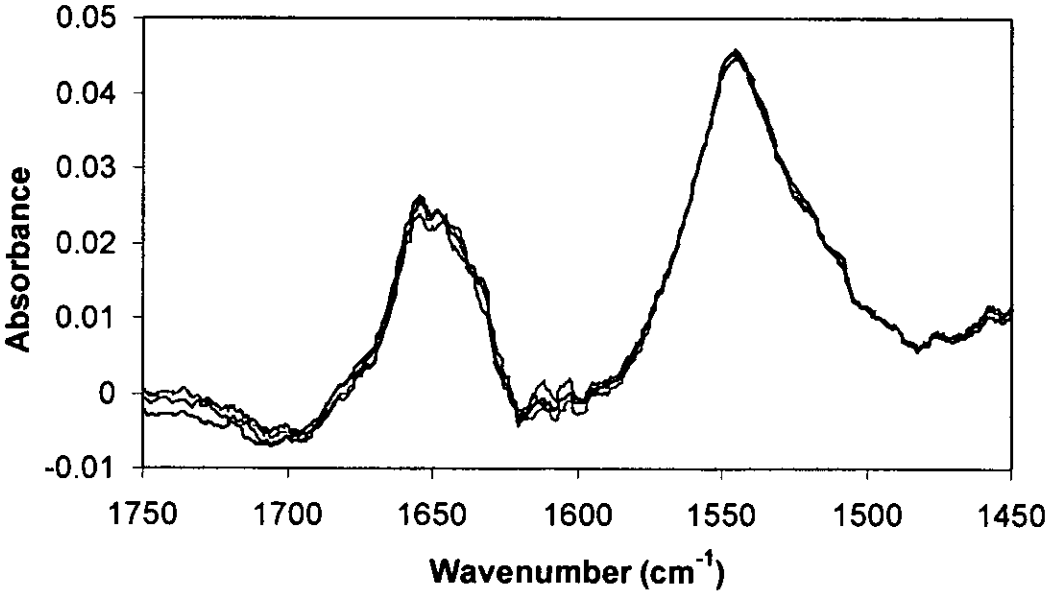

Figure 6.2.- The reproducibility of the ATR system was determined by independently running four replicate samples of bovine serum albumin (BSA, 1 mg ml^{-1}). Spectra were normalised to the maximum peak intensity of amide I bands of BSA.

6.2.2 Second derivative spectra.

ATR-FTIR has been shown to be useful for studying the secondary structure and other properties of proteins in a variety of matrices [27, 337 - 342]. The secondary structure of these proteins can be determined by infrared. Bands can be assigned in accordance with the particular physical arrangements of the amide bonds within the protein backbone. For example, the major amide I bands of β pleated sheets contain an intense absorption at 1620 to 1630 cm^{-1} and a weaker high frequency band at 1685 cm^{-1}, while random structures display broader spectra with a maximum centred around 1640 cm^{-1}. These bands contribute to the overall spectral envelope.

Most of the absorption band positions are easily found in second derivative spectra. Some difficulty arises in absorption bands showing as shoulder peaks in the second derivative. Information about frequency position, width, maximum intensity can be obtained from second derivative spectra but in practice are inaccurate due to neighbouring absorption bands. However, the second derivative spectra are more useful to assign absorption bands, as the derivative spectra will exactly show the positions of all the true absorption bands. The downward peaks corresponding exactly to the wavenumber of the component absorption band.

The second derivative spectra for each of the proteins are shown in **Figure 6.3**. The frequency range for the secondary structures as calculated by second derivative is given in **Table 6.1**. The ranges shown next to the secondary structural types are the values that are quoted in the literature [23 & 24].

Structure and amide I frequency		Aβ(1-40)	Aβ(1-42)	Aβ(1-43)	Extract	β_2M
Antiparallel β sheets	**(1675-1695)**	1683	1685	1678	1680	1684
α helix	**(1648-1660)**	1650	1649	1648	1648	1655
Random	**(1640-1648)**	1638	1640	1638	1635	1644
β sheet	**(1625-1640)**	1628	1630	1630	1627	1634
Aggregated strands	**(1610-1628)**	1611	1615	1610	1612	1616

Table 6.1 - The wavenumber of the absorption bands corresponding to the secondary structural features as calculated by the second derivative spectrum of amyloid proteins.

Figure 6.3

The second derivative spectrum of amyloid proteins of (**a**) Aβ(1-40), (**b**) Aβ(1-42), (**c**) Aβ(1-43), (**d**) Aβ extract, (**e**) β_2M. The corresponding spectrum is shown below.

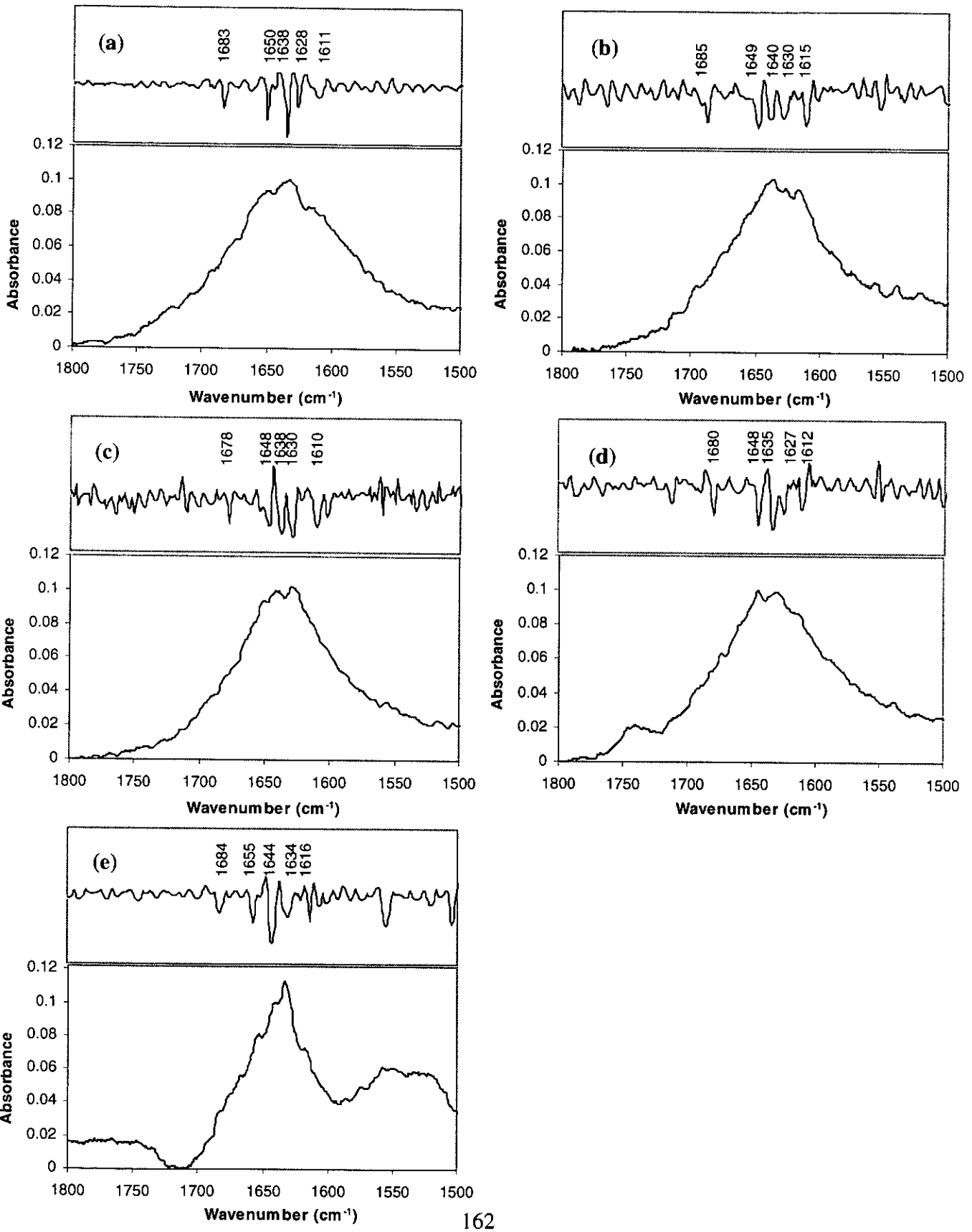

The main absorption bands corresponding to the various secondary structures are present. There are small shifts in the positions of the absorption bands comparing all the proteins. There was a maximum shift of about 5 cm^{-1}, which may be accounted for by effects such as side chains of the peptides and solvent interactions.

The second derivative spectra can give some indication of relative peak intensities of the individual absorption bands within the spectral envelope. Both the absorption bands at 1680 cm^{-1} and 1610 cm^{-1} are difficult to assign. The antiparallel β sheets at 1680 cm^{-1} are weak as seen in the second derivative spectra in **Figure 6.3**. This component is normally weak and is often overlapped by absorption from β turn and unordered structures. The absorption bands around 1610 cm^{-1} correspond to denatured aggregated strands but the range is also within the β sheet assignment and is difficult to interpret.

The precise percentages of secondary structure have not been calculated as this would require the use of curve fitting programs such as Gaussian curve fitting, which was not possible with the current system and software used. It should be noted that due to overlap of the secondary structural envelope, the direct calculation of secondary structures is not possible by absorbance measurements alone. A change in one component may cause an overall change in the spectral envelope and may mask changes of other secondary structure. Therefore, the absolute absorbance values assigned to particular secondary structures should be treated with caution without analysis by curve fitting programs. However, monitoring of the changes in position and intensity of the amide I bands gives an indication of the conformational changes within the protein. Spectra of peptides treated with metals can be directly compared with the native peptide spectra. The changes in the peak intensities within the base spectra can be used to empirically follow any changes in the secondary structures due to interaction with the metals.

6.2.3 Amyloid peptides.

The comparison of ATR spectra of amyloid proteins Aβ(1-40), Aβ(1-42), Aβ(1-43) and Aβ extract from Alzheimer's disease brain and β_2M are shown in **Figure 6.4**. The table shows the relative intensities of the amide I absorption bands corresponding to the secondary structural features. Little can be said about the various ratios of secondary structure between the different amyloid peptides. Further spectral deconvolution is necessary for the determination of the percentages of secondary structures, but this was not possible with the current system. However, much information can be obtained by monitoring changes within the spectra for individual peptides.

6.2.4 Amyloid proteins treated with metals.

The amyloid proteins treated with metals are shown in **Figure 6.5.** Aβ(1-43) treated with Cu^{2+} caused a decrease in α helix and β sheet and an increase in random structures (**Figure 6.5a**). Aβ(1-42) treated with both Cu^{2+} and Zn^{2+} showed a decrease in α helix and β sheet with an increase in random structures, albeit small changes (**Figure 6.5b**). The extracted protein treated with zinc caused a decrease in α helix and an increase in both random coil and β sheet (**Figure 6.5c**). Aβ(1-40) treated with Cu^{2+}, Zn^{2+} and Ca^{2+} show a decrease in α helix and random structures with increases in β sheet. There was also a shoulder developing at about 1660 cm^{-1} that may be associated with β turns (**Figure 6.5d**). β_2M with Cu^{2+}, Zn^{2+} show a decrease in α helix but an increase in both β sheets and random structures. Whereas calcium caused an overall decrease in β sheet and increases in both random and α helix structures (**Figure 6.5e**).

Figure 6.4

Comparison of ATR spectra of; Aβ(1-40), Aβ(1-42), Aβ(1-43), Aβ extract and β_2M. The relative intensities of the amide I absorption bands corresponding to the secondary structures are shown below.

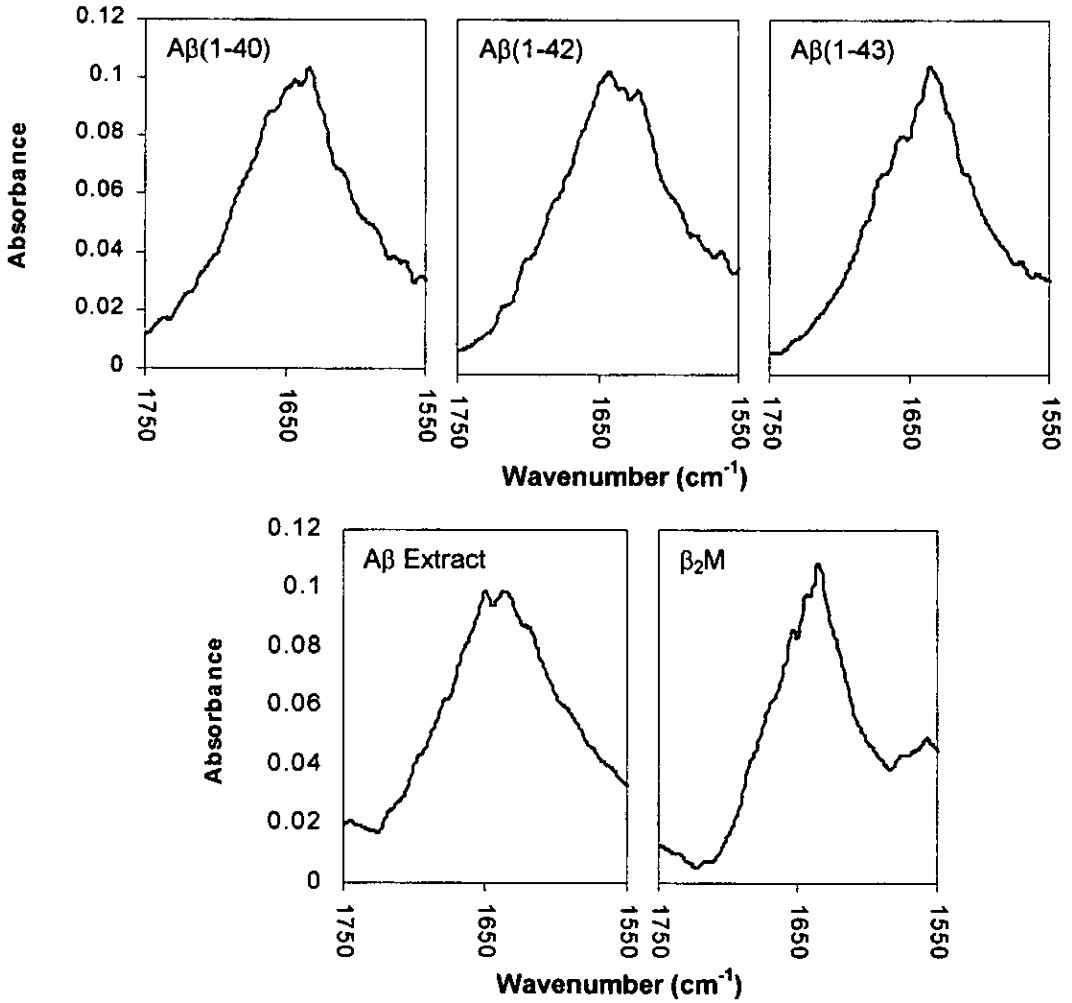

Secondary structures	Peak intensities				
	Aβ(1-40)	Aβ(1-42)	Aβ(1-43)	Aβ Extract	β_2M
Antiparallel β sheets	0.062	0.052	0.051	0.053	0.042
α helix	0.093	0.089	0.080	0.091	0.086
Random	0.099	0.100	0.092	0.099	0.099
β sheet	0.104	0.096	0.102	0.096	0.107

Figure 6.5a

The Aβ(1-43) peptide treated with $CaCl_2$, $CuCl_2$, and $ZnCl_2$ (100 μM). The relative intensities of the amide I absorption bands corresponding to the secondary structural features are shown below. Shaded values are changes greater than 0.003 absorbance units.

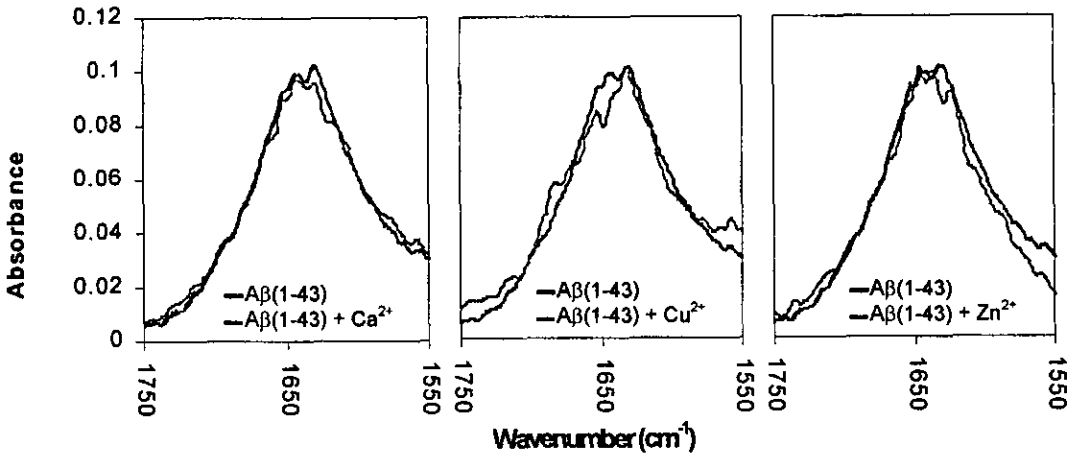

Secondary structures		Peak intensities			
		Aβ(1-43)	Ca^{2+}	Cu^{2+}	Zn^{2+}
Antiparallel β sheets	(1678 cm^{-1})	0.048	0.048	0.043	0.043
α helix	(1648 cm^{-1})	0.094	0.091	0.088	0.090
Random	(1638 cm^{-1})	0.099	0.097	0.106	0.097
β sheet	(1630 cm^{-1})	0.101	0.098	0.088	0.097

Figure 6.5b

The Aβ(1-42) peptide treated with $CaCl_2$, $CuCl_2$, and $ZnCl_2$ (100 μM). The relative intensities of the amide I absorption bands corresponding to the secondary structural features are shown below. Shaded values are changes greater than 0.003 absorbance units.

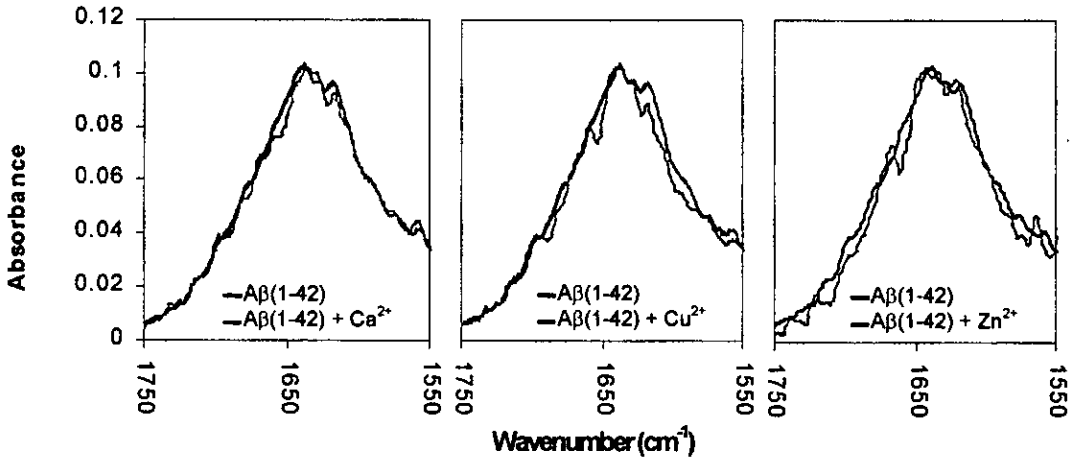

Secondary structures		Peak intensities			
		Aβ(1-42)	Ca^{2+}	Cu^{2+}	Zn^{2+}
Antiparallel β sheets	(1685 cm^{-1})	0.052	0.054	0.050	0.049
α helix	(1649 cm^{-1})	0.089	0.086	0.084	0.082
Random	(1640 cm^{-1})	0.100	0.098	0.106	0.105
β sheet	(1630 cm^{-1})	0.096	0.099	0.092	0.090

Figure 6.5c

The Aβ extract treated with $CaCl_2$, $CuCl_2$, and $ZnCl_2$ (100 μM). The relative intensities of the amide I absorption bands corresponding to the secondary structural features are shown below. Shaded values are changes greater than 0.003 absorbance units.

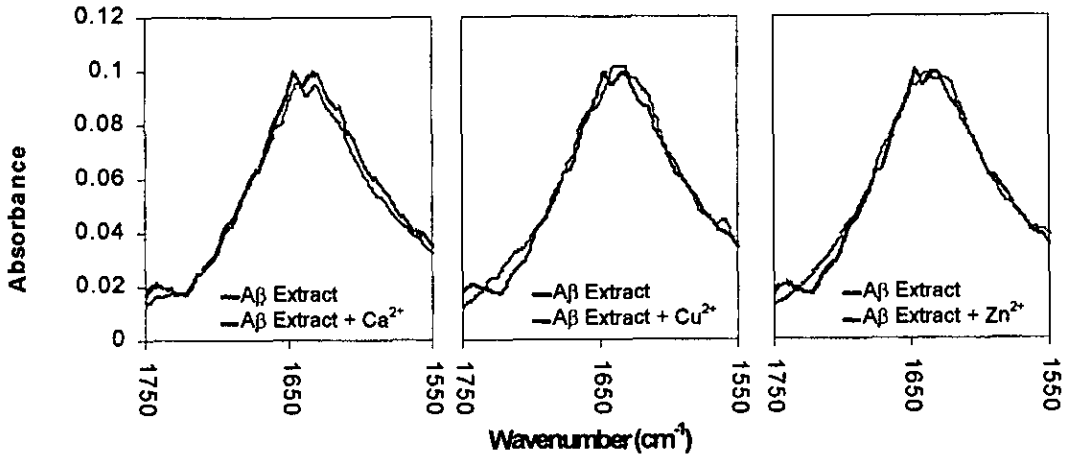

Secondary structures	Peak intensities			
	Aβ Extract	Ca^{2+}	Cu^{2+}	Zn^{2+}
Antiparallel β sheets (1680 cm^{-1})	0.053	0.053	0.055	0.054
α helix (1648 cm^{-1})	0.091	0.088	0.092	0.083
Random (1635 cm^{-1})	0.099	0.096	0.096	0.102
β sheet (1627 cm^{-1})	0.096	0.096	0.094	0.109

Figure 6.5d

The Aβ(1-40) peptide treated with $CaCl_2$, $CuCl_2$, $ZnCl_2$, and $MgCl_2$ (100 μM). The relative intensities of the amide I absorption bands corresponding to the secondary structural features are shown below. Shaded values are changes greater than 0.003 absorbance units.

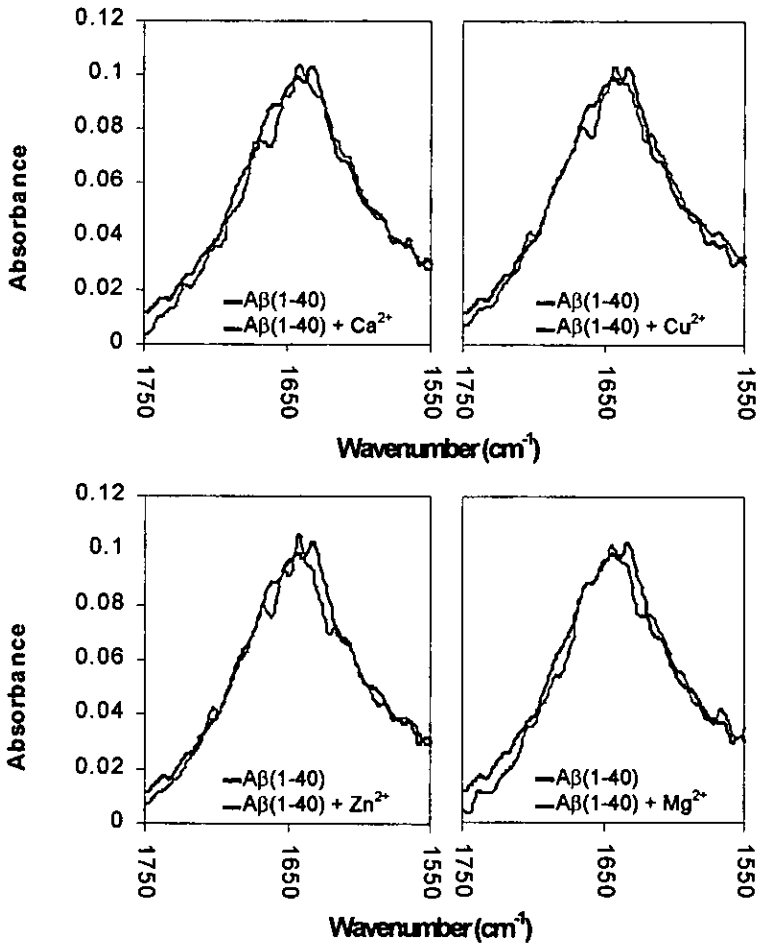

Secondary structures		Peak intensities				
		Aβ(1-40)	Ca^{2+}	Cu^{2+}	Zn^{2+}	Mg^{2+}
Antiparallel β sheets	(1683 cm^{-1})	0.062	0.068	0.065	0.062	0.058
α helix	(1650 cm^{-1})	0.093	0.090	0.078	0.081	0.091
Random	(1638 cm^{-1})	0.099	0.092	0.090	0.091	0.096
β sheet	(1628 cm^{-1})	0.104	0.108	0.108	0.109	0.105

Figure 6.5e

The β_2M peptide treated with $CaCl_2$, $CuCl_2$, $ZnCl_2$, and $MgCl_2$ (100 μM). The relative intensities of the amide I absorption bands corresponding to the secondary structural features are shown below. Shaded values are changes greater than 0.003 absorbance units.

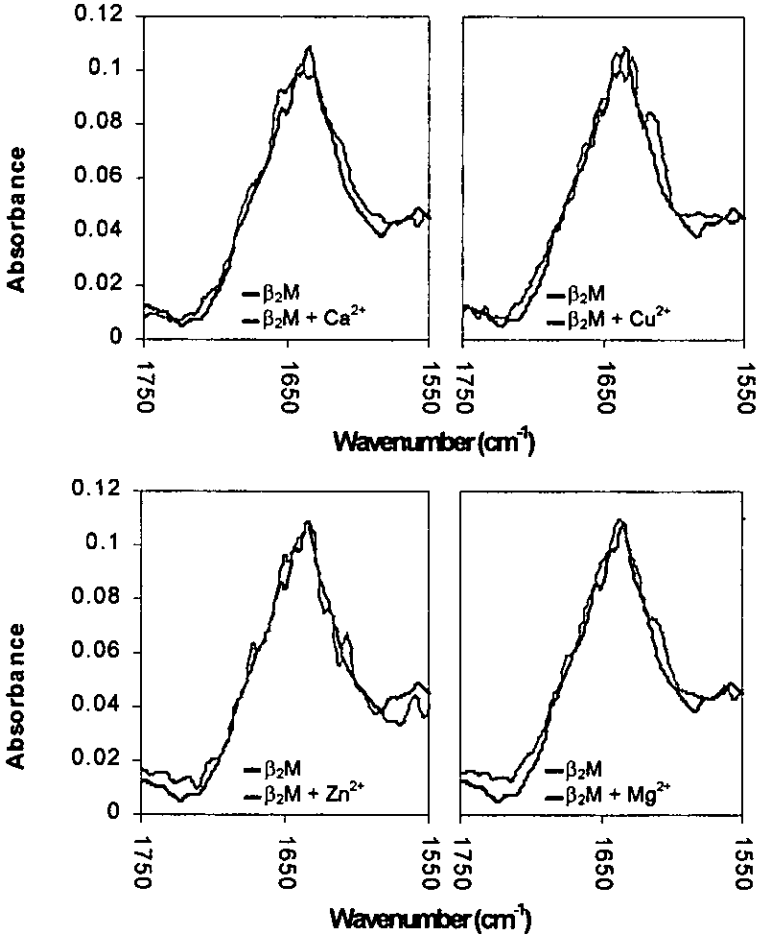

Secondary structures		Peak intensities				
		$ß_2M$	Ca^{2+}	Cu^{2+}	Zn^{2+}	Mg^{2+}
Antiparallel β sheets	(1684 cm^{-1})	0.042	0.051	0.039	0.046	0.039
α helix	(1655 cm^{-1})	0.086	0.090	0.080	0.083	0.087
Random	(1644 cm^{-1})	0.099	0.109	0.106	0.105	0.102
β sheet	(1634 cm^{-1})	0.107	0.103	0.111	0.112	0.106

6.2.5 Amyloid proteins treated with aluminium.

The effect of increasing Al^{3+} on the Aβ(1-43), Aβ(1-42) and Aβ extracted peptides are shown in **Figure 6.6.** Al^{3+} seems to have little effect on Aβ(1-43), Aβ(1-42) and the extracted amyloid as indicated by small changes in the peak intensities. There was a small increase in β sheet with both Aβ(1-42) and Aβ(1-43) treated with 300 μM Al^{3+} (**Figure 6.6a and Figure 6.6b**). Aβ(1-40) with increasing concentration of Al^{3+} caused an overall increase in random and β sheet with a decrease in α helix (**Figure 6.7a1**). β_2M, on the other hand, showed similar changes to that of the Aβ(1-40) but to a lesser extent. Addition of increasing concentration of Al^{3+} caused a small increase in β sheet and decreases in α helix (**Figure 6.7b1**).

6.2.6 Amyloid proteins treated with both aluminium and silicon.

Aβ(1-40) with increasing concentration of Al^{3+} caused an overall decrease in α helix and increases in both random and β sheet. Addition of silicate with the Al^{3+} treated peptide caused a slight reversal in the changes due to Al^{3+} (**Figure 6.7a2**). β_2M also showed similar changes with Al^{3+} with small increases in β sheet and decreases in α helix. Addition of silicate seemed to have little effect on the treated peptide (**Figure 6.7b2**).

6.2.7 Amyloid proteins treated with glycosaminoglycans and calcium.

Treatment of peptide with GAGs combined with calcium is shown in **Figure 6.8**. Aβ(1-40) treated with HSPG and HS caused a small decrease in α helix. Calcium had the effect of increasing β sheets and decreasing random structures (**Figure 6.5d**) but combination of the GAGs with calcium had the effect of reducing the β sheet but increasing the random coil structures (**Figure 6.8a**). The GAGs with β_2M caused small increasing in the α helix and β sheet. As shown in **Figure 6.5e**, calcium had the effect of increasing random structures but when combined with GAGs caused an increase in β sheet and a decrease in α helix (**Figure 6.8b**).

Figure 6.6a

The Aβ(1-43) peptide treated with $AlCl_3$ (50, 150, 300 and 400 μM); The relative intensities of the amide I absorption bands corresponding to the secondary structural features are shown below. Shaded values are changes greater than 0.003 absorbance units.

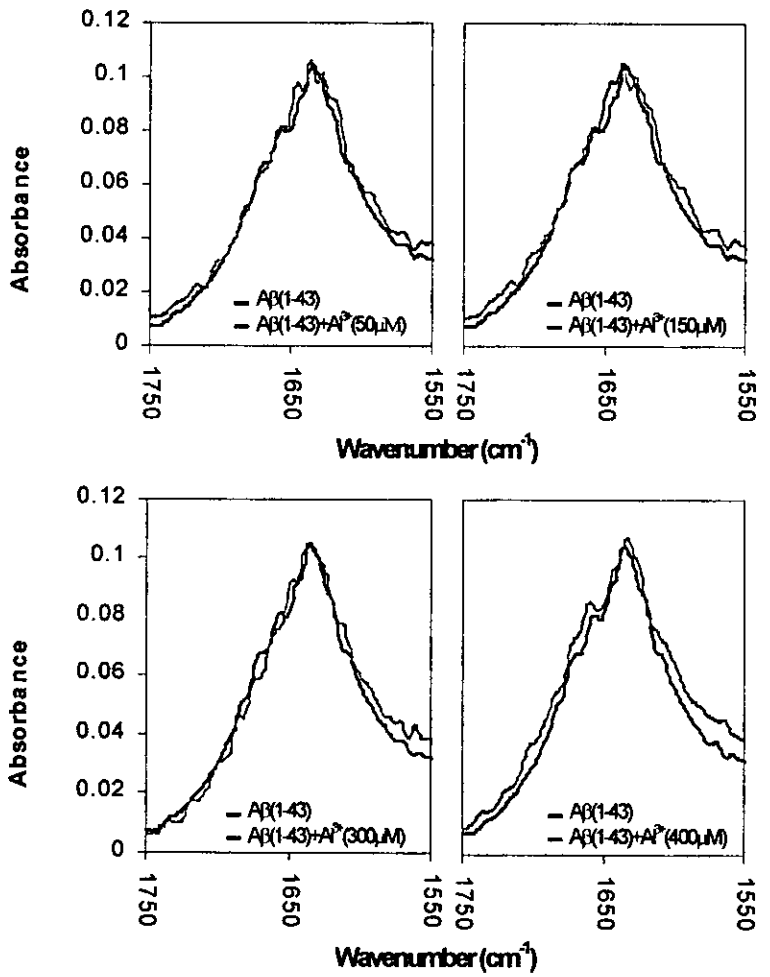

Secondary structures		Peak intensities				
		Aβ(1-43)	Al^{3+}(50μM)	Al^{3+}(150μM)	Al^{3+}(300μM)	Al^{3+}(400μM)
Antiparallel β sheets	(1678 cm^{-1})	0.051	0.050	0.050	0.048	0.053
α helix	(1648 cm^{-1})	0.079	0.082	0.083	0.077	0.080
Random	(1638 cm^{-1})	0.102	0.097	0.098	0.098	0.099
β sheet	(1630 cm^{-1})	0.098	0.099	0.097	0.105	0.101

Figure 6.6b

The Aβ(1-42) peptide treated with $AlCl_3$ (50, 150, 300 and 400 μM). The relative intensities of the amide I absorption bands corresponding to the secondary structural features are shown below. Shaded values are changes greater than 0.003 absorbance units.

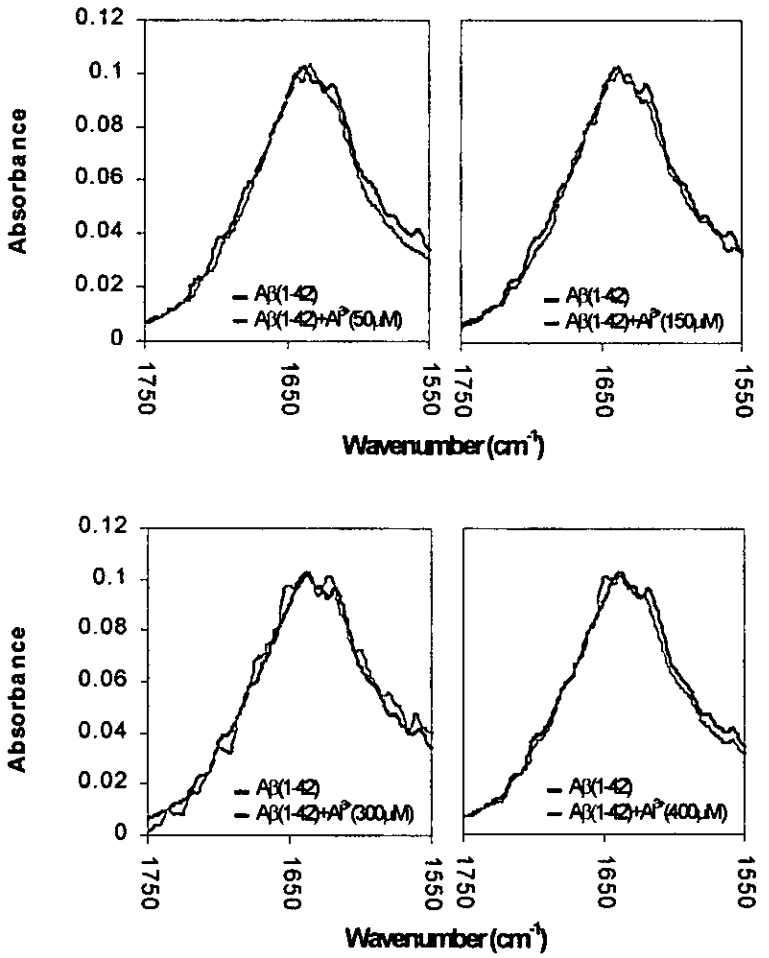

Secondary structures		Peak intensities				
		Aβ(1-42)	Al^{3+}(50μM)	Al^{3+}(150μM)	Al^{3+}(300μM)	Al^{3+}(400μM)
Antiparallel β sheets	(1685 cm^{-1})	0.052	0.052	0.052	0.049	0.050
α helix	(1649 cm^{-1})	0.089	0.091	0.095	0.091	0.098
Random	(1640 cm^{-1})	0.100	0.099	0.098	0.097	0.097
β sheet	(1630 cm^{-1})	0.096	0.097	0.101	0.104	0.098

Figure 6.6c

The Aβ extract treated with $AlCl_3$ (50, 150, 300 and 400 μM). The relative intensities of the amide I absorption bands corresponding to the secondary structural features are shown below. Shaded values are changes greater than 0.003 absorbance units.

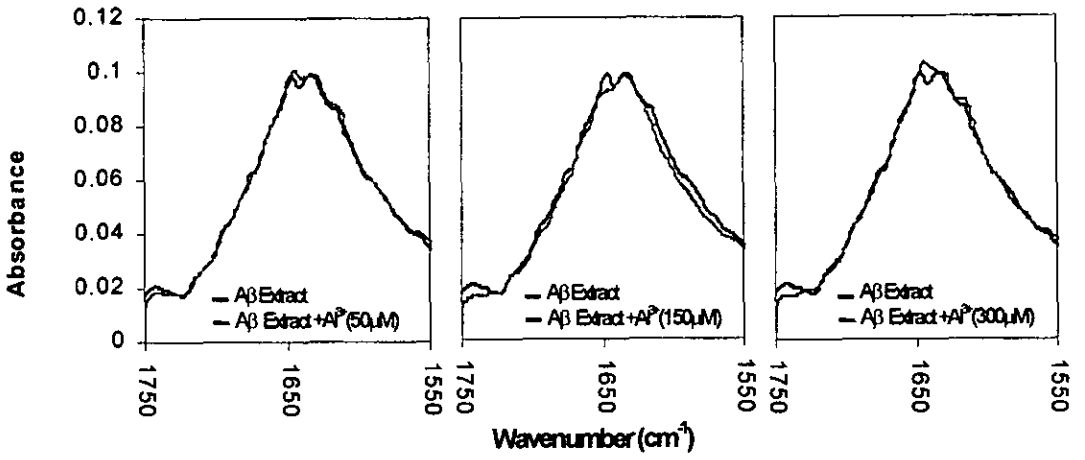

Secondary structures	Peak intensities			
	Aβ Extract	Al^{3+} (50 μM)	Al^{3+} (150 μM)	Al^{3+} (300 μM)
Antiparallel β sheets (1680 cm^{-1})	0.053	0.051	0.055	0.057
α helix (1648 cm^{-1})	0.091	0.090	0.093	0.092
Random (1635 cm^{-1})	0.099	0.093	0.098	0.099
β sheet (1627 cm^{-1})	0.096	0.098	0.099	0.099

Figure 6.7a1

The Aβ(1-40) peptide treated with $AlCl_3$ (50, 150, 300 and 400 μM). The relative intensities of the amide I absorption bands corresponding to the secondary structural features are shown below. Shaded values are changes greater than 0.003 absorbance units.

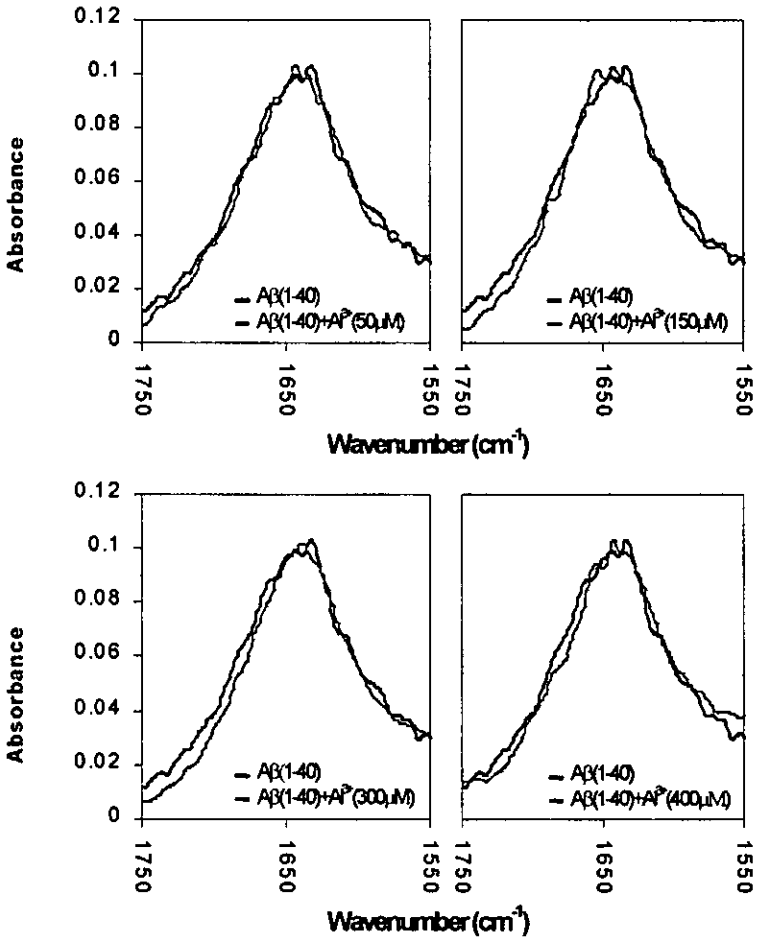

Secondary structures		Peak intensities				
		Aβ(1-40)	Al^{3+}(50μM)	Al^{3+}(150μM)	Al^{3+}(300μM)	Al^{3+}(400μM)
Antiparallel β sheets	(1683 cm^{-1})	0.062	0.059	0.052	0.048	0.050
α helix	(1650 cm^{-1})	0.095	0.091	0.098	0.084	0.088
Random	(1638 cm^{-1})	0.099	0.096	0.102	0.113	0.110
β sheet	(1628 cm^{-1})	0.104	0.103	0.105	0.108	0.107

Figure 6.7a2

The Aβ(1-40) peptide treated with $AlCl_3$ (150 and 300 μM) with SiO_4^{4-}(300 μM). The relative intensities of the amide I absorption bands corresponding to the secondary structural features are shown below. Shaded values are changes greater than 0.003 absorbance units.

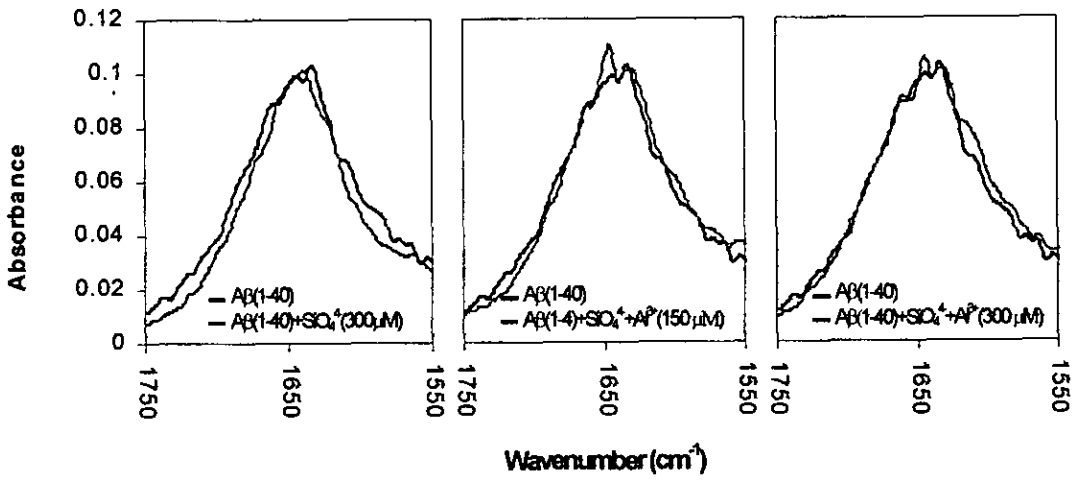

Secondary structures		Peak intensities			
		Aβ(1-40)	SiO_4^{4-}(300μM)	SiO_4^{4-}(300μM)+ Al^{3+}(150μM)	SiO_4^{4-}(300μM)+ Al^{3+}(300μM)
Antiparallel β sheets	(1683 cm^{-1})	0.062	0.062	0.059	0.060
α helix	(1650 cm^{-1})	0.095	0.092	0.090	0.089
Random	(1638 cm^{-1})	0.099	0.099	0.103	0.105
β sheet	(1628 cm^{-1})	0.104	0.101	0.102	0.107

Figure 6.7b1

The β_2M peptide treated with $AlCl_3$ (50, 150, 300 and 400 μM). The relative intensities of the amide I absorption bands corresponding to the secondary structural features are shown below. Shaded values are changes greater than 0.003 absorbance units.

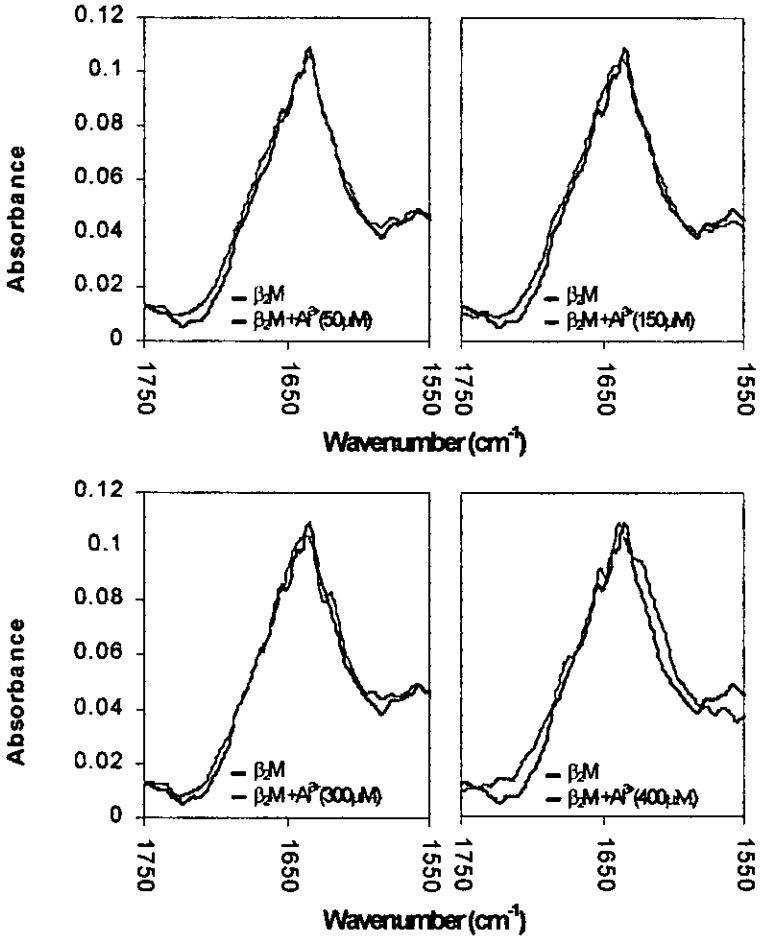

Secondary structures		Peak intensities				
		β_2M	Al^{3+}(50 μM)	Al^{3+}(150 μM)	Al^{3+}(300 μM)	Al^{3+}(400 μM)
Antiparallel β sheets	(1684 cm^{-1})	0.042	0.044	0.047	0.042	0.052
α helix	(1655 cm^{-1})	0.086	0.082	0.085	0.084	0.081
Random	(1644 cm^{-1})	0.099	0.099	0.102	0.105	0.104
β sheet	(1634 cm^{-1})	0.107	0.104	0.109	0.109	0.110

Figure 6.7b2

The β_2M peptide treated with $AlCl_3$ (150 and 300μM) with SiO_4^{4-} (300 μM). The relative intensities of the amide I absorption bands corresponding to the secondary structural features are shown below. Shaded values are changes greater than 0.003 absorbance units.

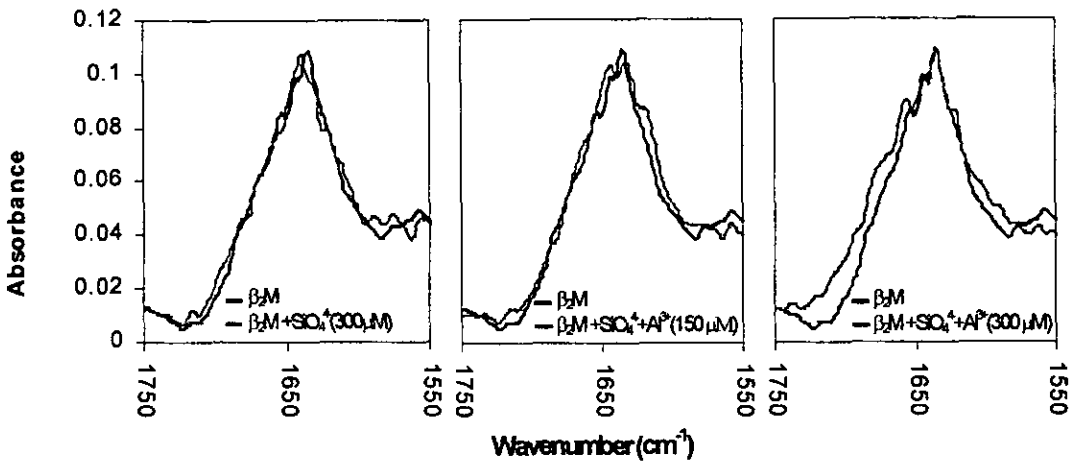

Secondary structures		Peak intensities			
		β_2M	SiO_4^{4-}(300μM)	SiO_4^{4-}(300μM)+ Al^{3+}(150μM)	SiO_4^{4-}(300μM)+ Al^{3+}(300μM)
Antiparallel β sheets	(1684 cm^{-1})	0.042	0.048	0.047	0.054
α helix	(1655 cm^{-1})	0.086	0.085	0.088	0.085
Random	(1644 cm^{-1})	0.099	0.100	0.102	0.101
β sheet	(1634 cm^{-1})	0.107	0.108	0.107	0.109

Figure 6.8a

The Aβ(1-40) peptide treated with heparan sulphate (HS) (500 μg ml^{-1}) and heparan sulphate proteoglycan (HSPG) (500 μg ml^{-1}) also combined with $CaCl_2$ (100 μM) The relative intensities of the amide I absorption bands corresponding to the secondary structural features are shown below. Shaded values are changes greater than 0.003 absorbance units.

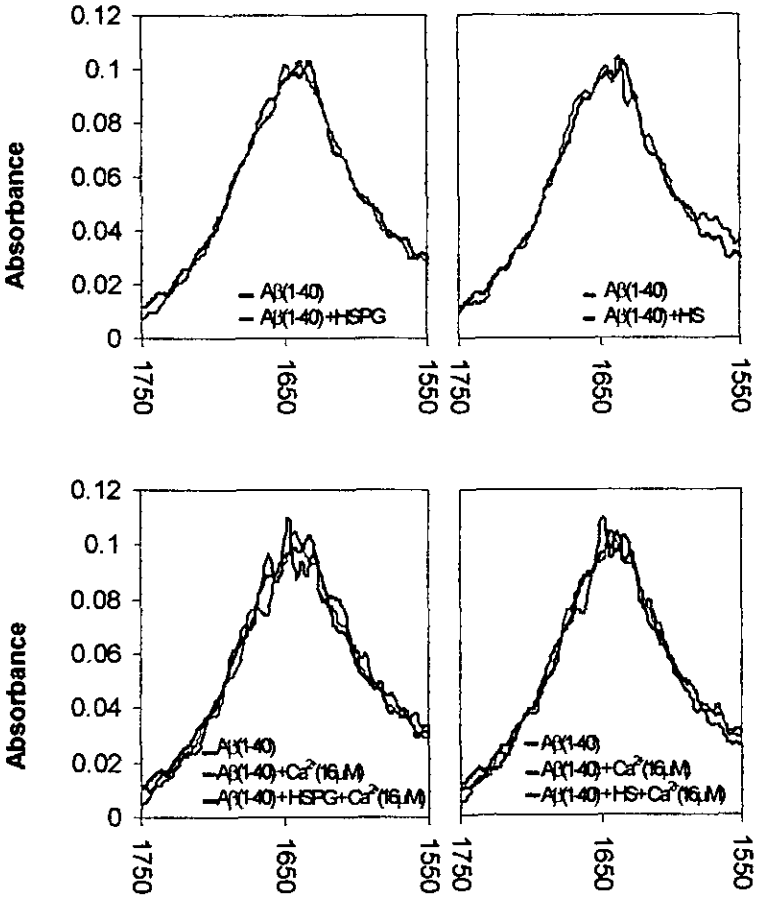

Secondary structures		Peak intensities					
		Aβ(1-40)	Ca^{2+}(16μM)	HSPG	HS	HSPG/Ca^{2+}	HS/Ca^{2+}
Antiparallel β sheets	(1683 cm^{-1})	0.062	0.068	0.059	0.057	0.066	0.052
α helix	(1650 cm^{-1})	0.093	0.090	0.089	0.090	0.083	0.095
Random	(1638 cm^{-1})	0.099	0.092	0.098	0.101	0.118	0.106
β sheet	(1628 cm^{-1})	0.104	0.108	0.100	0.101	0.107	0.105

Figure 6.8b

The β_2M peptide treated with heparan sulphate (HS) (500 μg ml^{-1}) and heparan sulphate proteoglycan (HSPG) (500 μg ml^{-1}) also combined with $CaCl_2$ (100 μM). The relative intensities of the amide I absorption bands corresponding to the secondary structural features are shown below. Shaded values are changes greater than 0.003 absorbance units.

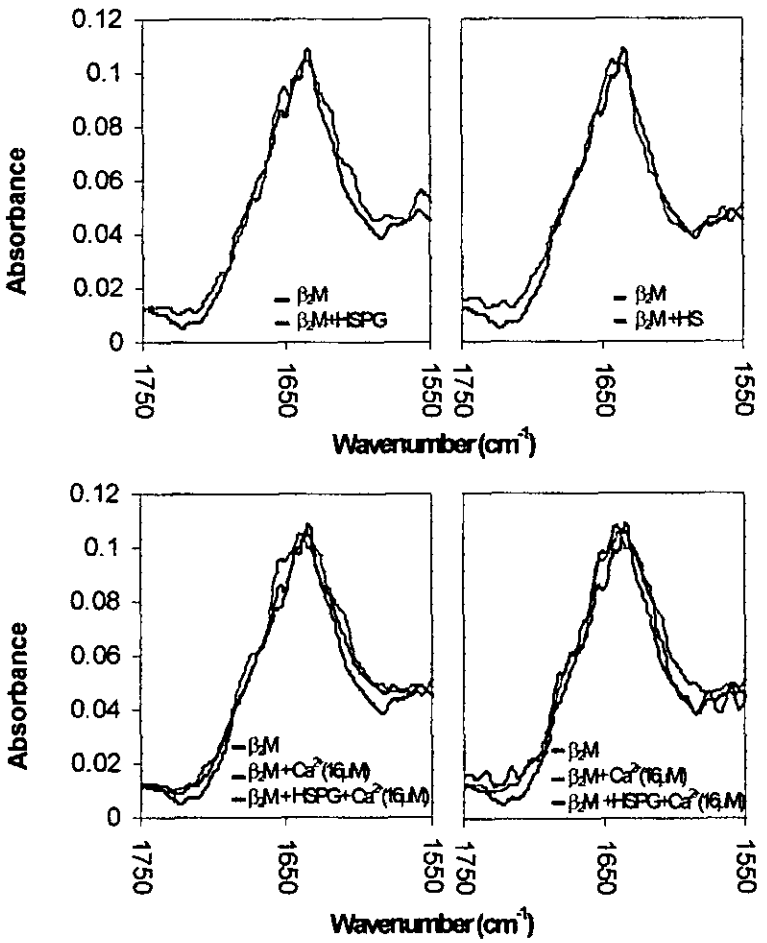

Secondary structures		Peak intensities					
		$ß_2M$	Ca^{2+}	HSPG	HS	HSPG/Ca^{2+}	HS/Ca^{2+}
Antiparallel β sheets	(1684 cm^{-1})	0.042	0.051	0.041	0.043	0.040	0.040
α helix	(1655 cm^{-1})	0.086	0.090	0.093	0.089	0.073	0.079
Random	(1644 cm^{-1})	0.099	0.109	0.102	0.100	0.100	0.105
β sheet	(1634 cm^{-1})	0.106	0.103	0.110	0.109	0.112	0.115

6.3 Summary of results.

The following tables show a summary of all the results.

Aβ(1-40)	α helix	Random	β sheet
Cu (100 μM)	↓↓	↓↓	↑
Zn (100 μM)	↓↓	↓↓	↑
Ca (100 μM)	↓	↓	↑↑
Mg (100 μM)	—	—	—
Al (50 μM)	↓	↓	—
Al (150 μM)	↓	↑	—
Al (300 μM)	↓↓	↑↑	↑
Al (400 μM)	↓↓	↑↑	↓
Si (300 μM)	—	—	—
Si (300 μM)/Al (150 μM)	—	—	—
Si (300 μM)/Al (300 μM)	—	↓	—
HSPG (500 μg ml^{-1})	—	—	—
HS (500 μg ml^{-1})	—	—	—
HSPG (500 μg ml^{-1})/Ca (100 μM)	↓↓	↑↑	—
HS (500 μg ml^{-1})/ Ca (100 μM)	↓	↑	—

Table 6.2a - Experiments with Aβ(1-40), the differences from the native peptide are indicated by: ↑ (>0.03 absorbance units), ↑↑ (>0.06 absorbance units) and ↑↑↑ (>0.1 absorbance units).

β_2M	α helix	Random	β sheet
Cu (100 μM)	↓	↑↑	↑
Zn (100 μM)	↓	↑↑	↑↑
Ca (100 μM)	↑	↑↑	↓
Mg (100 μM)	—	—	—
Al (50 μM)	—	—	—
Al (150 μM)	—	—	—
Al (300 μM)	↓	↑	—
Al (400 μM)	↓	↑	↑
Si (300 μM)	—	—	—
Si (300 μM)/Al (150 μM)	—	—	—
Si (300 μM)/Al (300 μM)	—	—	—
HSPG (500 μg ml^{-1})	—	—	↑
HS (500 μg ml^{-1})	—	—	↑
HSPG (500 μg ml^{-1})/Ca (100 μM)	↓↓	—	↑↑
HS (500 μg ml^{-1})/ Ca (100 μM)	—	↑	↑↑

Table 6.2b - Experiments with β_2M, the differences from the native peptide are indicated by: ↑ (>0.03 absorbance units), ↑↑ (>0.06 absorbance units) and ↑↑↑ (>0.1 absorbance units).

Aβ(1-43)	α helix	Random	β sheet
Cu (100 μM)	↓↓	↑	↓↓
Zn (100 μM)	↓	—	—
Ca (100 μM)	↑	↑↑	↓
Al (50 μM)	—	↓	—
Al (150 μM)	—	↓	—
Al (300 μM)	—	↓↓	↑
Al (400 μM)	↑	↓↓	↑

Table 6.2c - Experiments with Aβ(1-43), the differences from the native peptide are indicated by: ↑ (>0.03 absorbance units), ↑↑ (>0.06 absorbance units) and ↑↑↑ (>0.1 absorbance units).

Aβ(1-42)	α helix	Random	β sheet
Cu (100 μM)	—	↓	—
Zn (100 μM)	↓↓	↑	↑↑
Ca (100 μM)	↓	↓	—
Al (50 μM)	—	—	—
Al (150 μM)	—	—	↑
Al (300 μM)	—	—	↑
Al (400 μM)	↑↑	—	—

Table 6.2d - Experiments with Aβ(1-42), the differences from the native peptide are indicated by: ↑ (>0.03 absorbance units), ↑↑ (>0.06 absorbance units) and ↑↑↑ (>0.1 absorbance units).

Extract	α helix	Random	β sheet
Cu (100 μM)	—	↓	—
Zn (100 μM)	↓↓	↑	↑↑
Ca (100 μM)	↓	↓	—
Al (50 μM)	—	↓	—
Al (150 μM)	—	—	—
Al (300 μM)	—	—	—

Table 6.2e - Experiments with Aβ extract, the differences from the native peptide are indicated by: ↑ (>0.03 absorbance units), ↑↑ (>0.06 absorbance units) and ↑↑↑ (>0.1 absorbance units).

6.4 Discussion

The novel use of ATR-FTIR in the analysis of metals with amyloids has been demonstrated for the different amyloid peptides Aβ(1-40), Aβ(1-42), Aβ(1-43), the Aβ extract from Alzheimer's disease brain and β_2M. The developed method used an acetate 'cover-slip' to reduce the sample volume. The technique of ATR-FTIR has not been previously used to detect changes in the secondary structure of the amyloids treated with metals. Further spectral deconvolution is necessary for the determination of the percentages of secondary structures. However, much information can be obtained by monitoring changes within the spectra for individual peptides.

It should be noted that the buffer used in the ATR experiments only contained tris (10 mM, pH 7.4). The buffer used in the CD experiments contained trifluoroethanol, which stabilises α helices. Therefore, any changes in the secondary structures are more pronounced in CD especially if the α helices are altered. Also, the ATR method is less sensitive because of the inherent high absorbance of water. The different protein environments between the ATR and CD studies could account for any differences in the results or it may be the case that the ATR method is not sensitive enough to detect these changes.

6.4.1 Amyloid proteins treated with metals.

Most of the metals had the effect of decreasing α helices in all of the amyloids except Aβ(1-43). The changes are small for the treatment of metals with Aβ(1-43). With Cu^{2+} and Zn^{2+} with the Aβ(1-40) and the β_2M, there was a redistribution of α helices to β sheets and random coil secondary structures. These results are similar to those obtained in the CD spectra in **Chapter 5, section 5.2.3**, where there was also a decrease in α helices and an increase in β sheets with Aβ(1-40) and β_2M treated with Cu^{2+} and Zn^{2+}.

Zn^{2+} and Cu^{2+} ions have been implicated in both Aβ aggregation and neurotoxicity and have both been shown to cause aggregation of Aβ peptide *in vitro* [331 & 333]. Aβ preferentially and saturably binds Zn^{2+} [331], and induces synthetic Aβ aggregation in a pH-dependent and reversible manner [238, 332, 333, 345-347].

Copper is able to stabilise the formation of dimers of Aβ(1-40) as observed with affinity gel chromatography [331]. The Aβ(1-40) has both Cu^{2+} and Zn^{2+} binding sites and both can simultaneously bind [331 & 336]. Metal mediated radical damage of Aβ has been suggested as a causative agent for Aβ neurotoxicity [348-350].

6.4.2 Amyloid proteins treated with aluminium and silicon.

Addition of Al^{3+} increased the β sheets with a decrease α helix with both the Aβ(1-40) and β_2M and similarly there were no significant changes with both the Aβ(1-43) and Aβ(1-42). In the CD work in **Chapter 5, section 5.2.4.,** there was also a general decrease in α helices with an increase in β sheets with both the Aβ(1-40) and β_2M. Similar changes to that of the CD results (**Chapter 5, section 5.2.5**) were also observed with the Aβ(1-40) with Al^{3+} and SiO_4^{4-}. Addition of the silicate caused a reversal in the changes due to Al^{3+} itself. Therefore, interaction of SiO_4^{4-} and Al^{3+} to form aluminosilicates may mean less available soluble aluminium for interaction with the proteins.

It has been suggested that the binding of Al^{3+} to Aβ peptide [351] and tau proteins [352] results in the formation of senile plaques and neurofibrillary tangles as observed in AD brains. [264] Aluminium can promote the phosphorylation and aggregation of tau proteins and also induce the aggregation of conformationally modified Aβ peptide *in vitro* [353]. Amino acid-Al complexes such as D-Asp-Al and L-Glu-Al induce a larger random coil conformation in the Aβ peptide than the free Al^{3+} [278]. The putative toxicity of amyloids can be mediated by aluminium, aluminium silicates, and/or metal catalysed oxidative damage resulting in increased risk for premature amyloid deposition [94].

6.4.3 Amyloid proteins treated with GAGs and calcium.

There were some slight differences in the ATR results compared to those from the CD work in **Chapter 5, section 5.2.6-5.2.9**. The Aβ(1-40) with HSPG or HS and Ca^{2+} caused decreases in α helices and a redistribution to both random coil and β sheet, which was also seen in the CD. For β_2M, the CD showed that with combined calcium and HSPG and HS, there were further decreases in α helices and β sheets with increases in random coil. The ATR showed that these combinations of GAGs and

Ca^{2+} with β_2M caused a decrease in α helices but with an increase in β sheets and random coil. There was, however, a common decrease in α helices as seen in both studies. This still highlights the fact that combinations of GAGs and metals had additive effects compared to the GAGs or Ca^{2+} on its own.

Very specific high affinity interactions have been shown to occur between the HSPG and the various forms of the Alzheimer amyloid precursor protein [354]. The GAGs may bind to the region of His13-Lys16 of Aβ between two neighbouring filaments. In this way, the ultrastructure of the fibres would be maintained and the stability enhanced. GAGs could affect the nucleation and propagation of these fibres by stabilising the tertiary structure and inter-sheet interactions [355] and may serve as an anchor for fibril organisation [315].

6.5 Conclusion.

A novel technique for reducing the volume of sample required for the ATR-FTIR system has been demonstrated. The detection of amyloid treated with metals as seen with ATR-FTIR was similar to the results of the CD work. In the ATR study, the addition of copper, zinc, calcium and aluminium (>100 μM) to the amyloid proteins, in particular the Aβ(1–40) and β_2M, showed some changes with a general decrease in α helix and an increase in β sheet, though the results with the β_2M were smaller. Although no interaction between GAGs and the amyloids was seen, the binding of the GAGs could provide an anchor for the assembly of the fibrils or could allow binding of other factors such as metal ions leading to subsequent aggregation and amyloidosis.

Chapter 7. Polyacrylamide gel electrophoresis of amyloid proteins treated with metals.

7.1 Introduction.

Polyacrylamide gel electrophoresis (PAGE) is a useful technique for the separation of proteins with a net charge by the differential movement of the protein gel under an electric field. The polyacrylamide gel consists of uniform sized 'pores' formed from the polymerisation of acrylamide and methylenebisacrylamide. The mixture of proteins is denatured by first dissolving it in a solution of sodium dodecyl sulphate (SDS), that disrupts nearly all non-covalent interactions in native proteins, treatment with dithiothreitol to break disulphide bonds. The SDS coats the protein giving an overall negative charge, which is much greater than the charge of the native protein; thus separation is solely due to mass under denaturing conditions. The mobility of most polypeptide chains under these conditions is linearly proportional to the logarithm of their mass.

7.1.1 The use of PAGE in the study of amyloids.

SDS PAGE has been used extensively for the analysis of various amyloids and the determination of extracted amyloid proteins. It is an indispensable analytical tool for purification, detection, characterisation and determination of the molecular weight of the isolated amyloid protein [356]. SDS PAGE has been used in the extraction of Alzheimer's disease β amyloid [294, 356-359] and also in the extraction of β_2M from amyloid laden tissues [157, 167, 360-362]. The proteins are usually run on the polyacrylamide gels of uniform concentration (15-17%) or of linear gradient concentration (from 5% to 20%), using a continuous buffer system containing 0.025 M tris, 0.192 M glycine and 0.1% SDS [363]. Other techniques including the use of continuous buffers such as tris phosphate [363], and tricine (instead of glycine) and the use of discontinuous buffers systems such as tris-glycine [364], tris-tricine [365], trisbicine [366] and urea [367 & 368] have all been used in different amyloid studies.

Western blotting has also been extensively used for the immuno-detection of amyloids and has been shown to be effective for the determination of the type and

size of amyloid proteins when using the appropriate antibodies raised against different amyloid fibril proteins and their precursor proteins [356]. Two-dimensional PAGE has also been used to detect the presence of two or more acidic isoforms of β_2M with pI coordinates (5.3-5.7) [157 & 356]. More specifically SDS PAGE has been used in the study of amyloids treated with aluminium. Aluminium was revealed to promote the aggregation of synthetic amyloid β-protein Aβ(1-40) using immunoblotting and centrifugation [369 & 370]. Aluminium also caused aggregation of human recombinant amyloid precursor protein (APP) as investigated with SDS-PAGE [370].

7.1.1 The present study.

The present study investigated amyloid proteins treated with metals and glycosaminoglycans. Experiments showing the effect of metals on the charge and electrophoretic mobility of the amyloid peptides were carried out using gel electrophoresis. Any changes such as aggregation, fibril formation etc were detected using SDS PAGE. The synthetic amyloid peptides used were Aβ(1-43), Aβ(1-42), Aβ(1-40) peptides, as found in senile plaques in the brains of Alzheimer's disease sufferer. The Aβ extracted peptide and the synthetic β2 microglobulin, as found in dialysis related amyloidosis, were also used.

7.1.2 Method.

Experimental methods, instrumentation and reagent details are given in **Chapter 2, Section 2.6.**

7.2 Results.

7.2.1 Aβ(1-40) treated with metals.

The SDS-PAGE results of Aβ(1-40) amyloid protein treated with $AlCl_3$ (1 mM), $CuCl_2$ (1 mM), $ZnCl_2$ (1 mM), $CaCl_2$ (1 mM) and $MgCl_2$ (1 mM) are shown in **Figure 7.1**. The Aβ(1-40) was seen at 4.3 kDa corresponding to the monomer. The addition of the metals, with the exception of aluminium, did not affect the electrophoretic mobility of the Aβ(1-40) as seen in SDS PAGE. Aluminium caused a smearing of the band with a possible formation of the dimer of Aβ(1-40).

7.2.2 Aβ(1-40) treated with aluminium.

The Aβ(1-40) amyloid protein treated with increasing concentrations of Al^{3+} (12.5, 25, 50, 150, 300 and 400 μM) are shown in **Figure 7.2.** These concentrations are lower than the concentration used in the previous experiment with Aβ(1-40). These samples were run both with SDS and natively with no SDS. The SDS PAGE in **Figure 7.2a** show that treatment with increasing Al^{3+} did not have any affect on the Aβ(1-40). The non SDS treatment of the samples gave a PAGE as shown in **Figure 7.2b**. The bands show an elongation with a greater degree of smearing with higher concentration of Al^{3+}.

7.2.3 Aβ(1-40) treated with GAGs and metals.

The **Figures 7.3** and **Figure 7.4** show the SDS PAGE of Aβ(1-40) treated with various GAGs and combinations of GAGs with metals. There were no visible changes in the mobility of Aβ(1-40) with any of the combinations of GAGs and metals.

Figure 7.1

The Aβ(1-40) amyloid protein treated with Al^{3+} (1 mM), Cu^{2+} (1 mM), Zn^{2+} (1 mM), Ca^{2+} (1 mM) and Mg^{2+} (1 mM). The molecular weight markers are shown in the left lane.

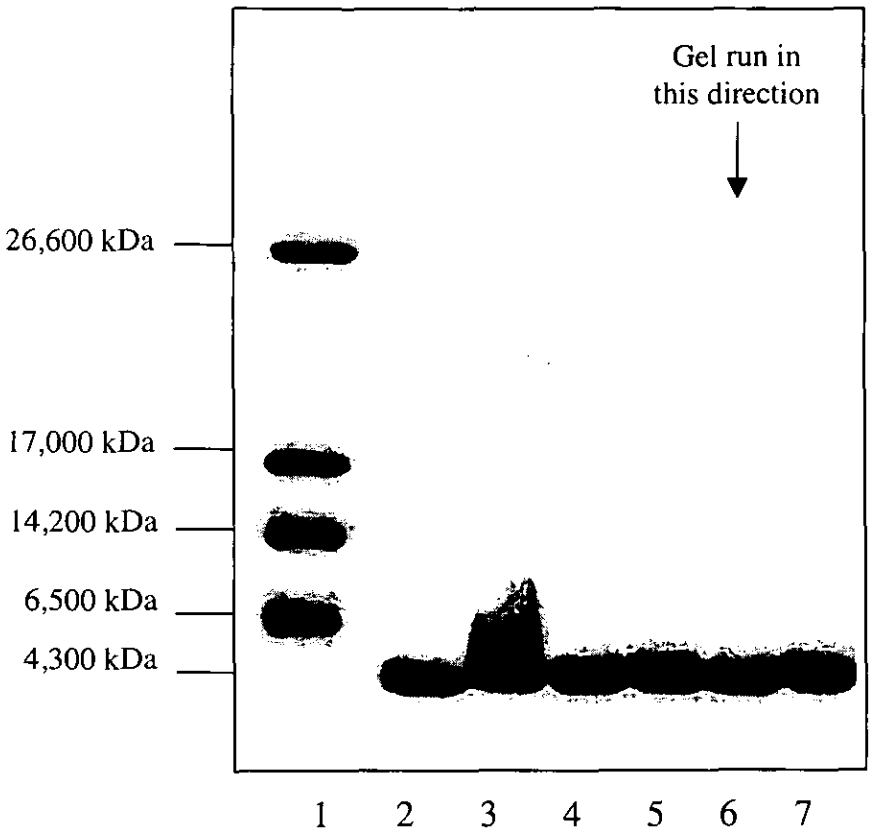

Lane	Sample
1	MW markers
2	Aβ(1-40)
3	Aβ(1-40) + Al^{3+} (1 mM)
4	Aβ(1-40) + Cu^{2+} (1 mM)
5	Aβ(1-40) + Zn^{2+} (1 mM)
6	Aβ(1-40) + Ca^{2+} (1 mM)
7	Aβ(1-40) + Mg^{2+} (1 mM)

Figure 7.2

The Aβ(1-40) amyloid protein treated with increasing concentrations of Al^{3+} (12.5, 25, 50, 150, 300 and 400 μM). These samples were run both (**a**) with SDS and (**b**) non SDS, i.e. natively run. Both the gels were processed with silver staining. The molecular weight markers are shown in the left lane.

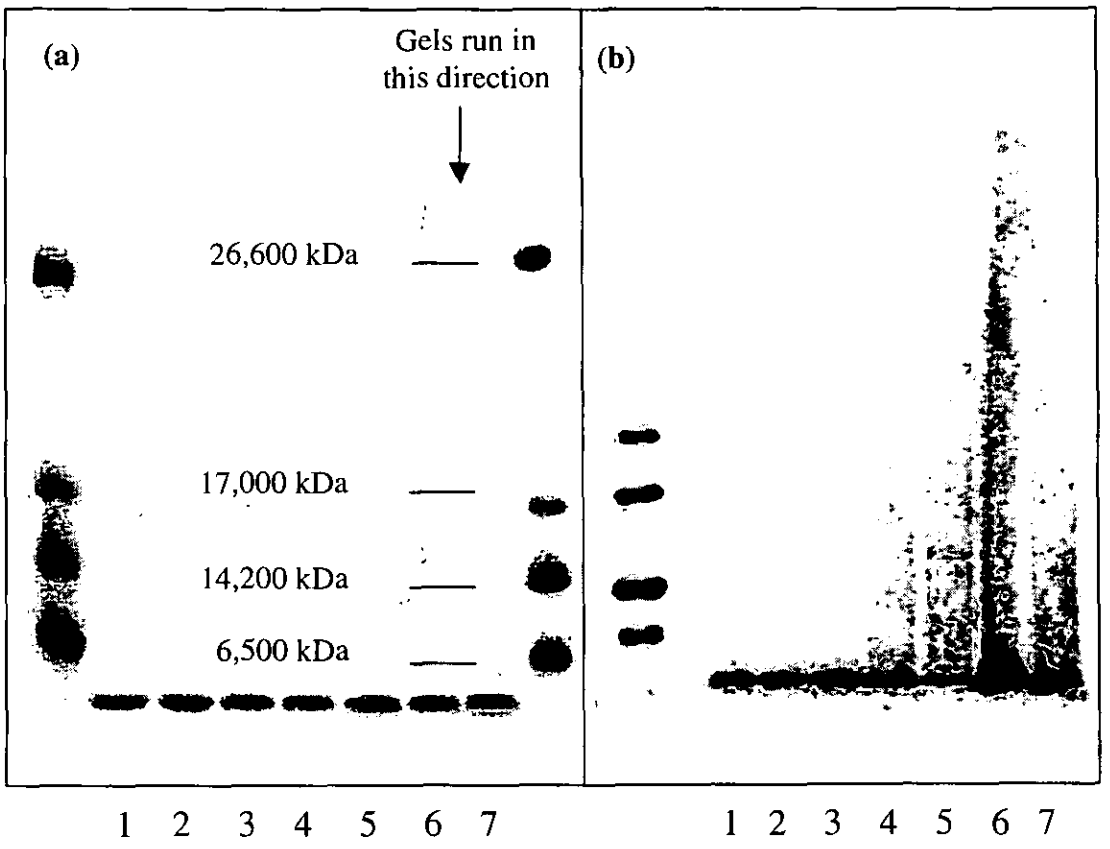

Lane	Sample
1	Aβ(1-40)
2	Aβ(1-40) + Al (12.5 μM)
3	Aβ(1-40) + Al (25 μM)
4	Aβ(1-40) + Al (50 μM)
5	Aβ(1-40) + Al (150 μM)
6	Aβ(1-40) + Al (300 μM)
7	Aβ(1-40) + Al (400 μM)

Figure 7.3

The Aβ(1-40) amyloid protein treated with (**a**) heparan sulphate, (**b**) heparan sulphate proteoglycan and (**c**) dermatan sulphate with Ca^{2+} (100 μM), Cu^{2+} (100 μM), Al^{3+} (300 μM), SiO_4^{4-} (300 μM) and Al^{3+} (300 μM) with SiO_4^{4-} (300 μM).

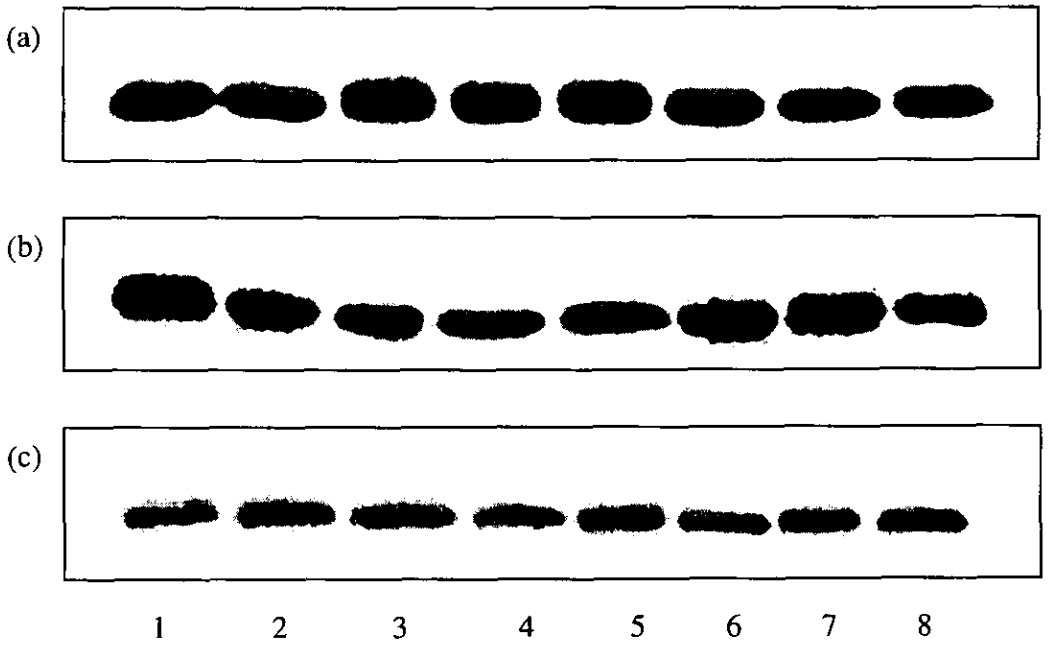

Lane	Sample
1	Aβ(1-40)
2	Aβ(1-40) + GAG (500 μg ml^{-1})
3	Aβ(1-40) + GAG (500 μg ml^{-1})
4	Aβ(1-40) + GAG (500 μg ml^{-1}) + Ca^{2+} (100 μM)
5	Aβ(1-40) + GAG (500 μg ml^{-1}) + Cu^{2+} (100 μM)
6	Aβ(1-40) + GAG (500 μg ml^{-1}) + Al^{3+} (300 μM)
7	Aβ(1-40) + GAG (500 μg ml^{-1}) + Al^{3+} + SiO_4^{4-} (both 300 μM)
8	Aβ(1-40) + GAG (500 μg ml^{-1}) + SiO_4^{4-} (300 μM)

Figure 7.4

The Aβ(1-40) amyloid protein treated with heparan sulphate, heparin and Na_2SO_4 with Ca^{2+} (100 μM). The molecular weight markers are shown in the left lane.

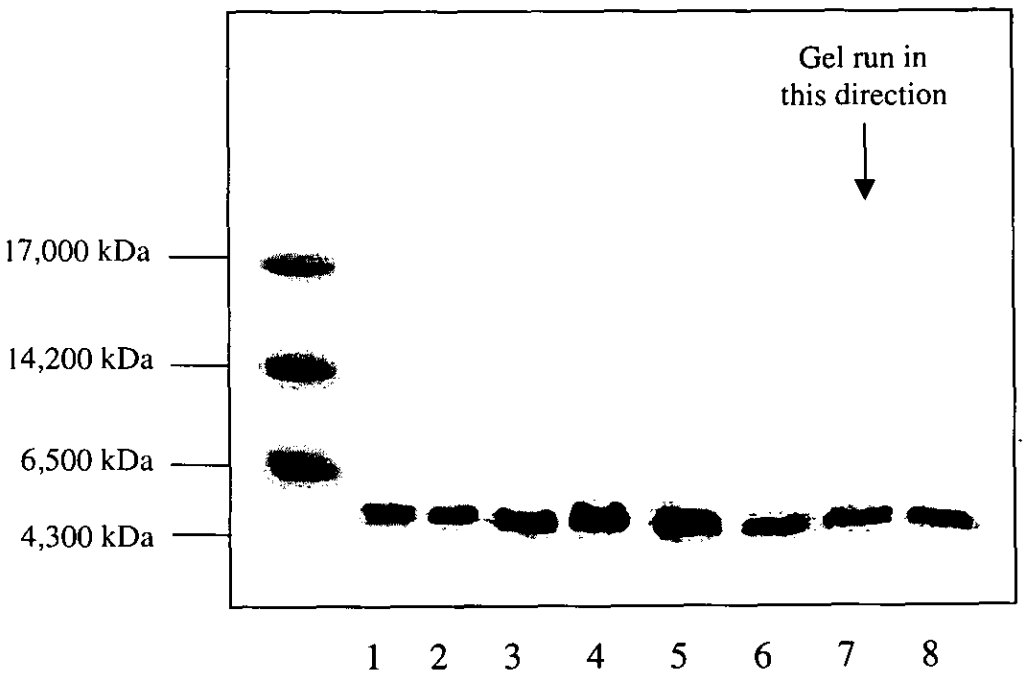

Lane	Sample
1	β(1-40)
2	β(1-40) + Heparin (500 μg.ml^{-1})
3	β(1-40) + Heparin (500 μg.ml^{-1}) + Ca^{2+} (100 μM)
4	β(1-40) + HS (500 μg.ml^{-1})
5	β(1-40) + HS (500 μg.ml^{-1}) + Ca^{2+} (100 μM)
6	β(1-40) + Na_2SO_4 (500 μg.ml^{-1})
7	β(1-40) + Na_2SO_4 (500 μg.ml^{-1}) + Ca^{2+} (100 μM)
8	β(1-40)

7.2.4 β_2M treated with metals.

The β_2M amyloid protein treated with Al^{3+}, Cu^{2+}, Zn^{2+}, Ca^{2+} and Mg^{2+} (1 mM) are shown in **Figure 7.5.** The β_2M was seen as a band at 12 kDa corresponding to the monomer. The addition of the metals, with the exception of Al^{3+}, did not affect the β_2M in SDS PAGE. Al^{3+} caused a smearing of the band with a possible formation of the dimer (24 kDa), and higher aggregates of β_2M. This result is similar to that of the Aβ(1-40) (**Figure 7.1**). There were no effects with Cu^{2+}, Mg^{2+}, Ca^{2+} or Zn^{2+}.

7.2.5 β_2M treated with aluminium and with aluminium and silicon.

The β_2M peptide treated with increasing concentrations of Al^{3+} (25, 50, 150, 300 and 400 μM) and mixtures of Al^{3+} with silicate are shown in **Figure 7.6**. These samples were run both (**Figure 7.6a**) with SDS and (**Figure 7.6b**) natively. The SDS PAGE in **Figure 7.6a** show that treatment with increasing Al^{3+} did not have any affect on the β_2M and may indicate a concentration as well as a time dependent effect. There were feint high molecular weight bands near the top of the gel, which may be related to the β_2M samples or may be due to artefacts in the experiment. There was no other high molecular weight protein in any of the samples, which indicates that the bands may be very high molecular weight polymers of the β_2M or aggregates.

Non SDS treatment of the samples gave a PAGE as shown in **Figure 7.6b**. Lanes 3, 4, 5, and 6 show two bands with Al^{3+} (50, 150, 300 and 400 μM) which correspond to dimers of the β_2M. There was a greater conversion of monomer to dimer with increasing Al^{3+} as seen by increasing intensity of the higher molecular weight bands and decreasing intensity of the monomer band. Addition of a higher concentration of silicon abolished this higher molecular weight band with a reversion back to the monomer as seen in lane 9.

7.2.6 Two dimensional PAGE of β_2M treated with aluminium.

A further experiment was performed with the aluminium treated β_2M sample. A two dimensional electrophoresis gel was run with the β_2M treated with aluminium (300 μM). The β_2M peptide (85 μM) was treated with aluminium (300 μM) and allowed to incubate at room temperature for 1 hour. The first dimension was run as an isoelectric focused gel. In 2 dimensional, the first tube gel was carefully removed and was laid on top of the second dimension gel and was run as an SDS PAGE gel. The two dimensional gels showed no bands except one spot corresponding to the β_2M itself indicating that no dimers or other isoforms were present (results not shown).

7.2.7 β_2M treated with GAGs and metals.

The **Figures 7.7** and **7.8** show the SDS PAGE of β_2M treated with various GAGs and combinations of GAGs with metals. There were no visible changes in the mobility of β_2M with any of the combinations of GAGs and metals. This may be due to the fact that the samples have not been allowed to incubate long enough.

7.2.8 Aβ(1-42) and Aβ(1-43) treated with metals and with silicon.

The **Figures 7.9** and **7.10** show the SDS PAGE of Aβ(1-42) and Aβ(1-43) treated with various metals and combinations of aluminium and silicon. There were no visible changes in the mobility of the amyloids with either the metals or any of the combinations of aluminium and silicon.

Figure 7.5

The β_2M amyloid protein treated with $AlCl_3$ (1 mM), $CuCl_2$ (1 mM), $ZnCl_2$ (1 mM), $CaCl_2$ (1 mM) and $MgCl_2$ (1 mM). The molecular weight markers are shown in the left lane.

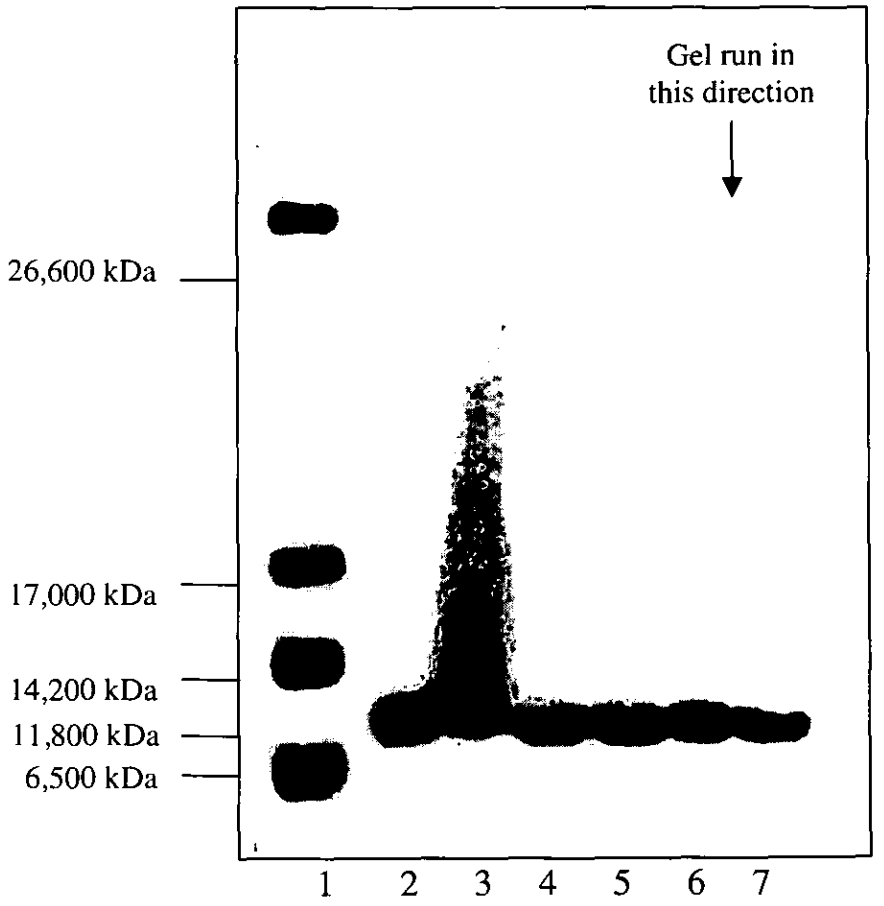

Lane	Sample
1	MW markers
2	β_2M
3	$\beta_2M + Al^{3+}$ (1 mM)
4	$\beta_2M + Cu^{2+}$ (1 mM)
5	$\beta_2M + Zn^{2+}$ (1 mM)
6	$\beta_2M + Ca^{2+}$ (1 mM)
7	$\beta_2M + Mg^{2+}$ (1 mM)

Figure 7.6

The β_2M treated with increasing concentrations of Al^{3+} (25, 50, 150, 300, and 400 μM) and with SiO_4^{4-} (100 and 300 μM) run **(a)** with SDS and **(b)** natively. Gels were processed with silver staining.

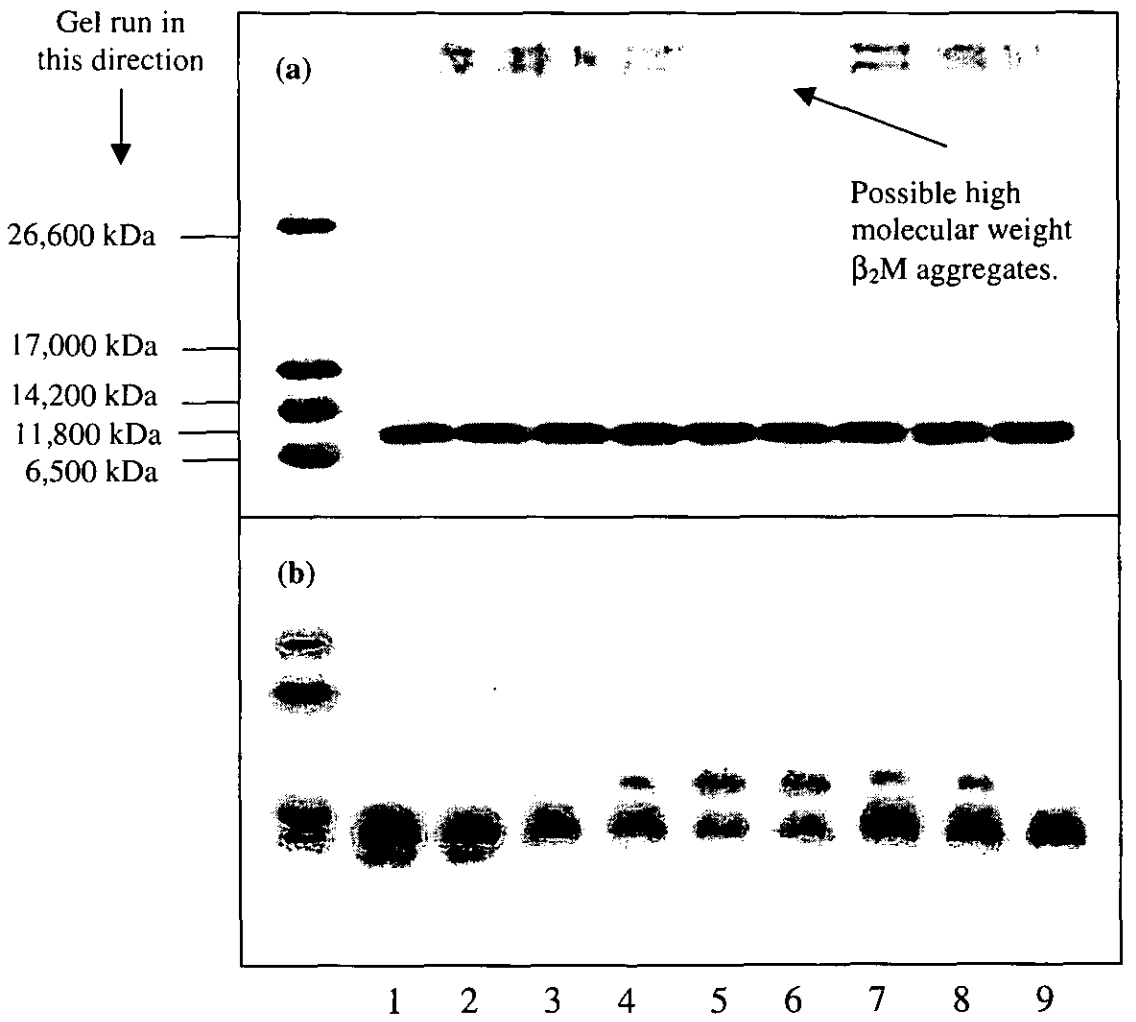

Lane	Sample
1	β_2M
2	$\beta_2M + Al^{3+}$ (25 μM)
3	$\beta_2M + Al^{3+}$ (50 μM)
4	$\beta_2M + Al^{3+}$ (150 μM)
5	$\beta_2M + Al^{3+}$ (300 μM)
6	$\beta_2M + Al^{3+}$ (400 μM)
7	$\beta_2M + Al^{3+}$ (150 μM) + SiO_4^{4-} (100μM)
8	$\beta_2M + Al^{3+}$ (300 μM) + SiO_4^{4-} (100μM)
9	$\beta_2M + Al^{3+}$ (300 μM) + SiO_4^{4-} (300μM)

Figure 7.7

The β_2M amyloid protein treated with **(a)** heparan sulphate, **(b)** heparan sulphate proteoglycan and **(c)** dermatan sulphate with Ca^{2+} (100 μM), Cu^{2+} (100 μM), Al^{3+} (300 μM), SiO_4^{4-} (300 μM) and Al^{3+} (300 μM) with SiO_4^{4-} (300 μM).

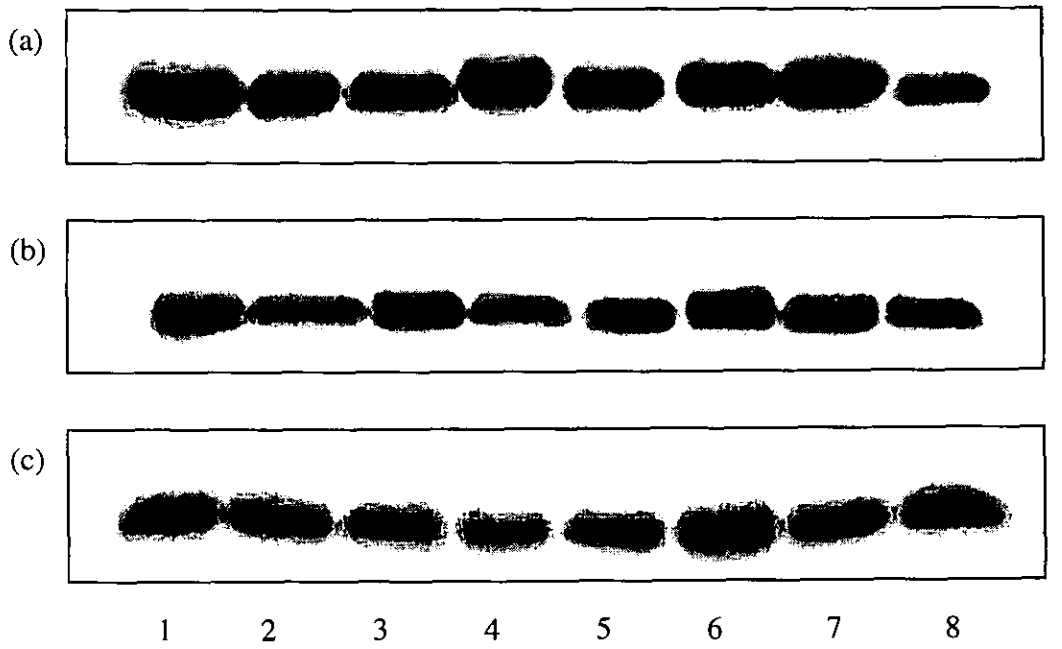

Lane	Sample
1	β_2M
2	β_2M + GAG (500 μg ml^{-1})
3	β_2M + GAG (500 μg ml^{-1})
4	β_2M + GAG (500 μg ml^{-1}) + Ca^{2+} (100 μM)
5	β_2M + GAG (500 μg ml^{-1}) + Cu^{2+} (100 μM)
6	β_2M + GAG (500 μg ml^{-1}) + Al^{3+} (300 μM)
7	β_2M + GAG (500 μg ml^{-1}) + Al^{3+} + SiO_4^{4-} (both 300 μM)
8	β_2M + GAG (500 μg ml^{-1}) + SiO_4^{4-} (300 μM)

Figure 7.8

The β_2M amyloid protein treated with heparan sulphate, heparin and Na_2SO_4 with Ca^{2+} (100 μM). The molecular weight markers are shown in the left lane.

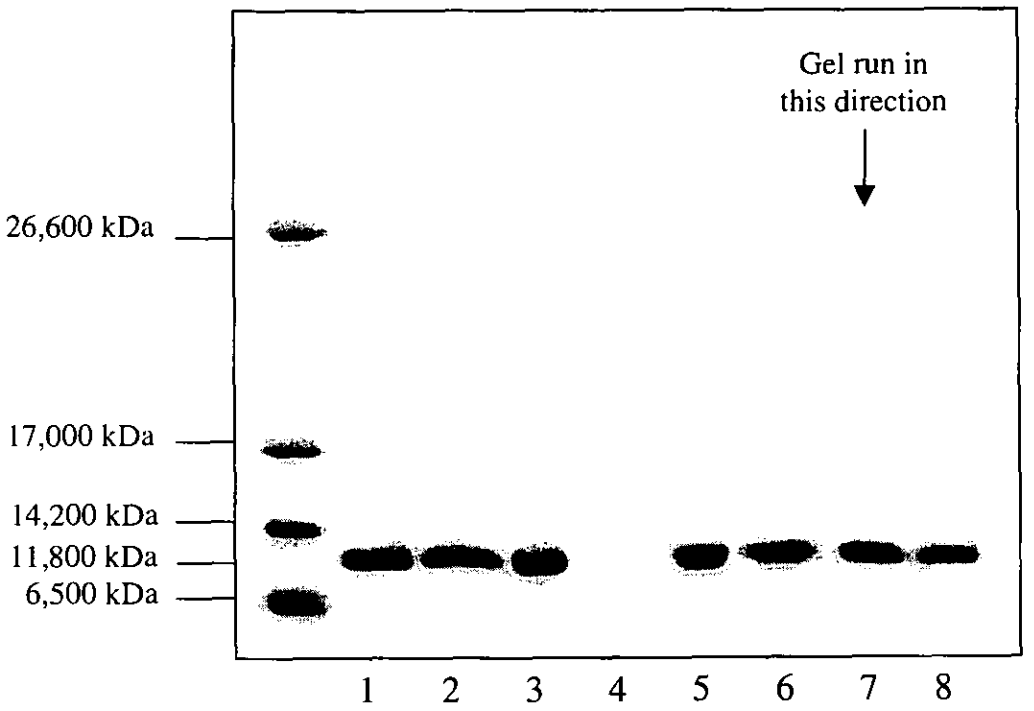

Lane	Sample
1	β_2M
2	β_2M + HS (500 $\mu g.ml^{-1}$)
3	β_2M + HS (500 $\mu g.ml^{-1}$) + Ca^{2+} (100 μM)
4	
5	β_2M + Heparin (500 $\mu g.ml^{-1}$)
6	β_2M + Heparin (500 $\mu g.ml^{-1}$) + Ca^{2+} (100 μM)
7	β_2M + Na_2SO_4 (500 $\mu g.ml^{-1}$)
8	β_2M + Na_2SO_4 (500 $\mu g.ml^{-1}$) + Ca^{2+} (100 μM)

Figure 7.9

The Aβ(1–42) amyloid protein treated with Al^{3+} (1 mM), Cu^{2+} (1 mM), Zn^{2+} (1 mM), Ca^{2+}(1 mM) and with Al^{3+} and SiO_4^{4-} (1 mM). The molecular weight markers are shown in the left lane.

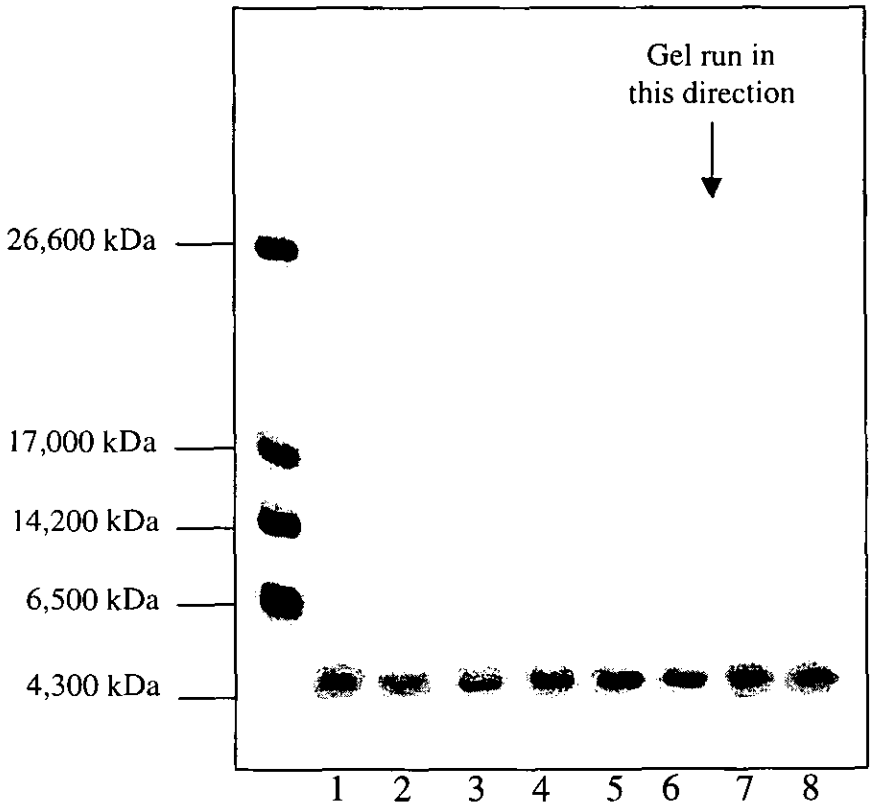

Lane	Sample
1	Aβ(1–42)
2	Aβ(1–42) + Al^{3+} (1 mM)
3	Aβ(1–42) + Cu^{2+} (1 mM)
4	Aβ(1–42) + Zn^{2+} (1 mM)
5	Aβ(1–42) + Ca^{2+} (1 mM)
6	Aβ(1–42) + Al^{3+} (1 mM)
7	Aβ(1–42) + SiO_4^{4-} (1 mM)
8	Aβ(1–42) + Al^{3+} + SiO_4^{4-} (both 1 mM)

Figure 7.10

The Aβ(1-43) amyloid protein treated with Al^{3+} (1 mM), Cu^{2+} (1 mM), Zn^{2+} (1 mM), Ca^{2+} (1 mM) and with Al^{2+} and SiO_4^{4-} (1 mM). The molecular weight markers are shown in the left lane.

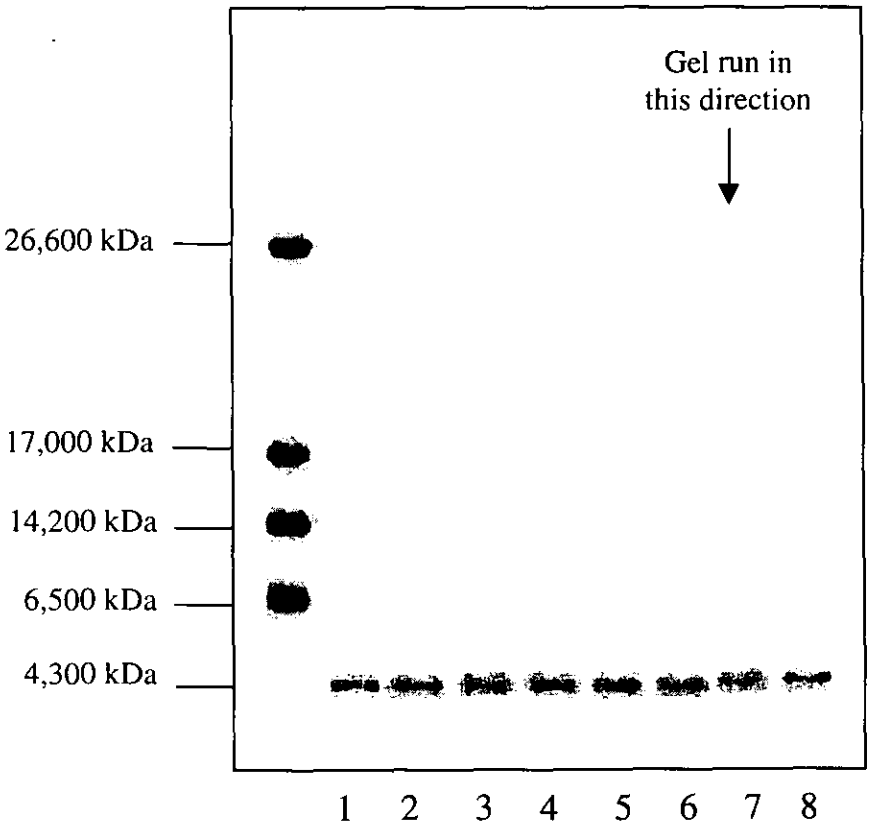

Lane	Sample
1	Aβ(1–43)
2	Aβ(1–43) + Al^{3+} (1 mM)
3	Aβ(1–43) + Cu^{2+} (1 mM)
4	Aβ(1–43) + Zn^{2+} (1 mM)
5	Aβ(1–43) + Ca^{2+} (1 mM)
6	Aβ(1–43) + Al^{3+} (1 mM)
7	Aβ(1–43) + SiO_4^{4-} (1 mM)
8	Aβ(1–43) + Al^{3+} + SiO_4^{4-} (both 1 mM)

7.3 Discussion

Metals have been shown to induce aggregations of amyloid and accelerate amyloid deposition. With the exception of Al^{3+}, the treatment of the amyloids, including Aβ(1-42) and Aβ(1-43), with most of the metals and GAGs showed no change in mobility as determined by SDS PAGE. Incubation time is very important for the experiments described in this chapter. The techniques of CD and ATR-FTIR as used in the previous chapters are more sensitive to the changes in the secondary structure. SDS-PAGE can only measure changes in the electrophoretic mobility or size of proteins. Therefore, these experiments were designed to have a short incubation period and any change in the mobility of the amyloid peptides would be due to the addition of metals and GAGs. It may simply be the case that a longer incubation period is necessary, but this may simply cause the spontaneous aggregation of the amyloid itself.

7.3.1 Aged amyloid.

The Aβ aggregation requires conformational changes that include the formation and stacking of β sheet structures. The lag phase of the initial nucleation process could account for the apparent delay in onset of Alzheimer's disease. It is possible that a soluble toxic Aβ conformation triggers a slow degenerative process that does not become apparent until after the peptide has proceeded to the stable aggregate stage. At a peptide concentration of 25 μM the solution contains essentially monomers with random coil structure, as evidenced by analytical ultra-centrifugation and CD spectroscopy. Solutions with higher peptide concentrations are characterised by equilibrium between random coil monomers and β structured aggregates [127]. Ageing may stabilise and/or accelerate this conformational change. Aggregation of Aβ protein, has been observed in aged peptides. Incubation of Aβ for 2-4 days at 37°C [80], and storing at 4°C for 1 week [316] have been reported to cause spontaneous aggregation. In fact, the self-assembly into fibrils by Aβ peptide analogues has been a major criticism of the role of GAG [371] and other factors in amyloidosis.

Therefore, since the amyloid proteins have been shown to self aggregate with time, the incubation period is very important for the present experiments. All the experiments were designed to have a short incubation period of 1 hour so that any changes in the peptide would be due to the added metals or GAGs rather than aged amyloid. It may be the case that a longer incubation period is necessary for a maximal effect, but this may simply cause the spontaneous aggregation of the amyloid itself. High concentrations of metals [369] and GAGs [315] may also cause greater aggregation within the short incubation time, but the physiological relevance of these concentrations may be questionable. The apparent ageing of synthetic amyloid *in vitro* may also be accounted for by a lag time, if the spontaneous formation of fibrils is via a nucleation dependent mechanism.

7.3.2 Amyloid peptides treated with metals.

The metals, copper, zinc calcium and magnesium (1 mM) did not appear to have any effect on the electrophoretic mobility of the amyloid peptides Aβ(1-40), Aβ(1-42), Aβ(1-43) and β_2M. Aβ(1-42) and Aβ(1-43) treated with combinations of aluminium and silicate also showed no changes in the PAGE gels. Aβ(1-40) treated with aluminium (1 mM) was shown to cause an elongation of the SDS PAGE band with the possible formation of the dimer. The β_2M in SDS PAGE also showed similar results to the Aβ(1-40). Al^{3+} caused a smearing of the band with a possible formation of the dimer (24 kDa), and higher aggregates of β_2M. The results for the Aβ(1-40) were similar to that of Kawahara et al. [369] although they did not test other peptides such as the β_2M. They also found that Aβ(1-40) treated with Al^{3+} (1 mM) caused an elongation of the band with the formation of higher molecular weight bands up to 94 kDa relating to higher order polymers of the Aβ(1-40).

The SDS treatment will break non-covalent bonds hence any ionic bound Al^{3+} will be removed. Therefore, the higher concentration of Al^{3+} (1 mM) must have interacted with both the Aβ(1-40) and the β_2M to form partial aggregates within the 1 hour incubation time. It can be assumed that a high concentration of aluminium has altered the electrophoretic mobility of the amyloid peptides by the formation of dimers and trimers. Since the SDS treatment is extremely thorough, any loosely

bound aluminium will be stripped off the protein. The high concentration of aluminium in solution may interact with the SDS coated protein, thus causing the streaking effect.

7.3.3 Amyloids peptides treated with an increasing concentration aluminium.

The SDS PAGE of the Aβ(1-40) and β_2M with increasing concentration of Al^{3+} (up to 400 μM) did not show any effects after a 1 hour incubation. This is in contrast to the 1 mM concentration of aluminium in the previous experiment. Kawahara et al [369] showed that addition of aluminium immediately before the electrophoresis did not alter the mobility of peptide, but caused the formation of higher molecular weight markers with incubation of the sample for 24 hours [369].

The additional incubation time may be necessary for aggregation or the formation of oligomers in the samples treated with lower concentrations of aluminium. Samples that had been left for more than one day did not run on the PAGE, they were retained at the top of the gel indicating, the formation of aggregates. The feint high molecular weight bands near the top of the gel in **Figure 7.6** could be due to higher molecular weight aggregates of β_2M. These bands could also be due to artefacts in the experiment. Too large a sample volume in the loading wells may mean that some of the protein sample runs into neighbouring wells and may give erroneous bands. Similar high molecular weight bands were seen in a study by Burdick et al. with Aβ(1-42) but they were attributed to gel artefacts [305].

The non SDS treatment of the amyloid peptide samples showed a concentration dependent effect with the aluminium. For the Aβ(1-40), a greater degree of smearing was seen with the addition of higher concentrations of Al^{3+}. This indicates that the Al^{3+} directly binds the Aβ(1-40). As the concentration of Al^{3+} increases, then the extent of Al^{3+} bound to the protein becomes greater. PAGE run under native conditions with no SDS treatment may be used to separate proteins according to charge as well as with size much like 2 dimensional electrophoresis. The smearing phenomena may be explained by the fact that, as the current passes through the

sample the aluminium was successively stripped off the protein, thereby changing the electrophoretic mobility of the protein. The smearing/tailing indicates that the Al^{3+} directly binds the Aβ(1-40). The amount of Al^{3+} bound to the protein is concentration dependent, with more Al^{3+} being bound at a greater concentration of Al^{3+} (400μM). With a lower concentration of Al^{3+} (50 μM) the streaking effect was minimal as less aluminium was initially bound to the Aβ(1-40).

With β_2M, the non SDS treatment of the samples showed two discrete bands with increasing Al^{3+} which correspond to dimers of the β_2M. Again there is a concentration effect with a greater conversion of monomer to dimer with increasing Al^{3+} as seen by the lower intensity of the monomer band with a corresponding increase in the intensity of dimer band. Addition of a silicate abolished this higher molecular weight band with a reversion back to the monomer as seen by the loss of the dimer band. Silicon has previously been shown to reverse the effect of Al^{3+} treated Aβ(1-40) and β_2M (see previous chapters).

7.3.4 Two dimensional PAGE of β_2M treated with aluminium.

The two dimensional PAGE of the β_2M treated with Al (300 μM) only showed one spot corresponding to the β_2M itself indicating that no other isoforms were present (results not shown). Reports of immunoblot analysis of SDS PAGE gels of partially solubilised amyloid fibrils extracted from tissue deposits have shown them to be composed of monomer, dimers, and higher polymers of β_2M. Two-dimensional gels show the presence of two or more isoforms of β_2M with pI coordinates (5.3-5.7) [157]. Acidic forms of β_2M have also been found, the presence and relevance of acidic β_2M isoforms in the pathogenesis of β_2M amyloidosis have been reported [167]. This is important because the above experiment was performed using β_2M isolated from urine (Sigma, UK) and treated with metals *in vitro*. Other reported studies have shown β_2M isolated from amyloid laden tissues and that may have already been subject to physiological processes such as proteolysis *in vivo* which leads to altered β_2M.

7.3.5 Amyloid peptides treated with GAGs and metals.

The combinations of GAGs with Ca^{2+} and Aβ(1-40) showed no visible changes in the mobility of Aβ(1-40) with either heparan sulphate or heparan sulphate proteoglycan. As with the Aβ(1-40), β_2M treated with various GAGs and combinations of GAGs with metals showed no visible changes in the mobility of β_2M. This may be due to the fact that the samples had not been allowed to incubate long enough. The incubation time was 1 hour, with a longer incubation the Aβ(1-40) may aggregate as the aggregation process is time dependent. Therefore, these GAGs may function by enhancing the structural features that favour a β sheet conformation or by accelerating the formation of the nucleation centre.

7.4 Conclusion.

With SDS PAGE, aluminium was seen to cause the aggregation of both Aβ(1-40) and β_2M as seen by a smearing of the bands. Again this was similar to the results of the CD and ATR studies. With β_2M, addition of a high concentration of silicate appeared to stop the formation of higher weight molecular with a reversion back to the monomer. The treatment of the amyloids with GAGs showed no change in SDS PAGE, as with the CD and ATR. Even if sulphate did not influence fibrillogenesis via conformation changes, binding of the GAGs could provide an anchor for the assembly of the fibrils. The high-affinity binding sites on the GAGs could then bind other factors such as metal ions altering the conformation and reducing the solubility of the peptide leading to aggregation and deposition. Highly sulphated species such as GAGs and the addition of sulphate ions have been reported to promote the aggregation of amyloid β protein [354].

8 General discussion

The present study involved the investigation of the effects of inorganic elements on the secondary structural integrity of amyloid proteins leading to aggregation and deposition. There is evidence in the literature for metals as trigger factors in the deposition of the Alzheimer's disease Aβ peptides, but not for the β_2M. The current results show that metals with both Aβ(1-40) or β_2M caused an increase in the peptide β sheets secondary structure and thus may accelerate amyloid deposition. Therefore, the data on Aβ and the new data on β_2M peptides indicates that metals may have an underlying role in the general process of amyloidosis independent of the type of amyloid protein involved.

The interaction of metals in the presence of GAGs as a possible trigger factor for amyloid deposition has not been previously reported in the literature. The treatment of metals and GAGs with Aβ(1-40) or β_2M showed a synergistic interaction indicating that GAGs may be acting in conjunction with metals leading to the aggregation of amyloid peptides. The fact that similar changes occurred for the interaction of metals and GAGs with metals, with both the Aβ(1-40) and β_2M, suggest similar mechanisms of interaction.

8.1 Common features of amyloids.

Amyloid deposits are associated with several human diseases, for example the prion diseases, Alzheimer's disease and dialysis-related amyloidosis. The major factor for amyloidosis appears to be an increase in the amount of amyloidogenic proteins, resulting in the deposition of aggregated amyloid. There are several suggested trigger factors for amyloidosis, for instance a genetic pre-disposition leading to enhanced susceptibility of an individual. GAGs are present as free chains and/or as intact PG and may be involved in the initiation or propagation of these deposits. An environmental component has been implicated and could involve damage from chemical agents such as metals [332]. Where these trigger factors interact in the amyloidosis pathway, and whether they act on their own or together are largely unknown. Although there might be various critical triggering events in the early stages of the disease, they seem to converge on a few characteristic final pathways in

the late stages of the disease. It appears that a possible common mechanism involves a nucleus formation with subsequent seeding. External factors may be important as they may accelerate the initial formation of fibrils necessary for seeding to occur and/or promote the subsequent polymerisation.

The characteristic feature of the amyloid deposits is a large quantity of intra- or inter-crossed β pleated sheets. The secondary structural values for the β_2M and Aβ(1-40) and the prion PrP^c were similar (37–42 % α helices and 15-18 % β sheets). All the Aβ amyloids including the β_2M and PrP^c prion protein showed a common structural feature of β sheets. The amyloid deposits in Alzheimer's disease [94 & 100], in the β_2M [164 & 165], and the prion PrP^{sc} [50, 196, 198 & 201], all have predominantly β sheet structures (>50 %). The Aβ extract was shown to contain Aβ(1-40) from the immunoblot assay but may also contain Aβ(1-42). It was shown to consist of a greater degree of β sheets than the Aβ(1-40) or Aβ(1-42) indicating that it could be an aggregated state. All the amyloids undergo a conformational change to adopt a new amyloidogenic conformation [318]. The β sheet formation and aggregation are closely coupled events that are difficult to separate suggesting that the transition to β sheets is critical for amyloid formation.

8.2 Metals as a possible trigger factor for amyloidosis.

A large number of studies of metal interaction and Aβ have shown that metals can induce aggregations of amyloid [332], others have suggested that the aggregation of amyloid may be accelerated by various metals [372]. In the present study, the addition of copper, zinc, calcium and aluminium (>100 μM) to the amyloid proteins, in particular the Aβ(1–40) and β_2M, showed some changes with a general decrease in α helix and an increase in β sheet. The CD and ATR spectrum of Aβ(1-40) amyloid protein treated with copper or zinc (10, 50 &100 μM) showed a shift from the α helix to the β sheet and that these effects in both copper and zinc were concentration dependent. There was no additive effect from the addition of combined copper and zinc, which may indicate competition for binding sites. The addition of aluminium (50, 150, 300 & 400 μM) was shown to have a concentration dependent effect on both the Aβ(1-40) and β_2M peptides as seen with an overall increase in β sheet and a

corresponding decrease in α helix. The changes with the β_2M peptide were smaller than that of the Aβ(1-40) peptide.

Aluminium (1 mM) caused the aggregation of both Aβ(1-40) and β_2M as seen by a smearing of the bands of the SDS PAGE indicating the formation of dimers and oligomers. Feint high molecular weight bands that were observed near the top of the gel for the β_2M treated with aluminium, which may relate to high molecular weight β_2M aggregates. Two distinct bands corresponding to the monomer and the dimer were observed with aluminium treated β_2M under non-denaturing conditions. Addition of a high concentration of silicate abolished this higher molecular weight band with a reversion back to the monomer. In the CD, addition of SiO_4^{4-} (300 μM) before the aluminium (300 μM) had the effect of reversing the changes in secondary structure caused by Al^{3+} for both the Aβ(1-40) and β_2M. Silicon may have no direct biological function other than to reduce the bioavailability of aluminium by the formation of a hydroxyaluminosilicates [279 & 373]. This property could be exploited as a therapeutic agent to reduce aluminium levels.

It may be argued that the concentrations of metals needed to elicit the above changes do not relate to physiological concentrations. The fact that the GAGs combined with physiological concentrations of metals enhanced this interaction, suggests that they could play a role in conjunction with metals. There has been considerable controversy as to the concentration of metals, such as zinc, that are required for Aβ aggregation [209 & 374]. Because the behaviour of Aβ is highly dependent on its concentration, and the concentration of the metals, the results can be viewed in two respects; the concentrations used can be extrapolated back to physiological concentrations or the levels represent an accumulated concentration from chronic exposure to low levels of metals *in vivo* [94].

Rapid, pH-sensitive aggregation has been shown to occur at low nanomolar concentrations of both Aβ(1-40) and Aβ(1-42) with sub-micromolar concentrations of Cu^{2+} [334] and Zn^{2+} [331 & 334]. The concentration of Cu^{2+} required for Aβ aggregation (~5 μM) [334] is well within the concentration range for copper found in the synapse (~15 μM) [375]. Concentrations of 25 μM or less of zinc are able to cause

the aggregation of amyloid β protein [331]. Extrapolation to physiological concentrations (10^{-9} M) from data gathered at $>10^{-6}$ M, indirectly indicates that Zn^{2+} [334 & 335], and Cu^{2+} [334] at physiologically relevant concentrations will also cause aggregation of Aβ.

High concentrations (0.15 to >300μM) of zinc have been found in neurons in regions of the brain that are vulnerable in AD such as the cortex and the hippocampus during neurotransmission in the hippocampus up to 300 μM Zn^{2+} is released into the extracellular space [252 & 257]. This increase in zinc levels may be sufficient to induce aggregation of Aβ. Although aluminium salts have been shown to precipitate soluble Aβ *in vitro* [289, 314, 320, 351 & 353], the concentrations of aluminium (> 50 μM) required to precipitate Aβ are far above those that are physiologically possible [331]. However, accumulation of aluminium from long term exposure to low levels of aluminium could increase the risk for premature amyloid deposition [94].

8.2.1 Metal binding sites in amyloids.

Although the mechanisms of aluminium interaction are still unclear, it has been shown that aluminium directly binds to the peptide and changes its conformation [289], and that silicate can reverse both the binding and conformational changes [320]. The capacity of aluminium to form polynuclear species acting as cross-linkers may play a role [376]. Aβ has six acidic amino acids that may be involved in metal binding [377]. At least two classes of metal binding site on Aβ exist; a Cu^{2+}/Ni^{2+} site that is responsible for significant Aβ assembly only under mildly acidic (pH 6.6-7.0) conditions and a Zn^{2+}/Co^{2+} site that mediates significant Aβ assembly at pH 7.4 [334]. The binding of metal ions with exposed binding sites resulting in a change in the protein structure. They could facilitate aggregation of amyloid filaments through cross-links, or seeding of amorphous amyloid into fibrils. Common metal binding sites may lead to an overall mechanism in the amyloidogenesis of these proteins.

Evidence of copper interaction with Aβ(1-40) was first observed by the stabilisation of an apparent Aβ(1-40) dimer by Cu^{2+} on gel chromatography [331]. Copper is also able to displace $^{65}Zn^{2+}$ from Aβ when co-incubated with excess Cu^{2+} [319] Subsequently aggregated Aβ was shown to exhibit multiple specific binding sites for

Cu^{2+} presented as a chelate, with both low and high binding affinity sites on Aβ(1-40) (0.025-1 nM and 16-40 nM) respectively. The stoichiometry of Cu^{2+} binding to soluble Aβ was <= 1, but it increased upon aggregation to 3 at both pH 7.4 and 6.6 [334]. Zinc also specifically and saturably binds Aβ itself, manifesting high binding affinity (K_{assoc} = 107 nM) with a 1:1 (zinc:Aβ) stoichiometry and a lower affinity binding of (K_{assoc} = 3.2-5.2 μM) with a 2:1 stoichiometry [331 & 320]. Zinc binding is histidine mediated [334] and has been mapped to a stretch of contiguous residues between positions 6 and 28 of the Aβ sequence [331]. Iminodiacetate (IDA) – Zn^{2+} affinity columns retain Aβ(1-40) at a pH of 7.0 and suggests that histidine (pKa ~6.6) residues are involved in this binding. [378]. Zinc binding to Aβ at the 16 Lysine position inhibits the α-secretase proteolysis leading to abnormal proteolysis [331].

8.2.2 Evidence for a histidine binding site.

The mechanism of Aβ modification appears to involve the oxidation of histidine, tyrosine, and methionine residues [379]. The β_2M contains six tyrosine residues, all located within the two β sheets of the immunoglobulin sandwich structure [168]. Tryptophan, tyrosine and methionine residues are likely to be important in the protein folding of β_2M [163]. The histidine, tyrosine, and methionine residues are associated with metal ion binding to amyloids [334]. One or more histidines are probably involved in binding [334 & 380] and they appear to be between residues 6 and 28 of the Aβ sequence [331]. The metal is likely to co-ordinate to histidine at position 13 and tyrosine at position 10 and may direct the aggregation of Aβ(1-40) [381]. Similar Aβ amyloid deposits has been detected in aged monkeys, dogs, and polar bears [383], but rarely have they been found in rats and mice [384]. Cerebral Aβ deposition is not a feature of aged rats [385]. The rat Aβ lacks the single tyrosine and one of the three histidine residues of human Aβ (Arg-5, Tyr-l0 and His-13 modifications). The rat Aβ and a histidine-modified human Aβ were not aggregated by Zn^{2+}, Cu^{2+}, or Fe^{3+}, indicating that histidine residues are essential for metal-mediated Aβ assembly [386].

The modulation of Aβ aggregation is commonly regulated through the affinities of many neurochemical factors such as zinc, copper, transthyretin, apolipoprotein E, and pH for the histidine residues of Aβ [334]. Both the rate and the extent of assembly are

much higher at lower pH in comparison with pH 7.4. Based on its measured isoelectric point Aβ(1-40) has a zero overall charge at a pH of 7.1 ± 0.2, based on its measured isoelectric point [243]. The loss if solubility at a pH of approximately 7.2 is consistent with the experimentally determined isoelectric point. The amphiphilic nature of the residues in a peptide is essential to the secondary structural conformation and the solubility of the protein [382]. Histidine has a pKa near neutrality and frequently serves as a controllable element of protein conformation, so slight changes in pH close to physiological conditions may protonate or deprotonate some or all of the histidines, altering the conformation or solubility of a protein [243]. It may be significant that abrupt change in solubility with pH occurs close to physiological pH. At pH values above the isoelectric point, some of the three histidine residues of Aβ(1-40) are deprotonated.

8.3 GAGs as a possible trigger factor for amyloidosis.

The current work showed that β_2M and Aβ(1-40) peptides did not appear to undergo any significant conformational change on binding sulphates and GAGs when analysed by CD, ATR-FTIR and SDS PAGE. Even if sulphate did not influence fibrillogenesis via conformation changes, binding of the GAGs could provide high-affinity binding ligands that could then bind other factors such as metal ions. They may; (i) initiate fibrillogenesis by promoting amyloidogenic protein conformation and structural transitions [107, 118 & 387]; (ii) enhance the stability of pre-formed fibrils [55, 354, 388 & 389]; (iii) decrease amyloid susceptibility to proteolysis; and (iv) direct the anatomical distribution of amyloid deposition.

Highly sulphated glycosaminoglycans and proteoglycans are common constituents of amyloid deposits. Immunohistochemical localisation of GAGs to regions containing neurofibrillary tangles [390], diffuse [391] and senile plaques have been reported [392]. Heparan sulphate, keratan sulphate, dermatan sulphate and chondroitin sulphate are associated with AD senile plaques and neurofibrillary tangles [393 - 395] and with articular connective tissue where β_2M amyloid is most often found [396 - 398]. An unusual feature of the fibrils of haemodialysis-associated amyloid is the presence of a peripheral layer composed of chondroitin sulphate proteoglycan (CSPG) rather than

of HSPG. CSPG is not tightly bound to the β_2M amyloid fibrils themselves, but may be involved in regulation of the amyloid deposition [372]. Abnormally high levels of HSPG are also associated with most types of PrP pathology including all plaque types and diffuse neuro-anatomically targeted forms [56, 399 & 400].

The presence of HSPG or other GAGs in a range of amyloids [57 & 389] suggests a common function or role [55]. It is unclear when GAG involvement with amyloid begins, although the association of HSPG with early diffuse Aβ plaque in the brains of young Down's syndrome patients suggests an early role [315 & 392]. In the latter stages of the amyloid pathway, GAGs may act by enhancing lateral aggregation of small fibrils. The acceleration of fibril formation induced by GAG-Aβ binding [54, 354, 387 & 389] may be particularly relevant at low nanomolar Aβ concentrations found *in vivo* where the nucleation lag is predicted to be extremely slow.

8.4 The interaction of both GAGs and metals with amyloids.

It appears that the GAGs do not illicit any conformational change on their own but can have a synergistic effect when combined with either Zn^{2+}, Cu^{2+}, Al^{3+} or Ca^{2+} at physiological concentrations. Both the Aβ(1-40) and β_2M peptides treated with physiological concentration of Al^{3+} combined with the GAGs showed that they had a synergistic effect. Neither the GAGs nor the Al^{3+} (1.5 μM) on their own cause an appreciable change in the secondary structure. Similar effects were also seen with Cu^{2+} and Zn^{2+} (10 μM), although the Cu^{2+} and Zn^{2+} initially alter the peptides at the concentrations used. These changes seemed independent of the type of GAG, which may suggest that it is the highly negatively charged sulphate groups on the GAGs that may exacerbate this interaction.

The importance of the sulphate groups in Aβ aggregation has been confirmed by a decrease in Aβ fibril formation in the presence of de-sulphated heparan sulphate [392]. Chondroitin sulphates are sulphated on a single face of the polymer and may represent an ideal distribution of sulphate groups for Aβ interactions [334]. GAGs possess substituent groups, which permits complex co-ordination and chelation of a range of inorganic and organic cations. Several cation-heparin interactions putatively

affecting the activities of either or both of the participants have been described. Zinc binds to heparin more readily than to other glycosaminoglycans [401] and such binding may have a role in Aβ deposition. Other metals that have high binding affinities with the GAGs [401] such as copper and aluminium may have similar effects on these amyloids.

The amyloidogenic peptides have been demonstrated to show a variation in their ability to interact with GAGs. In the present study, GAGs with calcium seemed to have interactions with the amyloids dependent on the type of GAG. The ability of GAGs to induce an amyloid-related structural transition may reflect variation in binding specificity of the GAGs to the amyloids and the metals to the GAGs. For example, the nucleation of Aβ(1-42) is greater for heparan sulphate at pH 7.0 than for heparin, though heparin is more highly charged than heparan sulphate. Heparin shows a higher binding activity compared with heparan sulphate [402], but both are known to have tighter binding properties compared to other GAGs [373 & 403].

Heparan sulphate with Serum AA causes an increase in its β sheet configuration [147 & 404]. Although serum amyloid A (SAA) analogues bind to both heparan and chondroitin sulphate, the effects on the SAA secondary structure vary greatly [59]. It may be that certain metals have different binding affinities with the various GAGs [401]. Zinc partially activates the binding serum amyloid protein (SAP) whilst other cations (Ba^{2+}, Mg^{2+}, Mn^{2+}, Fe^{2+}, Fe^{3+}, and Al^{3+}) are ineffective [406].

In the CD study, certain combinations of GAGs with calcium further decreased the α helices and increased the β sheet secondary structures of the Aβ(1-40) and β_2M, indicating that these combinations enhance the effects of Ca^{2+}. The Aβ(1-40) with either HSPG and CS combined with calcium caused further decreases in α helices compared to Ca^{2+} but only the CS and Ca^{2+} caused a further increase in β sheets. The β_2M treated with the combinations of HSPG, CS, KS or HS and calcium further enhanced the changes compared to calcium with a decrease in the α helices and an increase in the β sheets. Heparan sulphate in the presence of calcium has been found to increase the β sheet structures of certain amyloids [114]. Ca^{2+} and GAGs have been shown to cause changes in the secondary structure of mouse SAA, which is an acute

phase protein precursor of the AA amyloid [59]. This increase in β sheets caused by HS with Ca^{2+} was only detected at high concentration of Ca^{2+} (1-2 mM) [59]. SAP in affected vessels, bind in a calcium dependent manner, to amyloid fibrils and heparan sulphate, dermatan sulphate and heparan sulphate proteoglycans [405] but it is unclear if this is important for fibril formation. SAP is also seen to self aggregate in calcium free solutions, and forms small aggregates in 2 mM calcium and at 25 mM calcium, forms larger crystalline aggregates [406]. It has been reported that SAP has 2 calcium binding sites on each subunit and that 2 calcium ions form the binding site for the known ligands such as β D-galactose [405].

Most notably in both the CD and ATR studies, the treatment of the Aβ(1-40) peptide with combinations of heparin, HS, and Na_2SO_4 with calcium, appears to reverse the effect of calcium on its own with increases in the α helices and decreases in the β sheets. Since β sheets are a pre-requisite for aggregation, then this also indicates that addition of heparin/heparan sulphate with the calcium prevents aggregation due to calcium itself. A similar phenomena was seen with calcium induced aggregation of SAP. One study showed that SAP aggregation was enhanced by calcium but on addition of heparin or heparan sulphate to SAP before calcium completely prevented formation of aggregation but distribution of SAP fibrils was not evenly spread [406]. Serum amyloid P component plays a crucial role in amyloid fibril formation, directly influencing either the processing of a precursor proteins or protein folding rather than being deposited coincidentally as an innocent bystander [407]. Since SAP is an integral component of the amyloid deposits, metal interaction with or without the presence of GAGs could be important in the amyloidogenic process.

8.5 Conclusions.

The main aspects of the work presented in this thesis are highlighted below:

1. The novel use of ATR-FTIR for the analysis of metals with amyloids, and the use of CD for the detection of the protein secondary structure of amyloids treated with both metals and GAGs.
2. The present study indicates that metals may be involved in the amyloidogenesis of Aβ and β_2M amyloid. A change in the secondary structure of the amyloids Aβ(1–40) and β_2M with both metals and GAGs has been demonstrated.
3. There are many studies in the literature relating to the involvement of metals in the deposition Aβ peptides, in comparison, there are relatively few for the β_2M. The results showed that β_2M treated with metals displayed similar interactions to that of the Aβ peptides indicating that similar mechanisms may be involved.
4. The interaction of both metals with GAGs as a possible trigger factor has not been previously reported. The treatment of metals and GAGs with Aβ(1-40) or β_2M shows a synergistic interaction indicating that metals in the presence of GAGs may play a role in the amyloidogenic process.
5. The similarity of the results as seen with both β_2M and Aβ(1-40) suggests similar modes of interaction, and hence may lead to mechanisms of amyloid deposition.

It is clear that conformational changes in amyloidogenic proteins lead to fibril formation and aggregation. Several trigger factors may be involved in the initiation and propagation of these amyloid deposits. Metals have been shown to induce aggregations of both the Aβ(1-40) and β_2M amyloid *in vitro* and may accelerate amyloid deposition. The binding of GAGs could provide an anchor for the assembly of the fibrils. The high-affinity binding sites on the GAGs could then bind other factors such as metal ions altering the conformation of the peptide leading to aggregation and deposition. A transition from α helix to β sheet structures is critical for amyloid formation. The fact that similar changes occurred for the interaction of metals and GAGs with both the Aβ(1-40) and β_2M, suggest that similar mechanisms may be involved. Therefore, a mechanism for this conversion to β sheet secondary structures may provide an insight into the deposition of amyloid.

8.6 Future work.

Possible future work could include:

1. A trace element survey to determine an empirical link between metal levels and disease state. A study of trace element levels in tissues in which amyloid is deposited from various amyloid diseases. A more extensive study to include other organs and tissues to identify an overall change in element status of an individual. Emphasis on the disease state, tissue location, other factors such as diet, age, gender etc should be taken into account as these can affect metal levels.

2. Further development of the ion chromatography system to enable the detection of metals at physiological levels. A rapid and simple method should be adopted to avoid contamination and sample degradation. Other methods of metal detection should be used to enable comparison of results. Techniques such as inductively coupled plasma spectrometry and graphite furnace atomic absorption spectroscopy could be employed. Although sample size and detection limits will be a controlling factor in sensitivity with ICPOES.

3. Further CD studies of amyloid proteins and metals including the use of other amyloids, to elucidate a common mechanism of metal interaction and amyloid deposition. The use of other amyloid fragments and other factors such as serum amyloid P component and amyloid enhancing factor should be investigated. A study of metals with the amyloid precursor proteins should determine whether metals interact at this early stage of the deposition process.

4. The combination of ATR-FTIR with deconvolution and curve fitting techniques will allow the determination of secondary structural values. Current techniques for protein structure analysis include mass spectrometry, CD, FTIR, NMR, peptide mapping etc. Many of these techniques could be adopted for the analyses of amyloid proteins and with real time analysis.

5. There are now at least half a dozen mouse transgenic lines that develop one of the pathological characteristics of AD, amyloid plaques. An animal model for Alzheimer's disease would be extremely useful for basic research and for drug development. Therefore, animal models could be used for the investigation of amyloid deposition in relation to trace elements.

References

1. Pauling , L., 1953, *Discuss. Faraday. Soc.*, **13**, 170.
2. Anfinsen, C.B., 1973, *Science,* **181,** 223-230.
3. Stryer, L., *Biochemistry,* (Fourth Edition), New York, W.H. Freeman Company, 1995, pp 20.
4. Jaenicke, R., Seckler, R., 1997, *Advances in Protein Chemistry: Protein Missassembly,* **50,** 3.
5. Thomas, P.J., Qu, B-H. and Pederson, P.L., 1995, *Trends Biochem. Sci.,* **20**, 456-459.
6. Larvie, C.K., Lunte, S.M., Zhong, M., Perkins, M.D., Wilson, G.S., Gokulrangan, G., Williams, T., Afroz, F., Schoneich, C., Derrick, T.S., Middaugh, C.R., Bogdanowich-Knipp, S., 1999, *Anal.Chem.*, **71**, 389R.
7. Huhmer, A.F.S., Aced, G.I., Perkins, M.D., Gursoy, R.N., Jois, D.S.S., Larvie, C., Siahaan, T.J., Schoeich, C., 1997, *Anal. Chem.*, **69**, 29R.
8. Stryer, L., *Biochemistry,* (Fourth Edition), New York, W.H. Freeman Company, 1995, pp 63-65.
9. Adler, A.J., Greenfield, N.J., Fasman, G.D., 1973, *Meth. Enzymology,* **27**, 675.
10. Byler, D.M., Susi, H., 1986, *Biopolymers,* **25**, 469.
11. Dong, A., Huang, P., Caughy, W., 1990, *Biochemistry,* **29**, 3303.
12. Olinger, J.M., Hill, D.M., Jakobsen, R.J., Brody, R.S., 1986, *Biochim. Biophys. Acta.,* **869,** 89.
13. Campbell, I.D., Dwek, R.A., *Biological Spectroscopy*, Published by Benjamin Cummings Publishing Company Inc, London, 1984, pp 128
14. Wishart, D.S., Sykes, B.D., Richards, F.M., 1992, *Biochemistry*, **31**, 6, 1647.
15. Kuwajima, J.A., Bilsel, O., Luo, J., Jones, B.E., Matthews, C.R., 1995, *Biochemistry*, **34**, 12812.
16. Rodger, A.E, Norden, B., *Circular Dichroism Linear Dichroism,* Oxford Chemistry Masters, 1997, pp 1.
17. Sreerama, N., Woody, R.W., 1993, *Analytical Biochemistry,* **209**, 32.
18. Greenfield, N.J., Fasman, G.D., 1996, *Biochemistry,* **8**, 4108.
19. Cantor, C.R., Schimmel, P.R., 1980, *Biophysical Chemistry*, **2**, ch. 8.
20. Johnson, W.C., 1990, *Proteins*, **7**, 205.
21. Krimm, S., Bandekar, J., 1986, *Adv. Prot. Chem.*, **38,** 181.
22. Gazit, E., Miller, I.R., Biggin, P.C., Sansom, M. S. P., Shal, Y., 1996, *J. Mol. Biol.*, **258,** 860.
23. Jackson, M., Mantsch, M.H., 1995, *Crit. Rev. Biochem. Mol. Biol.*, **30**, 95.

24. Grivelli, L.A., 1995, *Crit. Rev. Biochem. Mol. Bol.*, **30**(2) 121.

25. Venyaminov, S.Y., Kalnin, N.N., 1990, *Biopolymers,* **30**, 1243.

26. Surewicz, W.K. Mantsch, H.H., 1988, *Biochim. Biophys. Acta,* **95**, 2115

27. Singh, B.R., Fuller, M.P., 1991, *Appl Spectrosc.*, **45**, 1017.

28. Sarver, R.W. Krueger, W.C., 1991, *Anal. Biochem.*, **194,** 89.

29. Lee, D.C., Harris, P.I., Chapman, D., Mitchell, R.C., 1990, *Biochemistry,* **29,** 9185.

30. Doussea, F., Pezolet, M., 1990, *Biochemistry,* **29,** 8771.

31. Mantsch, H.M., Jackson, M., 1995, *Crit. Rev. Biochem. Mol. Biol.*, **30**, 95.

32. Oberg, K., Fink, A.L., 1998, *Anal. Biochem.*, **256**, 92.

33. SpectraTech FT-IR Catalogue, 1998, SpectraTech, USA.

34. Cohen, A.S., 1967, *New Engl. J. Med.*, **277**, 523.

35. Virchow, R., 1854, *Virchows Arch. Patgol. Anal. Physiol.*, **6**, 426.

36. Sipe, J.D., 1992, *Ann. Rev. Biochem.*, **61**, 947.

37. Glenner, G.G., Keiser, H.R., Bladen, H.A., Cuatrecasas, P., Eanes, E.D., 1968, *J. Histochem. Cytochem.*, **16**, 633.

38. Campistol, J.M., Sole, M., 1992, *Am. J. Pathol.*, **141**, 241.

39. Ida, N., Masters, C.L., Beyreuther, K., 1996, *Febs Letters,* **394**, 174.

40. Kisilevsky, R., 1987, *Can. J. Physiol. Pharmacol.*, **65,** 1805.

41. Schwab, C., Steele, J.C., Akiyama, H., 1995, *Acta. Neuropathologica,* **90**, 287.

42. Glenner, G.G., Harbaugh, J., Ohms, J.I., Harada, M., Cuatrecasas, P., 1970, *Biochem. Biophys. Res. Commun.*, **41**, 1287.

43. Hoffman, J.S., Ericsson, L.H., Eriksen, N., Walsh, K.A., Benditt, E.P., 1984, *J. Exp. Med.*, **59**, 2934.

44. Hoffman, J.S., Benditt, E.P., 1982, *J. Biol. Chem.*, **257,** 10510.

45. Husebekk, A., Skogen, B., Husby, G., 1981, *Scand. J. Immunol.*, **25,** 375.

46. Kani, M., Raz, A., Goodman, DW., 1968, *J. Clin. Invest.*, **47,** 2044.

47. Westermark, P., Wernstedt, C., Wilander, E., Hayden, D.W., Johnson, B., 1987, *Proc. Natl. Acad. Sci. U.S.A.*, **84**, 3881.

48. Campistol, J.M., Skinner, M., 1993, *Seminars in Dialysis,* **6**, 117.

49. Masters, C.L., Multhaup, G., Simms, G., Pottgiesser, J., Martins, R.N., Beyreuther, K., 1985, *EMBO. J.*, **4,** 2757.

50. Prusiner, S.B., 1991, *Science,* **252**, 1515.

51. Adrian, G.S., Herbert, D.C., Robinson, L.K., Walter, C.A., Buchanan, J.M., Adrian, E.K., Weaker, F.J., Eddy, C.A., Yang, F.M., Bowman, B.H., 1992, *Biochimica. Biophysica. Acta,* **1132**, 168.

52. Scott, J.D., Marhaug, G., Husby, G., 1983, *Clin. Exp. Immunol.*, **52**, 701.

53. Baltz, M.L., Caspi, D., Evans, D.J., Rowe, I.F., Hind, C.R.K., Pepys, M.B., 1986, *Clin. Exp. Immunol.*, **66**, 691.

54. Snow, A.D., 1991, *J. Histochem. Cytochem.*, **39**, 1321.

55. Snow, A.D., Wight, T.N., 1989, *Neurobiol. Aging*, **10**.481.

56. Mcbride, P.A., Wilson, L.M.I., Eikelenboom, P., Tunstall, A., Bruce, M.E., 1998, *Exp. Neurol.*, **149**, 447.

57. Snow, A.D., Wight, T.N., Nochlin, D., Koike, Y., Kimata, K., DeArmond, S.J., Prusiner. S.B., 1990, *Lab. Invest.*, **63**: 601.

58. Snow, A.D., Kisilevski, R., 1988, *Lab. Invest.*, **57**, 687.

59. McCubbin, W.D., Kay, C.M., Narindrasorasak, S., Kislevsky, R., 1988, *Biochem, J.*, **256**, 755.

60. Wight, T.N., Kinsella, M.G., Qwarnstrom. E.E., 1992, *Curr. Opin. Cell. Biol.* **4,** 793.

61. Shirahama, T., Miura, K., Ju, S.T., 1990, *Lab. Invest.*, **62**, 61.

62. Varga, J., Flinn, M.S., Shirahama, T., 1986, *Virchows Arch. [B] Cell. Pathol.*, **51**, 177.

63. Axelrad, M.A., Kisilevsky, R., Willmer, J., 1982, *Lab. Invest.*, **47**, 139.

64. Campistol, J.M., Cohen, A.S., *Dialysis amyloid: Pathophysiology of amyloidogensis*, (Edited by Ypersele, C.V., Drueke, T.B.) Oxford University Press, 1996, p10.

65. Lansbury Jr., P.T., 1992, *Biochemistry*, **31**, 6865.

66. Jarrett, J.T., Lansbury Jr., P.T., 1993, *Cell*, **73**, 1055.

67. Alzheimer, A., 1907, *Allg. Z. Psychiat. Psych-Gericht. Med.*, **64**, 146.

68. Multhaup, G., Masters, C.L., Beckman, N.S., 1990, *Scand. J. Infect. Dis.*, **3,** 19.

69. McKhann, G., Drachman, D., Folstein, M., 1986, *Neurology*, **34**, 944.

70. Kidd, M., 1963, *Nature*, **197**, 193.

71. Husby, G., Sletten, K., Marrink, M, Van Rijswijk M.H., *Amyloidosis*, Dordrecht, pub. Martinus Nijhoff, 1986, pp 23.

72. Hardy, J., Allsop, D., 1991, *Tips*, **12**, 383.

73. Glenner, G.G., Wong, L., 1984, *Biochem. Biophys. Res. Commun.*, **120,** 855.

74. Miller, D.L., Papayannopolous, I.A., Styles, J., Bobin, S.A., Lin, Y.Y., Biemann, K., Iqbal, K., 1993, *Arch. Biochem. Biophys.*, **301**, 41.

75. Selkoe, D.J., 1999, *Nature*, Suppl., **399**, 6738.

76. Kang, J., Lemaire, H.G., Unterbeck, A., Salbaum, J.M., Masters, C.L., Grzeschick, K.H., Multhaup, G., Beyreuther, K., Muller-Hill, B., 1987, *Nature*, **325**, 733.

77. Sinha, S., Dovey, H.F., Seubert, P., 1990, *J. Biol. Chem.*, **265**, 8983.

78. Saitoh, T., Sunsdumo, M., Roch, J-M., 1989, *Cell,* **58**, 615.

79. Esch, F.S., Keim, P.S., Beattie, E.C., 1990, *Science*, **248**, 1122.

80. Yankner, B.A., Duffy, L.K., Kirschner, D.A., 1990, *Nature*, **250**, 279.

81. Lucia, M., Marco, A.C., Gyorgi, I.S., Laszlo, O.J., Pieruiling, B., Martin, V., Davide, F., Filippo, R., 1995, *Nature*, **374**, 647.

82. Mattson, M.P., 1992, *J. Neurosci.*, **12**, 379.

83. Pike, C.J., Burdick, D., Walencewicz, A.J., Glabe, C.G., Cotman, C.W., 1993, *J. Neurosci.*, **13,** 1676.

84. Snow, A.D., Sekiguchi, K, Nochlin, D., Fraser, P., Kimata, K, Mizutani, A, Arai, M., Schreier, W.A., Morgan, D.G., 1994, *Neuron,* **12**, 219.

85. Prior, K, Durso, D., Frank, R., Prikulis, I., Cleven, S., Ihl, R., Pavlakovic, G., 1996, *Am. J. Pathol.*, **148,** 1749.

86. Askanas, V., Engel, W.K., 1993, *Curr. Opin. Rheumatol.*, **5**, 732.

87. Joachim, C.L., Duffy, L.K, Morris, J.H., Selkoe, D.J., 1988, *Brain Res.*, **474**, 100.

88. Skodras, G., Peng, J. H., Parker Jr., J.C., Kragel, P. J., 1993, *Ann. Clin. Lab. Sci.* **23**, 275.

89. Joachim, C.L., Mori, H., Selkoe, D.J., 1989, *Nature,* **341**, 226.

90. Graham, D.I., Gentleman, S.M., Lynch, A, Roberts, G.W., 1995, *Neuropathol. Appl. Neurobiol.,* **21**, 27.

91. Mackenzie, I., 1993, *J. Neuropatnol. Exp. Neurol.*, **156**, 437.

92. Vaughan, D.W., Peters, A., 1981, *J. Neuropathol. Exp. Neurol.*, **40**, 472.

93. Shivers, B.D., Hilbich, C., Multhaup, G., Salbaum, M., Beyreuther, K, Seeburg, P.H., 1988, *EMBO J.*, **7**, 1365.

94. McLachlan, D.R.C., 1995, *Environmetrics*, **6,** 233.

95. Maggio, J.E., Stimson, E.R., Ghilardi, J.R., Allen, C.J., Dahl, C.E., Whitcomb, D.C., Vigna, S.R., Vinters, H.V., Labenski, M.E., Mantyh, P.W., 1992, *Proc. Natl., Acad. Sci. U.S.A.*, **89**, 5462.

96. Haass, C., Schlossmacher, M., Hung, A, Vigo-Pelfrey, C., Mellon, A, Ostaszewski, B.L., Lieberburg, I., Koo, E.H., Schenk, D., Teplow, D.B., Selkoe, D.S., 1992, *Nature,* **359,** 322.

97. Seubert, P., Vigo-Pelfrey, C., Esch, F., 1992, *Nature,* **359**, 325.

98. Nitsch, R.M., Rebeck, G.W., Deng, M., Richardson, U., Tennis, M., Schenk, D.B., Vigo-Peltrey, C., Lieberburg, I., Wurtman, R.J., Hyman, B.T., Growdon, J.H., 1995, *Ann. Neurol.*, **37,** 512.

99. Ida, N., Hartmann, T., Pantel, J., Schroder, J., Zerfass, K, Forstl, H., Sandbrink, R., Masters, C.L., Beyreuther, K., 1996, *J Biol. Chem.*, **271**, 22908-22914.

100. Sticht, H., Bayer, P., Willbold, D., Dames., S., Hilbich, C., Beyreuther, K., 1995, *Eur.J. Biochem.*, **233**, 293.

101. Durell, S.R., Guy, H.R., Arsipe, N., Rojas, E., Pollard, H., 1994, *Biophysical J.* **67**, 2137.

102. Barrow, J.B., 1999, *Protein Peptide letters*, **6**, 5, 217.

103. Gorevic, P.D., Castano, E.M., Sarma, R., Frangione, B., 1987, *Biochem. Biophys. Res. Commun.*, **147**, 854.

104. Kirschner, D.A., Inouye, H., Duffy, L.K., Sinclair, A., Lind, M., Selkoe, D.J., 1987, *Proc. Natl Acad. Sci. U.S. A.*, **84**, 6953.

105. Fraser, P.E., Duffy, L.K., O'Malley, M.B., Nguyen, J.T., Inouye, H., Kirschner, D.A., 1991, *J. Neurosci. Res.*, **28**, 474.

106. Castano, E.M., Ghiso, J., Prelli, F., Gorevic, P.D., Migheli, A., Frangione, B., 1986, *Biochem. Biophys. Res. Commun.*, **141**, 782.

107. Halverson, K., Fraser, P.E., Kirschner, D.A., Lansbury Jr., P.T., 1990, *Biochemistry*, **29**, 2639.

108. Barrow, C.J., Zagorski, M.G., 1991, *Science*, **253**,179.

109. Barrow, C.J., Yasuda, A., Kenny, P.T.M., Zagorski, M., 1992, *J. Mol. Biol.*, **225**, 1075.

110. Zagorski, M.G., Barrow, C.J., 1992, *Biochemistry*, **31**, 5621.

111. Yankner, B.A., Dawes, L.R., Fisher, S., Villa-Lormaroff, L., Oster-Granite, M.L., Neve, R.L., 1989, *Science*, **245**, 417.

112. Masters, C.L., Simms, G., Weinman, N.A., Multhaup, G., Macdonaldd, B.L., Beyreuther, K., 1985, *Proc. Natl. Acad. Sci. U.S.A.*, **82**, 4245.

113. Jarrett, J.T., Berger, E.P., Lansbury Jr., P.T., 1993, *Biochemistry*, **32**, 4693.

114. Roher, A E., Chaney, M.O., Kuo, Y.M., Webster, S.D., Stine, W.B:, Haverkamp, L.J., Woods, A.S., Cotter, K.J., Thohy, J.M., Krafft, G.A, Bonnell, B.S., Emmerling, M.K., 1996, *J. Biol. Chem.*, **271**, 20631.

115. Mann, D.M.A., Iwatsubo, T., Ihara, Y., Cairns, N.J., Lantos, P.L., Bog-danovic, N., Lannfelt, L., Winblad, B., Mast-Schieman, M.L.C., Rossor, M.N., 1996, *Am. J. Pathol.*, **148**, 1257.

116. Saido, T.C., Iwatsubo, T., Mann, D.M.A., Shimada, H., Ihara, Y. Kawashima, S., 1995, *Neuron*, **14**, 457.

117. Terzi, E., Holzemann, G., Seelig, J., 1994, *Biochemistry*, **33**, 1345.

118. Hilbich, C., Kister-Woike, B., Reed, J., Master, C.L., Beyreuther, K., 1991, *J. Mol. Biol.*, **218**, 149.

119. Hollosi, M., Otvos, L.J., Kajtar, J., Perzcel, A., Lee, V.M.J., 1989, *Peptide Res.*, **2**, 109.

120. Tjernberg, L.O., Naslund, J., Lindqvist, F., Johansson, J., Karlstrom, A R., Thyberg, J., Terenius, L., Nordstedt, C., 1996, *J Biol. Chem.*, **271**, 8545.

121. Selkoe, D.J., 1996, *J. Biol. Chem.*, **271**, 18295.

122. Lomakin, A., Chung, D. S., Benedek, G.B., Kirschner, D.A., Teplow, D.B., 1996, *Proc. Natl. Acad. Sci. U.S.A.*, **93**,1125.

123. Citron, M., Vigo-Pelfrey, C., Teplow, D.B., Miller, C., Schenk, D., Johnston. J., Winblad, B., Venizelos, N., Lannfelt, L., Selkoe, D., 1994, *Proc. Natl. Acad. Sci. U.S.A.*, **91**, 11993.

124. Suzuki, N.,Cheung, T.T., Cai, X.D., Odaika, A., Otvos, L. Jr. Eckman, C., Golde, TE., Younkin, S.G., 1994, *Science,* **264**.1336.

125. Simmons, L.K., May, P.C., Tomaselli, K.J., Rydel, R.E., Fuson, K.S., Brigham, E.F., Wright, S., Lieberburg, I., Becker, G.W., Brems, D.N., Li, W.Y., 1994, *Mol. Pharmacol.*, **45**, 373.

126. Garcon-Rodriguez, W., Sepulvede-Becerra, M., Milton, S., Glabe, C.G., 1997, *J. Biol. Chem.*, **272**, 21037.

127. Terzi, E., Holzemann, G., Seelig, J., 1995, *J. Mol. Biol.*, **252**, 633.

128. Mantyh, P.W., Ghilardi, J.R., Rogers, S., DeMaster, E., Allen, C.J., Stimson, E.R., Maggio, J.E., 1993, *J. Neurochem.*, **61,** 1171.

129. Strittmatter, W.J., Saunders, A.M., Schmechel, D., 1993, *Proc. Natl. Acad. Sci. U.S.A.*, **90**, 1977.

130. Rozemuller, J.M., Stam, F.C., Eikelenboom, P., 1990, *Neurosci. Lett.*, **119,** 75.

131. Benzi, G., Moretti, A., 1995, *Neurobiol. Aging*, **16**, 661.

132. Brownlee, M., 1995, *Annu. Rev. Med.*, **46**, 223.

133. Niwa, T., Sato, M., Katsuzaki, T., Tomoo, T., Miyazaki, T., Tatemichi, N., Takei, Y., Kondo, T., 1996, *Kidney Int.*, **50**, 1303.

134. Colaco, C.A.L.S., Ledesma, M.D., Harrington, C.R., Avila, 1996, *J. Nephrol. Dial. Transplant.*, **11**, 7.

135. Munch, G., Mayer, S., Michaelis, J., Hipkiss, A.R., Schnizel, R., Palm, D., Riederer, P., 1994, *J. Neural. Transm.*, **8**, 193.

136. Munch, G., Thome, J., Foley, P., Schnizel, R., Reiderer, P., 1997, *Brain Res. Rev.*, **23**, 134.

137. Gotz, M.E., Kunig, G., Riederer, P., Youdim, M.B., 1994, *Pharmacol. Ther.*, **63,** 37.

138. Wautier, J.L., Wautier, M.P., Schmidt, A.M., Anderson, G.M., Hori, O., Zoukourian, C., Capron, L., Chappy, O., Yan., S.D., Brett, J., 1994, *Proc. Natl. Acad. Sci. U.S.A.*, **91**, 7742.

139. Harrington, C.R., Colaco, C.A., 1994, *Nature,* **370**, 247.

140. Larner, A.J., 1995, *Trace Elem. Elec.*, **12**, 26.

141. Mera, S.L., 1991, *Medical Laboratory Sciences*, **48**, 283.

142. Candy, J.M., Oakley, A.E., Klinowski, J., Carpenter, T.A., Perry, R.H., Atack, J.R., Perry, E.K., Blessed, O., Fairbairn, A., Edwardson, J.A, 1986, *Lancet*, **i**, 354.

143. Nikaido, T., Shimoji, A., Kuramoto, R., 1982, *Virchows Arch.*, **40**, 129.

144. Beauchemin, D., Kisilevsky, R.J., 1998, *Anal. Chem.*, **70**, 1026.

145. Lovell, M.A., Robertson, J.D., Teesdale, W.J., Campbell, J.L., Markesbery, W.R., 1998, *J. Neurol. Sci.*, **158**, 47.

146. Ancsin, J.B., Kisilevsky, R.J., 1996, *J. Biol. Chem.*, **271**, 6845.

147. Narindrasorasak, S., Lowery, D.E., Altman, R.A., Gonzalez-De-Whitt, P.A., Greenberg, B.D., Kisilevsky, R., 1992, *J. Lab. Invest.*, **67**, 643.

148. Grant, D., Long, W.F., Williamson, F.B., 1992, *Biochem. J.*, **287**, 849.

149. Bush, A.I., Multhaup, G., Moir, R.D., Williamson, T.G., Small, D.H., Rumble, B., Pollwein, P., Beyreuther, K., Masters, C.L., 1993, *J. Biol. Chem.*, **268**, 16109.

150. Hesse, L., Beher, D., Masters, C.L., Multhaup, G., 1994, *FEBS lett.*, **49**, 109.

151. Multhaup, G., Schlicksupp, A., Hesse, L., Beher, D., Ruppert, T., Masters, C.L., Beyreuther, K., 1996, *Science*, **271**, 1406.

152. Campistol, J.M., Molina, R., Bernard, D., 1993, *Kidney Int.*, **44**, 1409.

153. Charra, B., Calemard, E., Laurent, G., 1982, *Blood purif.*, **6**, 117.

154. Ypersele V., Strihou, C., Honhon, B., Broucke, V.J.M., Huaux, J.P., Noel, H., Maldague, B., 1988, *Adv. Nephrol.*, **17**, 401.

155. Athanasou, NA., Ayers, D., Rainey, Al., Oliver, D.O., Duthie, R.B., 1991, *Q. J. Med.*, **78**, 205.

156. Farrell, J., Bastani, B., 1996, *J. Am. Soc. Nephrol.*, **8**, 509.

157. Gorevic, P.D., Munoz, P.C., Casey, T.T, DiRaimondo, C.R., Stone, W.J., Prelli, F.C., Rodrigues, M.M., Poulik, M.D., Frangione, B., 1986, *Proc. Natl. Acad. Sci. USA*, **83**, 7908.

158. Kay, J., 1997, *Amyloid: Int. J., Exp. Clin. Invest.*, **4**, 187.

159. Vincent, C., Revillard, J.P., Caudwell, V., 1992, *Kidney Int.*, **42**, 1434.

160. Campistol, J.M., Argiles, A., 1996, *Nephrol. Dial. Trans.*, **11**, 142.

161. Niwa, T., 1997, *Nephron*, **76**, 373.

162. Ogawa, H., Saito, A., Oda, O., Nakajima, M., Chung, T.G., 1988, *Clin. Nephrol.*, **30**, 158.

163. Bellotti, V., Merlini, G., 1996, *Nephrol. Dial. Trans.*, **11**, 53.

164. Milanka, V., Bray, P., Mire, Z., 1991, *Collect Czech Chem Commun*, **57**, 1148.

165. Durso, C.M., Wang, Z.G., Cao, Y., 1991, *J. Clin. Invest.*, **87**, 284.

166. Gejyo, F., Nishi, S., Arakawa, M., Dialysis Amyloid, (Ypersele, C.V., Drueke, T.B., eds.) Oxford University Press, Oxford, 1996, pp 159.

167. Campistol, J.M., Bernard, D., Papastoistsis, G., Sole, M., Kasirsky, J., Skinner, M., 1996, *Kidney Int.*, **50**, 1262.

168. Vucic, M., Bray, P., Zloh, M., Vucelic, D., 1992., *Collect. Czech, Chem. Commun.*, **57**, 1143.

169. Koch, K.M., 1992, *Kidney Int.*, **41**,1416.

170. Schwalbe, S., Holzauher, M., Schaeffer, J., Glanski, M., Koch, K.M., 1997, *Kidney. Int.*, **52**, 1077.

171. Athanasou NA, *Dialysis Amyloidosis*. (Van Ypersele C et al. eds.) Oxford: Oxford University Press, 1996, pp173.

172. Stevens, F.J., Westholm, F.A., Solomon, A., Schiffer, M., 1980, *Proc. Natl. Acad. Sci. U.S.A.*, **77**, 1144.

173. Myatt, E.A., Westholm, F.A., Weiss, G.C., Yankner, B.A., 1994, *Nature*, **368**, 756.

174. Miyata, T., Oda, O., Inagi, R., Iida, Y., Araki, N., Yamada, N., Horiuchi, S., Taniguchi, N., Maeda, K., Kinoshita, T., 1993, *J. Clin. Invest.*, **92**, 1243.

175. Vlassara, H., Moldawer, L., Chan, B., 1989, *J. Clin. Invest.*, **84**, 1820.

176. Miyata, T., Inagai, R., Iida, Y., Sate, M., Yamada, N., Oda, O., Maeda, K., Seo, H., 1994, *J. Clin. Invest.*, **93**, 521.

177. Cousins, R.J., 1985, *Physiol. Rev.*, **65**, 309.

178. Ong C.N., Ong, H.Y., Chua, L.H., 1988, *Anal. Biochem.*, **173**,64.

179. Gallieni, M., Brancacio, D., Cozzolino, P.W., 1982, *Ann. Int. Med.*, **96**, 302.

180. Kimmel, P.L., Phillips, T.M., Lew, S.Q., Longman, .B., 1996, *Kid. Int.*, **46**, 1407.

181. Nathan, E., Pederson, S., 1980, *Acta Paediatr Sci.*, **69**, 796.

182. Adler, A.J., Berlyne, G.M., 1996, *Nephron*, **44**, 36.

183. Gejyo, F., et al., Amyloid and Amyloidosis, (Natvig, J., et al. ed.) Kluwer, Dordecht, 1991, pp 377.

184. Gejyo, F., Arawaka, M., 1990, *Contrib Nephrol.*, **78**, 47.

185. Cary N.R.B., Sethi D., Brown E.A., Erhardt C.C., Woodrow D.F., Gower P.E., 1986, *Br. Med. J.* **293**; 1392.

186. Heller, D.S., Klein, M.J., Gordon, R.E., Good, P., Perl, D., 1989, *J. Bone Joint Surg.*, **714**; 1083.

187. Netter P, Kessler M, Garcher A, Bannworth B., 1990, *Ann. Rheum. Dis.*, **49**, 573.

188. Chaussidon, M., Netter, P., Kesler, M., Membre, H., Fener, P., Delons, S., Albarrede, F., 1993, *Nephron*, **65**, 559.

189. Dworkin, B.M., Rosenthal, W.S., Wormser, C.P., Weiss, L., 1986, *J. Parenteral Enteral. Nutr.*, **10**, 405.

190. Allavena, C., Dousset, B., May, T., Dubois, F., Canton, P., Belleville, F., 1995, *Biol. Trace Element Res.*, **42**, 133.

191. Alfrey, A.C., Mishell, J.M, Burks, J., 1972, *Trans, ASAIO*, **18**, 257.

192. Alfrey, A.C., LeGendre, G.R., Kheany, W.D., 1976, *New Eng. J. Med.*, **294**, 184.

193. Sprague, S.M., Corwin, H.L., Tanner, C.M., Wilson, R.S., Green, B.J., Goetz, C.G., 1988, *Archives of Internal Medicine*, **148**, 23.

194. Candy, J.M., McArthur, F.K., Oakley, A.E., Taylor, G.A., Chen, C.P., Mountfort, S.A., Thompson, J.E., Chalker, P.R., Bishop, H.E., Beyreuther, K., Perry, G., Ward, M.K., Martyn, C.N., Edwadrson, J.A., 1992, *J. Neurol. Sci.*, **107**, 210.

195. Sisodia, S.S., Koo, E.H., Beyreuther, K., Unterbeck, A., 1990, *Science,* **248**, 492.

196. Prusiner, S.B., DeArmond, S.J., 1995, *Amyloid: Int. J. Exp. Clin. Invest.*, **2**, 39.

197. Will, R.G., Ironside, J.W., Aeidler, M., Cousens, S.N., Estibeiro, K., Alperovitch, A., Poser, S., Pochiari, M., Hofman, A., Smith, P.G., 1996, *Lancet*, **347**, 921.

198. Safar, J., Roller, P.P., Gajdusek, D.C., Gibbs, C.J., 1993, *J. Biol. Chem.*, **268**, 20276.

199. Stahl, N., Baldwin, M.A., Teplow, D.B., Hood, L., Gibson, B.W., Burlingame, A.L., Prusiner, S.B., 1993, *Biochemistry,* **32**, 1991.

200. Pan, K.M., Baldwin, M., Nguyen, J., Gasset, M., Serban, A., Groth, D., Mehlhorn, I., Huang, Z., Fletterick, R.J., Cohen, F.E., Prusiner, S.B., 1993, *Proc. Natl. Acad. Sci. U.S.A.*, **90,** 10962.

201. Prusiner, S.B., 1997, *Science,* **278**, 245.

202. Liu, H., Farr-Jones, S., Ulyanov, B., Llinas, M., Marqusee, S., Groth, D., Cohen, F.E, Prusiner, S.B., James, T.L., 1999, *Biochemistry*, **38**, 5362.

203. Gajdusek, D.C., Gibbs, C.J., Alpers, M., 1966, *Nature*, **209**, 794.

204. Purdey, M., 1996, *Medical Hypothesis*, **46**, 429.

205. Stockel, J., Safar, J., Wallace, A.C., Cohen, F.E., Prusiner, S.B., 1998, *Biochemistry,* **37**, 7185.

206. Marshall, W.J., *Clinical chemistry,* London, Gower Medical publishing, 1988, pp 300.

207. Kaim, W., Chwederski, B., *Bioinorganic Chemistry: Inorganic Elements in the chemistry of Life, An Introduction Guide.,* New York, J.Wiley & Sons, 1994, pp 151.

208. Versieck, J., Cornelis, R., 1980, *Analytical Chimica. Acta.*, **116**, 217.

209. Fitzgerald, D.J., 1995, *Science*, **268**, 1920.

210. Emenaker, N.J., Disilvestro, R.A., Nahman, N.S., 1996, *Am. J. Clin.Nutr.*, **64**, 757.

211. Chappell, J.S., Birchall, J.D., 1988, *Inorganica. Chimica. Acta.*, **153**, 1.

212. Danks, D.M., in *The Metabolic Basis of Inherited Disease* (Editors, Scriber, C.R., Beaudet, A.L., Sly, W.S., Valle, B.D.) 6th ed., McGraw-Hill, Inc., New York., 1989, pp 1411.

213. Fahal, I.H., Ahmed, R., Bell, G.M., Birchall, J.D., Roberts, N.B., 1993, *J. Analytical Atomic Spectroscopy,* **8**, 911.

214. Vallee, B.L., Falchuk, K.H., 1993, *Physiol. Rev.*, **73**, 79.

215. Prasad, A.S., 1996, *Ann. Intern. Med.*, **125**, 142.

216. Ehmann, W.D., Markesbery, W.R., Allaudin, M., Hossain, T.I., Brubaker, E.H., 1986, *Neurotoxicology*, **7**, 195.

217. Frederickson, C.J., 1989, *Int. Res. Neurobiol.*, **31**, 145.

218. Fjerdingstad, E., Danscherer, G., Fjerdingstad, E.J., 1974, *Brain Res.*, **79**, 338.

219. Ebadi, M., 1991, *Meth. Enzymol.*, **205**, 363.

220. Ebadi, M., Hama, Y., 1986, *Adv. Exp. Med. Biol.*, **203**, 557.

221. Cuajungco, M.P., Lees, G.J., 1997, *Neurobiol. Dis.*, **4,** 137.

222. Cuajungco, M.P., Lees, G.J., 1997, *Brain Res. Rev.*, **23**, 219.

223. Linder, M.C., Hazegh-Azam, M., 1996, *Am. J. Clin. Nutr.*, **63**, 797.

224. Kaplan, J., O'Halloran, T.V., 1996, *Science*, **271**, 1510.

225. Harter, D.E., Barnea, A., 1988, *J. Biol. Chem.*, **263,** 799.

226. Nalbandyan, R.M., 1983, *Neurochem. Res.*, **8,** 1211.

227. Carlisle, E.M., 1972, *Science*, **178,**619.

228. Haag, W., Lago, R., Weisz, P., 1984, *Nature*, **309**, 589.

229. Alfrey, A.C., 1986, *Kid. Int.*, **S18**, s8.

230. Wenk, G.L., Stemmer, J.L., 1983, *Brain Res.*, **288**, 393.

231. Ohman, L.O., Martin, R.B., 1994, *Clin. Chem.*, **4014**, 59801.

232. Martin, R.B., 1986, *Clin. Chem.*, **32**: 1797.

233. Constantinidis, J., 1990, *Encephale.*, **16**, 231.

234. Agrimi,U., Di Guardo, G., 1993, *Medical Hypotheses,* **40**, 113.

235. Markesbery, W R., 1997, *Free Rad. Biol. Med.*, **23,** 134.

236. Halliwell, B., Gutteridge, J.M.C., 1990, *Meth. Enzymol.*, **186**, 1.

237. Lindeman, R.D., Yanice, A.A., Baxter, D.J., Miller, L.R, Nordquist, J., 1973, *J. Lab. Clin. Med.*, **81**, 194.

238. Huang, X., Atwood, C.S., Moir, R.D., Hartshorn, M.A., Vonstattel, J.P., Tanzi, R.E., Bush, A.I., 1997, *J. Biol. Chem.*, **272**, 26464.

239. Warren, P.J., Earl, C.J., Thompson, H.S., 1960, *Brain,* **83**,709.

240. Kisileveky, R., 1983, *Lab. Invest., **49**,* 381.

241. Gorevic, P.D., Cleveland, A.B., Franklin, E.C., 1982, *Ann. N.Y Acad. Sci.*, **389,** 380.

242. Yates, C.M., Butterworth, J., Tennet, M.C., Gordon, A., 1990, *J. Neurochem.*, **55**, 1624.

243. Tomski, S.J., Murphy, R.M., 1992, *Arch. Biochem. Biophys.*, **294**, 2, 630.

244. Tanzi, R E., Petrukin, K., Chernov, I., Pellequer, J.L., Wasco, W., Ross, B., Romano, D.M., Parano, E., Pavone, L., Brzustowicz, L.M, Devoto, M, Peppercorn, J., Bush, A I., Stemlieb, I., Piratsui, M., Gusella, J.F., Evgrafov, O.,

Penchazadeh, G.K, Honig, B., Edelman, I.S., Soares, M.B., Scheinberg, I.H., Gilliam, T.C., 1993, *Nat. Genet.*, **5**, 344.

245. Kapaki, E., Segditsa, J., Papageorgiou, C., 1989, *Acta Neurol Sci.*, **79**, 373.

246. Jeandel, C., Nicolas, M.B., Dubois, F., Nabet-Belleville, F., Penin, F., Cuny, G., 1989, *Gerontology*, **35**, 275.

247. Gronek, I., Kolomaznik, M., 1989, *Zh. Nevropatol Psikhiatr.*, **89**, 126.

248. Corrigan, F.M., Reynolds, G.P., Ward, N.I., 1993, *Biometals*, **6**, 149.

249. Constantinidis, J., 1992, *Drug Dev. Res.*, **27**, 1.

250. Corrigan, F.M., Reynolds, G.P., Ward, N.I., 1991, *Trace Elem. Med.*, **4**,117.

251. Hyman, B.T., Van Hoesen, G.W., Kroner, L.J., Damasio, A.R., 1986, *Ann. Neurol.*, **20**, 472.

252. Assaf, S.Y., Chung, S.H., 1984, *Nature*, **308**, 734.

253. Baba, A., Kihara, T., Sawada, T., Iwata, H., 1989, *Brain Res.*, **486**, 372.

254. Koh, J.Y., Choi, D.W., 1988, *Neurosci.*, **8**, 2164.

255. Provinciali, M., Di Stofano, G., Fabris, N., 1995, *J. Immunol. Pharmacol.*, **17**, 735.

256. Choi, D.W., Yokoyama, M., Koh, J., 1988, *Neuroscience*, **24**, 67.

257. Howell, G.A., Welch, M., Frederickson, C.J., 1984, *Nature*, **308**, 736.

258. Iyengar, O.V., Kolimer, W.E., Bowen, H.B.M., *The elemental composition of human tissues body fluids: a compilation of values for adults.* Verlag Chemie, New York, NY., 1978.

259. Smith, H., 1967, *J. Forens. Sci. Soc.*, **7**, 97.

260. Corder, E.H., Saunders, A.M., Strittmatter, W.J., 1993, *Science*, **261**, 921.

261. Blacker, D., Haines, J.L., Rodes, L., 1997, *Neurology*, **48**, 139.

262. Gallieni, M., Brancaccio, D., Cozzolio, M., Sabioni, E., 1996, *Nephrol. Dial. Trans.*, **11**, 1232.

263. Meiri, H., Banin, E., Roll, M., 1993, *Neurobiol.*, **40**, 89.

264. Munoz-Garcia, D., Pendlebury, W.W., Kessler J.B., 1986. *Acta. Neuropathol.*, **70**, 243.

265. Dedman, D.J., Trefry, M., Candy, J.M., Taylor, G.A.A., Morris, C.M., Bloxham, C.A., Perry, R.H., Edwardson, J.A., Harrison, P.M., 1992, *Biochem. J.*, **287**, 509.

266. Candy, J.M., Oakley, A.E., Mountfort, S., 1980, *Seconodary Ion Mass Spectrometry*, **4**, 323.

267. Garruto, R., Yase, Y., 1986, *Trends Neurosci.*, **9**, 268.

268. Shea, T.B., *1995*, *Mol. Chem. Neuropath.*, **24**, 151.

269. Shigematsu, K., McGeer, P.L., 1992, *Brain, Res.*, **593**, 117.

270. McDermott, J.R., Smith, A.I., Iqbal, K., Wisniewski, 1979, *Neurology*, **29**, 109.

271. Kowall, N.W., Pendlebury, W.W., Kessler, J.B., 1989, *Neuroscience*, **29**, 329.

272. Morris, C.M., Candy, J.M., Oakley, A.E., Taylor, G.A., Mountfort, S., Bishop, H., Ward, M.K., Bloxham, C.A., Edwardson, J.A., 1989, *Neurol. Sci.*, **94**, 295.

273. Roskams, A.J., Connor, J.R., 1990, *Proc. Natl. Acad. Sci. U.S.A.*, **87**, 9024.

274. Crapper, D., Krishman, S., Quittkat, S., 1976, *Brain*, **99**, 67.

275. Ward, N., Mason, J., Modern Trends in activation analysis (Isotope Division, Riso National Laboratory, Roskilde, 1989, pp 925.

276. Traub, R., Rains, T., Garruto, R., Gajdusek, D., Gibbs, C., 1981, *Neurology*, **31**, 709.

277. Markesbery, W., Ehmann, W., Hossain, B., Alauddin, M., Goodin, M., 1981, *Ann. Neurol.*, **10,** 511.

278. Ramesh, J., Madhav, T.R., Vatsala, S., Ramaknshna, T., Easwaran, K.R.K., Gulllard, O., Deloncle, R., 1999, *Alzheimer's Reports,* **2**, 1, 31.

279. Edwardson J.A., 1993, *Lancet,* **342**, 211.

280. Tokutake, H., Nagase, S., Morisake, S., 1995, *Neurosci. Lett.,* **185**, 99.

281. Edwardson, J.A., Candy, J.M., 1989, *Annals of Med.*, **21**, 95.

282. Iler, R., The chemistry of silica: Solubility, polymerisation, colloid surface properties & Biochemistry, Wiley, New York, 1979, pp.1.

283. Hershey, C.O., Hershey, L.A., Varneg.A., 1983, *Neurology,* **33,** 1350.

284. Canavesse, C., 1990, *Nephron*, **56**, 455.

285. Milacic, R., Benedik, M., Knezevic, S., 1997, *Clinica. Chimica. Acta.,* **265,** 169.

286. Gafter, U., Mamet, R., Karzets, A., Malachi, T Schoenfeld, N., 1996, *Nephrol. Dial. Transplant,* **11,** 1787.

287. Talbot, R.J., Newton, D., Priest, N.D., Austin, J.G., Day, J.P., 1995, *Human Exp. Tox.,* **14,** 595.

288. Yver, L., Blanchier, D., 1987, *Nephrol. Dial. Transplant,* **2**, 451.

289. Exley, C., Price, N.C., Kelly, S.M., Birchall, D., 1993, *FEBS Lett.*, **324**, 293.

290. Chang, T.M., Barre, P., 1983, *Lancet,* **8358**,1051.

291. Malluche, H., Faugere, M-C., 1990, *Kidney Int.,* **38,** 211.

292. Harrington, C.R., Wischik, C.M., McArthur, F.K., 1994, *Lancet*, **343,** 993.

293. Edwardson, J.A., Ferrier, I.N., McArthur, F.K., Aluminium in chemistry, biology medicine. New York Raven Press, 1992, pp 85.

294. Naslund, J., Schierhorn, A., Hellman, U., Lannfelt, L., Roses, A.D., Tjernberg, L.O., Silberring, J., G y, S.E., Winbald, B., Greengard, P., Norstedt, C., Terenius, L., 1994, *Proc. Natl. Acad. Sci. U.S.A.*, **91**, 8378.

295. Norred, W.P., Wade, A.E., 1972, *Biochem. Pharmacol.*, **21**, 2887.

296. Uesugi, Y., Uemichi, M., Koshioka, S., 1989, Saishin Noyaku Pesticide Data Book, Revised Edition. Soft Science, Tokyo.

297. Nomiyama, K., Nomiyama, H., 1989, *Nephrol Dial Trans.*, **4**, suppl. 114.

298. Hoenig, M., Cilissen, A., 1997, *Spectrochimica Acta*, **52**, part b, 1443.

299. Schoppenthau, J., Dunemann, L., 1994, *Fresenius J. Anal. Chem.*, **349**, 794.

300. Lane, E., Holden, A.J., Coward, R.A., 1999, *Analyst*, **124**, 245.

301. Pras, M., Schubert, D., Zucker-Franklin, A., Rimon, E.C., 1998, *J. Clin. Invest.*, **47**, 924.

302. Selkoe, D.J., Abraham, C.R., Podlinsy, M.B., Duffy, L.K., 1986, *J.Neurochem.*, **46**, 1820.

303. Prelli, F., Castano, E., Glenner, G.G., Frangione, B., 1988, *J. Neurochem.*, **51** 648.

304. Roher, A.E., Lowenson, J.D., Clarke, S., Woods, A.S., Cotter, R.J., Gowing, E., Ball, M.J., 1993, *Proc. Natl. Acad. Sci. U.S.A.*, **90**, 10836.

305. Burdick, D., Soreghan, B., Kwon, M., Kosmoski, J., Knauer, M., Henschen, A., Yates, J., Cotman, C., Glabe, C., 1992, *J. Biol. Chem.*, **276**, 546.

306. Duffy, L.K., Kates, J., Podlinsy, M.B., Walsh, R., Galibert, L., Selko, DJ., 1986, *Peptides Biol. Fluids Proc. Colloq.*, **34**, 193.

307. Mori, H., Takio, K., Ogawara, M., Selkoe, D.J., 1992, *J. Biol. Chem.*, **267**, 17082.

308. Gowing, E., Roher, A.E., Woods, A.S., Cotter, R.J., Chaney, M., Little, S.P., Ball, M.J., 1994, *J. Biol. Chem.*, **269**, 10987.

309. Soto, C., Castanos, E.M., Frangiones, B., Inestrosa, N.C., 1995, *J. Biol. Chem.*, **270**, 7, 3063.

310. Provencher, S.W., Glockner, J., 1981, *Biochemistry*, **20**, 33.

311. Bellotti, V., Stoppini, M., Mangione, P., Sunde, M., Robinson, C., Asti, L., Brancaaio, D., Ferri, G., 1998, *Eur. J. Biochem.*, **258**, 61.

312. Matsuzaki, K., Horikiri, C., 1999, *Biochemistry*, **38**, 4137.

313. Jarvet, J., Damberg, P., Bodell, K., Erikccon, L.E.G., Graslund, A., 2000, *J.Am.Chem.Soc.*, **122**, 4261.

314. Fasman, G.D., Perczel, A., Moore, C.D., 1995, *Proc. Natl. Acad. Sci. U.S.A.*, **92**, 369.

315. McLaurin, J., Franklin, T., Zhang, X., Deng, J., Fraser,P.E., 1999, *Eur. J. Biochem.*, **266**, 1101.

316. Koo, E.H., Park, L., Selkoe, D.J., 1993, *Proc. Natl. Acad. Sci. U.S.A.*, **90**,4748.

317. Mihara, H., Takahshi, Y., et al, 1998, *Biopolymers (Peptide Science)*, **47**, 83.

318. Kelly, J.W., 1996, *Curr. Opin. Struct. Biol.*, **6**, 11.

319. Clements, A., Allsop, D., Walsh, D.M., Williams, C.H., 1996, *J Neurochem.*, **66**, 740.

320. Fasman, G.D., Moore, C.D., 1994, *Proc. Natl. Acad. Sci. U.S.A.*, **91**, 11232.

321. Woody, R.W., *Peptides, Polypeptides Proteins*, New York, Wiley, 1974, pp 338.

322. Wille, H., Zhang, G.F., Baldwin, M.A., 1996, *J. Mol. Biol.*, **259**, 608.

323. Dyson, J., Rance, M., Houghton, R.A., Lerner, R.A., Wright, P.E., 1988, *J. Mol. Biol.*, **201**, 201.

324. Rajan, R., Barlaram, P., 1996, *Int. J. Peptide Protein Res.*, **48,** 328.

325. Sha, Y., Wang, Y.L.Q., Fan, K., Liu, D., Lai, L., Tang, Y., 1999, *Protein Peptide Letters*, **6,** 3, 137.

326. Greenfield, N.J., 1996, *Anal. Biochem,* **235**, 1.

327. Yankner, B.A., Mesulam, M.M., 1990, *New. Eng. J. Med.*, **325**, 1849.

328. Hayden, P.L., Rubin, A.J., *Aqueous Environmental Chemistry of Metals.* Michigan, Ann Arbor Science, 1974, pp 317.

329. Murphy Jr., G.M., Forno, L.S., Higgins, L., Scardina, J.M., Eng, L.F., Cordell, B., 1994, *Am. J. Pathol.*, **144**, 1082.

330. Smith, C and Clarke, A.R., *Structural properties of the prion proteins. In: Prion Diseases,* Collinge, J., Palmer, M.S., (Eds), Oxford University Press, Oxford, 1997, pp177.

331. Bush, A.I., Pettingell Jr., W.H., Paradis. M.D., Tanzi, R.E., 1994, *J.Biol. Chem.* **269**, 12152.

332. Mantyh, P.W., Ghilardi, J.R., Rogers, S., DeMaster, E., Allen, C.J., Stimson, E.R., Maggio, J.E., 1993, *J. Neurochem.*, **61,** 1171.

333. Bush, A.I., Pettingell, W.H., Multhaup, C., Paradis, M.D., Vonsattel, J.P., Gusella, J.F., Beyreuther, K., Masters, C.L., Tanzi, R.E., 1994, *Science,* **265**, 1464.

334. Atwood, C.S., Moir, R.D., Huang, X., Scarpa, R.C., Bacarra, N.M. E. Romano, D.M., Hartshorn, M.A., Tanzi, R.E., Bush, A.I., 1998, *J. Biol. Chem.*, **273**, 12817.

335. Bush, A.I., Moir, R.D., Rosenkranz, K.M., Tanzi, R.E., 1995, *Science*, **268**, 1921.

336. Sorehen, B., Kosmoski, J., Glabe, C., 1994, *J. Biol. Chem.* **269**, 28551.

337. Wasacz, F.M., Olinger, J.M., Jakobsen, R.J., 1987, *Biochemistry*, **28**, 1464.

338. Goormaghtigh, E., Cabiaux, V., Ruysschaert, J.M., 1990, *Eur. J. Biochem.*, **193,** 409.

339. Swedberg, S.A., Pesek, J.J., Fink, A.L., 1990, *Anal. Biochem.*, **188**, 153.

340. Buchet, B., Varga, S., Seidler, N.W., Molnar, E., Martonosi, A., 1991, *Biochim. Biophys. Acta,* **1068**, 201.

341. Uchida, K., Harada, L., Nskauchi, Y., Maruyama, K., 1991, *FEBS Letts.*, **195**, 35.

342. Oberg, K., Chrunyk, B.A., Wetzel, R., Fink, A.L., 1994, *Biochemistry*, **38**, 2628.

343. Cavillon, F., Elhaddoui, A., Alix, A.J.P., Turrell, S., Dauchez, M., 1997, *J. Mol. Struct.*, **408**, 185.

344. Fraser, P.E., McLachlan, D.R., Surewicz, W.K., Mizzen, C.A., Snow, D.A., Nguyen, J.T., Kirschner, D.A., 1994, *J. Mol. Biol.*, **244**, 64.

345. Esler, W.P., Stimson, E.R., Jennings, J.M., Ghilardi, J.R., Mantyh, P.W., Maggio, J.E., 1996, *.J. Neurochem.*, **66**, 723.

346. Brown, A.M., Tummolo, D.M., Rhodes, K.J., Hofmann, J.R., Jacobsen, J.S., Sonnenberg-Reines, J., 1997, *J. Neurochemistry*, **69**, 1204.

347. Kawahara, M.,Arispe, N., Kuroda, Y., Rojas, E., 1997, *Biophys. J.*, **73**, 67.

348. Behi, C., Davis, J., Cole, G.M., Schubert, D., 1992, *Biochem. Biophys. Res. Commun.*, **186**, 944.

349. Fabian, H., Szendrei, G.I., Mantsch, H.H., Greenberg, B.D., Otvos, L.,Jr., 1994, *Eur. J. Biochem.*, **221**, 959.

350. Hensley, K., Aksenova, M., Carney, J.M., Harris, M., Butterfield, D.A., 1995, *Neuroreport*, **6**, 493.

351. Ramakrishna T, Vatsala, S, Madhav, T.R., 1997, *Alz. Res.*, **3**, 223.

352. Madhav, T.R., Vatsala, S., Ramakrishna, T., 1996. *NeuroReport*, **7**, 1072.

353. Scott, C.W., Fieles, A., Sygowski, L.A., 1993, *Brain Res.*, **628**, 77.

354. Fraser, P.E., Nguyen, J.T., Chin, D.T., Kirschner, D.A., 1992, *J. Neurochem.*, **59**, 1531.

355. Sunde, M., Serpell, L.C., Bartlam, M., Fraser, PE.. Pepys, M.B., Blake, C.C.F., 1997, *J. Mol. Biol.*, **273** 789.

356. Kaplan, B., 1998, *Analytica chimica Acta*, **372**, 161.

357. Kaplan, B., German, G., Ravid, M., Pras, M., 1994, *Clin. Chim. Acta*, **224**, 171.

358. Wisniewski, T., Lalowski, M., Bobik, M., Russel, M., Strosznajder, B., Fragione, B., 1996, *Biochem, J.*, **313**, 575.

359. Frucht, S.J., Koo, E.H., 1993, *J.Neuropath. Exp. Neurol.*, **52**, 640.

360. Garcia-Garcia, M., Gouin- Charnet, A., Mourad, G., Argiles, A., 1997, *Nephrol. Dial. Trans.*, **12**, 1192.

361. Shoji, M., Golde, T., Ghiso, J., Cheung, T.T., Estus, S., Shaffer, L.M., Cai, X, D., McKay, D.M., Tintner, R., Frangione, B., Younkin, S.G., 1992, *Science*, **258**, 126.

362. Argiles, A., Garcia, M.G., Derancourt, J., Mourad, G., Demaille, J.G., 1995, *Kidney Int.*, **48**, 1397.

363. Swank, R.T., Munkres, K.D., 1971, *Anal. Biochem.*, **39**, 462.

364. Laemmli, U.K., 1970, *Nature*, **227** 680.

365. Schagger, H., Von Jagow, G., 1987, *Anal. Biochem.*, **166**, 166.

366. Wiltfang, J., Arold, N., Neuhoff, V., 1991, *Electrophoresis*, **12**, 352.

367. Onistein, L., 1964, *Ann. NY Acad. Sci. U.S.A.*, **121**, 321.

368. Davis, B.J., 1964, *Ann. NY Acad. Sci. U.S.A.*, **121**, 40.

369. Kawahara, M., Muramoto, K., Kobayashi, K., Mori, H., Kuroda, Y., 1994, *Biochem. Biophys. Res. Commun.*, **198,** 531.

370. Kuroda, Y., Kawahara, M., 1994, *Tohoku J. Exp. Med.*, **174** 263-2681.

371. Shirahama T., 1989, *Neurobiol Aging,* **10**,508.

372. Inoue, S., Kurorwa, M., Ohashi, K., Hara, M., Kisilevsky, R., 1997, *Kidney Int.*, **52**, 1543.

373. Exley, C., Birchall, J.D., 1995, *Biometals,* **8**, 271.

374. Maggio, J.E., Esler, W.P., Stimson, E.R., Jennings, J.M., Ghilardi, J.R., Mantyh, P.W., 1995, *Science*, **268**, 1921.

375. Barnea A., Cho, G., 1984, *Endocrinology*, **115**, 936.

376. Flaten, T.P., Garruto, R.M., 1992, *J. Theor. Biol.*, **156**, 129.

377. Chauhan, V.P.S., Indrani, R., Chauhan, A., Wegeil, J., Wisniewski, H.M., 1997, *Neurochem. Res.*, **22,** 7 , 805.

378. Balakrishnan, R., Parthasarathy, R., Sulkowski, E., 1998, *J.Peptide Res.*, **51**, 91.

379. Dyrks, T., Dyrks, E., Hartmann, T., Masters, C., Beyreuther, K., 1992, *J. Biol. Chem.*, **267**, 18210.

380. Atwood, C.S., Moir, R.D., Haung, X., Scarpa, R.C., Becarra, N.M.E., Stimson, E.R., Maggio, J.E., 1993, *J. Neurochem.*, **61**, 1171.

381. Liu, S.T., Howlett, G., Barrow, C.J., 1999, *Biochemistry*, **38**, 9373.

382. Iyer, H.V., Przybycien, T.M., 1995, *Biotech. Bioeng.*, **48**, 324.

383. Selkoe, D.J., Bell, D.S., Podlinsy, M.B., Price, D.L., Cork, L.C., 1987, *Science*, **235**, 873.

384. Selkoe, D.J., 1989, *Annu. Rev. Neurosci.*, **12**, 463.

385. Johnstone, E.M., Chaney, M.O., Norris, F.H., Pascual, R., Little, S.P., 1991, *Mol. Brain Res.*, **10**, 229.

386. Dyrks, T., Dyrks, E., Masters, C.L., Beyreuther, K., 1993, *FEBS Lett.*, **324**, 231.

387. Kirschner, D.A., Abraham, C., Selkoe, D.J., 1986, *Proc. Natl. Acad. Sci. U.S.A.*, **83**, 503.

388. Gasset, M., Baldwin, M.A., Fletterick, R.J., Prusiner, S.B., 1993, *Proc. Natl. Acad. Sci. U.S.A.*, **90**, 1.

389. Guiroy, D.C., Yanigihara, R., Gajdusek, D.C., 1991, *Acta Neuropathol,* **82,** 87.

390. DeWitt, D.A., Silver, J., Canning, D.R., Perry, G., 1993, *Exp. Neurol.*, **121**,149.

391. Buee, L., Ding, W., Delacourte, A., Fillit, H., 1993, *Brain Res.*, **601**, 154.

392. Snow, A.D., Mar, H., Nochlin, D., Sekiguchi, R.T., Kimata, K., Koike, Y., Wight, T.N., 1990, *Am. J. Pathol.*, **137**: 1253.

393. Snow, A.D., Mar, H., Nochim, D., Kimata, K., Kato, M., Suzuki, S., Hassell, J., Wight, T.N., 1988, *Am. J. Pathol.*, **133**, 456.

394. Snow, A.D., Nochim, D., Sekiguchi. R., Carlson, S.S., 1996, *J. Exp. Neurol.*, **138**, 305.

395. Snow, A.D., Mar. H., Nochim, D., Kresse. H., Wight, T.N., 1992, *J. Histochem Cytochem.*, **40**, 105.

396. Argua, E., Ozasa, H., Teraoka, S., Ota, K., 1993, *Lab. Invest.*, **69**, 223-230.

397. Iozzo, R.V., 1985, *Lab Invest.*, **53**, 373.

398. Athanasou, N.A., Puddle, B., Sallie, B., 1995, *Nephrol. Dial. Trans.*, **10,** 1672.

399. Caughey, B., Raymond, G.J., 1993, *J. Virol.*, **67,** 643.

400. Caughey, B., 1993, *Br. Med. Bull.*, **49,** 860.

401. Sato, C.S., Gyorkey, F.,1976, *J. Biochem. (Tokyo)*, **80**, 885.

402. Jiang, X., Myatt, E., Lykos, P., Stevens, F,S., 1997, *Biochemistry* **36**., 13187-13194.

403. Casu, B., Petitou, M., Provasoli, M., Sinay, P., 1988, *Trends Biochem. Sci.*, **13**, 221.

404. Narindrasorasak, S., Lowery, D., Gonzalezdewhitt, P., 1991, *J. Biol. Chem.*, **266**, 12878.

405. Hamazaki, H., 1987, *J. Biol. Chem.*, **262**, 1456.

406. Nielson, E.H., Sorenson, I.J., Vilsgarrd, K., Andersen, G.M., Svenhag, S.E., 1994, *APMIS,* **192**, 420.

407. Ono, K., Uchino, F., 1994, *Nephron,* **66,** 404.

Appendix

Reagents and their suppliers

Ammonium sulphate	Sigma, UK
Acetic acid	BDH, UK
Acrylamide stock solution	Sigma, UK
Aluminium chloride hexahydrate	Sigma, UK
Aluminium nitrate nonahydrate	Sigma, UK
Alcohol dehydrogenase	Sigma, UK
Ammonium acetate	Sigma, UK
Ammonium hydroxide	Sigma, UK
Ammonium persulfate	Sigma, UK
Ampholytes (pH 3-10)	Sigma, UK
APP(125-135)	Sigma, UK
Atomic absorption standards	Fisher, UK
Aβ(1-40)	Sigma, UK
Aβ(1-43)	MRC Neurochemicalpathology Unit, Newcastle, UK.
Aβ(25-35)	Sigma, UK
Aβ(1-42)	Sigma, UK
β_2 Microglobulin	Sigma, UK
Bisacrylamide stock solutions	Sigma, UK
Bovine serum albumin	Sigma, UK
Bromophenol blue	Sigma, UK
Calcium chloride dihydrate	Sigma, UK
Calcium nitrate tetrahydrate	Sigma, UK
Carbonic anhydrase,	Sigma, UK
Chloroform	Sigma, UK
Chondroitin sulphate	Sigma, UK
Coomasie Brilliant Blue R250	Sigma, UK
Coomasie brilliant blue G	Sigma, UK
Copper chloride dihydrate	Sigma, UK
Copper nitrate	Sigma, UK
Cytochrome C	Sigma, UK
Dermatan sulphate	Sigma, UK
Dithiothreitol	Sigma, UK
Ethanol	BDH, UK
Filters 0.45 μM	Millipore, UK
Formic acid	Sigma, UK
Glucose-6-phosphate	Sigma, UK
Glucose-6-phosphate dehydrogenase	Sigma, UK
Glutaraldehyde	Sigma, UK
Glycerol	Sigma, UK

Glycine	Sigma, UK
Heparan sulphate	Sigma, UK
Heparan sulphate proteogylcan	Sigma, UK
1,1,1,3,3,3 hexafluoroisopropanol	Sigma, UK
Hydrochloric acid	BDH, UK
Iso-butanol	Sigma, UK
Immuno-Blot immunoassay kit (protein G - horseradish peroxidase) (Cat no.170-6467)	Bio-Rad, UK
Keratan sulphate	Sigma, UK
Lithium hydroxide	BDH, UK
Molecular weight markers (1,060-26,600 kDa)	Sigma, UK
Methanol	BDH, UK
Magnesium chloride hexahydrate	Sigma, UK
Magnesium nitrate hexahydrate	Sigma, UK
NADPH	Sigma, UK
$NADP^+$	Sigma, UK
Nickel chloride hexahydrate	Sigma, UK
Nitric acid	BDH, UK
Nitro-cellulose membrane	Schleicher & Schuell
NP-40	Sigma, UK
Orthophosphoric acid	BDH, UK
Oxalic acid	BDH, UK
4-(2-pyridylazo) resorcinol	Dionex, UK
Phenyl methyl sulphonyl fluoride	Sigma, UK
Recombinant human prion protein	Imperial College London, UK
SDS	Sigma, UK
Sephadex G75, G150	Sigma, UK
Sodium carbonate	Sigma, UK
Sodium chloride	Sigma, UK
Sodium Citrate	Sigma, UK
Sodium heparin	Sigma, UK
Sodium hydroxide	Sigma, UK
Sodium metasilicate	Sigma, UK
Sodium sulphate	Sigma, UK
Sulphuric acid	BDH, UK
TEMED	Sigma, UK
Tiron	Sigma, UK
2,2,2-Trifluoroethanol	Sigma, UK
Tris (hydroxymethyl) aminomethane	Sigma, UK
Urea	Sigma, UK
Vitamin B_{12}	Sigma, UK
Zinc chloride	Sigma, UK
Zinc nitrate hexahydrate	Sigma, UK

Determination of copper and zinc in blood plasma by ion chromatography using a cobalt internal standard

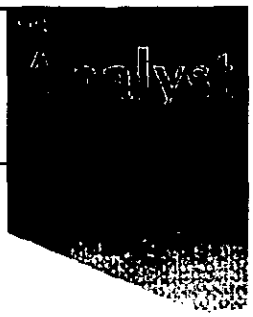

Edmund Lane,[a] Alexis J. Holden*[a] and Robert A. Coward[b]

[a] *Centre for Toxicology, University of Central Lancashire, Preston, UK PR1 2HE. E-mail: a.j.holden@uclan.ac.uk*

[b] *Dialysis Unit, Royal Preston Hospital, Sharoe Green Lane North, Fulwood, Preston, UK PR2 9HT*

Received 12th November 1998, Accepted 13th January 1999

Ion chromatography was used to detect levels of copper and zinc in blood plasma from renal dialysis patients on continuous ambulatory peritoneal dialysis (CAPD) and haemodialysis (HD). The developed method used cobalt as an internal standard and when combined with the standard additions method improved the overall precision of the results by between −0.3 and 6.0% and −0.8 and 5.7% for copper and zinc, respectively. The method was compared with inductively coupled plasma optical emission spectrometry (ICP-OES) and the results indicated no significant difference between the two methods with or without an internal standard. Without an internal standard, t_{calc} was 0.869 with a t_{crit} of 2.201 (n = 12, P = 0.05) and with an internal standard, t_{calc} was 0.189 compared to a t_{crit} of 2.201 (n = 12, P = 0.05). The copper and zinc levels in blood plasma in both dialysis groups were not significantly different to the copper and zinc levels in blood plasma of the control patients. A convenient method of analysis of trace elements in blood such as ion chromatography with UV/VIS detection is useful for determining whether inorganic elements may be disrupted in the body due to changes in the state of health.

Introduction

The trace elements copper and zinc serve chiefly as key components of proteins and of enzyme systems in the human body and are vital for their proper functions.[1] Zinc is involved in the synthesis of nucleic acids and proteins and is necessary for growth.[1] The majority of these enzymes act as antioxidants in biological systems [*e.g.*, Cu, Zn in superoxide dismutase (SOD) and Cu in caeruloplasmin]. Deficiencies or excess of the trace elements may have a detrimental effect on the function of these enzymes.[2,3] Levels of many trace elements are disturbed in various diseases, *e.g.*, abnormal levels of copper and zinc have been found in patients on renal dialysis,[4–8] lowered copper levels are associated with Wilson's disease and hypocupremia is observed with leukaemia and with a number of acute diseases.

The detection of trace elements in blood is an important factor for determining any disruption in trace element status of the body. The method used to determine elemental levels needs to be sensitive enough to detect the amounts present in blood (levels of Cu and Zn ~1 mg dm^{-3}) in an all too often limited sample volume.[3] Analysis of trace elements in biological samples requires: precise and accurate separation of the analyte from the bulk matrix for some measurements, a suitable means of detection which is of the appropriate sensitivity and to be free of contamination. Careful consideration of factors such as diet and disease state are critical in the assessment of the results before any conclusions can be made about cause–effect relationships for the disruption of metal status.[3]

Atomic absorption spectrometry (AAS) is widely used for the detection of many elements. Techniques such as flame atomic absorption spectrometry (FAAS) and electrothermal atomic absorption spectrometry (ETAAS) are suitable for the detection of Zn and Cu in blood serum and plasma. With the development of such routine methods often samples only require dilution.[9] Detection limits for flame AAS have been reported to be as low as 9.4 μg dm^{-3} for zinc [10] and 0.2 μg dm^{-3} for copper when preconcentration techniques have been employed.[11] Detection limits for ETAAS are typically 0.4 μg dm^{-3} and 0.1 μg dm^{-3} for Cu[12] and Zn,[13] respectively. However, for most of the AAS techniques, only one element can be determined at a time in many routine laboratories, although the relatively new Perkin-Elmer SIMAA 6000 method of simultaneous multi-element ETAAS is able to detect up to six elements with the same detection limits as conventional ETAAS analysis due to the very low noise of the solid-state detector.[14] Inductively coupled plasma optical emission spectrometry (ICP-OES) and mass spectrometry (ICP-MS) can be used in the direct analysis of biological fluids. The advantages include simultaneous detection of several elements in the one sample and its ability to overcome matrix interferences.[15] The sample is efficiently desolvated, vaporised, excited and ionised. Many chemical interferences are greatly reduced by the high temperature of 7000–8000 °C. Typical levels of detection range from <0.5 to 100 mg dm^{-3} for most metals. One of the major advantages of ICP-MS over ICP-OES is a three orders of magnitude higher sensitivity for metal detection although there may be problems due to the matrix.[15] Ion chromatography has been increasingly used for the determination of metals and is becoming an alternative to conventional spectrometric methods.[16,17] The main advantage is that multiple elements can be simultaneously determined in one sample using similar sample pre-treatment methods. Ion chromatography can separate a mixture of ions by their net charge according to the principles of ion exchange. Several detection methods are available including conductance and detection by UV by the use of a post column derivatisation reagent. Ion chromatography is suitable for small sample volumes, with injection volumes of 25 μl per analysis. Detection limits of less than 13 μg dm^{-3} have been reported by a number of workers.[18,19]

The current study involved the development of an ion chromatography (IC) method which would enable the determination of copper and zinc in the same aliquot of a sample. The final method made use of a cobalt internal standard which was used to minimise errors due to sample loading and fluctuations,

which occurred during the running of the column. The peak area results for the copper and zinc peaks were expressed as a ratio of the peak area result from the cobalt peak. Hence, if a varied volume of sample was injected or there was a variation in the flow rate of the mobile phase or the detector did not respond in a uniform manner throughout all the chromatography runs, then the results could still be used. The cobalt peak would be affected in the same manner as the copper and zinc peaks and so the ratio of the peak areas would remain the same although the raw peak area data values would change according to the inconsistencies within the instrument. Hence the use of an internal standard in analyses allows the use of data which may otherwise be deemed worthless. The method of standard additions was also used. To test the developed method a number of blood plasma samples from patients on haemodialysis (HD) and continuous ambulatory peritoneal dialysis (CAPD) as well as control samples were analysed.

Materials and methods

Specimens

Blood samples from eight renal dialysis patients, four on HD and four on CAPD, plus four control samples were obtained from the Royal Preston Hospital. The blood samples were collected from patients on renal dialysis in S-Monovette LH-Metall-Analytik tubes (Sarstedt Ltd., Leicester, UK) which contained lithium–heparin as an anticoagulant. These tubes are recommended by the suppliers for the collection of blood plasma which is to be analysed for analytes such as copper, zinc, lead, manganese, cadmium, iron, aluminium, nickel, selenium, chromium and mercury. The plasma was removed from the blood sample by centrifugation and the samples stored in the refrigerator at 4 °C before use. The time between sample collection and centrifugation was between 1–2 h because of the staggered collection time on the hospital ward. The dialysis subjects ranged in age (35–60 years) and in the number of years that they had received dialysis (2–25 years) (Table 1). The control samples were age matched where possible.

Reagents

All chemicals were of analytical-reagent grade and where possible all analyses were carried out in plasticware to reduce the risk of contamination during storage, transport and analysis. All containers were acid washed by soaking in 10% nitric acid (BDH-Merck, Poole, Dorset, UK) overnight and then in deionised water (Barnstead E-Pure, Fisons, Loughborough, Leicestershire, UK, 17.6 mΩ cm^{-1}) overnight. Stock standard solutions containing 1000 mg dm^{-3} of copper, zinc and cobalt were diluted to 5 mg dm^{-3} working solutions. All these solutions were prepared daily from copper, zinc and cobalt atomic absorption spectrometric standards (Fisher, Loughborough, Leicestershire, UK).

Table 1 Details of the patient sample used in each dialysis and control group

Dialysis type	Male	Years on dialysis	Female	Years on dialysisysis
CAPD	38	1	50	2
	73	10	52	11
HD	54	1	33	3
	70	4	52	1
Control	34	N/A	69	N/A
	50	N/A		
	61	N/A		

Instrumentation

A 1 cm^3 sample of the blood plasma sample was digested with 70% nitric acid in a ratio of 1:3 in pressure sealed Teflon bombs (150 cm^3 CEM, Buckingham, UK). An MDS 8D microwave (CEM) was used at 70% power for a total of 60 min in 3 × 20 min periods allowing the samples to cool for 10 min between each 20 min period. The digested material was diluted to 10 cm^3 with deionised water. For the standard additions method, four 1 cm^3 aliquots of the plasma digest were spiked with increasing amounts of copper (0, 0.2, 0.4, 0.8 cm^3 from the working solution) and zinc (0, 0.2, 0.4, 0.8 cm^3 from the working solution). A 0.6 mg dm^{-3} cobalt internal standard (0.6 cm^3 from the working solution) was also added to each sample. The solutions were made up to 5 cm^3 with deionised water.

Measurements were performed in triplicate on a Dionex DX500 ion chromatography system. A 25 cm HPIC-CS5 cation exchange column (Dionex, Camberley, Surrey, UK) with a 5 cm HPIC-CG5 guard column (Dionex) and a 25 μl sample loop was used. The column packing consisted of a cross-linked styrene and vinylbenzene polymer with sulfonic functional groups. The eluent was 50 mM oxalic acid and 95 mM lithium hydroxide at pH 4.8 (BDH-Merck) at a flow rate of 1 cm^3 min^{-1}. The post-column reagent used was 0.3 mM 4-(2-pyridylazo) resorcinol (PAR) (Dionex) in 1 M acetic acid and 3 M ammonium hydroxide solution at a flow rate of 0.7 cm^3 min^{-1}. The detection was at 520 nm using a Dionex A20 absorbance detector (Dionex).

An inductively coupled plasma optical emission spectrometer (ICP-OES) (Spectro, Halesowen, Worcestershire, UK, Analytical Model P) was used to detect copper and zinc. Copper was detected at 324.8 nm and zinc at 213.9 nm. The sample was introduced into the plasma at a flow rate of 1 cm^3 min^{-1} through silicone tubing *via* a peristaltic pump. Five replicate measurements were made and approximately 0.5 cm^3 of sample was required per sample. The system was flushed with deionised water between individual solutions.

Results and discussion

Copper, zinc and cobalt were easily separated by ion chromatography with elution times of 2.9, 4.8 and 6.6 min, respectively, as shown in Fig 1. With the oxalate eluent used it is reported that only cations lead, copper, zinc, manganese, cobalt, cadmium and nickel are detected. It was hypothesised that either iron(II) or iron(III) may interfere with the analysis of zinc or copper but preliminary experiments suggested that this was not the case. The cobalt internal standard was subjected to the same conditions as the sample, hence any fluctuations in the running conditions would be eliminated by plotting the absorbance ratio between copper and cobalt against the concentration of spiked copper. Similarly for zinc, the absorbance ratio between zinc

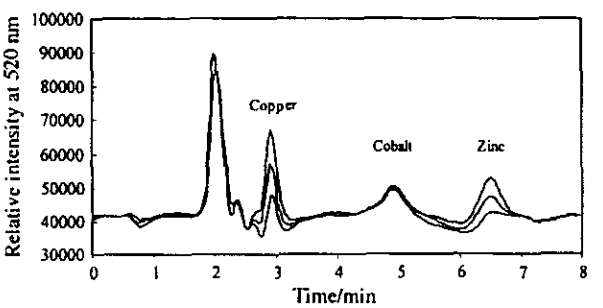

Fig. 1 Chromatograms of spiked blood plasma. Copper, cobalt and zinc eluted at 2.9, 4.8 and 6.6 min, respectively. Each of the three samples was spiked with cobalt (0.6 mg dm^{-3}) and with increasing concentrations of copper and zinc (0, 0.4, 0.8 mg dm^{-3}).

and cobalt against the concentration of spiked zinc was plotted. By using cobalt as an internal standard it is suggested that the ratio of the analyte to the internal standard provides a more accurate determination than the use of the analyte response alone. The precision was further improved by combining the internal standard method with the method of standard additions. This produced an overall improvement in the correlation coefficient of between −0.3 and 6% for copper and between −0.8 and 5.7% for zinc (Fig. 2 and Table 2). For this method to be reliable, the chosen internal standard must be well separated from the components but must appear close to the peaks of interest. Cobalt can be used as an internal standard as it is found in serum at very low levels (< 0.05 μg dm^{-3}),[1] well below the detection limit of IC with VIS detection and ICP-OES. The detection limit was calculated as three times the signal to noise ratio. The signal to noise ratio was calculated by measuring the concentration of the baseline noise in comparison with a peak of a 0.5 mg dm^{-3} sample of the analyte. The detection limits were calculated as 0.09 mg dm^{-3} for Cu and 0.03 mg dm^{-3} for Zn.

The results obtained from the ion chromatography analysis were validated by comparing the results with those obtained from ICP-OES. The *t*-test (at 95% confidence limit) revealed no significant differences between the values obtained by the two methods. There was reasonable agreement between both methods, although more samples would indicate if a better correlation was possible. The correlation coefficient for copper was 0.88 with an equation of $y = 1.04x - 0.019$ ($n = 12$) (Fig. 3) and the correlation coefficient for zinc was 0.89 with an equation of $y = 1.08x - 0.022$ ($n = 12$). A Bland–Altman plot is where the difference between the results from the two methods is expressed as a percentage of the mean of the two results for each sample, plotted against the mean concentration of the two measurements. If there is no systematic difference in the results from the two techniques then the data points would oscillate about the zero line on the *y*-axis. The Bland–Altman

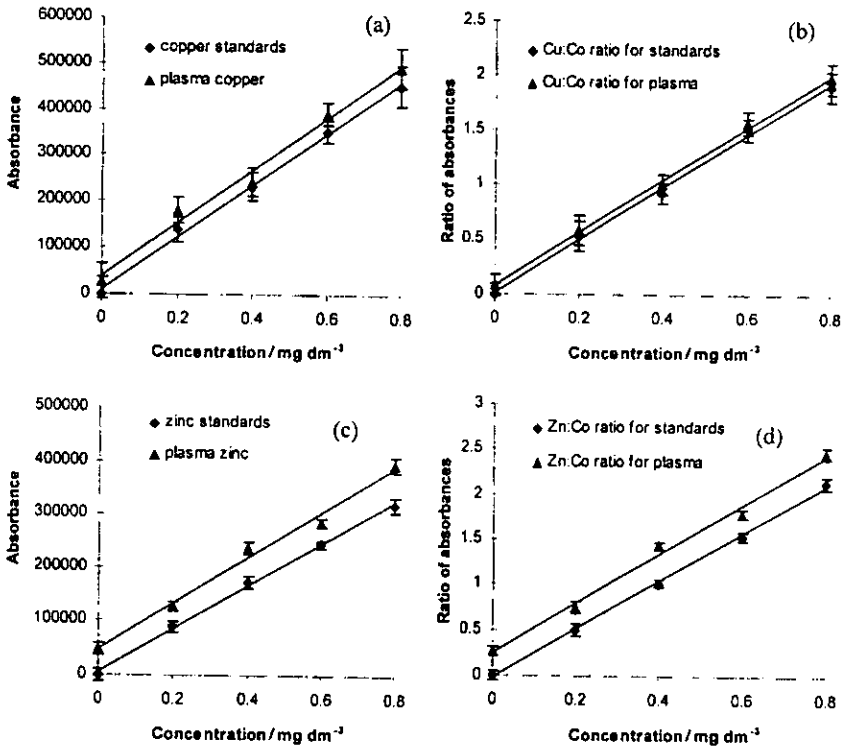

Fig. 2 Comparison of calibration and standard addition graphs of plasma from one haemodialysis patient (* in Table 2) for Cu [(a) and (b)] and Zn [(c) and (d)] with [(b) and (d)] and without [(a) and (c)] the use of an internal standard.

Table 2 Comparison of the correlation coefficient for each patient group when samples were analysed with and without an internal standard (IS). Results marked (*) correspond to data presented in Fig. 2

	Copper			Zinc		
Dialysis type	No IS	With IS	Improvement (%)	No IS	With IS	Improvement (%)
CAPD	0.917	0.976	6.05	0.951	0.943	−0.83
	0.922	0.954	3.35	0.907	0.951	4.64
	0.944	0.991	4.76	0.950	0.977	2.70
	0.954	0.991	3.75	0.921	0.976	5.64
HD	0.923	0.943	2.14	0.945	0.954	0.93
	0.943	0.951	0.82	0.928	0.932	0.43
	0.951	0.977	2.61	0.897	0.942	4.78
*	0.925	0.976	5.23	0.922	0.951	3.05
Control	0.931	0.954	2.41	0.944	0.977	3.33
	0.921	0.932	1.18	0.954	0.976	2.25
	0.945	0.942	−0.33	0.932	0.954	2.31
	0.914	0.951	3.89	0.934	0.991	5.77
Average			2.98 ± 1.89			2.92 ± 2.07

plot is used as Pollock *et al.* [20] suggested it to be more sensitive to potential bias within techniques than the standard regression techniques which can be used. In Fig. 4 if the difference between the results is 10%, this represents that one of the results is 1.1 times the value of the other, if the difference is 66%, then one result is twice the other and if the difference is 100%, one result is three times the other. Using the results from this work the Bland–Altman plot (Fig. 4) demonstrates that there is an overall positive bias for both copper and zinc of 0.006 mg dm^{-3} (0.35%) and 0.128 mg dm^{-3} (7.07%), respectively. This suggests that the results for zinc obtained from the ICP-OES method are higher than those obtained with IC-VIS analysis. This could result from matrix effects in either the IC-VIS or ICP-OES methods. Teixeira *et al.* [21] reported that the use of ICP-OES for the determination of zinc at low concentrations in matrices containing high concentrations of copper was difficult because of the interference by copper in the main emission wavelength of zinc at 213.856 nm.

There were no significant differences in both the copper and zinc levels between CAPD patients and HD patients and there was no significant difference when dialysis groups were compared to the control patients (Tables 3 and 4). It must be stressed that these individual values represent the levels of copper and zinc in different patients and thus the concentrations of copper and zinc may vary from patient to patient due to factors such as sex, age, and time on dialysis. The normal range for copper in serum is 0.8–1.5 mg dm^{-3} and for zinc it is 0.6 –1.3 mg dm^{-3}. Overall, the average control copper levels were lower than the normal levels expected in the blood. The measured copper concentration for this study was 0.501 ± 0.05 mg dm^{-3} for copper and was 1.350 ± 0.05 mg dm^{-3} for zinc in the control samples. This paper is concerned with the development of an alternative analytical method to conventional spectrometric methods for the determination of copper and zinc in biological samples and as such the levels of copper and zinc reported in this study should not be used exclusively as the measured concentration of the zinc in the samples was probably affected by the lapse time between collection and centrifugation as suggested by English and Hambridge.[22] They reported that

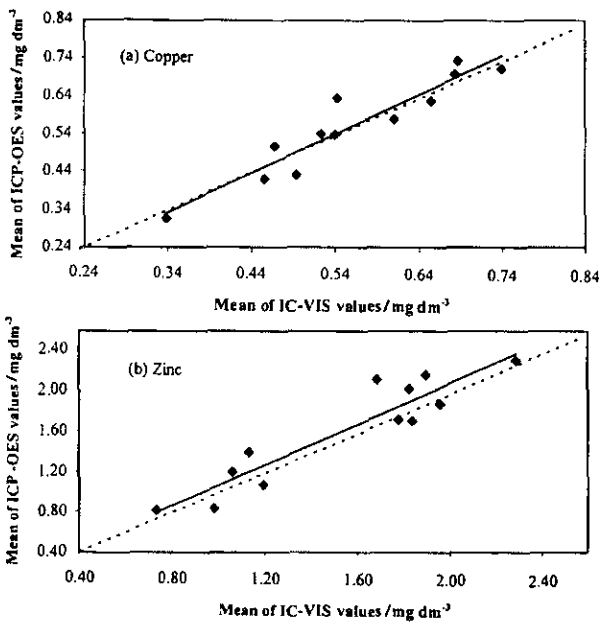

Fig. 3 The correlation between samples run on both ICP-OES and IC-VIS: (a) the correlation coefficient for copper values was $r = 0.88$ and the equation of the line is $y = 1.04x - 0.019$ ($n = 12$); (b) the correlation coefficient for zinc was $r = 0.89$ with an equation of the line $y = 1.08x - 0.022$ ($n = 12$).

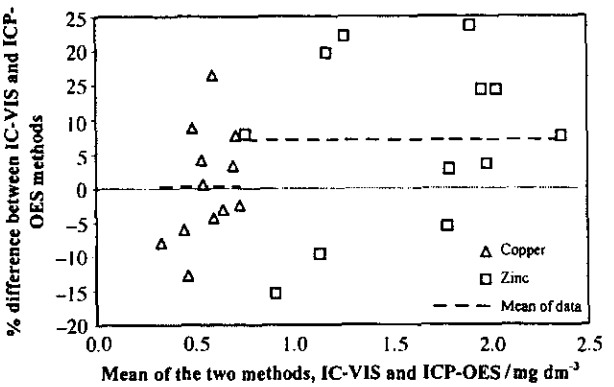

Fig. 4 The Bland–Altman plots for copper and zinc which compares the two methods IC-VIS and ICP-OES. The plots show a small positive bias indicating that the results obtained with ICP-OES are higher than those obtained using IC-VIS.

Table 3 Concentrations of copper and zinc in acid digested blood plasma as detected by ion chromatography with VIS detection using the standard additions method with a cobalt internal standard and with ICP-OES

Method	Dialysis type ($n = 4$)	Copper/mg dm^{-3}		Zinc/mg dm^{-3}	
		Average	Range	Average	Range
IC-VIS	Control	0.501 ± 0.05	0.45–0.67	1.350 ± 0.05	0.73–1.83
	CAPD	0.549 ± 0.05	0.33–0.68	1.576 ± 0.06	0.89–1.95
	HD	0.594 ± 0.05	0.46–0.78	1.348 ± 0.06	0.98–1.79
ICP-OES	Control	0.534 ± 0.03	0.31–0.62	1.417 ± 0.02	0.79–1.95
	CAPD	0.597 ± 0.02	0.51–0.70	1.789 ± 0.03	0.91–2.28
	HD	0.575 ± 0.02	0.43–0.73	1.481 ± 0.02	0.93–2.02

Table 4 One tailed *t*-test for unequal variances was used to compare between the means of the dialysis group with the control groups and between the two methods ($P < 0.05$)

Comparison	n	Copper		Zinc	
		t_{calc}	t_{crit}	t_{calc}	t_{crit}
IC-VIS (with IS) *vs.* ICP-OES	12	0.189	2.201	0.265	2.201
IC-VIS (no IS) *vs.* ICP-OES	12	0.869	2.201	1.170	2.201
CAPD *vs.* control	4	0.448	3.182	0.747	3.182
HD *vs.* control	4	0.938	3.182	0.007	3.182
CAPD *vs.* HD	4	0.427	3.182	0.747	3.182

the level of Zn determined in plasma and serum increased by 6% for the first 2 h after collection which was thought to be attributed to the release of some erythrocyte membrane zinc. A similar effect was not found for copper.

Many factors are involved in determining blood and tissue levels of individual elements in patients with renal failure. The processes involved in renal disease itself can result in either excretion or retention of individual elements whilst dialysis treatment can cause either removal or exposure to these elements. Trace metal disruption causes chronic renal insufficiency in dialysis patients that have been studied but many of these studies are contradictory due to different techniques that have been used. For instance, copper levels have shown conflicting results with high, low and normal levels with some evidence that the levels increase with age and the female sex but not with dialysis duration. Hypozincaemia is also common in patients with end stage renal disease and those on dialysis (haemodialysis and CAPD).

In haemodialysis the blood is pumped at 200–400 cm^3 min^{-1} into an artificial kidney where it is filtered by a semi-permeable dialysis membrane against the dialysate solution at a flow of 500 cm^3 min^{-1}. Transfer occurs across the membrane of waste products into the dialysate which is drained away. The dialysate solution is made from combining a concentrate with a filtered and reverse osmosis treated tap water.

In CAPD the dialysate (typically 2 dm^3) is introduced into the abdominal cavity *via* a catheter and remains there for 4–6 hours. During this time, excess fluid and waste products are transferred into the dialysate solution from the blood across the peritoneal membrane and subsequently drained out to be replaced by fluid dialysate.

Dialysis fluid (CAPD, haemodialysis concentrate and reverse osmosis treated tap water) has a role in contributing to trace element abnormalities in renal patients. Metal contaminants in dialysis fluid such as copper and zinc should be eliminated by the manufacturing process. Other sources of contamination such as dialysate tubing could be a possible source of metal contamination.[23] Further factors may be important in determining blood and tissue levels, in particular the ongoing ageing process with poor dietary intake and decreased gastrointestinal absorption of zinc, whilst copper absorption in the small intestine is facilitated by zinc deficiency owing to the loss of absorption competition.

Ion chromatography is an attractive alternative to the usually more conventional spectrometric methods for the determination of metals. Ion chromatography offers a more cost effective choice as the running expenses of ion chromatography often are cheaper than those faced by ICP-OES users. The most obvious advantage of this technique is that multiple elements can be determined in one sample of 25 µl volume and complete analysis can be performed when coupled with a suitable detection system or systems. Generally, the sample requires minimal sample pre-treatment.[16] Although it is accepted that microwave digestion seems laborious when compared to the simple dilution methods used with some atomic spectrometric methods, the use of acid digestion to totally breakdown the matrix of a sample in order to ensure all the analyte is recovered offers its own advantages. The selectivity and peak sharpness in IC can be enhanced by the use of complexing agents such as PAR for the detection of cations followed by spectrophotometric detection giving a highly sensitive method. The use of the standard additions method and of an internal standard can improve the precision of the results.

Acknowledgements

Thanks to Dr. Philip H. E. Gardiner and Heather Birtwistle at Sheffield Hallam University for the use of the ICP-OES system. This work was supported by a studentship from the Lancashire Centre for Medical Studies.

References

1 W. Kaim and B. Chwederski, *Bioinorganic Chemistry: Inorganic Elements in the Chemistry of Life, An Introduction and Guide*, Wiley, New York, 1994, pp. 151–161.
2 J. M. Campistol and A. Argiles, *Nephrol. Dial. Transplant*, 1996, **11**, 142.
3 M. Gallieni, D. Brancaccio, M. Cozzolio and E. Sabioni, *Nephrol. Dial. Transplant*, 1996, **11**, 1232.
4 N. J. Emenaker, R. A. Disilvestro and N. S. Nahman, *Am. J. Clin. Nutr.*, 1996, **64**, 757.
5 R. J. Cousins, *Physiol. Rev*, 1985, **65**, 309.
6 P. L. Kimmel, T. M. Philips and S. Q. Lew, *Kidney Int.* 1996, **49**, 1412.
7 L. Yver and D. Blanchier, *Nephrol. Dial. Transplant*, 1987, **2**, 451.
8 C. Canavesse, *Nephron*, 1990, **56**, 455.
9 K. Nomiyama and H. Nomiyama, *Nephrol. Dial. Transplant*, 1989, **4**, (suppl) 114.
10 K. Cundeva and T. Stafilov, *Talanta*, 1997, **44**(3), 451.
11 H. W. Chen, S. K. Xu and Z. L. Fang, *Anal. Chim. Acta*, 1994, **298**(2), 167.
12 P. B. Barrera, R. D. Gonzalez and A. B. Barrera, *Fresenius' J. Anal. Chem.*, 1997, **357**(4), 457.
13 S. D. Huang and K. Y. Shih, *Spectrochim. Acta, Part B*, 1995, **50**(8), 837.
14 M. Hoenig and A. Cilissen, *Spectrochim. Acta, Part B*, 1997, **52**, 1443.
15 J. Schoppenthau and L. Dunemann, *Fresenius' J. Anal. Chem.*, 1994, **349**, 794.
16 C. N. Ong, H. Y. Ong and L. H. Chua, *Anal. Biochem.*, 1988, **173**, 64.
17 M. En-ling and J. Zhu-ming, *Chin. Med. J.*, 1993, **106**(2), 118.
18 H. T. Lu, S. F. Mou, Y. Yan, S. Y. Tong and J. M. Riviello, *J. Chromatogr. A*, 1998, **800**(2), 247.
19 S. Okawa and T. Ishikawa, *Bunseki Kagaku*, 1998, **47**(1), 9.
20 M. A. Pollock, S. G. Jefferson, J. W. Kane, K. Lomax, G. MacKinnon and C. B. Winnard, *Ann. Clin. Biochem.*, 1992, **29**, 556.
21 L. S. G. Teixeira, J. O. N. Reis, A. C. S. Costa, S. L. C. Ferreira, M. D. S. G. Korn and J. B. deAndrade, *Talanta*, 1998, **46**(6), 1279.
22 J. L. English and K. M. Hambridge, *Clin. Chim. Acta*, 1988, **175**, 211.
23 R. Milacic, M. Benedik and S. Knezevic, *Clin. Chim. Acta*, 1997, **265**, 169.

Paper 8/08852G

Declaration

I declare that the work presented in this thesis is entirely my own, except where indicated or acknowledged, and includes nothing which is the outcome of work done in collaboration. It is not substantially the same as any work that I have submitted for a degree or diploma or any other qualification at this or any other university.

Edmund Lane

Date 25th oct 2000